LONG TERM PREDICTION OF HIGH ALTITUDE ORBITS

by

Sean Kevin Collins

B.S.A.E., University of Virginia
(1974)

S.M., Massachusetts Institute of Technology
(1977)

SUBMITTED IN PARTIAL FULFILLMENT
OF THE REQUIREMENT FOR
DOCTOR OF PHILOSOPHY

at the
Massachusetts Institute of Technology

MARCH 1981

© 1981 by Massachusetts Institute of Technology

Signature of Author _____
Department of Aeronautics & Astronautics
March 1981

Approved by _____ Walter M. Hollister
Chairman of Thesis Committee

Approved by _____ Richard H. Battin
Thesis Advisor

Approved by _____ John P. Vinti
Thesis Advisor

Approved by _____ Paul J. Cefola
Thesis Advisor

Accepted by _____ Manuel Martinez-Sanchez
Chairman, Departmental Doctoral Committee

Accepted by _____
Harold Y. Wachman, Chairman, Departmental
Graduate Committee

ARCHIVES
MASSACHUSETTS INSTITUTE
OF TECHNOLOGY
MAY 5 1981
LIBRARIES

LONG TERM PREDICTION OF HIGH ALTITUDE ORBITS

by
Sean Kevin Collins

Submitted to the Department of Aeronautics and Astronautics on 30 March 1981 in partial fulfillment of the requirements for the Degree of Doctor of Philosophy

ABSTRACT

This thesis develops a first order semi-analytical theory, based on the Generalized Method of Averaging and making extensive use of recursive algorithms, for the rapid and accurate calculation of the secular and long period changes in the elements of a high altitude satellite orbit caused by the action of the sun and moon. The theory is designed to assist the mission analyst concerned with testing the long term stability of selected orbits in the region above synchronous altitude where "third body" perturbations are a major determinant of orbital lifetime and stability.

A representation of the third body disturbing potential in satellite orbital elements is essential to the development. Non-singular equinoctial orbital elements are used as part of a unified approach to the elimination of artificial singularities in the satellite dynamical equations for near-circular and near-equatorial orbits. The potential is derived with respect to the reference frame of the satellite to minimize the analytical complexity of the first order theory. Special functions are employed wherever possible to modularize the analytical structure with a view towards efficient computation in a numerical program. The potential retains the parallax factor to an arbitrary power and no assumptions are made on the geometry of the third body orbit. The potential is expanded into the mean longitudes of the satellite and the disturbing body so that resonance can be studied.

An averaging theory, based on the Generalized Method of Averaging, is developed for removing frequencies from the satellite dynamical equations depending on rapidly varying linear combinations of the satellite and third body mean longitudes. The method for obtaining the analytical forms of the averaged equations of motion and the short periodic recovery functions is detailed.

The third body averaging theory has been numerically implemented and compared against Cowell integration for five test orbits. The principal conclusion of this thesis is that the first order semi-analytical third body theory can be used to accurately predict the long term motion of a high altitude satellite with an efficiency that makes it decisively superior to conventional mission analysis techniques.

Thesis Supervisor: Walter M. Hollister
Title: Associate Professor of Aeronautics and Astronautics

Thesis Supervisor: John P. Vinti
Title: Lecturer of Aeronautics and Astronautics

Thesis Supevisor: Richard H. Battin
Title: Adjunct Professor of Aeronautics and Astronautics
Associate Department Head, C. S. Draper Laboratory

Thesis Supervisor: Paul J. Cefola
Title: Lecturer of Aeronautics and Astronautics
Section Manager, C. S. Draper Laboratory

ACKNOWLEDGEMENTS

I wish to express my profound appreciation to the members of my doctoral thesis committee, whose support and counsel have made this work possible. This includes Professor Walter M. Hollister, who served as chairman, Dr. Richard H. Battin, who introduced me to astrodynamics, Dr. John P. Vinti, whose vast knowledge of Celestial Mechanics inspired me, and Dr. Paul J. Cefola, who acted as principal advisor. I would like to emphasize my gratitude to Dr. Cefola for his patience and technical guidance throughout my doctoral program. I am also indebted to Wayne D. McClain (CSDL) for his sage advice and criticisms during all phases of this thesis. Thanks are extended to Dr. Ronald J. Proulx (CSDL), Dr. Mark S. Slutsky (CSDL), Mr. Aaron F. Bobick (MIT/CSDL) and Captain Stephen P. Taylor (USA) for numerous helpful discussions, suggestions and support. Appreciation is also extended to Mr. Leo W. Early (CSDL) whose knowledge of GTDS was constantly exploited during the software development.

I would like to thank Captain (Dr.) Andrew J. Green (USA/ARMOR), a friend and prolific achiever. The software implementation of the third body theory developed in this thesis was greatly aided by work that he performed at CSDL as an MIT doctoral student. Special thanks go to Captain (Dr.) Jeffrey S. Shaver (USAF) for his reliable friendship and encouragement.

I wish to express appreciation to Mr. Bruce Baxter (The Aerospace Corporation) for a useful exchange of ideas regarding the concepts developed in this thesis and for the suggestion of research directions.

Thunderous applause is reserved for Ms. Karen M. Smith (CSDL), who forsook a normal life to ensure the completion of this document. I am very grateful to her for an effort that matches the highest professional standards.

My wife, Susie, deserves the lion's share of the accolades. Her unwavering understanding and compassion are the reasons for my success.

I would like to thank the Charles Stark Draper Laboratory of Cambridge, Massachusetts for providing financial support and research facilities for the entirety of my doctoral program at MIT.

TABLE OF CONTENTS

Chapter			Page
1.		INTRODUCTION	16
	1.1	Previous Work	20
	1.2	Overview	23
2.		THE THIRD BODY DISTURBING POTENTIAL	26
	2.1	Derivation of the Third Body Disturbing Potential in Inertial Coordinates	27
	2.2	Transformation of the Third Body Potential from Inertial Coordinates to Satellite Coordinates	35
	2.2.1	Reference Frame Choice and Implications	36
	2.2.2	Transformation of the Third Body Potential to Satellite Orbital Coordinates	39
	2.2.3	Induced Dependence of Third Body Orbital Elements on Satellite Orbital Elements	81
	2.2.3.1	The Meaning of h' and k'	81
	2.2.3.2	The Meaning of λ'	86
3.		ISOLATING LONG TERM MOTION IN THE SATELLITE DYNAMICAL EQUATIONS	91
	3.1	The Generalized Method of Averaging	94
	3.1.1	An Averaging Theory for Satellites Moving Under the Influence of a Disturbing Body	96
	3.1.2	A First Order Averaging Theory	110

TABLE OF CONTENTS
(cont.)

Chapter		Page
4.	MATHEMATICAL STRUCTURE OF A DYNAMICAL THIRD BODY MODEL FOR THE LONG TERM PREDICTION OF SATELLITE ORBITS USING NUMERICAL METHODS	118
4.1	First Order Averaged Equations of Motion for Third Body Perturbation	126
4.1.1	Criteria for Retaining Terms in the Averaged Equations of Motion	134
4.2	Mathematical Form of the Periodic Recovery Functions	137
4.3	Formulation of the Third Body Theory for Numerical Computation	151
4.4	Calculation of Special Functions	176
4.4.1	Calculation of $Z^m_{n,r}$	176
4.4.2	Calculation of Jacobi Polynomials and Their Partial Derivatives by Recurrence	180
4.4.3	Calculation of the Coefficients C^r_m, D^r_m and Their Partial Derivatives by Recurrence	183
4.4.4	Calculation of the Coefficients $A^{r,m}_{s,t}$, $B^{r,m}_{s,t}$ and Their Partial Derivatives	193
4.4.5	Recurrence Relations for the Third Body Hansen Coefficient Kernel $K_s^{-n-1,r}$ and its Derivative	201
4.5	Restriction of Indices in the Third Body Theory	211

TABLE OF CONTENTS
(cont.)

Chapter			Page
5.	NUMERICAL VERIFICATION OF THE FIRST ORDER THIRD BODY THEORY		219
	5.1	Initialization of the Averaged Equations of Motion	221
	5.2	The Computation of Third Body Ephemerides	228
	5.3	Analysis of the Numerical Results	231
	5.3.1	IUE Test Case	233
	5.3.2	ISEE Test Case	262
	5.3.3	VELA Test Case	273
	5.3.4	STRATSAT Test Case	285
	5.3.5	Lunar Resonance Test Case	296
6.	CONCLUSIONS AND FUTURE WORK		306
	6.1	Conclusions	310
	6.2	Future Work	312
Appendix A.	Computation and Storage of the Newcomb Operators in the Third Body Theory		316
Appendix B.	Software Implementation of the Third Body Theory		322
List of References			337

LIST OF FIGURES

Figure		Page
2-1	Geometry of the Third Body Problem	28
2-2	Orientation of the Satellite Reference Frame with Respect to the Inertial Reference Frame	40
2-3	Orientation of the Third Body Position Vector with Respect to the Satellite Frame	42
2-4	Geometry for the Rotation of Surface Spherical Harmonics	49
4-1	Admissible Values of the Index m vs. t	214
4-2	Admissible Values of the Index r vs. s	217
5-1	Osculating Semi-Major Axis Comparison within the 60 Day PCE Fit Span for the IUE Orbit/Semi-Analytical versus Cowell	239
5-2	Osculating Eccentricity Comparison within the 60 Day PCE Fit Span for the IUE Orbit/ Semi-Analytical versus Cowell	240
5-3	Osculating Inclination Comparison within the 60 Day PCE Fit Span for the IUE Orbit/ Semi-Analytical versus Cowell	241
5-4	Osculating Mean Longitude Comparison within the 60 Day PCE Fit Span for the IUE Orbit/ Semi-Analytical versus Cowell	242
5-5	Osculating Semi-Major Axis Differences within the 60 Day PCE Fit Span for the IUE Orbit/Semi-Analytical minus Cowell	243
5-6	Osculating Eccentricity Differences within the 60 Day PCE Fit Span for the IUE Orbit/ Semi-Analytical minus Cowell	244

LIST OF FIGURES
(cont.)

Figure		Page
5-7	Osculating Inclination Differences within the 60 Day PCE Fit Span for the IUE Orbit/ Semi-Analytical minus Cowell	245
5-8	Osculating Mean Longitude Differences within the 60 Day PCE Fit Span for the IUE Orbit/Semi-Analytical minus Cowell	246
5-9	Comparison of the Mean and Osculating Semi-Major Axis Histories for the 3 Year Integration of the IUE Orbit/AOG versus Cowell	248
5-10	Comparison of the Mean and Osculating Eccentricity Histories for the 3 Year Integration of the IUE Orbit/AOG versus Cowell	249
5-11	Comparison of the Mean and Osculating Inclination Histories for the 3 Year Integration of the IUE Orbit/AOG versus Cowell	250
5-12	Differences Between the Mean and Osculating Semi-Major Axis Histories for the 3 Year Integration of the IUE Orbit/AOG minus Cowell	251
5-13	Differences Between the Mean and Osculating Eccentricity Histories for the 3 Year Integration of the IUE Orbit/AOG minus Cowell	252
5-14	Differences Between the Mean and Osculating Inclination Histories for the 3 Year Integration of the IUE Orbit/AOG minus Cowell	253

LIST OF FIGURES
(cont.)

Figure		Page
5-15	Osculating Semi-Major Axis Comparison for the 3 Year IUE Integration/Semi-Analytical versus Cowell	255
5-16	Osculating Eccentricity Comparison for the 3 Year IUE Integration/Semi-Analytical versus Cowell	256
5-17	Osculating Inclination Comparison for the 3 Year IUE Integration/Semi-Analytical versus Cowell	257
5-18	Evolution of the Mean Eccentricity for the 100 Year AOG Prediction of the IUE Orbit	259
5-19	Evolution of the Mean Inclination for the 100 Year AOG Prediction of the IUE Orbit	260
5-20	Comparison of the Mean and Osculating Semi-Major Axis Histories for the 8 Year Integration of the ISEE Orbit/AOG versus Cowell	266
5-21	Comparison of the Mean and Osculating Eccentricity Histories for the 8 Year Integration of the ISEE Orbit/AOG versus Cowell	267
5-22	Comparison of the Mean and Osculating Inclination Histories for the 8 Year Integration of the ISEE Orbit/AOG versus Cowell	268

LIST OF FIGURES
(cont.)

Figure		Page
5-23	Comaprison of the Mean and Osculating Longitude of Ascending Node Histories for the 8 Year Integration of the ISEE Orbit/AOG versus Cowell	269
5-24	Comparison of the Mean and Osculating Argument of Perifocus Histories for the 8 Year Integration of the ISEE Orbit/AOG versus Cowell	270
5-25	Comparison of the Mean and Osculating Semi-Major Axis Histories for the 10 Year Integration of the VELA Orbit/AOG versus Cowell	278
5-26	Comparison of the Mean and Osculating h Element Histories for the 10 Year Integration of the VELA Orbit/AOG versus Cowell	279
5-27	Comparison of the Mean and Osculating k Element Histories for the 10 Year Integration of the VELA Orbit/AOG versus Cowell	280
5-28	Comparison of the Mean and Osculating p Element Histories for the 10 Year Integration of the VELA Orbit/AOG versus Cowell	281
5-29	Comparison of the Mean and Osculating q Element Histories for the 10 Year Integration of the VELA Orbit/AOG versus Cowell	282

LIST OF FIGURES
(cont.)

Figure		Page
5-30	Comparison of the Mean and Osculating Inclination Histories for the 10 Year Integration of the VELA Orbit/AOG versus Cowell	283
5-31	Comparison of the Mean and Osculating Semi-Major Axis Histories for the 8 Year Integration of the STRATSAT Orbit/AOG versus Cowell	291
5-32	Comparison of the Mean and Osculating Eccentricity Histories for the 8 Year Integration of the STRATSAT Orbit/AOG versus Cowell	292
5-33	Comparison of the Mean and Osculating Inclination Histories for the 8 Year Integration of the STRATSAT Orbit/AOG versus Cowell	293
5-34	Comparison of the Mean and Osculating Radius of Perifocus Histories for the 8 Year Integration of the STRATSAT Orbit/ AOG versus Cowell	294
5-35	Comparison of the Mean and Osculating Semi-Major Axis Histories for the 5 Year Integration of the Lunar Resonance Test Orbit/AOG versus Cowell	300
5-36	Comparison of the Mean and Osculating Eccentricity Histories for the 5 Year Integation of the Lunar Resonance Test Orbit/AOG versus Cowell	301

LIST OF FIGURES
(cont.)

Figure		Page
5-37	Comparison of the Mean and Osculating Inclination Histories for the 5 Year Integration of the Lunar Resonance Test Orbit/AOG versus Cowell	302
B-1	Subroutine Interaction Diagram for the Third Body Software	333

LIST OF TABLES

Table		Page
2-1	Form of the Function $S_{2n}^{(m,r)}(p',q')$	71
2-2	Form of the Function $S_{2n}^{(m,r)}(\alpha,\beta,\gamma)$	76
2-3	Functional Form of the Third Body Elements, h' and k'	85
3-1	Harmonic Contributions of the Trigonometric Argument $t\lambda + s\lambda'$	93
4-1	Nonzero Poisson Brackets of the Equinoctial Elements	122
4-2	Form of the First Order Averaged Equations of Motion for Third Body Perturbation	138
4-3	Partial Derivatives of the Third Body Mean Longitude with Respect to the Mean Satellite Elements p,q	172
5-1	Epoch Osculating Elements for the IUE Test Case	233
5-2	PCE Perturbation Models for the IUE Test Case	236
5-3	Epoch Mean Elements for the IUE Test Case	238
5-4	Epoch Osculating Elements for the ISEE Test Case	262
5-5	PCE Perturbation Models for the ISEE Test Case	264
5-6	Epoch Mean Elements for the ISEE Test Case	265
5-7	Comparison of Cowell and AOG Execution Times for the Eight Year ISEE Integration	272
5-8	Epoch Osculating Elements for the VELA Test Case	273

LIST OF TABLES
(cont.)

Table		Page
5-9	PCE Perturbation Models for the VELA Test Case	275
5-10	Epoch Mean Elements for the VELA Test Case	275
5-11	AOG Perturbation Model for the Ten Year VELA Integration	277
5-12	Comparison of Cowell and AOG Execution Times for the Ten Year VELA Integration	284
5-13	Epoch Osculating Elements for the STRATSAT Test Case	285
5-14	PCE Perturbation Models for the STRATSAT Test Case	287
5-15	Epoch Mean Elements for the STRATSAT Test Case	288
5-16	AOG Perturbation Model for the Eight Year STRATSAT Integration	289
5-17	Comparison of Cowell and AOG Execution Times for the Eight Year STRATSAT Integration	295
5-18	Epoch Osculating Elements for the Lunar Resonance Test Case	296
5-19	PCE Perturbation Models for the Lunar Resonance Test Case	297
5-20	Epoch Mean Elements for the Lunar Resonance Test Case	298
5-21	AOG Perturbation Model for the Five Year Lunar Resonance Integration	299
5-22	Comparison of Cowell and AOG Execution Times for the Five Year Lunar Resonance Integration	303
B-1	Datasets and Region Sizes Required for the Various Third Body Options	332

Chapter 1

Introduction

The central result of this thesis is a new first order theory, based on the Generalized Method of Averaging and making extensive use of recursive algorithms, for the rapid and accurate calculation of secular and long period changes in the elements of a high altitude Earth satellite caused by the action of the sun and moon. The theory is a valuable asset to the mission analyst concerned with testing the long term stability of selected orbits in the region above synchronous altitude where "third body" perturbations are a major determinant of orbital evolution and lifetime.

The third body theory is developed within the framework of semianalytical orbit theory. Semianalytical methods involve the removal of periodic components from a Variation of Parameters (VOP) formulation of the satellite dynamical equations. These periodic components unnecessarily restrict the step size of a conventional numerical integration. The resulting averaged equations of motion can then be integrated with an expanded step size at greatly reduced computational expense. This approach is superior to the use of purely analytical General Perturbations (GP) techniques since it permits the incorporation of realistic disturbing body models into a numerical orbit prediction program while

minimizing analytical complexity [1]. Furthermore, the artificial singularities associated with GP theories arising from critical arguments [2] are not introduced and non-canonical variable sets may be employed.

The generality of the semianalytical third body theory derived in this thesis represents a remarkable improvement over previous work. For the first time the following conceptual components are unified in a single theory:

1) Generalized Method of Averaging (GMA)

   In semianalytical orbit theory, the averaged equations of motion are an approximation to the long term dynamics contained in the high precision equations of motion. The rigorous mathematical structure of this approximation was developed by Krylov and Bogoliubov [3] in the area of non-linear oscillations and later extended by Mitropolsky [4]. Known as the Generalized Method of Averaging, the formalism unambiguously defines the order of an averaging theory and furnishes a straightforward protocol for obtaining the averaged equations of motion on an order by order basis.

To a specified order, the Generalized Method of Averaging also provides an approximation to the high precision orbital elements in terms of the averaged elements. This approximation is made possible through the construction of analytical functions of the averaged elements that represent the short periodic variations in the high precision trajectory. Short periodic functions are essential to the initialization of the averaged equations of motion given high precision orbital elements.

2) Third Body Resonance

For the case where the satellite and the disturbing body are nearly commensurable in their mean motions, long period terms arise in the satellite dynamical equations. This phenomenon, called third body resonance, is analogous to resonance with the tesseral harmonics of the Earth's gravity potential caused by a repeating ground-track. Third body resonance terms are included in the averaged equations of motion derived in this thesis.

3) Non-Singular Orbital Elements

The satellite VOP equations are formulated in terms of non-singular equinoctial orbital elements. This choice circumvents numerical instability for near-circular or near equatorial orbits that is characteristic of Keplerian VOP equations.

4) Special Functions

The use of special functions and coefficients in the third body theory permits an extremely compact and modular analytical structure.

5) General Disturbing Body Model

No assumptions are made on the number of third body terms available in a numerical orbit prediction program and no theoretical restrictions are placed on the orbital eccentricity of either the satellite or the disturbing body. Specification of program input parameters is sufficient to tailor the disturbing body model to the requirements of a particular satellite orbit. This attribute is in contrast to the "hard-wired" nature of explicit third body theories that require extensive reprogramming to extend capabilities.

6) Recursive Computation

The use of recurrence relations for the numerical computation of special functions allows complicated disturbing body models to be evaluated rapidly starting from simply determined initial values.

1.1 Previous Work

Major contributions have been made by several researchers to the study of semi-analytical techniques for determining the evolution of high altitude satellites moving under the influence of a third body. Most of the third body theories applicable to mission analysis over extended time intervals are based on successively averaging the satellite VOP equations over the fast angular variables of the satellite and disturbing body to remove all high frequency components of the motion. These theories are called double averaged. Each must be judged on its own merits. However, as a general criticism, the assumed independence of the satellite and disturbing body phase angles for the purposes of double averaging will exclude the presence of any long period dynamics in the averaged equations of motion induced by third body resonance.

A third body secular perturbation theory was developed by Gauss [5] in which the third body disturbing acceleration is doubly averaged to produce a system of Gaussian VOP equations from which all short periodic variations are eliminated. The average over the mean anomaly of the disturbing body is seen to reduce to the purely geometrical exercise of computing the attraction of an elliptical ring of matter that is distributed along the orbit of the third body. The subsequent average over the satellite mean anomaly is computed by numerical quadrature or any other available technique. A modified version of Gauss' theory, attributed to Halphen [5], was rederived by Musen [6] to modernize notation and programmed to study the long term effects of lunar and solar perturbations on high altitude satellites. In an effort to remove the possibility of numerical instability in the original Keplerian element formulation, Musen [7] later explained how Halphen's method could be reformulated in terms of a set of non-singular orbital elements. Initialization of the averaged equations of motion given high precision orbital elements at epoch remains a challenging problem. One technique, used by Smith [8], involves the numerical average of high precision elements over an appropriate interval. However, the averaged elements obtained in this way will contain short periodic contamination if the interval is not precisely

chosen. A more effective method, employed by Baxter [9], relies on a double angle harmonic analysis of high precision element histories to identify short periodic components.

Ash [10] developed a double averaged third body theory in Keplerian elements, based on Gauss' concept, which was used to physically interpret the numerical integration of high altitude satellite orbits. It differs from Halphen's method by starting from an infinite series expansion for the third body potential rather than directly from the perturbing acceleration which is closed form. Also, the average over the satellite orbit is performed analytically rather than numerically. Special functions imbedded in the literal averaged VOP equations are not recognized, leaving expressions which are unnecessarily complex. Furthermore, the third body orbital eccentricity is assumed to be zero. It can be shown that this assumption eliminates terms from the satellite equations representing significant dynamical contributions.

Sridharan and Seniw [11] followed the development of Lidov [12] to derive an explicit double averaged third body theory based on the first term in the Legendre polynomial expansion of the disturbing acceleration. The

Gaussian VOP equations and the short periodic recovery functions are formulated in terms of Keplerian orbital elements. As a consequence of the dramatically truncated force model the theory lacks the flexibility to handle a general high altitude satellite orbit. The theory is most applicable to satellites moving in the region below synchronous altitude.

A more general theory has been developed by Cook [13]. It includes an analytical double averaging capability based on Kaula's model for the third body disturbing potential in Keplerian elements [14]. The theory makes extensive use of special functions and attendant recurrence relations to simplify computation. Furthermore, no a priori assumptions are made to facilitate the truncation of the averaged equations of motion. However, there is no accompanying short periodic development, thereby making the initialization of the double averaging theory from high precision orbital elements an extremely difficult and uncertain task.

1.2 Overview

The Generalized Method of Averaging is applied to the conservative VOP equations describing the motion of an Earth satellite under the influence of a third body.

In Chapter 2, the third body disturbing potential is developed in non-singular orbital elements using the satellite orbit plane as the frame of reference. The mean longitude is taken as the fast angular variable for both the satellite and the disturbing body so that resonance can be accomodated.

In Chapter 3, the Generalized Method of Averaging is used to create an averaging theory applicable to a system of differential equations containing two rapidly rotating angles. The theory is then specialized to first order. The formal method for obtaining the first order averaged equations of motion and the short periodic functions is presented.

Chapter 4 details the results of applying the averaging theory of Chapter 3 to a system of VOP equations based on the disturbing potential derived in Chapter 2. The mathematical form of the averaged equations of motion and the short periodic functions, including all partial derivatives, are given. The recurrence relations and starting values for all special functions and their partial derivatives are presented. Truncation procedures for the disturbing body model are discussed.

The equations expressed in Chapter 4 are programmed and interfaced with a version of the Goddard Trajectory Determination System (GTDS) modified at the Charles Stark Draper Laboratory in Cambridge, Massachusetts. As a test bed program, GTDS furnishes numerical integrators, interpolation algorithms for the short periodic variations and auxiliary perturbation models. Speed and accuracy comparisons between high precision integration and the averaging theory developed in this thesis are presented in Chapter 5 for selected orbits.

Chapter 6 formulates conclusions and suggests some areas for future investigation.

Chapter 2

The Third Body Disturbing Potential

This chapter formulates the third body disturbing potential in terms of satellite orbital coordinates. Mathematical operations on the potential produce a system of high precision Variation of Parameters equations. These equations form the cornerstone of the third body averaging theory developed in this thesis.

The potential is expressed in non-singular equinoctial orbital elements as part of an approach to circumvent numerical instability for near-circular and near-equatorial orbits that is characteristic of satellite VOP equations formulated in terms of the classical Keplerian elements. The equinoctial elements are classically defined as [15]

$$a = a$$

$$h = e \sin(\omega + I\Omega)$$

$$k = e \cos(\omega + I\Omega)$$

$$p = \tan^{I}(i/2) \sin\Omega$$

$$q = \tan^{I}(i/2) \cos\Omega$$

$$\lambda = M + \omega + I\Omega$$

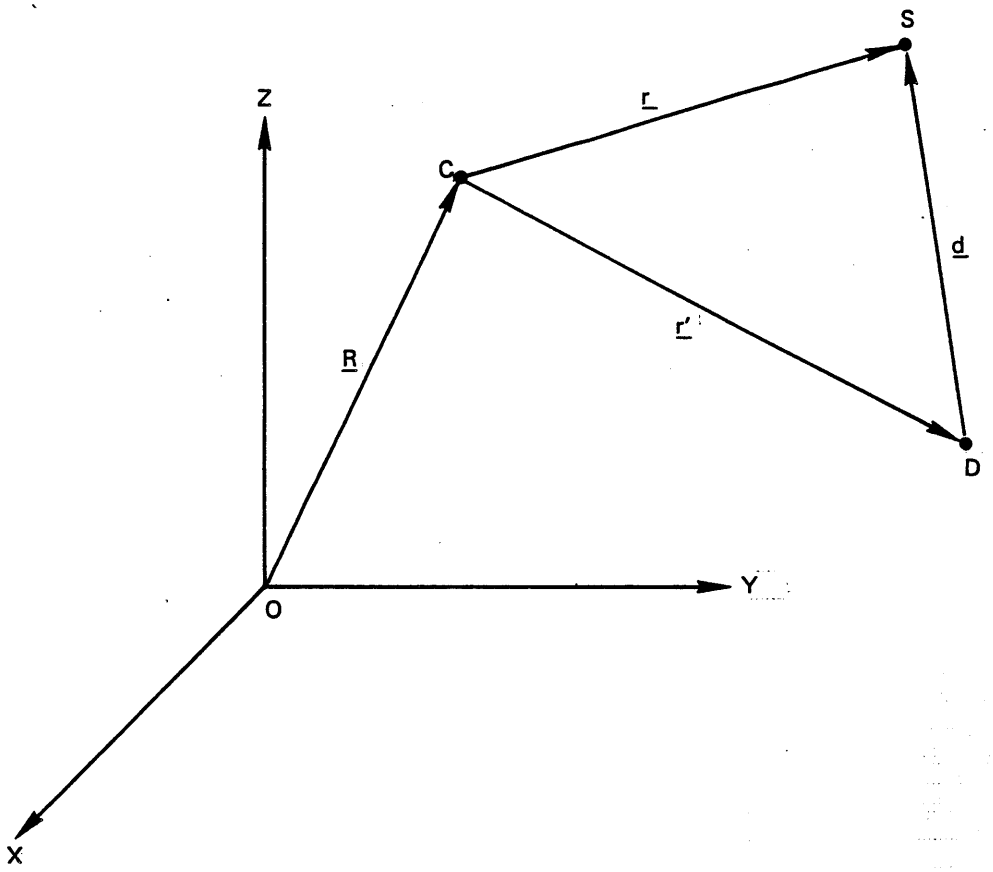
where a, e, i, ω, Ω, M are the Keplerian elements and I is the retrograde factor. The retrograde factor is present to eliminate a singularity in the element set for orbits with an inclination of 180 degrees. It is discussed in detail in Section 2.2.

Section 2.1 derives the third body disturbing potential in inertial rectangular coordinates. Section 2.2 details the transformation of the potential to equinoctial orbital elements.

2.1 Derivation of the Third Body Disturbing Potential in Inertial Coordinates

The development of the third body potential begins with an expression for the disturbing acceleration. In a strictly Newtonian formulation, this implies the postulate of an inertial frame XYZ with respect to which all motion may be referred. Figure 2-1 depicts the three body geometry. The vector $\underline{R}$ denotes the position of the central body (C) relative to the origin of coordinates. The vectors $\underline{r}$ and $\underline{r}'$ represent respectively the positions of the satellite (S) and the disturbing body (D) measured from the center of the central body. The vector $\underline{d}$, which is simply the difference $\underline{r} - \underline{r}'$, establishes the relative separation of

Figure 2-1. Geometry of the Third Body Problem



the satellite and the third body. Another useful parameter, soon to be employed, is the angle ψ between $\underline{r}$ and $\underline{r}'$. It is commonly referred to as the geocentric elongation in Earth centered orbital analyses.

Based on the stated geometry, a set of dynamical equations describing the motion of the three body system may be written as

$$m(\ddot{\underline{R}} + \ddot{\underline{r}}) = -\frac{G\,Mm}{r^3}\underline{r} - \frac{G\,m'\,m}{d^3}\underline{d} \qquad (2\text{-}1)$$

and

$$M\,\ddot{\underline{R}} = \frac{G\,Mm}{r^3}\underline{r} + \frac{G\,Mm'}{r'^3}\underline{r}' \qquad (2\text{-}2)$$

where the double dot notation indicates the second derivative with respect to time and

$m \equiv$ mass of satellite (kg)

$m' \equiv$ mass of the third body (kg)

$M \equiv$ mass of the central body (kg)

$G \equiv$ universal constant of gravitation ($km^3/kg\text{-}sec^2$)

From eq. (2-1) and (2-2) the inertial accelerations per unit mass of the satellite and central body are respectively given by

$$\ddot{\underline{R}} + \ddot{\underline{r}} = -\frac{GM}{r^3}\underline{r} - \frac{Gm'}{d^3}\underline{d} \qquad (2\text{-}3)$$

and

$$\ddot{\underline{R}} = \frac{Gm}{r^3}\underline{r} + \frac{Gm'}{r'^3}\underline{r}' \qquad (2\text{-}4)$$

Subtracting eq. (2-4) from eq. (2-3) yields

$$\ddot{\underline{r}} = -\frac{G(M+m)}{r^3}\underline{r} - Gm'\left(\frac{\underline{d}}{d^3} + \frac{\underline{r}'}{r'^3}\right) \qquad (2\text{-}5)$$

Eq. (2-5) may be simplified by defining the quantities

$$\mu = G(M+m) \qquad (2\text{-}6)$$

$$\mu' = Gm' \qquad (2\text{-}7)$$

Transposing the first term of the right hand side of eq. (2-5) and invoking eqs. (2-6) and (2-7) leads to

$$\ddot{\underline{r}} + \frac{\mu}{r^3}\underline{r} = -\mu'\left(\frac{\underline{d}}{d^3} + \frac{\underline{r}'}{r'^3}\right) \qquad (2\text{-}8)$$

Eq. (2-8) represents the motion of a satellite about a central body as forced by the third body disturbing acceleration

$$\underline{a}' = -\mu' \left(\frac{\underline{d}}{d^3} + \frac{\underline{r}'}{r'^3} \right) \tag{2-9}$$

Since gravitational forces are conservative, the specific force represented by eq. (2-9) can be expressed as the gradient, with respect to the satellite position, of a scalar potential function. This function of the satellite coordinates has the form

$$U' = \mu' \left(\frac{1}{d} - \frac{\underline{r}' \cdot \underline{r}}{r'^3} \right) \tag{2-10}$$

Subsequent analysis will require a more convenient version of eq. (2-10). Manipulation begins by recognizing that

$$d^2 = \underline{d} \cdot \underline{d} = (\underline{r} - \underline{r}') \cdot (\underline{r} - \underline{r}')$$

$$= r^2 - 2\underline{r} \cdot \underline{r}' + r'^2 \tag{2-11}$$

If the geocentric elongation, ψ, is introduced into eq. (2-11), then the inverse of the relative distance in eq. (2-10) is seen to be

$$\frac{1}{d} = (r^2 - 2rr' \cos \psi + r'^2)^{-1/2} \qquad (2\text{-}12)$$

To facilitate the expansion of the third body potential into satellite orbital coordinates, eq. (2-12) is more naturally developed in terms of the orthogonal Legendre polynomials defined by [16]

$$(h^2 - 2h\lambda + 1)^{-1/2} = \sum_{n=0}^{\infty} h^n P_n(\lambda) \qquad (2\text{-}13)$$

where

$P_n(\lambda)$ ≡ Legendre polynomial of degree n and argument λ

h ≡ parameter less than or equal to 1

Eq. (2-12) may be placed in correspondence with eq. (2-13) by factoring out r'^2 so that

$$\frac{1}{d} = \frac{1}{r'} \left\{ \left(\frac{r}{r'} \right)^2 - 2 \left(\frac{r}{r'} \right) \cos \psi + 1 \right\}^{-1/2} \qquad (2\text{-}14)$$

Comparing eq. (2-14) with eq. (2-13) yields the identifications

$$h = \left(\frac{r}{r'} \right) \tag{2-15}$$

and

$$\lambda = \cos \psi \tag{2-16}$$

This allows eq. (2-14) to take the final form

$$\frac{1}{d} = \frac{1}{r'} \sum_{n=0}^{\infty} \left(\frac{r}{r'}\right)^n P_n (\cos \psi) \tag{2-17}$$

Note that this representation assumes that the satellite describes an interior orbit with respect to the orbit of the perturbing body. This ensures that $(r/r') \leq 1$ as required. However, for an exterior orbit, the condition is obviously violated. In such a case r^2 must be factored from eq. (2-12). Only interior satellite orbits will be considered here.

Substituting eq. (2-17) into eq. (2-10) and rewriting $(\underline{r}' \cdot \underline{r})/r'^3$ as $(r/r'^2)\cos\psi$ yields

$$U' = \frac{\mu'}{r'}\left[\sum_{n=0}^{\infty}\left(\frac{r}{r'}\right)^n P_n(\cos\psi) - \left(\frac{r}{r'}\right)\cos\psi\right] \quad (2\text{-}18)$$

Further recognizing that $P_0(\cos\psi)=1$ and $P_1(\cos\psi)=\cos\psi$, eq. (2-18) becomes, after cancelling terms,

$$U' = \frac{\mu'}{r'}\left[1 + \sum_{n=2}^{\infty}\left(\frac{r}{r'}\right)^n P_n(\cos\psi)\right] \quad (2\text{-}19)$$

The satellite equations of motion in cartesian coordinates depend solely on the gradient of the disturbing potential with respect to the elements of the satellite position vector. Accordingly, the leading term in eq. (2-19) will not contribute to the satellite motion by virtue of having no satellite dependencies. In view of this fact the third body disturbing potential may be rewritten in the commonly used form

$$U' = \frac{\mu'}{r'}\sum_{n=2}^{\infty}\left(\frac{r}{r'}\right)^n P_n(\cos\psi) \quad (2\text{-}20)$$

2.2 Transformation of the Third Body Potential from Inertial Coordinates to Satellite Coordinates

The Lagrangian VOP formulation of the orbit prediction problem requires partial derivatives of the disturbing potential with respect to the orbital elements of the satellite. It is therefore highly desirable to express the third body potential, represented by eq. (2-20), directly in terms of satellite elements. One approach, typified by Kaula [14], entails a straightforward but tedious application of standard identities in spherical trigonometry and algebraic manipulations. Although such a method is in principle correct, it tends to ignore the presence of mathematical special functions in the satellite theory and the reduction in analytical complexity that derives from their use.

An alternate technique involves employing a powerful transformation theorem for spherical harmonics under a rotation of coordinates to provide an expression for the potential which is substantially more compact. This technique has been used with success by McClain [17] and Cefola [18] and will be adopted in the ensuing analysis.

2.2.1 Reference Frame Choice and Implications

Before transforming the third body potential to satellite orbital elements, a reference frame must be chosen for computing the cosine of the geocentric elongation in eq. (2-20). The potential is a scalar quantity and therefore must be numerically invariant under a change of coordinates that leaves the datum unaffected. Hence, the selection of a reference frame can be made principally as a matter of convenience or practicality to provide a more elegant analytical form of the potential or to reduce the computational load in a numerical orbit prediction program.

In broad terms, the choice of a reference frame may be made between absolute and relative. Absolute frames are inertial reference systems commonly oriented in the equatorial plane of the Earth or in the ecliptic plane. Within the context of developing the third body disturbing function such frames have the advantage of maintaining the independence of the third body orbital elements from the satellite orbital elements. Hence, at each integration step the disturbing body elements are simply constant parameters taken from an external ephemeris. This decoupling is consistent with the notion that the integrated satellite elements are affected by the movement of the third body rather than the reverse.

On the debit side of the ledger, the use of an absolute frame may be undesirable from the viewpoint of a numerical program. In the expansion of the Earth's gravity potential in equinoctial variables, as referred to the equatorial inertial frame [18], an inclination function is introduced relating the satellite orbital plane to the equatorial system. However, in the case of third body perturbation, a second inclination function is introduced. This results in the appearance of an additional summation in the potential and extra computational complexity. The end product could be a reduction in the overall efficiency of a numerical prediction program.

Selecting a relative reference frame in the satellite or disturbing body orbital plane serves to eliminate one or the other of the inclination functions and the associated summation. The result is an analytically simpler form of the disturbing potential. An obvious drawback would appear to be induced dependencies. For example, if the third body potential is developed using the satellite reference system, then the orbital elements of the disturbing body will be referred to a frame that is in motion with respect to absolute space. However, the satellite dynamical equations were derived in an inertial frame of reference. Hence the third body elements must be chained to the inertial frame through the motion of the satellite frame. Similarly, if the third body reference frame is chosen, then the elements of the satellite orbit will be non-inertially defined and consequently will be related to the integrated elements through the motion of the disturbing body system [ ].

This characteristic of relative frames does not preclude their use since an analytical framework exists for relating non-inertially referred elements to the inertial dynamical reference frame. Accordingly, for the purpose of demonstrating the power of averaging in the third body problem, a relative frame is chosen. In particular, the satellite frame is selected to develop the potential since it leaves the satellite elements expressed directly in the system of integration.

2.2.2 Transformation of the Third Body Potential to Satellite Orbital Coordinates

The transformation of eq. (2-20) to the equinoctial elements of the satellite begins by expressing the cosine of the geocentric elongation as the dot product,

$$\cos \psi = 1_r \cdot 1_{r'} \tag{2-21}$$

where the symbol 1 denotes a unit vector. In coordinates measured with respect to the satellite reference frame, the unit vector 1_r has the form,

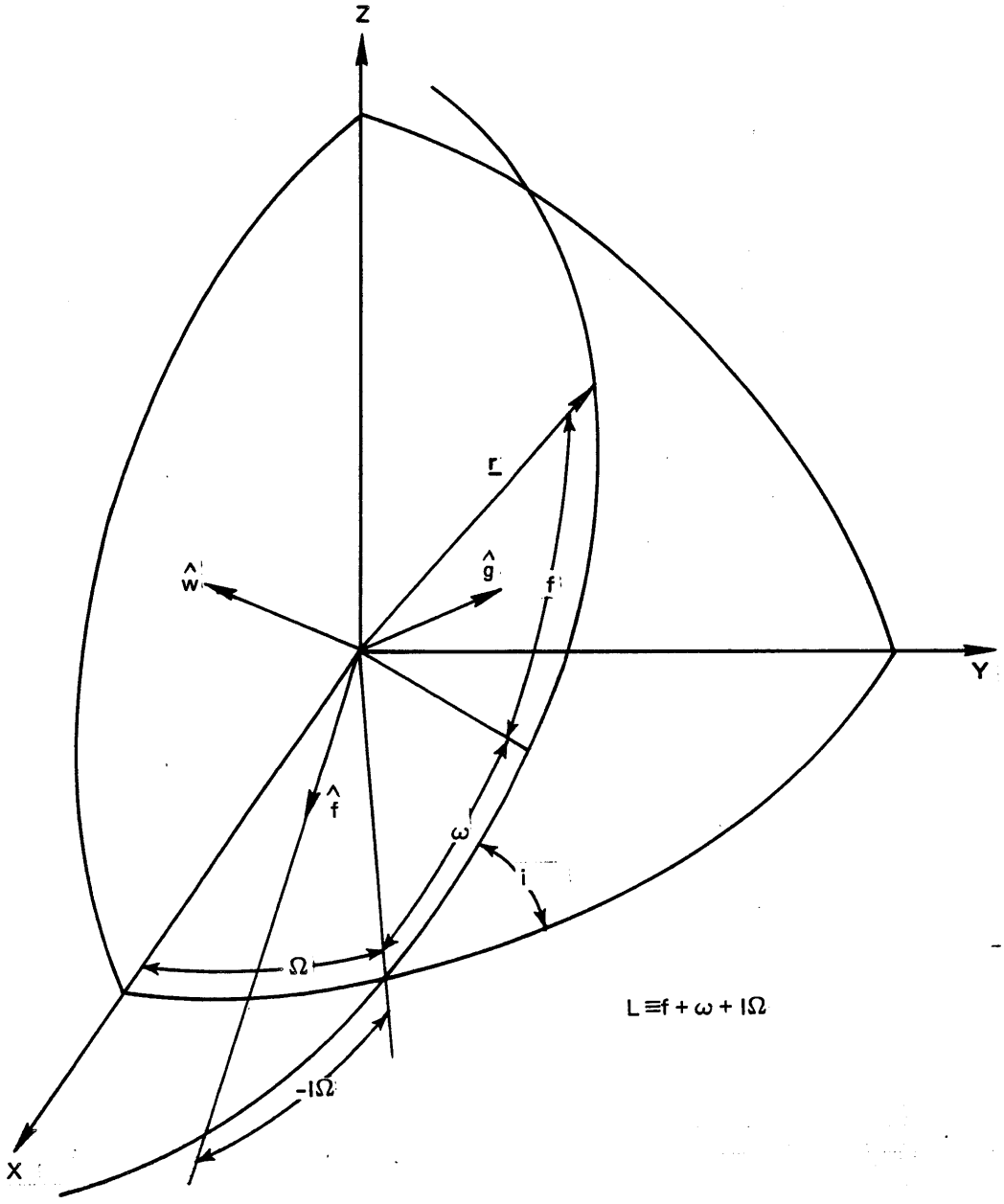
$$1_r = \cos(L)\ \hat{f} + \sin(L)\ \hat{g} + 0\ \hat{w} \tag{2-22}$$

where L is the true longitude of the satellite and the vectors $\hat{f}$, $\hat{g}$, $\hat{w}$ are the inertially referred satellite frame unit vectors depicted graphically in Figure 2-2 and defined by

$$\hat{f}^T = \frac{1}{1+p^2+q^2}\,[1 + q^2 - p^2,\ 2pq,\ -2pI] \tag{2-23}$$

$$\hat{g}^T = \frac{1}{1+p^2+q^2}\,[2pqI,\ (1 + p^2 - q^2)I,\ 2q] \tag{2-24}$$

Figure 2-2. Orientation of the Satellite Reference Frame with Respect to the Inertial Reference Frame



$$\hat{w}^T = \frac{1}{1+p^2+q^2} [2p, -2q, (1 - p^2 - q^2)I] \qquad (2\text{-}25)$$

The variables p and q are the equinoctial elements that specify the orientation of the satellite frame relative to the inertial frame. The retrograde factor, I, is present to circumvent a singularity in the satellite equations of motion for orbits with inclinations of 180 degrees. The factor is +1 when the orbital inclination is 0° and -1 when the inclination is 180°. In between either value may be used.

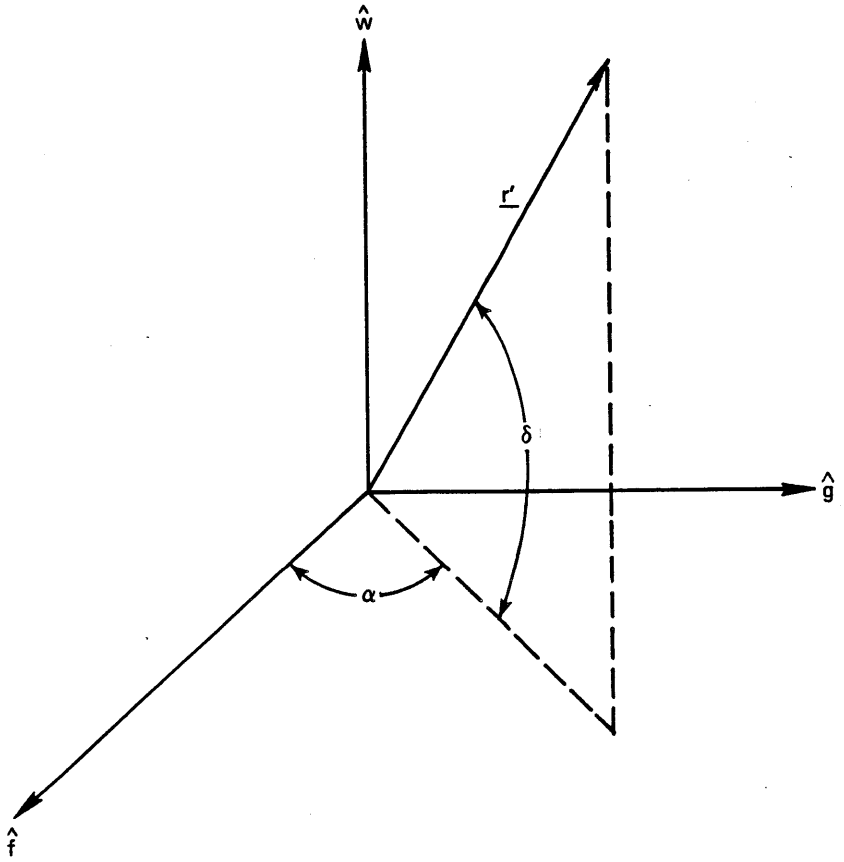
The third body unit vector is given by

$$1_{r'} = \cos\delta \cos\alpha \hat{f} + \cos\delta \sin\alpha \hat{g} + \sin\delta \hat{w} \qquad (2\text{-}26)$$

where α and δ are the right ascension and declination of the third body relative to the satellite frame. The geometry is shown in Figure 2-3. Substituting eqs. (2-22) and (2-26) into eq. (2-21) yields

$$\cos\psi = \cos\delta \cos\alpha \cos(L) + \cos\delta \sin\alpha \sin(L) + \sin(0) \sin\delta \qquad (2\text{-}27)$$

Figure 2-3. Orientation of the Third Body Position Vector with Respect to the Satellite Frame



Apply the standard trigonometric identity cos(x-y) = cos(x) cos(y)+ sin(x) sin(y), eq. (2-27) becomes

$$\cos\psi = \sin(0)\sin\delta + \cos\delta\cos(\alpha - L) \qquad (2\text{-}28)$$

At this point the Addition Theorem for spherical harmonics should be invoked. It decomposes $P_n[\sin(0)\sin\delta + \cos\delta\cos(\alpha - L)]$ into simple functions of the satellite and third body coordinates. The Addition Theorem has the form [19]

$$P_n[\sin(y)\sin(y') + \cos(y)\cos(y')\cos(x - x')] =$$

$$= P_n[\sin(y)]\, P_n[\sin(y')]$$

$$+ 2\sum_{m=1}^{n} \frac{(n-m)!}{(n+m)!} P_{nm}[\sin(y)]\, P_{nm}[\sin(y')]\cos m(x - x') \qquad (2\text{-}29)$$

The function $P_{nm}(z)$ is the associated Legendre function defined by [16]

$$P_{nm}(z) = (1 - z^2)^{m/2} \frac{d^m}{dz^m} P_n(z) \qquad (2\text{-}30)$$

If one makes the identifications

$$\begin{aligned} \sin(y) &= 0 \\ \sin(y') &= \sin\delta \\ \cos(y) &= 1 \\ \cos(y') &= \cos\delta \\ x &= \alpha \\ x' &= L \end{aligned}$$

then eq. (2-29) becomes

$$P_n(\cos\psi) = P_n(0)\, P_n(\sin\delta) + 2 \sum_{m=1}^{n} \frac{(n-m)!}{(n+m)!} P_{nm}(0)\, P_{nm}(\sin\delta) \cos[m(\alpha - L)] \qquad (2\text{-}31)$$

From eq. (2-30) it is clear that

$$P_{n0}(z) = P_n(z) \tag{2-32}$$

Hence eq. (2-31) may be rewritten as

$$P_n(\cos\psi) = P_{n0}(0)\, P_{n0}(\sin\delta)$$

$$+ 2 \sum_{m=1}^{n} \frac{(n-m)!}{(n+m)!} P_{nm}(0)\, P_{nm}(\sin\delta) \cos[m(\alpha-L)] \tag{2-33}$$

Defining

$$K_m = \begin{cases} 1 & m = 0 \\ 2 & m > 0 \end{cases}$$

allows the summation in eq. (2-33) to begin at zero, producing

$$P_n(\cos\psi) = \sum_{m=0}^{n} K_m \frac{(n-m)!}{(n+m)!} P_{nm}(0)\, P_{nm}(\sin\delta) \cos[m(\alpha-L)]$$

(2-34)

If the function $V_{n,m}$ is defined to be,

$$V_{n,m} = \frac{(n-m)!}{(n+m)!} P_{nm}(0) \qquad (2\text{-}35)$$

then eq. (2-33) may be restated as,

$$P_n(\cos\psi) = \sum_{m=0}^{n} K_m V_{n,m} P_{nm}(\sin\delta) \cos[m(\alpha-L)] \qquad (2\text{-}36)$$

Substituting eq. (2-36) into eq. (2-20) produces the intermediate form of the third body potential,

$$U' = \frac{\mu'}{r'} \sum_{n=2}^{\infty} \left(\frac{r}{r'}\right)^n \sum_{m=0}^{n} K_m V_{n,m} P_{nm}(\sin\delta) \cos[m(\alpha-L)] \qquad (2\text{-}37)$$

In order to use the rotational transformation theorem for spherical harmonics, the potential in eq. (2-37) is rewritten in complex notation. Doing so yields

$$U' = \mathrm{Re}\left\{\frac{\mu'}{r'}\sum_{n=2}^{\infty}\left(\frac{r}{r'}\right)^{n}\sum_{m=0}^{n}K_m V_{n,m} P_{nm}(\sin\delta)\, e^{j[m(\alpha-L)]}\right\} \tag{2-38}$$

where Re { } denotes the real part of the bracketed expression and $j = \sqrt{-1}$. Breaking apart the complex exponential produces

$$U' = \mathrm{Re}\left\{\frac{\mu'}{r'}\sum_{n=2}^{\infty}\left(\frac{r}{r'}\right)^{n}\sum_{m=0}^{n}\left[K_m V_{n,m} e^{-jmL}\right] P_{nm}(\sin\delta)\, e^{jm\alpha}\right\} \tag{2-39}$$

The surface spherical harmonics, $P_{nm}(\sin\delta)e^{jm\alpha}$, will now be rotated from the satellite reference frame into the third body frame. A theorem exists which describes the transformation of any linearly independent set of spherical harmonics under a simple rotation of coordinates when the origin is held fixed. With appropriate changes of notation, the theorem is formally stated by[20],

$$P_{nm}(\cos\theta)e^{jm\xi} = \sum_{r=-n}^{n} \frac{(n-r)!}{(n-m)!} S_{2n}^{(m,r)}(\rho,\sigma,\tau) \cdot$$

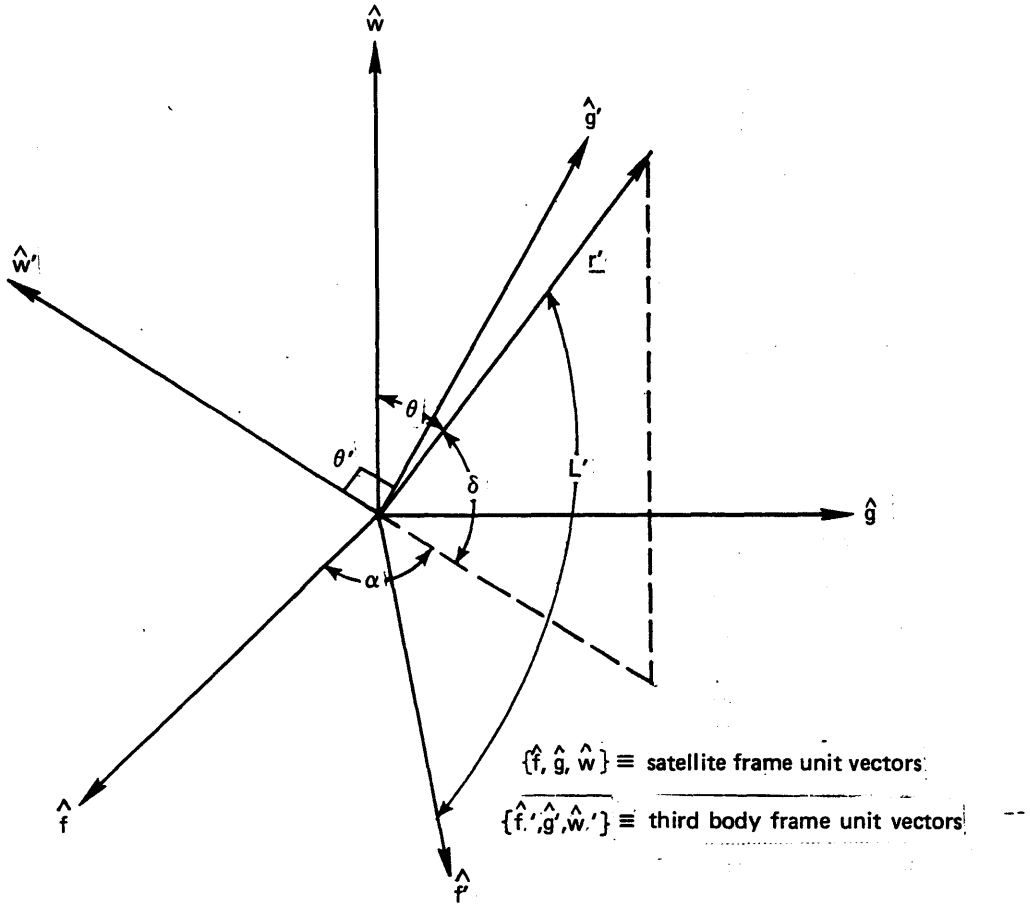
$$\cdot P_{nr}(\cos\theta') e^{jr\xi'}$$

(2-40)

The unprimed quantities θ and ξ are the angular coordinates of a point as measured from the axes of the satellite frame. The primed angles θ' and ξ' are the spherical coordinates of the same point as measured from the satellite referred axes of the third body frame. The parameters ρ,σ,τ are related to the Euler angles defining a rotation of coordinates from the third body reference frame to the satellite frame. These parameters will be discussed shortly.

Eq. (2-40) is now used to express the surface spherical harmonics, $P_{nm}(\sin\delta)e^{jm\alpha}$, as a linear combination of spherical harmonics expressed in the third body reference frame. This is done by identifying the geometrical quantities shown in Figure 2-4. The parameter θ, generally called the colatitude in spherical coordinates, is measured from the positive $\hat{w}$ axis of the satellite coordinate frame to the

Figure 2-4. Geometry for the Rotation of Surface Spherical Harmonics



plane of the disturbing body orbit. It is related to the third body declination, δ, through the relation $\theta = \pi/2 - \delta$. The angle ξ in eq. (2-40) holds the place of the third body right ascension, α. In the coordinate system of the perturbing body, the angle θ' has the value $\pi/2$ since the third body orbital plane is normal to the $\hat{w}'$ axis. Finally, the parameter, ξ', corresponds to the true longitude of the third body, L'. The angle, L', is measured from the $\hat{f}'$ axis in the plane of the perturbing body orbit.

Making the indicated substitutions, eq. (2-40) becomes

$$P_{nm}(\sin\delta)\, e^{jm\alpha} = \sum_{r=-n}^{n} \frac{(n-r)!}{(n-m)!}\, S_{2n}^{(m,r)}(\rho,\sigma,\tau) \cdot$$

$$\cdot\, P_{nr}(0)\, e^{jrL'} \qquad (2\text{-}41)$$

Making the definition

$$V_{n,r}^{m} = \frac{(n-r)!}{(n-m)!}\, P_{nr}(0) \qquad (2\text{-}42)$$

eq. (2-41) may be rewritten as

$$P_{nm}(\sin\delta)\, e^{jm\alpha} = \sum_{r=-n}^{n} V_{n,r}^{m}\, S_{2n}^{(m,r)}(\rho,\sigma,\tau)\, e^{jrL'} \tag{2-43}$$

Substituting eq. (2-43) into eq. (2-39) produces,

$$U' = \mathrm{Re}\left\{\frac{\mu'}{r'} \sum_{n=2}^{\infty} \left(\frac{r}{r'}\right)^{n} \sum_{m=0}^{n} K_m V_{n,m} \sum_{r=-n}^{n} V_{n,r}^{m}\, S_{2n}^{(m,r)}(\rho,\sigma,\tau) \cdot \right.$$

$$\left. \cdot\, e^{jrL'}\, e^{-jmL}\right\} \tag{2-44}$$

The explicit dependence of $S_{2n}^{(m,r)}(\rho,\sigma,\tau)$ on known quantities will now be determined. As defined in Courant and Hilbert [20], $S_{2n}^{(m,r)}(\rho,\sigma,\tau)$ has the form

$$S_{2n}^{(m,r)}(\rho,\sigma,\tau) = U_{2n}^{(m,r)}(\tau)\exp\{-j[(r+m)\rho + (r-m)\sigma]\}$$

(2-45)

where

$$U_{2n}^{(m,r)} = (-1)^{n+m}\binom{n-m}{n+r}(\cos\tau)^{-m-r}(\sin\tau)^{m-r} \cdot$$

$$\cdot {}_2F_1(-n-r,\ n+1-r;\ 1-m-r;\ \cos^2\tau)$$

$$m + r \leq 0 \qquad (2-46)$$

and

$$U_{2n}^{(m,r)} = (-1)^{n+r} \binom{n+m}{n-r} (\cos\tau)^{m+r} (\sin\tau)^{r-m} \cdot$$

$$\cdot {}_2F_1(r-n,\ n+r+1;\ 1+m+r;\ \cos^2\tau)$$

$$r + m \geq 0 \qquad (2\text{-}47)$$

The expression ${}_2F_1(a,b;c;\cos^2\tau)$ is a hypergeometric function in the argument $(\cos^2\tau)$ and $\binom{d}{e}$ is the binomial coefficient.

In view of eq. (2-43), the quantities ρ, σ, and τ are related to a rotation <u>from</u> the third body orbital plane <u>to</u> the satellite orbital plane. They are actually orthogonal coordinates defining a four parameter representation of the rotation matrix from the third body frame to the satellite frame, viz.,

$$M = \frac{1}{\nu^2} \begin{pmatrix} q_4^2+q_1^2-q_2^2-q_3^2 & 2(q_1q_2+q_3q_4) & 2(q_1q_3-q_2q_4) \\ 2(q_1q_2-q_3q_4) & q_4^2+q_2^2-q_1^2-q_3^2 & 2(q_2q_3+q_1q_4) \\ 2(q_1q_3+q_2q_4) & 2(q_2q_3-q_1q_4) & q_4^2+q_3^2-q_1^2-q_2^2 \end{pmatrix} \tag{2-48}$$

where $\nu^2 = q_1^2 + q_2^2 + q_3^2 + q_4^2$ and

$$q_1 = -\nu \sin\tau \sin\sigma \tag{2-49}$$

$$q_2 = \nu \sin\tau \cos\sigma \tag{2-50}$$

$$q_3 = \nu \cos\tau \sin\rho \tag{2-51}$$

$$q_4 = \nu \cos\tau \cos\rho \tag{2-52}$$

The parameters q_1, q_2, q_3, q_4 are determined through a comparison of eq. (2-48) with the rotation matrix

$$M = \frac{1}{1+p'^2+q'^2} \begin{pmatrix} 1-p'^2+q'^2 & 2p'q'I' & 2p' \\ 2p'q' & (1+p'^2-q'^2)I' & -2q' \\ -2p'I' & 2q' & (1-p'^2-q'^2)I' \end{pmatrix}$$

(2-53)

The quantities p' and q' are the equinoctial elements that specify the orientation of the third body reference frame relative to the satellite frame. Hence, they are related to the mutual inclination of the third body and satellite orbit planes. The symbol I' is the retrograde factor, which is ordinarily set to +1 but assumes the value of -1 when the mutual inclination is 180°. This circumvents an apparent singularity in the equations of motion when the satellite moves in the plane of the third body orbit, but in the opposite direction. The singularity is not dynamical. Instead, it appears because the satellite frame was used to develop the disturbing potential.

Taking into account both the direct and retrograde cases of eq. (2-53), the parameters, q_i, of eq. (2-48) are found to be,

$$q_1 = \pm \frac{1}{2} \left[(1 - I') + (1 + I')q'\right] \qquad (2\text{-}54)$$

$$q_2 = \pm \frac{(1 + I')}{2} p' \qquad (2\text{-}55)$$

$$q_3 = \pm \frac{(1 - I')}{2} p' \qquad (2\text{-}56)$$

$$q_4 = \pm \frac{1}{2} \left[(1 + I') + (1 - I')q'\right] \qquad (2\text{-}57)$$

Also, it is evident that

$$\nu = (1 + p'^2 + q'^2)^{1/2} \qquad (2\text{-}58)$$

Now that the parameters, q_i, have been identified, it is possible to determine the dependence of ρ, σ, and τ on the elements p' and q'. Substituting eqs. (2-54) and (2-55) into eqs. (2-49) and (2-50) yields an expression for $\sin\tau$, after squaring and adding, viz.,

$$\sin\tau = (1 + p'^2 + q'^2)^{-1/2} (p'^2 + q'^2)^{(1+I')/4} \qquad (2\text{-}59)$$

Automatically, $\cos\tau$ must be

$$\cos\tau = (1 + p'^2 + q'^2)^{-1/2} (p'^2 + q'^2)^{(1-I')/4}$$

(2-60)

The plus or minus ($\pm$) designation in eqs. (2-54) through (2-57) does not imply that an arbitrary distribution of signs over the parameter set will satisfy the conditions of the rotation matrix given in eq. (2-53). Only two combinations of signs will produce the desired result, those being (-,-,-,+) and (+,+,+,-). The analysis that follows adopts the former convention although the other would be valid.

Substituting eqs. (2-54), (2-58) and (2-59) into eq. (2-49) and solving for $\sin\sigma$ yields

$$\sin\sigma = \frac{(1 - I')\sqrt{p'^2 + q'^2} + (1 + I')q'}{2\sqrt{p'^2 + q'^2}}$$

(2-61)

Substituting eqs. (2-55), (2-58) and (2-59) into eq. (2-50) produces

$$\cos\sigma = -\frac{(1 + I')p'}{2\sqrt{p'^2 + q'^2}} \tag{2-62}$$

Similar manipulations with eqs. (2-51) and (2-52) provide the desired forms of $\sin\rho$ and $\cos\rho$, viz.,

$$\sin\rho = -\frac{(1 - I')p'}{2\sqrt{p'^2 + q'^2}} \tag{2-63}$$

and

$$\cos\rho = \frac{(1 + I')\sqrt{p'^2 + q'^2} + (1 - I')q'}{2\sqrt{p'^2 + q'^2}} \tag{2-64}$$

Making use of eqs. (2-61) through (2-64), the complex exponential in eq. (2-45) is seen to be

$$\exp\{-j[(r + m)\rho + (r - m)\sigma]\} =$$

$$= (-1)^{m-r} (p'^2 + q'^2)^{(m-r)/2} (p'I' + jq')^r (p' + jq')^{-m} \tag{2-65}$$

The dependence of $U_{2n}^{(m,r)}(\tau)$ on the elements p' and q' will now be determined. The range $r \leq -m$ will be considered first. Substituting eqs. (2-59) and (2-60) into eq. (2-46),

$$U_{2n}^{(m,r)} = (-1)^{n+m} \binom{n-m}{n+r} \left[(1+p'^2+q'^2)^{-1/2}(p'^2+q'^2)^{(1-I')/4}\right]^{-m-r}$$

$$\cdot \left[(1 + p'^2 + q'^2)^{-1/2} (p'^2 + q'^2)^{(1+I')/4}\right]^{m-r} \cdot$$

$$\cdot {}_2F_1 \left[-n-r,\ n+1-r;\ 1-m-r;\ \frac{(p'^2 + q'^2)^{(1-I')/2}}{(1 + p'^2 + q'^2)}\right]$$

$$r \leq -m \qquad (2\text{-}66)$$

After some manipulation, eq. (2-66) becomes

$$U_{2n}^{(m,r)} = (-1)^{n+m} \binom{n-m}{n+r} (1+p'^2+q'^2)^{r}(p'^2+q'^2)^{(I'm-r)/2} \cdot$$

$$\cdot {}_2F_1\left[-n-r,\ n+1-r;\ 1-m-r;\ \frac{(p'^2+q'^2)^{(1-I')/2}}{(1 + p'^2 + q'^2)}\right]$$

$$r \leq -m \qquad (2\text{-}67)$$

The hypergeometric function may be replaced by the orthogonal Jacobi polynomials $P_n^{(a,b)}(x)$ by using the definition [16]

$$P_\ell^{(a,b)}(x) = \binom{\ell+a}{\ell} {}_2F_1(-\ell, \ell+a+b+1;\ a+1;\ \frac{1-x}{2}) \tag{2-68}$$

if $\ell = n+r$, $a = -m-r$, and $b = m-r$. Hence,

$$\frac{1}{\binom{n-m}{n+r}} P_{n+r}^{(-m-r,m-r)}(x) = {}_2F_1(-n-r,\ n+1-r;\ 1-m-r;\ \frac{1-x}{2}) \tag{2-69}$$

The argument of the Jacobi polynomial, x, may be determined by solving the algebraic equation

$$\frac{1-x}{2} = \frac{(p'^2 + q'^2)(1-I')/2}{(1 + p'^2 + q'^2)} \tag{2-70}$$

The solution is given by

$$x = -\frac{(1 - p'^2 - q'^2)I'}{(1 + p'^2 + q'^2)} \tag{2-71}$$

An interpretation of eq. (2-71) is made by examining the dot product representation of the rotation matrix in eq. (2-53), viz.,

$$M = \begin{pmatrix} (\hat{f} \cdot \hat{f}') & (\hat{f} \cdot \hat{g}') & (\hat{f} \cdot \hat{w}') \\ (\hat{g} \cdot \hat{f}') & (\hat{g} \cdot \hat{g}') & (\hat{g} \cdot \hat{w}') \\ (\hat{w} \cdot \hat{f}') & (\hat{w} \cdot \hat{g}') & (\hat{w} \cdot \hat{w}') \end{pmatrix} \tag{2-72}$$

The columns of eq. (2-72) are the components of the third body frame basis vectors as coordinatized in the satellite frame. Comparison of the (3,3) element of eq. (2-72) with the same element of eq. (2-53) shows

$$\hat{w} \cdot \hat{w}' = \frac{(1 - p'^2 - q'^2)I'}{1 + p'^2 + q'^2} \tag{2-73}$$

The dot product of the unit normals to the satellite and third body orbital planes, denoted in eq. (2-73), is equal to the cosine of the mutual inclination and is evidently the negative of the x in eq. (2-71). Representing the dot product by the symbol γ, eq. (2-69) can be rewritten as

$$\frac{1}{\binom{n-m}{n+r}} P_{n+r}^{(-m-r,m-r)}(-\gamma) = {}_2F_1\left(-n-r,n+1-r;1-m-r;\frac{1+\gamma}{2}\right) \tag{2-74}$$

Replacing the hypergeometric function in eq. (2-67) by eq. (2-74) produces

$$U_{2n}^{(m,r)} = (-1)^{n+m} (1+p'^2+q'^2)^r (p'^2+q'^2)^{(I'm-r)/2} \cdot P_{n+r}^{(-m-r,m-r)}(-\gamma)$$

$$r \leq -m \tag{2-75}$$

Using the identity for Jacobi polynomials [17]

$$P_n^{(a,b)}(-x) = (-1)^n P_n^{(b,a)}(x) \qquad (2\text{-}76)$$

transforms eq. (2-75) into

$$U_{2n}^{(m,r)} = (-1)^{m+r} (1+p'^2+q'^2)^r (p'^2+q'^2)^{(I'm-r)/2} \cdot$$

$$\cdot P_{n+r}^{(m-r,-m-r)}(\gamma)$$

$$r \leq -m \qquad (2\text{-}77)$$

Substituting eqs. (2-77) and (2-65) into eq. (2-45) provides an expression for $S_{2n}^{(m,r)}(p',q')$,

$$S_{2n}^{(m,r)}(p',q') = (1+p'^2+q'^2)^r (p'^2+q'^2)^{[(I'+1)m/2]-r} \cdot$$

$$\cdot (p'I' + jq')^r (p'+jq')^{-m} P_{n+r}^{(m-r,-m-r)}(\gamma)$$

$$r \leq -m \qquad (2\text{-}78)$$

Examination of the direct and retrograde cases of eq. (2-78) leads to the more compact expression,

$$S_{2n}^{(m,r)}(p',q') = (I')^r (1 + p'^2 + q'^2)^r \cdot$$

$$\cdot (p' - jq' I')^{I'm-r} P_{n+r}^{(m-r,-m-r)}(\gamma)$$

$$r \leq -m \qquad (2\text{-}79)$$

A similar procedure is used to determine the function $S_{2n}^{(m,r)}(p',q')$ when $r \geq -m$. However, there is an important proviso. Whereas the hypergeometric function in eq. (2-47) is valid over the entire range $r \geq -m$, care must be taken to ensure that the Jacobi polynomial representation is also valid. In fact, it is necessary to break the range $r \geq -m$ into the subranges $-m \leq r \leq m$ and $r \geq m$ to satisfy the requirement. A different Jacobi polynomial is required corresponding to each subrange. This will now be demonstrated. Substituting eqs. (2-59) and (2-60) into eq. (2-47) leads to, after some simplification,

$$U_{2n}^{(m,r)} = (1 + p'^2 + q'^2)^{-r} (p'^2 + q'^2)^{(r-I'm)/2} \cdot$$

$$\cdot P_{n-r}^{(r-m,r+m)} (\gamma)$$

(2-80)

The validity of the Jacobi polynomial in eq. (2-80) is determined by the restriction that the two superscripts satisfy the constraints [16]

$$r - m > -1 \qquad (2\text{-}81)$$

$$r + m > -1 \qquad (2\text{-}82)$$

Since r and m can only be integers, the constraint relations may be rewritten as

$$r - m \geq 0 \qquad (2\text{-}83)$$

$$r + m \geq 0 \qquad (2\text{-}84)$$

Only $r \geq m$ will satisfy the inequality relations in eqs. (2-83) and (2-84). As a result, eq. (2-80) is only valid over the range $r \geq m$. Substituting eqs. (2-80) and (2-65) into eq. (2-47) yields

$$S_{2n}^{(m,r)}(p',q') = (-1)^{m-r} (1+p'^2+q'^2)^{-r} (p'^2+q'^2)^{(1-I')m/2} \cdot$$

$$\cdot (p'I'+jq')^r (p'+jq')^{-m} P_{n-r}^{(r-m,r+m)}(\gamma)$$

$$r \geq m \qquad (2\text{-}85)$$

Examination of the direct and retrograde cases of eq. (2-85) allows the more compact expression

$$S_{2n}^{(m,r)}(p',q') = (I')^r (-1)^{m-r} (1 + p'^2 + q'^2)^{-r} \cdot$$

$$\cdot (p' + jq'I')^{r-I'm} P_{n-r}^{(r-m,r+m)}(\gamma)$$

$$r \geq m \qquad (2\text{-}86)$$

Finding a form of eq. (2-47) over the remaining subrange, $-m \leq r \leq m$, is accomplished by using a linear transformation of the hypergeometric function, [16], viz.,

$$ {}_2F_1(a,b;c;z) = (1 - z)^{c-a-b} \, {}_2F_1(c-a,c-b;c;z) \tag{2-87} $$

After matching the parameters in eq. (2-47) with those of eq. (2-87), one obtains

$$ {}_2F_1(r-n,n+r+1;1+m+r;\cos^2\tau) = $$

$$ = (\sin^2\tau)^{m-r} \, {}_2F_1(1+m+n,m-n;1+m+r;\cos^2\tau) \tag{2-88} $$

Recalling that the first two arguments of a hypergeometric function may be interchanged and applying eq. (2-68), leads to

$$P_{n-r}^{(r+m,r-m)}(-\gamma) = \frac{\binom{n+m}{n+r}}{\binom{n+r}{n-m}} (\sin^2\tau)^{m-r} P_{n-m}^{(r+m,m-r)}(-\gamma)$$

(2-89)

Finally, substituting eq. (2-59) for $\sin\tau$ and using the Jacobi polynomial identity of eq. (2-76), eq. (2-89) becomes

$$P_{n-r}^{(r-m,r+m)}(\gamma) = (-1)^{r-m} \frac{(n+m)!(n-m)!}{(n+r)!(n-r)!} (1+p'^2+q'^2)^{r-m} \cdot$$

$$\cdot (p'^2+q'^2)^{(1+I')(m-r)/2} P_{n-m}^{(m-r,r+m)}(\gamma)$$

(2-90)

Replacing $P_{n-r}^{(r-m,r+m)}(\gamma)$ in eq. (2-86) by the right hand side of eq. (2-90) yields the result, after some simplification,

$$S_{2n}^{(m,r)}(p',q') = (I')^r \frac{(n+m)!(n-m)!}{(n+r)!(n-r)!} (1+p'^2+q'^2)^{-m} \cdot$$

$$\cdot (p'-jq')^{m-I'r} P_{n-m}^{(m-r,r+m)}(\gamma)$$

$$-m \leq r \leq m \qquad (2\text{-}91)$$

A collection of the final expressions for the function $S_{2n}^{(m,r)}(p',q')$ is given in Table 2-1.

The right hand sides of the Lagrangian VOP equations contain partial derivatives of the disturbing potential with respect to the inertially referred p and q elements of the satellite orbit. The Earth's gravity potential in equinoctial variables is already formulated directly in terms of the p and q elements. By contrast, an inclination function that depends on the relative quantities p' and q' was introduced when the third body disturbing potential was derived with respect to the satellite frame. The element pair (p',q') must be related to the element pair (p,q) through a set of intermediate quantities, so that the dynamical par-

Table 2-1. Form of the function $S_{2n}^{(m, r)}(p', q')$.

$$S_{2n}^{(m, r)}(p', q') = (I')^r (1 + p'^2 + q'^2)^r (p' - j q' I')^{I'm - r} P_{n+r}^{(m-r, -m-r)}(\gamma)$$

$$r \leqslant -m$$

$$S_{2n}^{(m, r)}(p', q') = (I')^r \frac{(n+m)!\,(n-m)!}{(n+r)!\,(n-r)!} (1 + p'^2 + q'^2)^{-m} (p' - j q')^{m - I'r} P_{n-m}^{(m-r, r+m)}(\gamma)$$

$$-m \leqslant r \leqslant m$$

$$S_{2n}^{(m, r)}(p', q') = (I')^r (-1)^{m-r} (1 + p'^2 + q'^2)^{-r} (p' + j q' I')^{r - I'm} P_{n-r}^{(r-m, r+m)}(\gamma)$$

$$r \geqslant m$$

tial derivatives can be taken. The problem is solved by recognizing that a dot product is numerically invariant under a change of coordinates although the analytical form may appear different. The direction cosines of the third body orbital plane unit normal with respect to the satellite reference frame are formally represented by the dot products

$$\alpha = \hat{f} \cdot \hat{w}' \tag{2-92}$$

$$\beta = \hat{g} \cdot \hat{w}' \tag{2-93}$$

$$\gamma = \hat{w} \cdot \hat{w}' \tag{2-94}$$

The right hand sides of eq. (2-92) through (2-94) form the third column of the dot product rotation matrix that relates the third body frame to the satellite frame. This can be verified by looking at eq. (2-72). Matching that column to its counterpart in eq. (2-53) leads to

$$\alpha = \frac{2p'}{1+p'^2+q'^2} \tag{2-95}$$

$$\beta = \frac{-2q'}{1+p'^2+q'^2} \tag{2-96}$$

$$\gamma = \frac{(1-p'^2-q'^2)I'}{1+p'^2+q'^2} \tag{2-97}$$

Eqs. (2-95) through (2-97) are the result of using satellite frame coordinates to compute the direction cosines. By contrast, if inertial coordinates are used to compute the direction cosine dot products, then the elements p and q are introduced naturally through the unit vectors of the satellite frame. Hence, α, β and γ form the bridge between (p',q') space and (p,q) space. Thus, transforming the third body potential inclination function to direction cosines would allow the dynamical partial derivatives to be taken through the chain rules,

$$\frac{\partial S_{2n}^{(m,r)}}{\partial p} = \frac{\partial S_{2n}^{(m,r)}}{\partial \alpha}\ \frac{\partial \alpha}{\partial p} + \frac{\partial S_{2n}^{(m,r)}}{\partial \beta}\ \frac{\partial \beta}{\partial p} + \frac{\partial S_{2n}^{(m,r)}}{\partial \gamma}\ \frac{\partial \gamma}{\partial p} \tag{2-98}$$

and

$$\frac{\partial S_{2n}^{(m,r)}}{\partial q} = \frac{\partial S_{2n}^{(m,r)}}{\partial \alpha} \frac{\partial \alpha}{\partial q} + \frac{\partial S_{2n}^{(m,r)}}{\partial \beta} \frac{\partial \beta}{\partial q} +$$

$$+ \frac{\partial S_{2n}^{(m,r)}}{\partial \gamma} \frac{\partial \gamma}{\partial q} \qquad (2\text{-}99)$$

The transformation from p' and q' to α, β, and γ is made by manipulating eqs. (2-95) to (2-97). Eq. (2-97) leads to the relation

$$(1 + p'^2 + q'^2) = \frac{2}{1+I'\gamma} \qquad (2\text{-}100)$$

Using eq. (2-100) in conjunction with eqs. (2-95) and (2-96) produces the set of identities

$$(p' - jq'I') = \frac{(\alpha + j\beta I')}{1 + I'\gamma} \qquad (2\text{-}101)$$

$$(p' - jq') = \frac{(\alpha + j\beta)}{1 + I'\gamma} \tag{2-102}$$

$$(p' + jq'I') = \frac{(\alpha - j\beta I')}{1 + I'\gamma} \tag{2-103}$$

Substitution of eqs. (2-100) through (2-103) into Table 2-1 yields Table 2-2 after simplification and regard for both the direct and retrograde cases. The formulae in Table 2-2 are used in the numerical implementation. To aid in the analysis which follows, the matrix relating the third body frame to the satellite frame should be converted to direction cosines. Using the newly developed identities, the result is

$$M = \frac{1}{1+I'\gamma} \begin{pmatrix} 1+I'\gamma-\alpha^2 & \alpha\beta I' & \alpha(1+I'\gamma) \\ -\alpha\beta & I'+\gamma-\beta^2 I' & \beta(1+I'\gamma) \\ -\alpha(\gamma+I') & -\beta(1+I'\gamma) & \gamma(1+I'\gamma) \end{pmatrix} \tag{2-104}$$

Table 2-2. Form of the function $S_{2n}^{(m, r)}(\alpha, \beta, \gamma)$

$$S_{2n}^{(m, r)}(\alpha, \beta, \gamma) = (l')^r 2^r (1 + l'\gamma)^{-l'm} (\alpha + j\beta l')^{l'm - r} P_{n+r}^{(m-r, -m-r)}(\gamma)$$

$$r \leqslant -m$$

$$S_{2n}^{(m, r)}(\alpha, \beta, \gamma) = (l')^r 2^{-m} \frac{(n+m)!\,(n-m)!}{(n+r)!\,(n-r)!} (1 + l'\gamma)^{l'r} (\alpha + j\beta)^{m - l'r} P_{n-m}^{(m-r, r+m)}(\gamma)$$

$$-m \leqslant r \leqslant m$$

$$S_{2n}^{(m, r)}(\alpha, \beta, \gamma) = (l')^r (-1)^{m-r} 2^{-r} (1 + l'\gamma)^{l'm} (\alpha - j\beta l')^{r - l'm} P_{n-r}^{(r-m, r+m)}(\gamma)$$

$$r \geqslant m$$

At present the potential is expressed in terms of the true longitude. This formulation is particularly useful for high eccentricity satellite orbits, since it retains the orbital eccentricity in closed form. However, there are times when changing to the mean longitude, λ, can be an essential choice. This is true in the case of third body resonance where the satellite and disturbing body are commensurable in their mean motions. Since the unperturbed time derivative of the mean longitude is equal to the mean motion, it is a more natural choice for the study of resonance than the true longitude whose dependence on the mean motion is nonlinear. Using the mean longitude also has the collateral effect of simplifying the structure of the short periodic recovery functions that are discussed in Chapter 3.

The transformation from the true longitude to the mean longitude is made through the Hansen expansion which has the form [18]

$$\left(\frac{r}{a}\right)^n e^{jmL} = \sum_{t=-\infty}^{\infty} Y_t^{n,m} e^{jt\lambda} \qquad (2\text{-}105)$$

where the index t is an integer and the modified Hansen coefficients, $Y_t^{n,m}$, are polynomials in the eccentricity defined by

$$Y_t^{n,m} = (k + jh)^{m-t} \sum_{\sigma=0}^{\infty} X_{\sigma+m-t,\sigma}^{n,-m} (h^2 + k^2)^{\sigma}$$

$$t \leq m \qquad (2\text{-}106)$$

$$Y_t^{n,m} = (k - jh)^{t-m} \sum_{\sigma=0}^{\infty} X_{\sigma+t-m,\sigma}^{n,m} (h^2 + k^2)^{\sigma}$$

$$t \geq m \qquad (2\text{-}107)$$

The Newcomb operators, $X_{\rho,\sigma}^{n,m}$, in eqs. (2-106) and (2-107) are numerical constants which are governed by simple recurrence relations. For a further discussion of these operators see Appendix A.

Multiplying numerator and denominator of eq. (2-44) by $(r/a)^n$ produces

$$U' = \mathrm{Re}\left\{ \frac{\mu'}{r'} \sum_{n=2}^{\infty} \left(\frac{a}{r'}\right)^n \sum_{m=0}^{n} K_m V_{n,m} \sum_{r=-n}^{n} V_{n,r}^{m} \cdot \right.$$

$$\left. \cdot S_{2n}^{(m,r)} (\alpha,\beta,\gamma) e^{jrL'} \left(\frac{r}{a}\right)^n e^{-jmL} \right\}$$

(2-108)

Applying the Hansen expansion of eq. (2-105) with appropriate changes yields

$$U' = \mathrm{Re}\left\{ \frac{\mu'}{r'} \sum_{n=2}^{\infty} \left(\frac{a}{r'}\right)^n \sum_{m-0}^{n} K_m V_{n,m} \sum_{r=-n}^{n} V_{n,r}^{m} \cdot \right.$$

$$\left. \cdot S_{2n}^{(m,r)} (\alpha,\beta,\gamma) e^{jrL'} \sum_{t=-\infty}^{\infty} Y_t^{n,-m} (k,h) e^{jt\lambda} \right\}$$

(2-109)

Similarly, multiplying numerator and denominator of eq. (2-109) by $(r'/a')^{n+1}$ and using eq. (2-105) with the required notation changes leads to the final result

$$U' = \mathrm{Re}\left\{ \frac{\mu'}{a'} \sum_{n=2}^{\infty} \left(\frac{a}{a'}\right)^n \sum_{m=0}^{n} K_m V_{n,m} \sum_{r=-n}^{n} V_{n,r}^m \cdot \right.$$

$$\cdot S_{2n}^{(m,r)}(\alpha,\beta,\gamma) \sum_{s=-\infty}^{\infty} \sum_{t=-\infty}^{\infty} Y_s^{-n-1,r}(k',h') \cdot$$

$$\left. \cdot Y_t^{n,-m}(k,h) \exp[j(t\lambda + s\lambda')] \right\} \qquad (2\text{-}110)$$

Compare this with the potential derived in the equatorial frame which contains the additional inclination function and corresponding summation, viz.,

$$U' = \mathrm{Re}\left\{ \frac{\mu'}{a'} \sum_{n=2}^{\infty} \left(\frac{a}{a'}\right)^n \sum_{m=0}^{n} K_m \sum_{r=-n}^{n} V_{n,r}^m S_{2n}^{(m,r)}(p,q) \cdot \right.$$

$$\cdot \sum_{s=-n}^{n} V_{n,s}^m S_{2n}^{*(m,s)}(p',q') \sum_{u=-\infty}^{\infty} \sum_{t=-\infty}^{\infty} Y_u^{-n-1,s}(k',h') \cdot$$

$$\left. \cdot Y_t^{n,r}(k,h) \exp[j(t\lambda + u\lambda')] \right\}$$

(2-111)

The asterisk (*) represents the complex conjugate. The primed parameters in eq. (2-111) are the equinoctial elements of the third body as computed in the equatorial reference frame and are not to be confused with the third body elements of eq. (2-110).

2.2.3 Induced Dependence of Third Body Orbital Elements on Satellite Orbital Elements

The primed parameters in eq. (2-110) describe the geometry of the perturbing body orbit. However, since the third body potential was developed with respect to the satellite frame, these parameters are not inertially referred. The next sections discuss the functional dependence of the third body elements on the satellite elements that is induced by the choice of a non-inertial reference frame. These results are necessary before eq. (2-110) can be used to develop the satellite equations of motion.

2.2.3.1 The Meaning of h' and k'

The elements h' and k' are formally defined by

$$k' = \underline{e}' \cdot \hat{f}' \qquad (2\text{-}112)$$

$$h' = \underline{e}' \cdot \hat{f}' \qquad (2\text{-}113)$$

The third body eccentricity vector can be computed from the inertial position and velocity vectors, $(\underline{r}')_I$ and $(\underline{v}')_I$, through the formula

$$(\underline{e}')_I = \left(\frac{1}{\mu^*} v'^2 - \frac{1}{r'}\right) (\underline{r}')_I - \frac{1}{\mu^*} \left((\underline{r}')_I \cdot (\underline{v}')_I\right) (\underline{v}')_I \qquad (2\text{-}114)$$

The symbol $(\ )_I$ indicates that the vector is expressed in inertial coordinates. The notation is unnecessary for vector magnitudes since they are independent of the reference frame. The parameter μ^* is the product of the universal gravitational constant and the sum of the masses of the central body and the perturbing body.

The vectors in eqs. (2-112) and (2-113) must be expressed in a common coordinate system for the dot products to be performed. The first two columns of the rotation matrix in eq. (2-104), give the $\hat{f}'$ and $\hat{g}'$ unit vectors in satellite (S) coordinates, viz.,

$$(\hat{f}'^{T})_S = \frac{1}{1+I'\gamma} \left[1+I'\gamma-\alpha^2,\ -\alpha\beta,\ -\alpha(\gamma+I')\right] \tag{2-115}$$

$$(\hat{g}'^{T})_S = \left[-\alpha\beta I',\ I'+\gamma-\beta^2 I',\ -\beta(1+I'\gamma)\right] \tag{2-116}$$

The eccentricity is transformed from inertial coordinates to satellite coordinates by the operation

$$(\underline{e}')_S = \begin{pmatrix} \text{———} & (\hat{f}^T)_I & \text{———} \\ \text{———} & (\hat{g}^T)_I & \text{———} \\ \text{———} & (\hat{w}^T)_I & \text{———} \end{pmatrix} (\underline{e}')_I \tag{2-117}$$

Eq. (2-117) can be rewritten in terms of dot products as,

$$(\underline{e}')_S = \begin{pmatrix} (\hat{f})_I \cdot (\hat{\underline{e}}')_I \\ (\hat{g})_I \cdot (\hat{\underline{e}}')_I \\ (\hat{w})_I \cdot (\hat{\underline{e}}')_I \end{pmatrix} \qquad (2\text{-}118)$$

Using the transpose operator to denote the scalar product and recognizing that the order of the vectors is immaterial, eqs. (2-112) and (2-113) may be written in satellite frame coordinates as

$$k' = (\hat{f}'^T)_S (\underline{e}')_S \qquad (2\text{-}119)$$

and

$$h' = (\hat{g}'^T)_S (\underline{e}')_S \qquad (2\text{-}120)$$

Finally, substituting eqs. (2-115), (2-116) and (2-118) into eqs. (2-119) and (2-120) yields the final expressions for h' and k'. They are given in Table 2-3. For the special case of $\alpha = \beta = 0$ and $\gamma = 1$, the third body frame axes coincide with those of the satellite. In that case, the expressions for h' and k' assume the well known forms

$$k' = \frac{1}{1+I'\gamma}\{[1 + I'\gamma - \alpha^2][(\hat{f})_I \cdot (\underline{e}')_I] - \alpha\beta[(\hat{g})_I \cdot (\underline{e}')_I] - \alpha(\gamma + I')[(\hat{w})_I \cdot (\underline{e}')_I]\}$$

$$h' = \frac{1}{1+I'\gamma}\{-\alpha\beta I'[(\hat{f})_I \cdot (\underline{e}')_I] + [I' + \gamma - \beta^2 I'][(\hat{g})_I \cdot (\underline{e}')_I] - \beta(1 + I'\gamma)[(\hat{w})_I \cdot (\underline{e}')_I]\}$$

Table 2-3. Functional Form of the Third Body Elements, h' and k'

$$k' = (\hat{f})_I \cdot (\underline{e}')_I \qquad (2\text{-}121)$$

and

$$h' = (\hat{g})_I \cdot (\underline{e}')_I \qquad (2\text{-}122)$$

2.2.3.2 The Meaning of λ'

The mean longitude of the third body, λ', is determined from Kepler's equation in equinoctial elements

$$\lambda' = F' - k' \sin F' + h' \cos F' \qquad (2\text{-}123)$$

where F' is the third body eccentric longitude defined through the relations [15]

$$\cos F' = k' + \frac{(1 + k'^2\beta')\, X' - h'k'\beta'Y'}{a' \sqrt{1 - h'^2 - k'^2}} \qquad (2\text{-}124)$$

$$\sin F' = h' + \frac{(1 - h'^2\beta')\, Y' - h'k'\beta'X'}{a'\sqrt{1 - h'^2 - k'^2}} \qquad (2\text{-}125)$$

The parameter β' has the meaning

$$\beta' = \frac{1}{1 + \sqrt{1 - h'^2 - k'^2}} \qquad (2\text{-}126)$$

while X' and Y' are formally represented by

$$X' = \underline{r}' \cdot \hat{f}' \qquad (2\text{-}127)$$

and

$$Y' = \underline{r}' \cdot \hat{g}' \qquad (2\text{-}128)$$

The procedure leading to Table 2-3 is applicable to the decomposition of any vector that lies in the plane of the third body orbit. Hence, by analogy, X' and Y' may be computed according to

$$X' = \frac{1}{1+I'\gamma} \{[1 + I'\gamma - \alpha^2] [(\hat{f})_I \cdot (\underline{r}')_I] -$$

$$- \alpha\beta[(\hat{g})_I \cdot (\underline{r}')_I] - \alpha(\gamma + I')[(\hat{w})_I \cdot (\underline{r}')_I]\} \quad (2\text{-}129)$$

and

$$Y' = \frac{1}{1+I'\gamma} \{-\alpha\beta I'[(\hat{f})_I \cdot (\underline{r}')_I] +$$

$$+ [I' + \gamma - \beta^2 I'] [(\hat{g})_I \cdot (\underline{r}')_I] -$$

$$- \beta(1 + I'\gamma) [(\hat{w})_I \cdot (\underline{r}')_I]\}. \quad (2\text{-}130)$$

2.2.4 Steps for the Evaluation of Third Body Quantities

The following steps are used to compute the third body parameters α, β, γ, h', k' and λ' in eq. (2-110):

1) Given the position and velocity components of the third body in inertial coordinates, $(\underline{r}')_I$ and $(\underline{v}')_I$, compute the third body eccentricity vector, $(\underline{e}')_I$, from eq. (2-114) and the unit normal to the disturbing body orbital plane from the cross product,

$$(\hat{w}')_I = \text{Unit}\left[(\underline{r}')_I \times (\underline{v}')_I\right] \qquad (2\text{-}131)$$

2) Given the p and q elements of the satellite, construct the inertially referred $(\hat{f})_I$, $(\hat{g})_I$, $(\hat{w})_I$ unit vectors of the satellite reference frame using eqs. (2-23) through (2-25).

3) Compute the direction cosines, α, β, and γ, of the disturbing body unit orbital normal with respect to the satellite frame from eqs. (2-92) through (2-94).

4) Compute the third body elements h' and k' from Table 2-3 using the results of steps (1) through (3).

5) Compute the third body mean longitude, λ', from the expressions presented in Section 2.2.3.2.

Chapter 3

Isolating Long Term Motion in the Satellite Dynamical Equations

The previous chapter developed a form of the third body disturbing potential in non-singular equinoctial orbit elements. The result has the structure

$$U' = \mathrm{Re}\left\{ \sum_{t=-\infty}^{\infty} \sum_{s=-\infty}^{\infty} \psi_{t,s}\, e^{j(t\lambda+s\lambda')} \right\} \qquad (3\text{-}1)$$

The complex quantity $\psi_{t,s}$ consolidates constants and factors that depend on the slow equinoctial elements of both the satellite and the disturbing body. A system of high precision dynamical equations are obtained by substituting the potential directly into the Lagrange Planetary equations.

The harmonic content of the high precision satellite equations is determined by the linear combination of fast angles $t\lambda + s\lambda'$ as well as the more slowly varying $\psi_{t,s}$. Contributions to the satellite motion stemming from $\psi_{t,s}$ are most noticeably a result of variations in the third body orbital parameters. Examples are the thirty day oscillation

in the lunar eccentricity and the 8.9 year period of lunar perigee advance. The combination $t\lambda + s\lambda'$ contributes several classes of dynamical frequencies, each of which has an analogous counterpart in the theory of a satellite moving under the influence of the Earth's non-spherical gravity potential. These classes are summarized in Table 3-1.

Mission analysis provides an excellent illustration of a case where much of the harmonic information in the satellite equations of motion is dispensable and serves solely to restrict the step size of a numerical integration. In mission analysis, the goal may be to verify prior to launch that a satellite orbit will satisfy geometrical constraints over the projected operational lifetime of the satellite. On the other hand, the goal may be to ensure a minimum perigee height over a time span that is quite long in comparison to the anticipated utility of the satellite. In either case, a knowledge of the long term evolution of the satellite orbit is sufficient.

DESIGNATION	CONSTRAINTS ON INDICES IN $t\lambda + s\lambda'$	PERIOD OF TRIGONOMETRIC ARGUMENT, $t\lambda + s\lambda'$ P = SATELLITE PERIOD P' = DISTURBING BODY PERIOD	REMARKS
ZONAL ANALOGS	$t \neq 0,\ s = 0$	$P/\lvert t\rvert,\ \lvert t\rvert = 1,2,3,\ldots$	DEPENDS SOLELY ON SATELLITE MEAN MOTION
"M-DAILY" ANALOGS	$t = 0,\ s \neq 0$	$P'/\lvert s\rvert,\ \lvert s\rvert = 1,2,3,\ldots$	DEPENDS SOLELY ON THIRD BODY MEAN MOTION
TESSERAL ANALOGS	$t \neq 0,\ s \neq 0$	$P/\lvert t + sP/P'\rvert$ $\lvert t\rvert = 1,2,3,\ldots$ $\lvert s\rvert = 1,2,3,\ldots$	RESONANT TERMS (i.e., $t+sP/P' \simeq 0$) PRODUCE OSCILLATIONS WITH LONG PERIODS IN RELATION TO THE SATELLITE PERIOD
SECULAR	$t = 0,\ s = 0$	∞	DOUBLE AVERAGED TERM

Table 3-1. Harmonic Contributions of the Trigonometric Argument $t\lambda + s\lambda'$

This chapter derives an averaging theory, based on the Generalized Method of Averaging, that can be used to remove high frequency components from the high precision dynamical equations arising from rapidly varying combinations of λ and λ'. Methods for smoothing $\psi_{t,s}$ are outside the scope of this thesis.

3.1 The Generalized Method of Averaging

The Generalized Method of Averaging (GMA) is an asymptotic technique which can be used to eliminate dynamical frequencies from a system of differential equations. The mathematical formalism was developed by Krylov and Bogoliubov [3], and extended by Mitropolsky [4], for use in the study of non-linear oscillations. In the context of satellite theory, the method is employed to remove short periodic oscillations from the equations of motion that restrict the step size of the numerical integration. The resulting averaged equations of motion in mean elements may be integrated at reduced computational expense. The GMA also allows for the analytical recovery of the short periodic variations at the output points of the averaged orbit generator. Hence, an approximation to the high precision orbital elements is available at each output time of the averaged orbit generator by evaluating the

periodic corrections to the mean elements. The accuracy depends on the order of the asymptotic averaging theory. Chapter 5 demonstrates how this approximation is used to initialize the averaged equations of motion.

The Generalized Method of Averaging has already been used for the high precision prediction and the short arc determination of low and medium altitude satellite orbits [21, 22]. Efficient algorithms have usually been based on an application of the method of averaging to remove the satellite fast variable. However, in some cases a single average is not appropriate. Researchers in the area of central body perturbations have found examples where an additional averaging operation, to remove frequencies that depend on the rotation rate of the central body, is essential to algorithmic efficiency [23].

There is an analogous consideration for high altitude satellites moving under the influence of the sun and moon when extensive mission analysis and very long term stability studies are attempted. Variations in the satellite motion induced by the moon moving in its orbit can restrict the step size of numerical integration to at most 3.5 days [23]. Similarly, the apparent motion of the sun about the Earth can place an upper bound on the step size of around 45

days. Any averaging operation that removes the satellite fast variable from the equations of motion, but ignores periodic variations caused by the motion of a third body is inappropriate. An effective average of the satellite dynamical equations must be based on eliminating the rapidly varying members in the set $\{\phi_{t,s}\}$ where $\phi_{t,s}$ is a linear combination of the satellite and third body mean longitudes given by,

$$\phi_{t,s} = t\lambda + s\lambda' \qquad (3-2)$$

The following section derives an averaging theory, based on the Generalized Method of Averaging, that removes frequencies associated with the composite angles, $\phi_{t,s}$.

3.1.1 An Averaging Theory for Satellites Moving Under the Influence of a Disturbing Body

Given the potential as schematically represented in eq. (3-1), the equations of motion describing the orbital evolution for a satellite perturbed by a third body have the form [15]

$$\frac{da_i}{dt} = -\sum_{k=1}^{6} (a_i, a_k) \frac{\partial}{\partial a_k} \operatorname{Re}\left\{ \sum_{t=-\infty}^{\infty} \sum_{s=-\infty}^{\infty} \psi_{t,s} e^{j\phi_{t,s}} \right\}$$

$$i = 1,\ldots,5 \qquad (3-3)$$

and

$$\frac{d\lambda}{dt} = n(a_1) - \sum_{k=1}^{6} (a_6, a_k) \frac{\partial}{\partial a_k} \operatorname{Re}\left\{ \sum_{t=-\infty}^{\infty} \sum_{s=-\infty}^{\infty} \psi_{t,s} e^{j\phi_{t,s}} \right\} \tag{3-4}$$

where (a_i, a_k) is a Poisson bracket and $n(a_1)$ is the satellite mean motion.

The asymptotic formalism of the Generalized Method of Averaging depends on the presence of a small parameter, ν. Hence, the high precision dynamical equations are required to have the form,

$$\frac{da_i}{dt} = \nu F_i (\underline{a}, \{\phi_{t,s}(\underline{a}, \lambda)\}; \underline{a}'(\underline{a}))$$

$$i = 1, \ldots, 5 \tag{3-5}$$

and

$$\frac{d\lambda}{dt} = n(a_1) + \nu F_6(\underline{a}, \{\phi_{t,s}(\underline{a},\lambda)\}; \underline{a}'(\underline{a})) \qquad (3\text{-}6)$$

where

$\underline{a}$ ≡ vector of the slowly varying satellite orbital elements; $\underline{a}^T = [a,h,k,p,q]$

λ ≡ mean longitude of the satellite

$\underline{a}'(\underline{a})$ ≡ vector of satellite dependent slowly varying parameters of the perturbing body orbit; $\underline{a}'^T = [a',h',k',\alpha,\beta,\gamma]$

$\phi_{t,s}(\underline{a},\lambda)$ ≡ $t\lambda + s\lambda'(\underline{a})$

$\lambda'(\underline{a})$ ≡ satellite dependent mean longitude of the third body

The dependence of $\phi_{t,s}$ and $\underline{a}'$ on the slowly varying satellite orbital elements reflects the decision made in Chapter 2 to develop the disturbing potential in the non-inertial satellite frame. The averaging theory developed in this chapter can be specialized to the case of a potential developed in inertial coordinates by neglecting the induced dependencies.

In the analysis that follows, $\{\phi_{t,s}\}$ is broken into two subsets. One is the set of rapidly varying angles, $\{\sigma_{\ell,m}\}$. The other is the set of slowly varying angles, $\{\mu_{j,k}\}$. The averaged equations of motion are to be determined so that no members of $\{\sigma_{\ell,m}\}$ appear. Accordingly, the assumed form of the averaged dynamics is

$$\frac{d\bar{a}_i}{dt} = \sum_{p=1}^{N} \nu^p A_{i,p}\left(\underline{\bar{a}}, \{\bar{\mu}_{j,k}(\underline{\bar{a}},\bar{\lambda})\}; a'(\underline{\bar{a}})\right)$$

$$i = 1,\ldots,5 \qquad (3\text{-}7)$$

and

$$\frac{d\bar{\lambda}}{dt} = n(\bar{a}_1) + \sum_{p=1}^{N} \nu^p A_{6,p}(\bar{\underline{a}}, \{\bar{\mu}_{j,k}(\bar{\underline{a}},\bar{\lambda})\};\underline{a}'(\bar{\underline{a}}))$$

(3-8)

where the symbol (-) denotes the mean and

$$\bar{\mu}_{j,k}(\bar{\underline{a}},\bar{\lambda}) = j\bar{\lambda} + k\lambda'(\bar{\underline{a}}) \qquad (3-9)$$

The Generalized Method of Averaging assumes the existence of a near-identity transformation in the small parameter that connects the mean element space to the high precision element space. The transformation equations are

$$a_i = \bar{a}_i + \sum_{p=1}^{N} \nu^p \eta_{i,p}(\bar{\underline{a}}, \{\bar{\sigma}_{\ell,m}(\bar{\underline{a}},\bar{\lambda})\}; \underline{a}'(\bar{\underline{a}}))$$

$$i = 1,\ldots,6 \qquad (3-10)$$

where $\eta_{i,p}$ is a function that is required to be jointly periodic in the members of the set $\{\bar{\sigma}_{\ell,m}(\bar{\underline{a}},\bar{\lambda})\}$ on the interval $[0,2\pi]$. Also,

$$\bar{\sigma}_{\ell,m}(\bar{\underline{a}},\bar{\lambda}) = \ell\bar{\lambda} + m\lambda'(\bar{\underline{a}}) \qquad (3\text{-}11)$$

The objective is to create expressions relating the as yet undetermined $A_{i,p}$ and $\eta_{i,p}$ to functions which are known. The approach is to develop both sides of the high precision equations of motion in terms of mean elements. The near identity transformation, in conjunction with the assumed form of the averaged equations of motion, is used to transform the left hand sides of the high precision equations. The right hand sides of the osculating equations are expanded in a Taylor series about the mean elements with the aid of the near identity transformation. Both sides of the transformed dynamical equations are then equated on an order by order basis in the small parameter to produce expressions relating the functions $A_{i,p}$ and $\eta_{i,p}$ to known quantities. These expressions are then averaged to remove all dependence on the set $\{\bar{\sigma}_{\ell,m}\}$ to yield the functional form of $A_{i,p}$. The periodic recovery function $\eta_{i,p}$ is then known.

To begin, the near identity transformation is differentiated with respect to time. It is assumed that there is no <u>explicit</u> time variation of the slow third body orbital elements and that whatever change occurs comes from the motion of the satellite orbital plane. Accordingly

$$\frac{da_i}{dt} = \frac{d\bar{a}_i}{dt} + \sum_{p=1}^{N} \nu^p \{ \sum_{n=1}^{5} [\frac{\partial \eta_{i,p}}{\partial \bar{a}_n} + \sum_{(\ell,m)} \frac{\partial \eta_{i,p}}{\partial \bar{\sigma}_{\ell,m}} \frac{\partial \bar{\sigma}_{\ell,m}}{\partial \bar{a}_n} +$$

$$+ \sum_{q=1}^{5} \frac{\partial \eta_{i,p}}{\partial a'_q} \frac{\partial a'_q}{\partial \bar{a}_n}] \frac{d\bar{a}_n}{dt} + \sum_{(\ell,m)} \frac{\partial \eta_{i,p}}{\partial \bar{\sigma}_{\ell,m}} \frac{\partial \bar{\sigma}_{\ell,m}}{\partial t}$$

$$i = 1,\ldots,6 \qquad (3\text{-}12)$$

The partial derivatives of the disturbing body parameters with respect to the satellite orbital elements are the consequence of expressing the third body disturbing potential in a coordinate frame which is not the reference system of the numerical integration.

The function $A_{i,p}$ is now introduced by substituting the assumed form of the averaged equations of motion into eq. (3-12). The result is

$$\frac{da_i}{dt} = \sum_{p=1}^{N} \nu^p A_{i,p} + \sum_{p=1}^{N} \nu^p \left\{ \sum_{n=1}^{5} \left[\frac{\partial \eta_{i,p}}{\partial \bar{a}_n} + \right. \right.$$

$$\left. + \sum_{(\ell,m)} \frac{\partial \eta_{i,p}}{\partial \bar{\sigma}_{\ell,m}} \frac{\partial \bar{\sigma}_{\ell,m}}{\partial \bar{a}_n} + \sum_{q=1}^{5} \frac{\partial \eta_{i,p}}{\partial a'_q} \frac{\partial a'_q}{\partial \bar{a}_n} \right] \left[\sum_{r=1}^{N} \nu^r A_{n,r} \right] +$$

$$\left. + \sum_{(\ell,m)} \frac{\partial \eta_{i,p}}{\partial \bar{\sigma}_{\ell,m}} \left[(\ell \bar{n} + mn') + \ell \sum_{r=1}^{N} \nu^r A_{6,r} \right] \right\}$$

$$i = 1,\ldots,5 \qquad (3\text{-}13)$$

and

$$\frac{d\lambda}{dt} = \bar{n} + \sum_{p=1}^{N} \nu^p A_{6,p} + \sum_{p=1}^{N} \nu^p \{ \sum_{n=1}^{5} [\frac{\partial \eta_{6,p}}{\partial \bar{a}_n} +$$

$$+ \sum_{(\ell,m)} \frac{\partial \eta_{6,p}}{\partial \bar{\sigma}_{\ell,m}} \frac{\partial \bar{\sigma}_{\ell,m}}{\partial \bar{a}_n} + \sum_{q=1}^{5} \frac{\partial \eta_{6,p}}{\partial \bar{a}_q} \frac{\partial a'_q}{\partial \bar{a}_n}] [\sum_{r=1}^{N} \nu^r A_{n,r}]$$

$$+ \sum_{(\ell,m)} \frac{\partial \eta_{6,p}}{\partial \bar{\sigma}_{\ell,m}} [(\ell\bar{n} + mn') + \ell \sum_{r=1}^{N} \nu^r A_{6,r}]\}$$

(3-14)

where n' is the disturbing body mean motion. Eqs. (3-13) and (3-14) can be expressed as a pure power series in ν, viz, [15]

$$\frac{da_i}{dt} = \sum_{p=1}^{N} \nu^p \{A_{i,p} + \sum_{(\ell,m)} (\ell\bar{n} + mn') \frac{\partial \eta_{i,p}}{\partial \bar{\sigma}_{\ell,m}} +$$

$$+ \sum_{n=1}^{5} \sum_{w=1}^{p-1} [\frac{\partial \eta_{i,p-w}}{\partial \bar{a}_n} + \sum_{(\ell,m)} \frac{\partial \eta_{i,p-w}}{\partial \bar{\sigma}_{\ell,m}} \frac{\partial \bar{\sigma}_{\ell,m}}{\partial \bar{a}_n} +$$

$$+ \sum_{q=1}^{5} \frac{\partial \eta_{i,p-w}}{\partial a'_q} \frac{\partial a'_q}{\partial \bar{a}_n}] A_{n,w} +$$

$$+ \sum_{w=1}^{p-1} \sum_{(\ell,m)} \ell \frac{\partial \eta_{i,p-w}}{\partial \bar{\sigma}_{\ell,m}} A_{6,w}\} + O(\nu^{N+1})$$

$$i = 1,\ldots,5 \qquad (3\text{-}15)$$

and

$$\frac{d\lambda}{dt} = \bar{n} + \sum_{p=1}^{N} \nu^p \{A_{6,p} + \sum_{(\ell,m)} (\ell\bar{n} + mn') \frac{\partial \eta_{6,p}}{\partial \bar{\sigma}_{\ell,m}} +$$

$$+ \sum_{n=1}^{5} \sum_{w=1}^{p-1} [\frac{\partial \eta_{6,p-w}}{\partial \bar{a}_n} + \sum_{(\ell,m)} \frac{\partial \eta_{6,p-w}}{\partial \bar{\sigma}_{\ell,m}} \frac{\partial \bar{\sigma}_{\ell,m}}{\partial \bar{a}_n} +$$

$$+ \sum_{q=1}^{5} \frac{\partial \eta_{6,p-w}}{\partial a'_q} \frac{\partial a'_q}{\partial \bar{a}_n}] A_{n,w} +$$

$$+ \sum_{w=1}^{p-1} \sum_{(\ell,m)} \ell \frac{\partial \eta_{6,p-w}}{\partial \bar{\sigma}_{\ell,m}} A_{6,w}\} + O(\nu^{N+1})$$

(3-16)

The summation on w is not performed when p = 1 so that no contribution is made at first order.

The right hand sides of the high precision equations of motion are now expressed in terms of mean elements. Substituting the transformation equations into the right hand sides of eqs. (3-5) and (3-6) yields

$$\frac{da_i}{dt} = \nu F_i\Big[\bar{\underline{a}} + \sum_{p=1}^{N} \nu^p \underline{\eta}_p\ ,$$

$$,\ \{\phi_{t,s}\ (\bar{\underline{a}} + \sum_{p=1}^{N} \nu^p \underline{\eta}_p,\ \bar{\lambda} + \sum_{p=1}^{N} \nu^p \eta_{6,p})\}\ ;$$

$$;\ \underline{a}'\ (\bar{\underline{a}} + \sum_{p=1}^{N} \nu^p \underline{\eta}_p)\Big]_{\ i\ =\ 1,\ldots,5}$$

(3-17)

and

$$\frac{d\lambda}{dt} = n(\bar{a}_1 + \sum_{p=1}^{N} \nu^p \eta_{1,p}) +$$

$$+ \nu F_6\Big[\bar{\underline{a}} + \sum_{p=1}^{N} \nu^p \eta_p\ ,\{\phi_{t,s}(\bar{\underline{a}} + \sum_{p=1}^{N} \nu^p \underline{\eta}_p, \bar{\lambda} + \sum_{p=1}^{N} \nu^p \eta_{6,p})\}$$

$$;\ \underline{a}'\ (\bar{\underline{a}} + \sum_{p=1}^{N} \nu^p \underline{\eta}_p)\Big]$$

(3-18)

where $\underline{\eta}_p$ is a vector of periodic recovery functions associated with the slow satellite elements. Expanding in a Taylor series about the mean elements,

$$\frac{da_i}{dt} = \nu F_i \left(\bar{\underline{a}}, \{\bar{\phi}_{t,s}(\bar{\underline{a}},\bar{\lambda})\}; \underline{a}'(\bar{\underline{a}})\right) +$$

$$+ \nu \sum_{n=1}^{\infty} \frac{1}{n!} \left\{ \sum_{k=1}^{5} \sum_{p=1}^{N} \nu^p \eta_{k,p} \left(\frac{\partial}{\partial a_k} + \sum_{(t,s)} \frac{\partial \phi_{t,s}}{\partial a_k} \frac{\partial}{\partial \phi_{t,s}} \right.\right.$$

$$\left. + \sum_{q=1}^{5} \frac{\partial a'_q}{\partial a_k} \frac{\partial}{\partial a'_q} \right) +$$

$$\left. + \sum_{p=1}^{N} \nu^p \eta_{6,p} \sum_{(t,s)} t \frac{\partial}{\partial \phi_{t,s}} \right\}^n F_i \Bigg|_{\substack{\underline{a} = \bar{\underline{a}} \\ \phi_{t,s} = \bar{\phi}_{t,s}}}$$

$$i = 1,\ldots,5 \qquad (3\text{-}19)$$

and

$$\frac{d\lambda}{dt} = \bar{n} + \sum_{n=1}^{\infty} \frac{1}{n!} \left\{ \sum_{p=1}^{N} \nu^p \eta_{1,p} \frac{\partial}{\partial a_1} \right\}^n n(a_1) \Big|_{a_1 = \bar{a}_1} +$$

$$+ \nu F_6 \left(\underline{\bar{a}}, \{\bar{\phi}_{t,s}(\underline{\bar{a}}, \bar{\lambda})\}; \underline{a}'(\underline{\bar{a}})\right) +$$

$$+ \nu \sum_{n=1}^{\infty} \frac{1}{n!} \left\{ \sum_{k=1}^{5} \sum_{p=1}^{N} \nu^p \eta_{k,p} \left(\frac{\partial}{\partial a_k} + \sum_{(t,s)} \frac{\partial \phi_{t,s}}{\partial a_k} \frac{\partial}{\partial \phi_{t,s}} \right.\right.$$

$$\left.\left. + \sum_{q=1}^{5} \frac{\partial a'_q}{\partial a_k} \frac{\partial}{\partial a'_q} \right) + \sum_{p=1}^{N} \nu^p \eta_{6,p} \sum_{(t,s)} t \frac{\partial}{\partial \phi_{t,s}} \right\}^n F_6$$

(3-20)

The right hand sides of eqs. (3-19) and (3-20) represent the osculating element rates. The same is true of the right hand sides of eqs. (3-15) and (3-16). Consequently, it follows that these expressions must be equal to each other. Equating them and matching coefficients of like powers of the small parameter leads to equations that relate the A and η functions to the known F function on an order by order basis.

In many instances, the first order approximation produces results of striking accuracy with minimal analytical complexity. A first order formulation of the averaged equations of motion and periodic recovery functions will now be developed to provide the basis for the numerical demonstration.

3.1.2 A First Order Averaging Theory

Using the methods described in the preceding section, the set of first order equations for $A_{i,p}$ and $\eta_{i,p}$ are found to be

$$F_i(\bar{\underline{a}},\ \{\bar{\phi}_{t,s}(\bar{\underline{a}},\bar{\lambda})\};\ \underline{a}'\ (\bar{\underline{a}})) =$$

$$= A_{i,1}\ (\bar{\underline{a}},\ \{\bar{\mu}_{j,k}(\bar{\underline{a}},\bar{\lambda})\};\ a'\ (\bar{\underline{a}})) +$$

$$+ \sum_{(\ell,m)} (\ell\bar{n} + mn')\ \frac{\partial \eta_{i,p}}{\partial \bar{\sigma}_{\ell,m}}\ (\bar{\underline{a}},\ \{\bar{\sigma}_{\ell,m}(\bar{\underline{a}},\bar{\lambda})\};\ \underline{a}'\ (\bar{\underline{a}}))$$

$$i = 1,\ldots,5 \qquad (3\text{-}21)$$

and, recognizing that $n(a_1) = \mu^{1/2}\, a_1^{-3/2}$,

$$-\frac{3}{2}\,\frac{\bar{n}}{\bar{a}_1}\,\eta_{1,1}\,(\bar{\underline{a}},\ \{\bar{\sigma}_{\ell,m}(\bar{\underline{a}},\bar{\lambda})\};\ \underline{a}'\ (\bar{\underline{a}})) +$$

$$+ F_6\,(\bar{\underline{a}},\ \{\bar{\phi}_{t,s}(\bar{\underline{a}},\bar{\lambda})\};\ \underline{a}'\ (\bar{\underline{a}})) =$$

$$= A_{6,1}\,(\bar{\underline{a}},\ \{\bar{\mu}_{j,k}(\bar{\underline{a}},\bar{\lambda})\};\ \underline{a}'\ (\bar{\underline{a}})) +$$

$$+ \sum_{(\ell,m)} (\ell\bar{n} + mn')\ \frac{\partial \eta_{6,1}}{\partial \bar{\sigma}_{\ell,m}}\ (\bar{\underline{a}},\ \{\bar{\sigma}_{\ell,m}(\bar{\underline{a}},\bar{\lambda})\};\ \underline{a}'(\bar{\underline{a}}))$$

(3-22)

The desired expressions for the A functions are determined by successively averaging eqs. (3-21) and (3-22) over each member of the set $\{\bar{\sigma}_{\ell,m}\}$ on the interval $[0,2\pi]$ to remove all dependence on the rapidly varying angles. At first order, the slow elements of the satellite and the third body are held fixed over the averaging interval and mutual independence of the angles is assumed. The periodic recovery functions are required to be jointly 2π periodic in the angles of the set $\{\bar{\sigma}_{\ell,m}\}$. Hence if the elements of the set are denoted by $\{\bar{\sigma}_{\ell_1,m_1},\ldots,\bar{\sigma}_{\ell_n,m_n},\ldots\}$ then the following properties hold [15]

$$\frac{1}{2\pi}\int_0^{2\pi}\left[\frac{1}{2\pi}\int_0^{2\pi}\cdots\left[\frac{1}{2\pi}\int_0^{2\pi}\left\{\sum_{(\ell,m)}(\ell\bar{n}+mn')\frac{\partial\eta_{i,p}}{\partial\bar{\sigma}_{\ell,m}}\right\}\cdot\right.\right.$$

$$\left.\left.\cdot\, d\bar{\sigma}_{\ell_1,m_1}\right]\cdots d\bar{\sigma}_{\ell_{n-1},m_{n-1}}\right] d\bar{\sigma}_{\ell_n,m_n} = 0$$

$$i = 1,\ldots,6 \qquad (3\text{-}23)$$

and

$$\frac{1}{2\pi}\int_0^{2\pi}\left[\frac{1}{2\pi}\int_0^{2\pi}\cdots\left[\frac{1}{2\pi}\int_0^{2\pi}\left\{-\frac{3}{2}\frac{\bar{n}}{\bar{a}_1}\eta_{1,1}\right\}d\bar{\sigma}_{\ell_1,m_1}\right]\cdot\right.$$

$$\left.\cdot\ \ldots\ d\bar{\sigma}_{\ell_{n-1},m_{n-1}}\right]d\bar{\sigma}_{\ell_n,m_n} \;=\; 0$$

(3-24)

The right hand sides of the averaged equations of motion are then seen to be

$$A_{i,1}\left(\underline{\bar{a}},\ \{\bar{\mu}_{j,k}(\underline{\bar{a}},\bar{\lambda})\};\ \underline{a}'\ (\underline{\bar{a}})\right) =$$

$$= \frac{1}{2\pi}\int_0^{2\pi}\left[\frac{1}{2\pi}\int_0^{2\pi}\cdots\left[\frac{1}{2\pi}\int_0^{2\pi}F_i\left(\underline{\bar{a}},\{\bar{\phi}_{t,s}(\underline{\bar{a}},\bar{\lambda})\};\underline{a}'(\underline{\bar{a}})\right)\cdot\right.\right.$$

$$\left.\left.\cdot\ d\bar{\sigma}_{\ell_1,m_1}\right]\ldots\ d\bar{\sigma}_{\ell_{n-1},m_{n-1}}\right]d\bar{\sigma}_{\ell_n,m_n}$$

$$i = 1,\ldots,6 \qquad (3\text{-}25)$$

Eq. (3-25) shows that at first order, the averaged equations of motion are obtained by substituting mean quantities into the right hand sides of the high precision satellite equations, followed by a removal of all terms depending on any of the rapidly rotating phases.

Now that the $A_{i,1}$ functions are known, the periodic recovery functions are given by the partial differential equations,

$$\sum_{(\ell,m)} (\ell\bar{n} + mn') \frac{\partial \eta_{i,1}}{\partial \bar{\sigma}_{\ell,m}} = F_i - A_{i,1}$$

$$i = 1,\ldots,5 \qquad (3\text{-}26)$$

and

$$\sum_{(\ell,m)} (\ell\bar{n} + mn') \frac{\partial \eta_{6,1}}{\partial \bar{\sigma}_{\ell,m}} = (F_6 - A_{6,1}) - \frac{3}{2} \frac{\bar{n}}{\bar{a}_1} \eta_{1,1}$$

(3-27)

If the notation $[\quad]_{(\ell,m)}$ is used to denote a term in the right hand sides of eqs. (3-26) and (3-27) that depends on $\bar{\sigma}_{\ell,m}$,

$$\sum_{(\ell,m)} (\ell\bar{n} + mn') \frac{\partial \eta_{i,1}}{\partial \bar{\sigma}_{\ell,m}} = \sum_{(\ell,m)} [F_i - A_{i,1}]_{(\ell,m)}$$

$$i = 1,\ldots,5 \qquad (3\text{-}28)$$

and

$$\sum_{(\ell,m)} (\ell\bar{n} + mn') \frac{\partial \eta_{6,1}}{\partial \bar{\sigma}_{\ell,m}} = \sum_{(\ell,m)} \left[(F_6 - A_{6,1}) - \frac{3}{2} \frac{\bar{n}}{\bar{a}_1} \eta_{1,1}\right]_{(\ell,m)}$$

(3-29)

For a given pair (ℓ^*,m^*), the solutions to eqs. (3-28) and (3-29) are

$$\eta_{i,1} = \frac{1}{\ell^*\bar{n}+m^*n'} \int [F_i - A_{i,1}]_{(\ell^*,m^*)} d\bar{\sigma}_{\ell^*,m^*} +$$

$$+ f(\{\bar{\sigma}_{\ell,m}\}')$$

$$i = 1,\ldots,5 \qquad (3\text{-}30)$$

and

$$\eta_{6,1} = \frac{1}{\ell^*\bar{n}+m^*n'} \int [(F_6 - A_{6,1}) - \frac{3}{2}\frac{\bar{n}}{\bar{a}_1}\eta_{1,1}]_{(\ell^*,m^*)} \cdot$$

$$\cdot d\bar{\sigma}_{\ell^*,m^*} + g(\{\bar{\sigma}_{\ell,m}\}') \qquad (3\text{-}31)$$

where $f(\{\bar{\sigma}_{\ell,m}\}')$ and $g(\{\bar{\sigma}_{\ell,m}\}')$ are functions of the set of fast angles that excludes $\bar{\sigma}_{\ell^*,m^*}$. It is straightforward to show that these functions must be a sum of terms each of which depends on exactly one of the angles in the

set $\{\bar{\sigma}_{\ell,m}\}'$. Further, each term has a form that is identical to that of the leading term of eqs. (3-30) and (3-31). This shows that the periodic recovery functions may be separated into a sum of functions, $\eta_{i,1,\ell,m}$, that have the form

$$\eta_{i,1,\ell,m} = \frac{1}{\ell\bar{n}+mn'} \int \left[F_i - A_{i,1}\right]_{(\ell,m)} d\bar{\sigma}_{\ell,m}$$

$$i = 1,\ldots,5 \qquad (3\text{-}32)$$

and

$$\eta_{6,1,\ell,m} = \frac{1}{\ell\bar{n}+mn'} \int \left[(F_6 - A_{6,1}) - \right.$$

$$\left. - \frac{3}{2} \frac{\bar{n}}{\bar{a}_1} \eta_{1,1}\right]_{(\ell,m)} d\bar{\sigma}_{\ell,m}$$

(3-33)

Chapter 4

Mathematical Structure of a Dynamical Third Body Model for the Long Term Prediction of Satellite Orbits Using Numerical Methods

The goal of this thesis is to construct a flexible numerical tool for the long term prediction of satellite orbits for which third body perturbation is significant. Chapters 2 and 3 furnish the analytical components. This chapter synthesizes these components into an orbit prediction algorithm that is numerically efficient and free from singularities.

In Chapter 2, the third body disturbing potential was derived. It is formulated in terms of non-singular equinoctial orbital elements in order to avoid singularities in the satellite dynamical equations. Wherever possible, the potential is expressed in terms of functions which are governed by recurrence relations. This was done to eliminate the inefficiency associated with explicit calculations. Furthermore, the potential was developed with respect to the satellite reference frame. This reference frame choice eliminates a summation and the corresponding

inclination function. A side-effect of this choice is that the third body elements h', k', and λ' acquire a dependence on the satellite orientation elements p and q. The potential is restated here in the functional form,

$$U' = \mathrm{Re}\Big\{ \sum_{t=-\infty}^{\infty} \sum_{s=-\infty}^{\infty} \psi_{t,s}[\underline{a};\, a', h'(p,q), k'(p,q), \alpha, \beta, \gamma] \cdot e^{j\phi_{t,s}[p,q,\lambda]} \Big\} \tag{4-1}$$

where

$\mathrm{Re}\{\ \}$ $\equiv$ real part of a complex quantity

$\underline{a}^T$ $\equiv$ $\{a,h,k,p,q\}$

$\phi_{t,s}[p,q,\lambda]$ $\equiv$ $t\lambda + s\lambda'(p,q)$

j $\equiv$ $\sqrt{-1}$

and $\psi_{t,s}$ has the structure

$$\psi_{t,s}[\underline{a};\ a',\ h'(p,q),\ k'(p,q),\ \alpha,\beta,\gamma] =$$

$$= \frac{\mu'}{a'} \sum_{n=2}^{\infty} \left(\frac{a}{a'}\right)^n \sum_{m=0}^{n} K_m V_{n,m} \sum_{r=-n}^{n} V_{n,r}^{m}\, S_{2n}^{(m,r)}(\alpha,\beta,\gamma) \cdot$$

$$\cdot\, Y_s^{-n-1,r}[k'(p,q),\ h'(p,q)]\ Y_t^{n,-m}(k,h) \qquad (4\text{-}2)$$

The definitions of the various blocks in eq. (4-2) are found in Chapter 2.

The high precision satellite equations for third body perturbations are obtained by substituting the disturbing potential of eq. (4-1) into the expressions,

$$\frac{da_i}{dt} = -\sum_{k=1}^{6} (a_i, a_k) \frac{\partial U'}{\partial a_k}$$

$$i = 1,\ldots,5 \qquad (4\text{-}3)$$

and

$$\frac{d\lambda}{dt} = n - \sum_{k=1}^{6} (\lambda, a_k) \frac{\partial U'}{\partial a_k} \qquad (4-4)$$

where

$$[a_1, a_2, a_3, a_4, a_5, a_6] \equiv [a, h, k, p, q, \lambda]$$

U' ≡ third body disturbing potential

(a_i, a_k) ≡ Poisson bracket

n ≡ satellite mean motion

A table of the non-zero Poisson brackets in equinoctial orbital elements is found in Reference 16 and is reproduced in Table 4-1. The result of the substitution is

Table 4-1. Nonzero Poisson brackets of the equinoctial elements.

$$(a, \lambda) = -2as_1 \qquad (h, p) = -kps_5$$

$$(\lambda, h) = -hs_4 \qquad (h, q) = -kqs_5$$

$$(\lambda, k) = -ks_4 \qquad (k, p) = hps_5$$

$$(\lambda, p) = -ps_5 \qquad (k, q) = hqs_5$$

$$(\lambda, q) = -qs_5 \qquad (p, q) = -\frac{1}{2}s_2 s_5 I$$

$$(h, k) = -s_1 s_3$$

where

$$s_1 = \frac{1}{na^2}$$

$$s_2 = 1 + p^2 + q^2$$

$$s_3 = \sqrt{1 - h^2 - k^2}$$

$$s_4 = \frac{s_1 s_3}{1 + s_3}$$

$$s_5 = \frac{s_1 s_3}{2s_3}$$

$$\dot{a}_i = n\delta_{i6} - \mathrm{Re}\Big\{ \sum_{t=-\infty}^{\infty} \sum_{s=-\infty}^{\infty} \Big[\sum_{k=1}^{5} (a_i, a_k) \frac{\partial}{\partial a_k} \psi_{t,s} + (a_i, \lambda)\, jt\psi_{t,s} \Big] e^{j\phi_{t,s}} \Big\} -$$

$$- \mathrm{Re}\Big\{ \sum_{t=-\infty}^{\infty} \sum_{s=-\infty}^{\infty} \big[(a_i, p)\, P_{t,s} + (a_i, q)\, Q_{t,s} \big] e^{j\phi_{t,s}} \Big\}$$

$$i = 1, \ldots, 6 \qquad (4\text{-}5)$$

where δ_{i6} is the Kronecker delta function defined by

$$\delta_{i6} = \begin{cases} 0 \; ; & i = 1, \ldots, 5 \\ 1 \; ; & i = 6 \end{cases} \qquad (4\text{-}6)$$

Also,

$$P_{t,s} = \frac{\partial \psi_{t,s}}{\partial h'} \frac{\partial h'}{\partial p} + \frac{\partial \psi_{t,s}}{\partial k'} \frac{\partial k'}{\partial p} + j\, \psi_{t,s} \frac{\partial \phi_{t,s}}{\partial p} \qquad (4\text{-}7)$$

and

$$Q_{t,s} = \frac{\partial \psi_{t,s}}{\partial h'} \frac{\partial h'}{\partial q} + \frac{\partial \psi_{t,s}}{\partial k'} \frac{\partial k'}{\partial q} + j \psi_{t,s} \frac{\partial \phi_{t,s}}{\partial q}$$

(4-8)

The form of eq. (4-5) hinges on the auxiliary expressions,

$$\frac{\partial \psi_{t,s}}{\partial p} = \frac{\partial \psi_{t,s}}{\partial \alpha} \frac{\partial \alpha}{\partial p} + \frac{\partial \psi_{t,s}}{\partial \beta} \frac{\partial \beta}{\partial p} + \frac{\partial \psi_{t,s}}{\partial \gamma} \frac{\partial \gamma}{\partial p}$$

(4-9)

and

$$\frac{\partial \psi_{t,s}}{\partial q} = \frac{\partial \psi_{t,s}}{\partial \alpha} \frac{\partial \alpha}{\partial q} + \frac{\partial \psi_{t,s}}{\partial \beta} \frac{\partial \beta}{\partial q} + \frac{\partial \psi_{t,s}}{\partial \gamma} \frac{\partial \gamma}{\partial q}$$

(4-10)

The partial derivatives $\partial(h',k')/\partial(p,q)$ are obtained from Table 2-3. The specific results are given in Section 4.3.

The operators $\partial/\partial\alpha$, $\partial/\partial\beta$, $\partial/\partial\gamma$ act on $\psi_{t,s}$ solely through the explicit appearance of the direction cosines in the inclination function $S^{(m,r)}_{2n}(\alpha,\beta,\gamma)$. The functions $P_{t,s}$ and $Q_{t,s}$ connect the third body elements to the inertial frame through the orientation of the satellite orbital plane. When the disturbing potential is developed with respect to an inertial frame, $P_{t,s}$ and $Q_{t,s}$ vanish.

In Chapter 3, a first order averaging theory was developed, for the elimination of frequencies from a system of differential equations that are produced by linear combinations of two fast angles. The benefit of the theory is that the averaged equations can be numerically integrated with a much larger step size than the high precision equations. Initialization of the averaged equations is made possible by the feature of the theory that allows for the recovery of the short periodics at the output times of the numerical integration.

The remainder of this chapter discusses the results of applying first order averaging methods to the high precision satellite equations in eq. (4-5). The mathematical form of the partial derivatives is fully explored. Finally, the recursive nature of the orbit prediction algorithm is detailed.

4.1 First Order Averaged Equations of Motion for Third Body Perturbation

The first order averaging theory developed in Chapter 3 transforms a system of high precision differential equations of the form,

$$\frac{da_i}{dt} = \nu F_i (\underline{a}, \{\phi_{t,s} (\underline{a},\lambda)\}; \underline{a}' (\underline{a}))$$

$$i = 1,\ldots,5 \qquad (4\text{-}11)$$

and

$$\frac{d\lambda}{dt} = n + \nu F_6(\underline{a},\{\phi_{t,s}(\underline{a},\lambda)\}; \underline{a}' (\underline{a})) \qquad (4\text{-}12)$$

into a system of averaged equations of motion in mean elements having the form

$$\frac{d\bar{a}_i}{dt} = \nu A_{i,1} (\bar{\underline{a}}, \{\bar{u}_{j,k} (\bar{\underline{a}},\bar{\lambda})\}; \underline{a}' (\bar{\underline{a}}))$$

$$i = 1,\ldots,5 \qquad (4\text{-}13)$$

and

$$\frac{d\bar{\lambda}}{dt} = \bar{n} + \nu A_{6,1}\left(\underline{\bar{a}}, \{\bar{\mu}_{j,k}(\underline{\bar{a}}, \bar{\lambda})\}; \underline{a}'(\underline{\bar{a}})\right) \tag{4-14}$$

where $\bar{n}$ is the mean mean motion defined by

$$\bar{n} = n(\bar{a}) = \mu^{1/2}\,\bar{a}^{-3/2} \tag{4-15}$$

and $\{\bar{\mu}_{j,k}\}$ is a set of slowly varying mean angles.

The transformation is begun by comparing the right hand sides of eqs. (4-11) and (4-12) to the right hand sides of eq. (4-5). This leads to a representation for the high precision forcing function, viz.,

$$\nu F_i = - \mathrm{Re}\Big\{ \sum_{t=-\infty}^{\infty} \sum_{s=-\infty}^{\infty} \Big[\sum_{k=1}^{5} (a_i, a_k) \frac{\partial}{\partial a_k} \psi_{t,s} +$$

$$+ (a_i, \lambda)\ jt\psi_{t,s} \Big] e^{j\phi_{t,s}} \Big\} -$$

$$- \mathrm{Re}\Big\{ \sum_{t=-\infty}^{\infty} \sum_{s=-\infty}^{\infty} \big[(a_i, p)\ P_{t,s} + (a_i, q)\ Q_{t,s} \big] e^{j\phi_{t,s}} \Big\}$$

$$i = 1, \ldots, 6 \qquad (4\text{-}16)$$

Mean elements are then substituted directly in place of high precision satellite elements in eq. (4-16) to yield

$$\nu \bar{F}_i = - \mathrm{Re}\Big\{ \sum_{t=-\infty}^{\infty} \sum_{s=-\infty}^{\infty} \Big[\sum_{k=1}^{5} (\bar{a}_i, \bar{a}_k) \frac{\partial}{\partial \bar{a}_k} \bar{\psi}_{t,s} +$$

$$(\bar{a}_i, \bar{\lambda})\ jt\bar{\psi}_{t,s} \Big] e^{j\bar{\phi}_{t,s}} \Big\} -$$

$$- \mathrm{Re}\Big\{ \sum_{t=-\infty}^{\infty} \sum_{s=-\infty}^{\infty} \big[(\bar{a}_i, \bar{p})\ \bar{P}_{t,s} + (\bar{a}_i, \bar{q})\ \bar{Q}_{t,s} \big] e^{j\bar{\phi}_{t,s}} \Big\}$$

$$i = 1, \ldots, 6 \qquad (4\text{-}17)$$

Successively averaging eq. (4-17) with respect to each of the rapidly varying members of the set $\{\bar{\phi}_{t,s}\}$ on the interval $[0,2\pi]$ produces expressions for the mean functions, $\nu A_{i,1}$. At first order, the slow elements of the satellite and disturbing body are held fixed over the averaging interval. In addition, the angles in the set $\{\bar{\phi}_{t,s}\}$ are taken to be mutually independent. The stipulation of independence ensures that terms in νF_i that do not contain an angle $\bar{\phi}_{t^*,s^*}$ are unaffected by an average over a cycle of that angle. Hence, one is concerned with evaluating integrals of the form

$$I = -\frac{1}{2\pi}\int_0^{2\pi} \mathrm{Re}\{[\sum_{k=1}^{5}(\bar{a}_i,\bar{a}_k)\frac{\partial}{\partial \bar{a}_k}\bar{\psi}_{t^*,s^*} +$$

$$+ (\bar{a}_i,\bar{\lambda})jt^*\bar{\psi}_{t^*,s^*}]e^{j\bar{\phi}_{t^*,s^*}}\}d\bar{\phi}_{t^*,s^*} -$$

$$-\frac{1}{2\pi}\int_0^{2\pi}\mathrm{Re}\{[(\bar{a}_i,\bar{p})\bar{P}_{t^*,s^*} + (\bar{a}_i,\bar{q})\bar{Q}_{t^*,s^*}]e^{j\bar{\phi}_{t^*,s^*}}\}d\bar{\phi}_{t^*,s^*}$$

$$i = 1,\ldots,6 \qquad (4\text{-}18)$$

According to the rules of first order averaging, the first integral of eq. (4-18) vanishes. The second integral is also identically zero, although the reasons for this deserve some consideration. Eqs. (4-7) and (4-8) provide the definitions for $\bar{P}_{t,s}$ and $\bar{Q}_{t,s}$. Substitution of these definitions into eq. (4-18) produces integrals of the form,

$$\frac{1}{2\pi} \int_0^{2\pi} \mathrm{Re}\left\{\left[(\bar{a}_i,\bar{p})j\ \bar{\psi}_{t^*,s^*} \frac{\partial\bar{\phi}_{t^*,s^*}}{\partial\bar{p}} + \right.\right.$$

$$\left.\left. + (\bar{a}_i,\bar{q})j\ \bar{\psi}_{t^*,s^*} \frac{\partial\bar{\phi}_{t^*,s^*}}{\partial\bar{q}} \right] e^{j\bar{\phi}_{t^*,s^*}}\right\} d\bar{\phi}_{t^*,s^*}$$

$$i = 1,\ldots,6 \qquad (4\text{-}19)$$

These integrals vanish if the partial derivatives $\partial\bar{\phi}_{t^*,s^*}/\partial\bar{p}$ and $\partial\bar{\phi}_{t^*,s^*}/\partial\bar{q}$ are independent of $\bar{\phi}_{t^*,s^*}$. This can be shown by returning to the expression for $\bar{\phi}_{t^*,s^*}$. Differentiating this relation with respect to $\bar{p}$ and $\bar{q}$ leads to,

$$\frac{d\bar{\phi}_{t^*,s^*}}{\partial \bar{p}} = \frac{\partial}{\partial \bar{p}} \left[t^*\bar{\lambda} + s^*\lambda'(\bar{p},\bar{q})\right] = s^* \frac{\partial \lambda'}{\partial \bar{p}}$$

(4-20)

and

$$\frac{\partial \bar{\phi}_{t^*,s^*}}{\partial \bar{q}} = \frac{\partial}{\partial \bar{q}} \left[t^*\bar{\lambda} + s^*\lambda'(\bar{p},\bar{q})\right] = s^* \frac{\partial \lambda'}{\partial \bar{q}}$$

(4-21)

The mean longitude of the third body, λ', may be thought of as the sum of a dynamical term and a geometrical term, viz.,

$$\lambda'(t,\bar{p},\bar{q}) = \underbrace{\sqrt{\frac{\bar{\mu}}{\bar{a}'}}\ (t - t_0)}_{\text{DYNAMICAL}} + \underbrace{\lambda'_0(\bar{p},\bar{q})}_{\text{GEOMETRICAL}}$$

(4-22)

where

t ≡ current time

t_0 ≡ reference time

λ'_0 ≡ reference value of the mean longitude

The dynamical term describes how λ' changes as the third body moves in its orbit. It is reference frame independent since it depends only on the elapsed time from a reference and on the third body semi-major axis which is invariant under coordinate transformations. At a point in the third body orbit, the geometrical term reflects the variation of λ' as resulting from changes in the satellite $\bar{p}$ and $\bar{q}$ elements. Variations in the orientation of the satellite orbital plane map into a rotation of the third body unit vectors, $\hat{f}'$ and $\hat{g}'$, in the plane of the disturbing body orbit. The rotation changes the datum with respect to which λ'_0 is measured, causing λ' to vary in turn. Differentation of eq. (4-22) with respect to $\bar{p}$ and $\bar{q}$ yields the intuitively satisfying results

$$\frac{\partial \lambda}{\partial \bar{p}} = \frac{\partial \lambda'_0}{\partial \bar{p}} \qquad (4\text{-}23)$$

and

$$\frac{\partial \lambda'}{\partial \bar{q}} = \frac{\partial \lambda'_0}{\partial \bar{q}} \tag{4-24}$$

Substituting eqs. (4-23) and (4-24) into eqs. (4-20) and (4-21) leads to the desired relations

$$\frac{\partial \bar{\phi}_{t^*,s^*}}{\partial \bar{p}} = s^* \frac{\partial \lambda'_0}{\partial \bar{p}} \tag{4-25}$$

and

$$\frac{\partial \bar{\phi}_{t^*,s^*}}{\partial \bar{q}} = s^* \frac{\partial \lambda'_0}{\partial \bar{q}} \tag{4-26}$$

Hence, $\partial\bar{\phi}_{t^*,s^*}/\partial\bar{p}$ and $\partial\bar{\phi}_{t^*,s^*}/\partial\bar{q}$ do not depend on the angle $\bar{\phi}_{t^*,s^*}$. The variation of $\bar{\phi}_{t^*,s^*}$ is simply caused by the change in the reference line from which λ' is measured. At first order, the partial derivatives $\partial\lambda'_0/\partial\bar{p}$ and $\partial\lambda'_0/\partial\bar{q}$ are constant over the averaging interval, so that the integral of eq. (4-19) vanishes.

The preceding result leads to an extremely simple procedure for obtaining the $\nu A_{i,1}$ functions of the first order averaged equations of motion. Those angles in $\{\bar{\phi}_{t,s}\}$ that are to be retained in the averaged equations of motion map into specific members of the index set $\{(t,s)\}$. Restricting the summations on t and s in eq. (4-17) to produce only those index pairs gives the defining expressions for the $\nu A_{i,1}$. At first order, terms depending on other indices cannot contribute to the averaged equations of motion.

A philosophy for retaining index pairs in the averaged equations of motion will now be developed.

4.1.1 Criteria for Retaining Terms in the Averaged Equations of Motion

Averaging is merely a formal technique for eliminating dynamical frequencies from a system of differential

equations. It is therefore the task of the mission analyst to judiciously specify those frequencies that are to be retained in the averaged equations of motion, so that the computational advantages of averaging can be realized. For the third body problem, this entails identifying the long period dynamics in eq. (4-17).

The dynamical kernel of eq. (4-17) consists of the double averaged terms. These are terms which depend on the trivial linear combination of the satellite and disturbing body mean longitudes, viz.,

$$\bar{\phi}_{t=0,s=0} = 0 \qquad (4\text{-}27)$$

If no further transformations are made, then these dynamics represent the irreducible minimum of harmonic information, as embodied in $\bar{\psi}_{0,0}$. Hence, they determine the maximum admissible step size for a numerical integration. Accordingly, additional terms considered for inclusion in the averaged equations of motion should have periods that do not restrict the integration step size to less than that dictated by the double averaged dynamics. Candidates satisfying such a requirement could be introduced in the

case when the satellite and the third body are nearly commensurable in their mean motions. This phenomenon, known as third body resonance, may be expressed mathematically as

$$\frac{\bar{n}}{n'} \simeq \frac{N}{N'} \tag{4-28}$$

where N and N' are integers. Eq. (4-28) states that the geometrical relationship of satellite to third body will repeat every N' revolutions of the disturbing body. Since long periodic variations in the satellite motion occur for linear combinations of $\bar{\lambda}$ and λ' that are slowly varying, one obtains the auxiliary condition

$$\dot{\bar{\phi}}_{t,s} = t\dot{\bar{\lambda}} + s\dot{\bar{\lambda}}' \simeq 0 \tag{4-29}$$

If two body relations are used, then eq. (4-29) can be rewritten in terms of the mean motions of the satellite and third body, viz.,

$$\dot{\bar{\phi}}_{t,s} = t\bar{n} + sn' \simeq 0 \tag{4-30}$$

The union of eq. (4-30) with the statement of resonance in eq. (4-28) leads to the constraint relation

$$tN + sN' = 0 \qquad (4\text{-}31)$$

which provides a filter for the values of t and s that give rise to long period terms in eq. (4-17) that could be included in the averaged equations of motion. Notice that eq. (4-31) is a generalized constraint that includes double averaging as a special case. Hence the functions $\nu A_{i,1}$ are found by restricting the indices in eq. (4-17) so as to satisfy eq. (4-31). Given this, the averaged equations of motion are seen to have the form found in Table 4-2.

4.2 Mathematical Form of the Periodic Recovery Functions

Those terms in eq. (4-17) for which $tN + sN' \neq 0$ contribute periods to the satellite motion that are deemed to unecessarily restrict the step size of a numerical integration. In accordance with the methods detailed in Chapter 3, the amplitudes of these periodic variations can be recovered as a function of the mean element output of the averaged orbit generator through the evaluation of the indefinite integrals

Table 4-2. Form of the first order averaged equations of motion for third body perturbation.

$$\dot{\bar{a}}_i = \underbrace{\bar{n}\,\delta_{i6} - \mathrm{Re}\left\{\sum_{k=1}^{5} (\bar{a}_i, \bar{a}_k)\frac{\partial}{\partial \bar{a}_k}\bar{\psi}_{0,0} + (\bar{a}_i, \bar{p})\,\bar{P}_{0,0} + (\bar{a}_i, \bar{q})\,\bar{Q}_{0,0}\right\}}_{\text{DOUBLE AVERAGED TERMS}}$$

$$\underbrace{- \mathrm{Re}\left\{\sum_{\substack{t=-\infty \\ tN + sN' = 0 \\ t \neq 0,\ s \neq 0}}^{\infty}\ \sum_{s=-\infty}^{\infty}\left[\sum_{k=1}^{5} (\bar{a}_i, \bar{a}_k)\frac{\partial}{\partial \bar{a}_k}\bar{\psi}_{t,s} + (\bar{a}_i, \bar{\lambda})\,jt\,\bar{\psi}_{t,s} + (\bar{a}_i, \bar{p})\,\bar{P}_{t,s} + (\bar{a}_i, \bar{q})\,\bar{Q}_{t,s}\right] e^{j\bar{\phi}_{t,s}}\right\}}_{\text{RESONANT TERMS}} \qquad (4\text{-}32)$$

$$\bar{P}_{0,0} = \frac{\partial \bar{\psi}_{0,0}}{\partial h'}\frac{\partial h'}{\partial \bar{p}} + \frac{\partial \bar{\psi}_{0,0}}{\partial k'}\frac{\partial k'}{\partial \bar{p}};\quad \bar{Q}_{0,0} = \frac{\partial \bar{\psi}_{0,0}}{\partial h'}\frac{\partial h'}{\partial \bar{q}} + \frac{\partial \bar{\psi}_{0,0}}{\partial k'}\frac{\partial k'}{\partial \bar{q}}$$

$$\nu\ \eta_{i,1} = \underbrace{\sum_{t=-\infty}^{\infty}\ \sum_{s=-\infty}^{\infty}}_{tN+sN'\neq 0}\ \nu\ \eta_{i,1,t,s}$$

$$= -\underbrace{\sum_{t=-\infty}^{\infty}\ \sum_{s=-\infty}^{\infty}}_{tN+sN'\neq 0}\ \frac{1}{\bar{tn}+sn'}\ \int \mathrm{Re}\{[\sum_{k=1}^{5}\ (\bar{a}_i,\bar{a}_k)\ \frac{\partial}{\partial \bar{a}_k}\ \bar{\psi}_{t,s} +$$

$$+\ (\bar{a}_i,\bar{\lambda})\ jt\ \bar{\psi}_{t,s} + (\bar{a}_i,\bar{p})\bar{P}_{t,s} + (\bar{a}_i,\bar{q})\bar{Q}_{t,s}]\ e^{j\bar{\phi}_{t,s}}\}d\bar{\phi}_{t,s}$$

$$i = 1,\ldots,5 \qquad (4\text{-}33)$$

and

$$\nu\ \eta_{6,1} = \underbrace{\sum_{t=-\infty}^{\infty}\ \sum_{s=-\infty}^{\infty}}_{tN+sN'\neq 0}\ \nu\ \eta_{6,1,t,s}$$

$$= -\underbrace{\sum_{t=-\infty}^{\infty}\ \sum_{s=-\infty}^{\infty}}_{tN+sN'\neq 0}\ \frac{1}{t\bar{n}+sn'}\int\Big[\mathrm{Re}\Big\{\Big[\sum_{k=1}^{5}(\bar{\lambda},\bar{a}_k)\ \frac{\partial}{\partial\bar{a}_k}\ \bar{\psi}_{t,s} +$$

$$+ (\bar{\lambda},\bar{p})\bar{P}_{t,s} + (\bar{\lambda},\bar{q})\bar{Q}_{t,s}\ \Big]\ e^{j\bar{\phi}_{t,s}}\Big\} + \frac{3}{2}\ \frac{\bar{n}}{\bar{a}}\ \nu\ \eta_{1,1,t,s}\Big]d\bar{\phi}_{t,s} \qquad (4\text{-}34)$$

where

$$\begin{bmatrix}\Delta a\\ \Delta h\\ \Delta k\\ \Delta p\\ \Delta q\\ \Delta\lambda\end{bmatrix} = \begin{bmatrix}\nu\eta_{1,1}\\ \nu\eta_{2,1}\\ \nu\eta_{3,1}\\ \nu\eta_{4,1}\\ \nu\eta_{5,1}\\ \nu\eta_{6,1}\end{bmatrix} \qquad (4\text{-}35)$$

and

$$\Delta a_i = a_i - \bar{a}_i \qquad i = 1,\ldots,6 \tag{4-36}$$

Notice that eq. (4-34) has taken into account that the Poisson bracket $(\bar{\lambda},\bar{\lambda})$ is equal to zero. A simplification of notation can be achieved by defining the slowly varying complex quantities

$$M_{i,t,s} = -\sum_{k=1}^{5} (\bar{a}_i,\bar{a}_k) \frac{\partial}{\partial \bar{a}_k} \bar{\psi}_{t,s} - (\bar{a}_i,\bar{\lambda})\ jt\ \bar{\psi}_{t,s} - (\bar{a}_i,\bar{p})\ \bar{P}_{t,s} - (\bar{a}_i,\bar{q})\ \bar{Q}_{t,s}$$

$$i = 1,\ldots,5 \tag{4-37}$$

and

$$M_{6,t,s} = -\sum_{k=1}^{5} (\bar{\lambda},\bar{a}_k) \frac{\partial}{\partial \bar{a}_k} \bar{\psi}_{t,s} - (\bar{\lambda},\bar{p})\bar{P}_{t,s} - (\bar{\lambda},\bar{q})\bar{Q}_{t,s} \tag{4-38}$$

Eqs. (4-33) and (4-34) may then be rewritten as

$$\nu\, \eta_{i,1} = \underbrace{\sum_{t=-\infty}^{\infty} \sum_{s=-\infty}^{\infty}}_{tN+sN' \neq 0} \frac{1}{t\bar{n}+sn'} \int \mathrm{Re}\{M_{i,t,s}\, e^{j\bar{\phi}_{t,s}}\}\, d\bar{\phi}_{t,s}$$

$$i = 1,\ldots,5 \qquad (4\text{-}39)$$

and

$$\nu\, \eta_{6,1} = \underbrace{\sum_{t=-\infty}^{\infty} \sum_{s=-\infty}^{\infty}}_{tN+sN' \neq 0} \frac{1}{t\bar{n}+sn'} \int \left[\mathrm{Re}\{M_{6,t,s}\, e^{j\bar{\phi}_{t,s}}\} - \right.$$

$$\left. - \frac{3}{2} \frac{\bar{n}}{\bar{a}}\, \nu\, \eta_{1,1,t,s}\right] d\bar{\phi}_{t,s} \qquad (4\text{-}40)$$

Expressions for the periodic variations in the five slowly varying satellite elements are obtained by the straightforward integration of eq. (4-39). The result is:

$$\nu\,\eta_{i,1} = -\underbrace{\sum_{t=-\infty}^{\infty}\sum_{s=-\infty}^{\infty}}_{tN+sN'\neq 0} \frac{1}{\bar{tn}+sn'} \operatorname{Re}\{j\,M_{i,t,s}\,e^{j\bar{\phi}_{t,s}}\}$$

$$i = 1,\ldots,5 \qquad (4\text{-}41)$$

The periodic correction for the satellite mean longitude is determined in two steps. From eq. (4-41), one finds,

$$\nu\,\eta_{1,1,t,s} = -\frac{1}{\bar{tn}+sn'} \operatorname{Re}\{j\,M_{1,t,s}\,e^{j\bar{\phi}_{t,s}}\}$$

(4-42)

Substituting eq. (4-42) into eq. (4-40) and integrating,

$$\nu\,\eta_{6,1} = \frac{3}{2}\,\frac{\bar{n}}{\bar{a}} \underbrace{\sum_{t=-\infty}^{\infty}\sum_{s=-\infty}^{\infty}}_{tN+sN'\neq 0} \frac{1}{(t\bar{n}+sn')^2}\,\mathrm{Re}\{M_{1,t,s}\,e^{j\bar{\phi}_{t,s}}\} -$$

$$-\underbrace{\sum_{t=-\infty}^{\infty}\sum_{s=-\infty}^{\infty}}_{tN+sN'\neq 0} \frac{1}{t\bar{n}+sn'}\,\mathrm{Re}\{j\,M_{6,t,s}\,e^{j\bar{\phi}_{t,s}}\} \qquad (4\text{-}43)$$

Eqs. (4-41) and (4-43) can be rewritten by breaking $M_{i,t,s}$ into its real and imaginary parts, viz.,

$$M_{i,t,s} = \mathrm{Re}(M_{i,t,s}) + j\,\mathrm{Im}(M_{i,t,s}) \qquad (4\text{-}44)$$

and by recalling that

$$e^{j\bar{\phi}_{t,s}} = \cos\bar{\phi}_{t,s} + j\sin\bar{\phi}_{t,s} \qquad (4\text{-}45)$$

After performing the complex multiplications and extracting the real part, one obtains,

$$\nu\ \eta_{i,1} = \underbrace{\sum_{t=-\infty}^{\infty}\ \sum_{s=-\infty}^{\infty}}_{tN+sN'\neq 0} \left\{ \frac{\mathrm{Im}(M_{i,t,s})}{t\bar{n}+sn'} \cos\bar{\phi}_{t,s} + \right.$$

$$\left. + \frac{\mathrm{Re}(M_{i,t,s})}{t\bar{n}+sn'} \sin\bar{\phi}_{t,s} \right\}$$

$$i = 1,\ldots,5 \qquad (4\text{-}46)$$

and

$$\nu\ \eta_{6,1} = \underbrace{\sum_{t=-\infty}^{\infty}\ \sum_{s=-\infty}^{\infty}}_{tN+sN'\neq 0} \left\{ \frac{\frac{3}{2}\ \frac{\bar{n}}{\bar{a}}\ \frac{\mathrm{Re}(M_{1,t,s})}{t\bar{n}+sn'} + \mathrm{Im}(M_{6,t,s})}{t\bar{n} + sn'} \cdot \right.$$

$$\left. \cdot \cos\bar{\phi}_{t,s} + \frac{-\frac{3}{2}\ \frac{\bar{n}}{\bar{a}}\ \frac{\mathrm{Im}(M_{1,t,s})}{t\bar{n}+sn'} + \mathrm{Re}(M_{6,t,s})}{t\bar{n} + sn'} \sin\bar{\phi}_{t,s} \right\}$$

$$(4\text{-}47)$$

The problem of third body perturbations, as formulated in two fast variables, is analogous to the problem of non-spherical central body perturbations, as formulated in terms of the satellite mean longitude and the Greenwich hour angle. The common structure shared by the two problems can be exploited to simplify the computational flow of a software package that includes both perturbations. Accordingly, eqs. (4-46) and (4-47) may be cast into three distinct classes of short periodic functions, the forms of which are mathematically identical to those found in the central body problem. The results are:

Zonal analogs; $t \neq 0$, $s = 0$

$$[\nu n_{i,1}]_{zonals} = \sum_{t=1}^{\infty} \{\bar{C}_{i,t,0} \cos \bar{\phi}_{t,0} + \bar{S}_{i,t,0} \sin \bar{\phi}_{t,0}\}$$

$$i = 1,\ldots,6 \qquad (4\text{-}48)$$

where

$$\bar{\phi}_{t,0} = t\bar{\lambda} \qquad (4\text{-}49)$$

and

$$\left.\begin{aligned} \bar{C}_{i,t,0} &= \frac{1}{t\bar{n}} \left[\mathrm{Im}(M_{i,t,0}) - \mathrm{Im}(M_{i,-t,0})\right] \\ \bar{S}_{i,t,0} &= \frac{1}{t\bar{n}} \left[\mathrm{Re}(M_{i,t,0}) + \mathrm{Re}(M_{i,-t,0})\right] \end{aligned}\right\} \quad i = 1,\ldots,5 \qquad (4\text{-}50)$$

$$\bar{C}_{6,t,0} = \frac{1}{t\bar{n}} \left[\frac{3}{2} \frac{\bar{n}}{\bar{a}} \frac{\mathrm{Re}(M_{1,t,0}) - \mathrm{Re}(M_{1,-t,0})}{t\bar{n}} + \right.$$

$$\left. + \mathrm{Im}(M_{6,t,0}) - \mathrm{Im}(M_{6,-t,0}) \right] \qquad (4\text{-}51)$$

$$\bar{S}_{6,t,0} = \frac{1}{t\bar{n}} \left[-\frac{3}{2} \frac{\bar{n}}{\bar{a}} \frac{\mathrm{Im}(M_{1,t,0}) + \mathrm{Im}(M_{1,-t,0})}{t\bar{n}} + \right.$$

$$\left. + \mathrm{Re}(M_{6,t,0}) + \mathrm{Re}(M_{6,-t,0}) \right] \qquad (4\text{-}52)$$

<u>s-monthly or s-yearly terms; t = 0, s ≠ 0</u>

$$[\nu\ \eta_{i,1}]_{s\text{-}''\ ''} = \sum_{s=1}^{\infty} \{\bar{C}_{i,0,s} \cos \bar{\phi}_{0,s} + \bar{S}_{i,0,s} \sin \bar{\phi}_{0,s}\}$$

$$i = 1,\ldots,6 \qquad (4\text{-}53)$$

where

$$\bar{\phi}_{0,s} = s\lambda' \tag{4-54}$$

and

$$\bar{C}_{1,0,s} = \frac{1}{sn'} \left[\mathrm{Im}(M_{1,0,s}) - \mathrm{Im}(M_{1,0,-s}) \right] = 0 \tag{4-55}$$

$$\bar{S}_{1,0,s} = \frac{1}{sn'} \left[\mathrm{Re}(M_{1,0,s}) + \mathrm{Re}(M_{1,0,-s}) \right] = 0 \tag{4-56}$$

$$\left.\begin{aligned} \bar{C}_{i,0,s} &= \frac{1}{sn'} \left[\mathrm{Im}(M_{i,0,s}) - \mathrm{Im}(M_{i,0,-s}) \right] \\ \bar{S}_{i,0,s} &= \frac{1}{sn'} \left[\mathrm{Re}(M_{i,0,s}) + \mathrm{Re}(M_{i,0,-s}) \right] \end{aligned}\right\} i = 2,\ldots,6 \tag{4-57}$$

Tesseral analogs; $t \neq 0$, $s \neq 0$

$$[\nu\ \eta_{i,1}]_{\text{tesseral}} = \underbrace{\sum_{t=-\infty,\ t\neq 0}^{\infty} \sum_{s=1}^{\infty}}_{tN-sN' \neq 0} \{\bar{C}_{i,t,s} \cos \bar{\phi}_{t,-s} + \bar{S}_{i,t,s} \sin \bar{\phi}_{t,-s}\} \qquad i = 1,\ldots,6 \qquad (4\text{-}58)$$

where

$$\bar{\phi}_{t,-s} = t\bar{\lambda} - s\lambda' \qquad (4\text{-}59)$$

and

$$\left.\begin{aligned} \bar{C}_{i,t,s} &= \frac{1}{t\bar{n}-sn'} \left[\mathrm{Im}(M_{i,t,-s}) - \mathrm{Im}(M_{i,-t,s}) \right] \\ \bar{S}_{i,t,s} &= \frac{1}{t\bar{n}-sn'} \left[\mathrm{Re}(M_{i,t,-s}) + \mathrm{Re}(M_{i,-t,s}) \right] \end{aligned}\right\} i=1,\ldots,5 \qquad (4\text{-}60)$$

$$\bar{C}_{6,t,s} = \frac{1}{t\bar{n}-sn'} \left[\frac{3}{2} \frac{\bar{n}}{\bar{a}} \frac{Re(M_{1,t,-s}) - Re(M_{1,-t,s})}{t\bar{n} - sn'} + \right.$$

$$\left. + Im(M_{6,t,-s}) - Im(M_{6,-t,s}) \right]$$

(4-61)

$$\bar{S}_{6,t,s} = \frac{1}{t\bar{n}-sn'} \left[-\frac{3}{2} \frac{\bar{n}}{\bar{a}} \frac{Im(M_{1,t,-s}) + Im(M_{1,-t,s})}{t\bar{n} - sn'} + \right.$$

$$\left. + Re(M_{6,t,-s}) + Re(M_{6,-t,s}) \right]$$

(4-62)

The union of the three classes of short periodic functions just described exactly reproduces eqs. (4-46) and (4-47). Eqs. (4-48), (4-53) and (4-58) are Fourier expansions of the periodic variations for the third body problem. The expansion coefficients $\bar{C}$ and $\bar{S}$ are functions of only the slowly varying elements of the satellite and the disturbing body. This property allows the coefficients to be calculated explicitly on the integration grid of the averaged orbit generator and interpolated at any intermediate times. The form of the Fourier series

developed for the third body perturbation problem is compatible with interpolator software already created by Early [24] for the central body theory so that implementation is straightforward.

4.3 Formulation of the Third Body Theory for Numerical Computation

Sections 4.1 and 4.2 described the formal representations of the third body averaged equations of motion and the short periodic functions. However, a numerical implementation of an averaged orbit prediction theory requires a detailed knowledge of the quantities to be computed and an efficient methodology for their computation. For third body perturbations, this entails an understanding of the properties of the complex function $\bar{\psi}_{t,s}$ and its partial derivatives with respect to satellite related quantities. It also involves establishing the functional form of the partial derivatives of the third body mean longitude, λ', with respect to the mean equinoctial $\bar{p},\bar{q}$ elements of the satellite. The nature of $\bar{\psi}_{t,s}$ will be considered first.

For convenience, $\bar{\psi}_{t,s}$ is restated here

$$\bar{\psi}_{t,s} = \frac{\mu'}{\bar{a}'} \sum_{n=2}^{\infty} \left(\frac{\bar{a}}{\bar{a}'}\right)^n \sum_{m=0}^{n} K_m V_{n,m} \sum_{r=-n}^{n} V_{n,r}^{m} S_{2n}^{(m,r)}(\alpha,\beta,\gamma) \cdot$$

$$\cdot Y_s^{-n-1,r}\,[k'(\bar{p},\bar{q}),\ h'(\bar{p},\bar{q})]\ Y_t^{n,-m}\,(\bar{k},\bar{h}) \qquad (4\text{-}63)$$

The complex factors of $\bar{\psi}_{t,s}$ are imbedded in the inclination function $S_{2n}^{(m,r)}$ and the Hansen coefficients $Y_s^{-n-1,r}$ and $Y_t^{n,-m}$. The S function may be formally broken into its real and imaginary parts to yield the expression,

$$S_{2n}^{(m,r)}(\alpha,\beta,\gamma) = [C_m^r(\alpha,\beta) + j\, D_m^r(\alpha,\beta)]\,\Lambda(\gamma) \qquad (4\text{-}64)$$

where depending on the relationship of r to m, one of the following definitions is used

$$S_{2n}^{(m,r)} = \underbrace{(\alpha+j\beta I')^{I'm-r}}_{C_m^r+jD_m^r} \underbrace{(I')^r 2^r (1+I'\gamma)^{-I'm} P_{n+r}^{(m-r,-m-r)}(\gamma)}_{\Lambda(\gamma)}$$

$$r \leq -m \qquad (4\text{-}65)$$

$$S_{2n}^{(m,r)} = (\alpha+j\beta)^{m-I'r} (I')^r 2^{-m} \frac{(n+m)!(n-m)!}{(n+r)!(n-r)!} (1+I'\gamma)^{I'r} \cdot$$

$$\cdot \underbrace{\underbrace{P_{n-m}^{(m-r,r+m)}(\gamma)}_{\Lambda(\gamma)}}_{C_m^r+jD_m^r}$$

$$-m \leq r \leq m \qquad (4\text{-}66)$$

$$S_{2n}^{(m,r)} = \underbrace{(\alpha-j\beta I')^{r-I'm}}_{C_m^r + jD_m^r} \underbrace{(I')^r (-1)^{m-r} 2^{-r} (1+I'\gamma)^{I'm} P_{n-r}^{(r-m,r+m)}}_{\Lambda(\gamma)}$$

$$r \geq m \qquad (4\text{-}67)$$

The third body Hansen coefficient may be broken into the product of a complex polynomial in h' and k' and a purely real power series in the square of the disturbing body orbital eccentricity, viz.,

$$Y_s^{-n-1,r} = (k' - j\eta'h')^{|r-s|} K_s^{-n-1,r} \qquad (4\text{-}68)$$

where

$$K_s^{-n-1,r} = \sum_{i=0}^{\infty} X^{-n-1,r}_{i+\frac{|q|+q}{2},\, i+\frac{|q|+q}{2}} e'^{2i} \tag{4-69}$$

$$q = s - r \tag{4-70}$$

$$\eta' = \text{sign}(q) \tag{4-71}$$

The expansion coefficients, X, are the Newcomb operators. Their computation and storage are discussed in detail in Appendix A. The satellite Hansen coefficients have the similar form

$$Y_t^{n,-m} = (\bar{k} - j\eta\bar{h})^{|-m-t|} K_t^{n,-m} \tag{4-72}$$

where

$$K_t^{n,-m} = \sum_{i=0}^{\infty} X^{n,-m}_{i+\frac{|q|+q}{2},\, i+\frac{|q|-q}{2}} \bar{e}^{\,2i} \tag{4-73}$$

$$q = t + m \tag{4-74}$$

$$n = \text{sign}(q) \tag{4-75}$$

Substituting eqs. (4-64), (4-68) and (4-72) into the expression for $\bar{\psi}_{t,s}$ yields

$$\bar{\psi}_{t,s} = \frac{\mu'}{a'} \sum_{n=2}^{\infty} \left(\frac{\bar{a}}{a'}\right)^n \sum_{m=0}^{n} K_m V_{n,m} \sum_{r=-n}^{n} V_{n,r}^m \Lambda(\gamma) \cdot$$

$$\cdot K_s^{-n-1,r} K_t^{n,-m} \{(C_m^r + j D_m^r)(k' - jn'h')^{|r-s|} \cdot$$

$$\cdot (\bar{k} - jn\bar{h})^{|-m-t|}\} \tag{4-76}$$

If the designation is made

$$A^{r,m}_{s,t} + j\, B^{r,m}_{s,t} = (k' - j\eta' h')^{|r-s|}\ (\bar{k} - j\eta\bar{h})^{|-m-t|}$$

(4-77)

and the complex multiplication in eq. (4-76) is performed, then $\bar{\psi}_{t,s}$ is seen to have the form

$$\bar{\psi}_{t,s} = \frac{\mu'}{a'} \sum_{n=2}^{\infty} \left(\frac{\bar{a}}{a'}\right)^n \sum_{m=0}^{n} K_m\, V_{n,m} \sum_{r=-n}^{n} V^m_{n,r}\ \Lambda(\gamma) \cdot$$

$$\cdot\ K_s^{-n-1,r}\ K_t^{n,-m}\ \{(A^{r,m}_{s,t}\ C^r_m - B^{r,m}_{s,t}\ D^r_m) +$$

$$+\ j(B^{r,m}_{s,t}\ C^r_m + A^{r,m}_{s,t}\ D^r_m)\}$$

(4-78)

If $V_{n,m}$ and $V^m{}_{n,r}$ are grouped into the aggregate function

$$Z^m_{n,r} = V_{n,m}\ V^m_{n,r} \qquad (4\text{-}79)$$

then eq. (4-78) becomes

$$\bar{\psi}_{t,s} = \frac{\mu'}{a'} \sum_{n=2}^{\infty} \left(\frac{\bar{a}}{a'}\right)^n \sum_{m=0}^{n} K_m \sum_{r=-n}^{n} Z_{n,r}^{m} \Lambda(\gamma) K_s^{-n-1,r} \cdot$$

$$\cdot K_t^{n,-m} \{(A_{s,t}^{r,m} C_m^r - B_{s,t}^{r,m} D_m^r) + j(B_{s,t}^{r,m} C_m^r + A_{s,t}^{r,m} D_m^r)\}$$

(4-80)

The final form of $\bar{\psi}_{t,s}$ is shaped by practical considerations. The Jacobi polynomial embedded in $\Lambda(\gamma)$ is governed by a recurrence relation which will soon be introduced. It is advantageous to ensure that the recurrence is employed to compute Jacobi polynomials in the direction of increasing subscript, since it is for that direction that convenient starting values can be determined. Accordingly, the summations of eq. (4-80) are reordered so that the summation over n is innermost. Furthermore, for the purposes of a numerical program, the indices must be restricted to run over finite ranges. Hence, the form of $\bar{\psi}_{t,s}$ used in the numerical implementation is

$$\bar{\psi}_{t,s} = \frac{\mu'}{a'^{\tau}} \sum_{r=R_1}^{R_2} \sum_{m=0}^{M} K_m \sum_{n=\max(2,m,|r|)}^{N} (\bar{a}/a')^n \, Z^m_{n,r} \, \Lambda(\gamma) \cdot$$

$$\cdot K_s^{-n-1,r} \, K_t^{n,-m} \, \{(A^{r,m}_{s,t} \, C^r_m - B^{r,m}_{s,t} \, D^r_m) + j(B^{r,m}_{s,t} \, C^r_m + A^{r,m}_{s,t} \, D^r_m)\}$$

(4-81)

The software implementation of the third body theory requires the following partial derivatives:

$\bar{a}$ partial

$$\bar{a} \frac{\partial \bar{\psi}_{t,s}}{\partial \bar{a}} = \frac{\mu'}{a'^{\tau}} \sum_{r=R_1}^{R_2} \sum_{m=0}^{M} K_m \sum_{n=\max(2,m,|r|)}^{N} n \, (\bar{a}/a')^n \cdot$$

$$\cdot Z^m_{n,r} \, \Lambda(\gamma) \, K_s^{-n-1,r} \, K_t^{n,-m} \cdot$$

$$\cdot \{(A^{r,m}_{s,t} \, C^r_m - B^{r,m}_{s,t} \, D^r_m) + j(B^{r,m}_{s,t} \, C^r_m + A^{r,m}_{s,t} \, D^r_m)\}$$

(4-82)

$\bar{h}$ partial

$$\frac{\partial \bar{\psi}_{t,s}}{\partial \bar{h}} = \frac{\mu'}{a'} \sum_{r=R_1}^{R_2} \sum_{m=0}^{M} K_m \sum_{n=\max(2,m,|r|)}^{N} (\bar{a}/a')^n \, Z_{n,r}^m \, \Lambda(\gamma) \cdot$$

$$\cdot K_s^{-n-1,r} \Big[2\bar{h} \frac{dK_t^{n,-m}}{d\bar{e}^2} \{(A_{s,t}^{r,m} C_m^r - B_{s,t}^{r,m} D_m^r) +$$

$$+ j(B_{s,t}^{r,m} C_m^r + A_{s,t}^{r,m} D_m^r)\} +$$

$$+ K_t^{n,-m} \{(\frac{\partial A_{s,t}^{r,m}}{\partial \bar{h}} C_m^r - \frac{\partial B_{s,t}^{r,m}}{\partial \bar{h}} D_m^r) + j(\frac{\partial B_{s,t}^{r,m}}{\partial \bar{h}} C_m^r + \frac{\partial A_{s,t}^{r,m}}{\partial \bar{h}} D_m^r)\}\Big]$$

(4-83)

Eq. (4-83) has been derived by employing the relation

$$\frac{\partial K_t^{n,-m}}{\partial \bar{h}} = \frac{d K_t^{n,-m}}{d \bar{e}^2} \frac{\partial \bar{e}^2}{\partial \bar{h}} \qquad (4\text{-}84)$$

where

$$\frac{\partial \bar{e}^{\,2}}{\partial \bar{h}} = \frac{\partial}{\partial \bar{h}} (\bar{h}^{\,2} + \bar{k}^{\,2}) = 2\bar{h} \qquad (4\text{-}85)$$

$\bar{k}$ partial

$$\frac{\partial \bar{\psi}_{t,s}}{\partial \bar{k}} = \frac{\mu'}{a'} \sum_{r=R_1}^{R_2} \sum_{m=0}^{M} K_m \sum_{n=\max(2,m,|r|)}^{N} (\bar{a}/a')^n Z_{n,r}^{m} \Lambda(\gamma) \cdot$$

$$\cdot K_s^{-n-1,r} \left[2\bar{k} \frac{dK_t^{n,-m}}{d\bar{e}^{\,2}} \{(A_{s,t}^{r,m} C_m^r - B_{s,t}^{r,m} D_m^r) + \right.$$

$$+ j(B_{s,t}^{r,m} C_m^r + A_{s,t}^{r,m} D_m^r) +$$

$$\left. + K_t^{n,-m} \{(\frac{\partial A_{s,t}^{r,m}}{\partial \bar{k}} C_m^r - \frac{\partial B_{s,t}^{r,m}}{\partial \bar{k}} D_m^r) + j(\frac{\partial B_{s,t}^{r,m}}{\partial \bar{k}} C_m^r + \frac{\partial A_{s,t}^{r,m}}{\partial \bar{k}} D_m^r)\}\right]$$

(4-86)

α partial

$$\frac{\partial \bar{\psi}_{t,s}}{\partial \alpha} = \frac{\mu'}{a'} \sum_{r=R_1}^{R_2} \sum_{m=0}^{M} K_m \sum_{n=\max(2,m,|r|)}^{N} (\bar{a}/a')^n \, Z_{n,r}^m \, \Lambda(\gamma) \cdot$$

$$\cdot K_s^{-n-1,r} \, K_t^{n,-m} \{ \left(A_{s,t}^{r,m} \frac{\partial C_m^r}{\partial \alpha} - B_{s,t}^{r,m} \frac{\partial D_m^r}{\partial \alpha} \right) +$$

$$+ j \left(B_{s,t}^{r,m} \frac{\partial C_m^r}{\partial \alpha} + A_{s,t}^{r,m} \frac{\partial D_m^r}{\partial \alpha} \right) \}$$

(4-87)

β partial

$$\frac{\partial \bar{\psi}_{t,s}}{\partial \beta} = \frac{\mu'}{a'} \sum_{r=R_1}^{R_2} \sum_{m=0}^{M} K_m \sum_{n=\max(2,m,|r|)}^{N} (\bar{a}/a')^n \; Z_{n,r}^{m} \; \Lambda(\gamma) \cdot$$

$$\cdot K_s^{-n-1,r} \; K_t^{n,-m} \; \{ \left(A_{s,t}^{r,m} \frac{\partial C_m^r}{\partial \beta} - B_{s,t}^{r,m} \frac{\partial D_m^r}{\partial \beta} \right) +$$

$$+ j \left(B_{s,t}^{r,m} \frac{\partial C_m^r}{\partial \beta} + A_{s,t}^{r,m} \frac{\partial D_m^r}{\partial \beta} \right) \}$$

(4-88)

γ partial

$$\frac{\partial \overline{\psi}_{t,s}}{\partial \gamma} = \frac{\mu'}{a'} \sum_{r=R_1}^{R_2} \sum_{m=0}^{M} K_m \sum_{n=\max(2,m,|r|)}^{N} (\bar{a}/a')^n \, Z_{n,r}^m \, \frac{d\Lambda}{d\gamma} \cdot$$

$$\cdot K_s^{-n-1,r} \, K_t^{n,-m} \{ (A_{s,t}^{r,m} \, C_m^r - B_{s,t}^{r,m} \, D_m^r) +$$

$$+ j(B_{s,t}^{r,m} \, C_m^r + A_{s,t}^{r,m} \, D_m^r) \}$$

(4-89)

h' partial

$$\frac{\partial \bar{\psi}_{t,s}}{\partial h'} = \frac{\mu'}{a'} \sum_{r=R_1}^{R_2} \sum_{m=0}^{M} K_m \sum_{n=\max(2,m,|r|)}^{N} (\bar{a}/a')^n \, Z_{n,r}^{m} \, \Lambda(\gamma) \cdot$$

$$\cdot K_t^{n,-m} \Big[2h' \frac{dK_s^{-n-1,r}}{de'^2} \{ (A_{s,t}^{r,m} C_m^r - B_{s,t}^{r,m} D_m^r) +$$

$$+ j(B_{s,t}^{r,m} C_m^r + A_{s,t}^{r,m} D_m^r) \} +$$

$$+ K_s^{-n-1,r} \{ (\frac{\partial A_{s,t}^{r,m}}{\partial h'} C_m^r - \frac{\partial B_{s,t}^{r,m}}{\partial h'} D_m^r) + j(\frac{\partial B_{s,t}^{r,m}}{\partial h'} C_m^r \frac{\partial A_{s,t}^{r,m}}{\partial h'} D_m^r \} \Big]$$

(4-90)

k' partial

$$\frac{\partial \bar{\psi}_{t,s}}{\partial k'} = \frac{\mu'}{a'} \sum_{r=R_1}^{R_2} \sum_{m=0}^{M} K_m \sum_{n=\max(2,m,|r|)}^{N} (\bar{a}/a')^n \, Z_{n,r}^m \, \Lambda(\gamma) \cdot$$

$$\cdot K_t^{n,-m} \left[2k' \frac{dK_s^{-n-1,r}}{de'^2} \{(A_{s,t}^{r,m} C_m^r - B_{s,t}^{r,m} D_m^r) + \right.$$

$$+ j(B_{s,t}^{r,m} C_m^r + A_{s,t}^{r,m} D_m^r)\} +$$

$$+ K_s^{-n-1,r} \{(\frac{\partial A_{s,t}^{r,m}}{\partial k'} C_m^r - \frac{\partial B_{s,t}^{r,m}}{\partial k'} D_m^r) +$$

$$\left. + j(\frac{\partial B_{s,t}^{r,m}}{\partial k'} C_m^r + \frac{\partial A_{s,t}^{r,m}}{\partial k'} D_m^r)\} \right]$$

(4-91)

In view of eqs. (4-7) through (4-10), the following auxiliary partial derivatives are also required:

$$\frac{\partial h'}{\partial \bar{p}} = \frac{2}{\bar{c}} \frac{1}{(1+I'\gamma)} \{-\alpha I'h' + \alpha(\hat{g} \cdot \underline{e}') - \beta(\hat{f} \cdot \underline{e}')\} +$$

$$+ \frac{2}{\bar{c}} I\, I'\, \bar{q}\, k' \qquad (4\text{-}92)$$

where

$$\bar{c} = 1 + \bar{p}^{\,2} + \bar{q}^{\,2} \qquad (4\text{-}93)$$

$$\frac{\partial h'}{\partial \bar{q}} = \frac{2}{\bar{c}} I\, I' \{(1 - I'\gamma)(\hat{w} \cdot \underline{e}') - \bar{p}\, k'\} +$$

$$+ \frac{2}{\bar{c}} \frac{I\, I'}{1+I'\gamma} \{\beta h' - \gamma[\alpha(\hat{f} \cdot \underline{e}') + \beta(\hat{g} \cdot \underline{e}')]\} \qquad (4\text{-}94)$$

$$\frac{\partial k'}{\partial \bar{p}} = \frac{2}{\bar{c}} \frac{1}{1+I'\gamma} \{-\alpha I'k' + \gamma[\alpha(\hat{f} \cdot \underline{e}') + \beta(\hat{g} \cdot \underline{e}')]\} -$$

$$- \frac{2}{\bar{c}} \{(1 - I'\gamma)(\hat{w} \cdot \underline{e}') + I\, I'\, \bar{q}\, h'\} \qquad (4\text{-}95)$$

$$\frac{\partial k'}{\partial \bar{q}} = \frac{2}{\bar{c}} \frac{I\, I'}{(1+I'\gamma)} \{\beta k' + \alpha(\hat{g} \cdot \underline{e}') - \beta(\hat{f} \cdot \underline{e}')\} +$$

$$+ \frac{2}{\bar{c}} I\, I'\, \bar{p}\, h' \qquad (4\text{-}96)$$

and [17]

$$\frac{\partial \alpha}{\partial \bar{p}} = -\frac{2}{\bar{c}} [\bar{q}\, I\, \beta + \gamma] \qquad (4\text{-}97)$$

$$\frac{\partial \alpha}{\partial \bar{q}} = \frac{2}{\bar{c}} I\, \bar{p}\, \beta \qquad (4\text{-}98)$$

$$\frac{\partial \beta}{\partial \bar{p}} = \frac{2}{\bar{c}} I\, \bar{q}\, \alpha \qquad (4\text{-}99)$$

$$\frac{\partial \beta}{\partial \bar{q}} = -\frac{2}{\bar{c}} I\, (\bar{p}\alpha - \gamma) \qquad (4\text{-}100)$$

$$\frac{\partial \gamma}{\partial \bar{p}} = \frac{2}{\bar{c}} \alpha \qquad (4\text{-}101)$$

$$\frac{\partial \gamma}{\partial \bar{q}} = -\frac{2}{\bar{c}} I\beta \qquad (4\text{-}102)$$

The partial derivatives of the third body mean longitude with respect to the mean satellite elements $\bar{p}$ and $\bar{q}$ are determined as follows. The functional dependence of λ' may be given by,

$$\lambda' = \lambda'[(\underline{r}')_s, (\underline{v}')_s] \tag{4-103}$$

where $(\underline{r}')_s$ and $(\underline{v}')_s$ are the third body position and velocity vectors in the satellite frame coordinates. By the chain rule, the partial derivatives of λ' with respect to $\bar{p}$ and $\bar{q}$ have the form

$$\frac{\partial \lambda'}{\partial \bar{p}} = \left[\frac{\partial \lambda'}{\partial (\underline{r}')_s}\right]^T \frac{\partial (\underline{r}')_s}{\partial \bar{p}} + \left[\frac{\partial \lambda'}{\partial (\underline{v}')_s}\right]^T \frac{\partial (v')_s}{\partial \bar{p}}$$

(4-104)

and

$$\frac{\partial \lambda'}{\partial \bar{q}} = \left[\frac{\partial \lambda'}{\partial (\underline{r}')_s}\right]^T \frac{\partial (\underline{r}')_s}{\partial \bar{q}} + \left[\frac{\partial \lambda'}{\partial (\underline{v}')_s}\right]^T \frac{\partial (\underline{v}')_s}{\partial \bar{q}}$$

(4-105)

where the superscript denotes the transpose. Since the third body ephemerides are generally available in an inertial coordinate system, eqs. (4-104) and (4-105) are rewritten using the transformation relations:

$$(\underline{r}')_S = [\hat{f} \,\vdots\, \hat{g} \,\vdots\, \hat{w}]^T (\underline{r}')_I \qquad (4\text{-}106)$$

and

$$(\underline{v}')_S = [\hat{f} \,\vdots\, \hat{g} \,\vdots\, \hat{w}]^T (\underline{v}')_I \qquad (4\text{-}107)$$

where $(\underline{r}')_I$ and $(\underline{v}')_I$ are the position and velocity vectors of the third body in inertial coordinates. The result of substituting eqs. (4-106) and (4-107) into eqs. (4-104) and (4-105) is,

$$\frac{\partial \lambda'}{\partial \bar{p}} = \left[\frac{\partial \lambda'}{\partial (\underline{r}')_s}\right]^T \left[\frac{\partial \hat{f}}{\partial \bar{p}} \vdots \frac{\partial \hat{g}}{\partial \bar{p}} \vdots \frac{\partial \hat{w}}{\partial \bar{p}}\right]^T (\underline{r}')_I +$$

$$+ \left[\frac{\partial \lambda'}{\partial (\underline{v}')_s}\right]^T \left[\frac{\partial \hat{f}}{\partial \bar{p}} \vdots \frac{\partial \hat{g}}{\partial \bar{p}} \vdots \frac{\partial \hat{w}}{\partial \bar{p}}\right]^T (\underline{v}')_I \qquad (4\text{-}108)$$

and

$$\frac{\partial \lambda'}{\partial \bar{q}} = \left[\frac{\partial \lambda'}{\partial (\underline{r}')_s}\right]^T \left[\frac{\partial \hat{f}}{\partial \bar{q}} \vdots \frac{\partial \hat{g}}{\partial \bar{q}} \vdots \frac{\partial \hat{w}}{\partial \bar{q}}\right]^T (\underline{r}')_I +$$

$$+ \left[\frac{\partial \lambda'}{\partial (\underline{v}')_s}\right]^T \left[\frac{\partial \hat{f}}{\partial \bar{q}} \vdots \frac{\partial \hat{g}}{\partial \bar{q}} \vdots \frac{\partial \hat{w}}{\partial \bar{q}}\right]^T (\underline{v}')_I \qquad (4\text{-}109)$$

Analytical expressions exist for the partial derivatives of the satellite frame unit vectors with respect to the satellite $\bar{p}$ and $\bar{q}$ elements. As taken from a work by McClain [17] they are,

$$\frac{\partial \hat{f}}{\partial \bar{p}} = -\frac{2}{\bar{c}} \left(\bar{q} \; I \; \hat{g} + \hat{w}\right) \tag{4-110}$$

$$\frac{\partial \hat{f}}{\partial \bar{q}} = \frac{2}{\bar{c}} \; I \; \bar{p} \; \hat{g} \tag{4-111}$$

$$\frac{\partial \hat{g}}{\partial \bar{p}} = \frac{2}{\bar{c}} \; I \; \bar{q} \; \hat{f} \tag{4-112}$$

$$\frac{\partial \hat{g}}{\partial \bar{q}} = -\frac{2}{\bar{c}} \; I\left(\bar{p} \; \hat{f} - \hat{w}\right) \tag{4-113}$$

$$\frac{\partial \hat{w}}{\partial \bar{p}} = \frac{2}{\bar{c}} \; \hat{f} \tag{4-114}$$

$$\frac{\partial \hat{w}}{\partial \bar{q}} = -\frac{2}{\bar{c}} \; I \; \hat{g} \tag{4-115}$$

Making use of eqs. (4-110) through (4-115) leads to Table 4-3. The partial derivatives of the third body mean longitude with respect to the disturbing body position and velocity vectors have closed form representations which are found in a work by Shaver [25]. They are:

Table 4-3. Partial derivatives of the third body mean longitude with respect to the mean satellite elements $\bar{p}, \bar{q}$.

$$\frac{\partial \lambda'}{\partial \bar{p}} = -\frac{2}{\bar{c}}\left\{\left[\frac{\partial \lambda'}{\partial (\underline{r}')_S}\right]^T \left[\bar{q}\,\hat{g} + \hat{w} \;\middle|\; -\bar{q}\,\hat{f} \;\middle|\; -\hat{f}\right]^T (\underline{r}')_I \right.$$

$$\left. + \left[\frac{\partial \lambda'}{\partial (\underline{v}')_S}\right]^T \left[\bar{q}\,\hat{g} + \hat{w} \;\middle|\; -\bar{q}\,\hat{f} \;\middle|\; -\hat{f}\right]^T (\underline{v}')_I \right\} \qquad (4\text{-}116)$$

$$\frac{\partial \lambda'}{\partial \bar{q}} = \frac{2}{\bar{c}}\left\{\left[\frac{\partial \lambda'}{\partial (\underline{r}')_S}\right]^T \left[\bar{p}\,\hat{g} \;\middle|\; -(\bar{p}\,\hat{f} - \hat{w}) \;\middle|\; -\hat{g}\right]^T (\underline{r}')_I \right.$$

$$\left. + \left[\frac{\partial \lambda'}{\partial (\underline{v}')_S}\right]^T \left[\bar{p}\,\hat{g} \;\middle|\; -(\bar{p}\,\hat{f} - \hat{w}) \;\middle|\; -\hat{g}\right]^T (\underline{v}')_I \right\} \qquad (4\text{-}117)$$

$$\frac{\partial \lambda'}{\partial \underline{r}'} = -\frac{\underline{v}'}{n'a'^2} - \frac{\beta'\sqrt{1-h'^2-k'^2}}{n'a'^2}\left[\left(h'\frac{\partial \dot{X}'}{\partial h'} + k'\frac{\partial \dot{X}'}{\partial k'}\right)\hat{f}' + \right.$$

$$\left. + \left(h'\frac{\partial \dot{Y}'}{\partial h'} + k'\frac{\partial \dot{Y}'}{\partial k'}\right)\hat{g}'\right] -$$

$$- \frac{1}{G'}\left(q'\dot{Y}'I' - p'\dot{X}'\right)\hat{w}'$$

(4-118)

and

$$\frac{\partial \lambda'}{\partial \underline{v}'} = -\frac{2}{n'a'^2}\,\underline{r}' + \frac{\beta'\sqrt{1-h'^2-k'^2}}{n'a'^2} \cdot$$

$$\cdot \left[\left(h'\frac{\partial X'}{\partial h'} + k'\frac{\partial X'}{\partial k'}\right)\hat{f}' + \right.$$

$$\left. + \left(h'\frac{\partial Y'}{\partial h'} + k'\frac{\partial Y'}{\partial k'}\right)\hat{g}'\right] + \frac{1}{G'}\left(q'Y'I' - p'X'\right)\hat{w}'$$

(4-119)

where it is understood that all calculations are performed in satellite frame coordinates and [25]

$$\beta' = \frac{1}{1+\sqrt{1-h'^2-k'^2}} \tag{4-120}$$

$$X' = r' \cos L' = \underline{r}' \cdot \hat{f}' \tag{4-121}$$

$$Y' = r' \sin L' = \underline{r}' \cdot \hat{g}' \tag{4-122}$$

$$\dot{X}' = \frac{-n'a'(h' + \sin L')}{\sqrt{1 - h'^2 - k'^2}} \tag{4-123}$$

$$\dot{Y}' = \frac{n'a'(k' + \cos L')}{\sqrt{1 - h'^2 - k'^2}} \tag{4-124}$$

$$G' = n'a'^2 \sqrt{1 - h'^2 - k'^2} \tag{4-125}$$

$$\frac{\partial X'}{\partial h'} = - \frac{k'\beta'\dot{X}'}{n'} + \frac{a'}{G'} Y' \dot{Y}' \tag{4-126}$$

$$\frac{\partial Y'}{\partial h'} = - \frac{k'\beta'\dot{Y}'}{n'} - \frac{a'}{G'} (X'\dot{Y}' + G') \tag{4-127}$$

$$\frac{\partial \dot{X}'}{\partial k'} = \frac{h'\beta'\dot{X}'}{n'} + \frac{a'}{G'}(\dot{X}'Y' - G') \qquad (4\text{-}128)$$

$$\frac{\partial \dot{Y}'}{\partial k'} = \frac{h'\beta'\dot{Y}'}{n'} - \frac{a'}{G'} X' \dot{X}' \qquad (4\text{-}129)$$

$$\frac{\partial \dot{X}'}{\partial h'} = \frac{a'}{G'} \dot{Y}'^{2} + \frac{a'}{r'^{3}\sqrt{1-h'^{2}-k'^{2}}} (G'k'\beta'X' - n'a'Y'^{2})$$

(4-130)

$$\frac{\partial \dot{Y}'}{\partial h'} = -\frac{a'}{G'} \dot{X}'\dot{Y}' + \frac{a'}{r'^{3}\sqrt{1-h'^{2}-k'^{2}}} (G'k'\beta'Y' + n'a'X'Y')$$

(4-131)

$$\frac{\partial \dot{X}'}{\partial k'} = \frac{a'}{G'} \dot{X}'\dot{Y}' - \frac{a'}{r'^{3}\sqrt{1-h'^{2}-k'^{2}}} (G'h'\beta'X' + n'a'X'Y')$$

(4-132)

$$\frac{\partial \dot{Y}'}{\partial k'} = -\frac{a'}{G'} \dot{X}'^{2} - \frac{a'}{r'^{3}\sqrt{1-h'^{2}-k'^{2}}} (G'h'\beta'Y' - n'a'X'^{2})$$

(4-133)

4.4 Calculation of Special Functions

4.4.1 Calculation of $Z^m_{n,r}$

The coefficient $Z^m_{n,r}$ is defined by

$$Z^m_{n,r} = V_{n,m} V^m_{n,r} \tag{4-134}$$

where

$$V_{n,m} = \frac{(n-m)!}{(n+m)!} P_{n,m}(0) \tag{4-135}$$

$$V^m_{n,r} = \frac{(n-r)!}{(n-m)!} P_{n,r}(0) \tag{4-136}$$

and the functions $P_{n,m}(0)$ and $P_{n,r}(0)$ are associated Legendre functions of argument zero. Substituting eqs. (4-135) and (4-136) into eq. (4-134) yields

$$Z^m_{n,r} = \frac{(n-r)!}{(n+m)!} P_{n,m}(0) P_{n,r}(0) \tag{4-137}$$

The indices n and m are constrained to run over only the positive integers. However, the index r may assume both positive and negative values. Hence, there are two cases of eq. (4-137) to consider, those being $r \geq 0$ and $r \leq 0$. A computational form for eq. (4-137) is now determined for positive r. A simple symmetry relation will then be used to compute $Z^{m}_{n,r}$ when r is negative.

$\underline{r \geq 0}$

Eq. (4-137) is written in terms of double factorials [17] by recognizing that

$$P_{n,m}(0) = (-1)^{(n-m)/2} \frac{(n+m-1)!!}{(n-m)!!} \qquad (4\text{-}138)$$

and

$$P_{n,r}(0) = (-1)^{(n-r)/2} \frac{(n+r-1)!!}{(n-r)!!} \qquad (4\text{-}139)$$

where the definition is made

$$(-1)!! = 1 \qquad (4\text{-}140)$$

Substituting eqs. (4-138) and (4-139) into eq. (4-137) yields

$$Z^m_{n,r} = \frac{(n-r)!}{(n+m)!}\,(-1)^{(n-m)/2}\,\frac{(n+m-1)!!}{(n-m)!!}\,(-1)^{(n-r)/2}\,\frac{(n+r-1)!!}{(n-r)!!} \qquad (4\text{-}141)$$

or after simplification

$$\boxed{Z^m_{n,r} = (-1)^{n-[(r+m)/2]}\,\frac{(n-r-1)!!\;(n+r-1)!!}{(n+m)!!\;(n-m)!!} \qquad r \geq 0 \qquad (4\text{-}142)}$$

$r \leq 0$

Replacing r by -r in eq. (4-142) produces the expression

$$Z^{m}_{n,-r} = (-1)^{n+[(r-m)/2]} \frac{(n+r-1)!!\ (n-r-1)!!}{(n+m)!!\ (n-m)!!} \qquad (4\text{-}143)$$

Comparing eq. (4-143) to eq. (4-142) leads immediately to

$$\boxed{Z^{m}_{n,-r} = (-1)^{r} Z^{m}_{n,r} \qquad r \geq 0 \qquad (4\text{-}144)}$$

The coefficient $Z^{m}_{n,r}$ has an interesting property. The exploitation of this property helps to minimize calculations in a numerical program. It is easy to show that the following relations are true

$$P_{n,r}(0) = 0 \ ; \ |n-r| = \text{odd} \qquad (4\text{-}145)$$

and

$$P_{n,m}(0) = 0 \ ; \ |n-m| = \text{odd} \qquad (4\text{-}146)$$

Hence, $Z^{m}_{n,r}$ vanishes if the indices r, m and n are not all even or all odd. Thus the members of the triad (r,m,n) must have the same parity if a term in $\bar{\psi}_{t,s}$ corresponding to that set of indices is to be non-zero.

4.4.2 Calculation of Jacobi Polynomials and Their Partial Derivatives by Recurrence

The function $\Lambda(\gamma)$, the forms of which can be found in eqs. (4-65) through (4-67) depending on the relationship of m to r, contains the orthogonal Jacobi polynomial $P_{\sigma}^{(\varepsilon,\tau)}(\gamma)$, where

$$\left.\begin{aligned} \sigma &= n + r \\ \varepsilon &= m - r \\ \tau &= -m - r \end{aligned}\right\} \qquad r \leq -m \qquad (4\text{-}147)$$

$$\left.\begin{aligned} \sigma &= n - m \\ \varepsilon &= m - r \\ \tau &= r + m \end{aligned}\right\} \qquad -m \leq r \leq m \qquad (4\text{-}148)$$

$$\left.\begin{aligned} \sigma &= n - r \\ \varepsilon &= r - m \\ \tau &= r + m \end{aligned}\right\} \qquad r \geq m \qquad (4\text{-}149)$$

The Jacobi polynomial and its derivative with respect to γ are governed by the standard recurrence relations [16]

$$P_{\sigma+1}^{(\varepsilon,\tau)}(\gamma) = \frac{(a_{2\sigma} + a_{3\sigma}\,\gamma)}{a_{1\sigma}} P_{\sigma}^{(\varepsilon,\tau)}(\gamma) - \frac{a_{4\sigma}}{a_{1\sigma}} P_{\sigma-1}^{(\varepsilon,\tau)}(\gamma) \qquad (4\text{-}150)$$

and

$$\frac{dP_{\sigma+1}^{(\varepsilon,\tau)}}{d\gamma}(\gamma) = \frac{(a_{2\sigma} + a_{3\sigma}\,\gamma)}{a_{1\sigma}} \frac{dP_{\sigma}^{(\varepsilon,\tau)}(\psi)}{d\gamma} + \frac{a_{3\sigma}}{a_{1\sigma}} P_{\sigma}^{(\varepsilon,\tau)}(\gamma) - \frac{a_{4\sigma}}{a_{1\sigma}} \frac{dP_{\sigma-1}^{(\varepsilon,\tau)}(\psi)}{d\gamma} \qquad (4\text{-}151)$$

where

$$a_{1\sigma} = 2(\sigma + 1)(\sigma + \varepsilon + \tau + 1)(2\sigma + \varepsilon + \tau) \quad (4\text{-}152)$$

$$a_{2\sigma} = (2\sigma + \varepsilon + \tau + 1)(\varepsilon^2 - \tau^2) \quad (4\text{-}153)$$

$$a_{3\sigma} = (2\sigma + \varepsilon + \tau)(2\sigma + \varepsilon + \tau + 2)(2\sigma + \varepsilon + \tau + 1) \quad (4\text{-}154)$$

$$a_{4\sigma} = 2(\sigma + \varepsilon)(\sigma + \tau)(2\sigma + \varepsilon + \tau + 2) \quad (4\text{-}155)$$

Starting values for the recurrences are given by the explicit expressions [16]

$$P_0^{(\varepsilon,\tau)} = 1 \tag{4-156}$$

$$P_1^{(\varepsilon,\tau)} = \frac{1}{2}\left[\varepsilon - \tau + (\varepsilon + \tau + 2)\gamma\right] \tag{4-157}$$

$$\frac{P_0^{(\varepsilon,\tau)}}{d\gamma} = 0 \tag{4-158}$$

$$\frac{dP_1^{(\varepsilon,\tau)}}{d\gamma} = 1 + \frac{\varepsilon + \tau}{2} \tag{4-159}$$

4.4.3 Calculation of the Coefficients C_m^r, D_m^r and Their Partial Derivatives by Recurrence

The coefficients C_m^r and D_m^r are defined according to

$$C_m^r + jD_m^r = \begin{cases} (\alpha + j\beta I')^{I'm-r} & ; \ r \leq -m \quad (4\text{-}160) \\ (\alpha + j\beta)^{m-I'r} & ; \ -m \leq r \leq m \quad (4\text{-}161) \\ (\alpha - j\beta I')^{r-I'm} & ; \ r \geq m \quad (4\text{-}162) \end{cases}$$

This section develops recurrence relations for the coefficients C_m^r, D_m^r and their partial derivatives with respect to α and β. Starting values for these recurrences are also determined. The task is simplified by recognizing that eqs. (4-160) through (4-162) can be collapsed into two cases, viz,

$$C_m^r + j\, D_m^r = (\alpha + j\beta I')^{I'm-r} \qquad r \leq I'm \qquad (4\text{-}163)$$

and

$$C_m^r + j\, D_m^r = (\alpha - j\beta I')^{r-I'm} \qquad r \geq I'm \qquad (4\text{-}164)$$

The exponents of the complex polynomials of eqs. (4-163) and (4-164) are greater than or equal to zero. Hence, recurrence relations are required only for increasingly positive exponents. Furthermore, since it has been shown that the indices r and m must have the same parity, recurrence relations should connect coefficients corresponding to exponents that differ by two. This is because the sum or difference of two integers having the same parity must be even. The recurrence relations follow directly:

Case I

For clarity, it is appropriate to rewrite eq. (4-163) as

$$C_{I'm-r} + j\, D_{I'm-r} = (\alpha + j\beta I')^{I'm-r} \quad r \leq I'm \qquad (4\text{-}165)$$

Incrementing I'm-r by 2 leads to

$$C_{(I'm-r)+2} + j\, D_{(I'm-r)+2} = (\alpha + j\beta I')^{(I'm-r)+2}$$

$$= (\alpha + j\beta I')^{I'm-r} (\alpha + j\beta I')^2 \qquad (4\text{-}166)$$

Substituting eq. (4-165) into (4-166)

$$C_{(I'm-r)+2} + j\, D_{(I'm-r)+2} = (C_{I'm-r} + j\, D_{I'm-r}) \cdot$$

$$\cdot [(\alpha^2 - \beta^2) + j\, 2\alpha\, \beta I']$$

(4-167)

Performing the complex multiplication and equating the real and imaginary parts yields the recurrence relations

$$C_{(I'm-r)+2} = (\alpha^2 - \beta^2)\, C_{I'm-r} - 2\alpha\, \beta I'\, D_{I'm-r}$$

(4-168)

$$D_{(I'm-r)+2} = 2\alpha\beta I'\, C_{I'm-r} + (\alpha^2 - \beta^2)\, D_{I'm-r}$$

$$r \leq I'm \qquad (4-169)$$

The recurrences of eq. (4-168) and (4-169) are initialized at the point r = I'm, where

$$\left.\begin{aligned} C_0 &= 1 \\ D_0 &= 0 \end{aligned}\right\} \quad r = I'm \qquad (4\text{-}170),\ (4\text{-}171)$$

Recurrence relations for the partial derivatives of $C_{I'm-r}$ and $D_{I'm-r}$ with respect to α may be found by differentiating eq. (4-165)

$$\frac{\partial C_{I'm-r}}{\partial \alpha} + j \frac{\partial D_{I'm-r}}{\partial \alpha} = (I'm - r)(\alpha + j\beta I')^{I'm-r-1} \qquad (4\text{-}172)$$

Incrementing $I'm - r$ by 2

$$\frac{\partial C_{(I'm-r)+2}}{\partial \alpha} + j \frac{\partial D_{(I'm-r)+2}}{\partial \alpha} = [(I'm-r)+2](\alpha+j\beta I')^{(I'm-r)+1}$$

$$= [(I'm-r)+2](\alpha+j\beta I')^{I'm-r}(\alpha+j\beta I') \qquad (4\text{-}173)$$

Substituting eq. (4-165) into eq. (4-173)

$$\frac{\partial C_{(I'm-r)+2}}{\partial \alpha} + j \frac{\partial D_{(I'm-r)+2}}{\partial \alpha} = [(I'm-r)+2](C_{I'm-r} + jD_{I'm-r})$$

$$\cdot (\alpha + j\beta I')$$

(4-174)

After performing the complex multiplication and equating the real and imaginary parts, one obtains the recurrence relations

$$\frac{\partial C_{(I'm-r)+2}}{\partial \alpha} = [(I'm-r) + 2] (\alpha C_{I'm-r} - \beta I' D_{I'm-r})$$

(4-175)

$$\frac{\partial D_{(I'm-r)+2}}{\partial \alpha} = [(I'm-r) + 2] (\beta I' C_{I'm-r} + \alpha D_{I'm-r})$$

$$r \leq I'm \qquad (4-176)$$

Again, the initialization is found at the point r = I'm

$$\left.\begin{aligned} \frac{\partial C_0}{\partial \alpha} &= 0 \\ \frac{\partial D_0}{\partial \alpha} &= 0 \end{aligned}\right\} \quad r = I'm \qquad (4\text{-}177),\ (4\text{-}178)$$

In similar fashion, the recurrence relations for the partial derivatives with respect to β are given by

$$\frac{\partial C_{(I'm-r)+2}}{\partial \beta} = -I'[(I'm-r) + 2](\beta I' C_{I'm-r} + \alpha D_{I'm-r}) \qquad (4\text{-}179)$$

$$\frac{\partial D_{(I'm-r)+2}}{\partial \beta} = I'[(I'm-r) + 2](\alpha C_{I'm-r} - \beta I' D_{I'm-r}) \qquad (4\text{-}180)$$

$$r \leq I'm$$

with initial conditions

$$\left.\begin{aligned} \frac{\partial C_0}{\partial \beta} &= 0 \\ \frac{\partial D_0}{\partial \beta} &= 0 \end{aligned}\right\} \quad r = I'm \qquad (4\text{-}181),\ (4\text{-}182)$$

Case II

Having rewritten eq. (4-164) as

$$C_{r-I'm} + j\, D_{r-I'm} = (\alpha - j\beta I')^{r-I'm} \qquad r \geq I'm \qquad (4\text{-}183)$$

the recurrence relations for $C_{r-I'm}$ and $D_{r-I'm}$ are found to be

$$C_{(r-I'm)+2} = (\alpha^2 - \beta^2)C_{r-I'm} + 2\alpha\beta I'\, D_{r-I'm} \qquad (4\text{-}184)$$

$$D_{(r-I'm)+2} = -2\alpha\beta I'\, C_{r-I'm} + (\alpha^2 - \beta^2)\, D_{r-I'm}$$

$$r \geq I'm \qquad (4\text{-}185)$$

with the initial values

$$\left.\begin{aligned} C_0 &= 1 \\ D_0 &= 0 \end{aligned}\right\} r = I'm \qquad (4\text{-}186),\ (4\text{-}187)$$

The recurrence relations for the α partial derivatives are given by

$$\frac{\partial C_{(r-I'm)+2}}{\partial \alpha} = [(r-I'm) + 2](\alpha C_{r-I'm} + \beta I' D_{r-I'm}) \qquad (4\text{-}188)$$

$$\frac{\partial D_{(r-I'm)+2}}{\partial \alpha} = [(r-I'm) + 2](-\beta I' C_{r-I'm} + \alpha D_{r-I'm}) \qquad (4\text{-}189)$$

$$r \geq I'm$$

The initialization is furnished by

$$\left.\begin{aligned} \frac{\partial C_0}{\partial \alpha} &= 0 \\ \frac{\partial D_0}{\partial \alpha} &= 0 \end{aligned}\right\} \quad r = I'm \qquad (4\text{-}190),\ (4\text{-}191)$$

Finally, the recurrence relations for the β partial derivatives have the form

$$\frac{\partial C_{(r-I'm)+2}}{\partial \beta} = -I'[(r-I'm)+2](\beta I' C_{r-I'm} - \alpha D_{r-I'm}) \qquad (4\text{-}192)$$

$$\frac{\partial D_{(r-I'm)+2}}{\partial \beta} = -I'[(r-I'm) + 2](\alpha C_{r-I'm} + \beta I' D_{r-I'm}) \qquad (4\text{-}193)$$

$$r \geq I'm$$

The initial values are

$$\left.\begin{aligned} \frac{\partial C_0}{\partial \beta} &= 0 \\ \frac{\partial D_0}{\partial \beta} &= 0 \end{aligned}\right\} \quad r = I'm \qquad (4\text{-}194),\ (4\text{-}195)$$

4.4.4 Calculation of the Coefficients $A_{s,t}^{r,m}$, $B_{s,t}^{r,m}$ and their Partial Derivatives

The definition of the coefficients $A_{s,t}^{r,m}$ and $B_{s,t}^{r,m}$ come from the expression

$$A_{s,t}^{r,m} + jB_{s,t}^{r,m} = (k' - j\eta'h')^{|r-s|}(\bar{k} - j\eta\bar{h})^{|-m-t|} \tag{4-196}$$

where

$$\eta' = \text{sign}(s - r) \tag{4-197}$$

and

$$\eta = \text{sign}(t + m) \tag{4-198}$$

If the following definitions are made

$$e_{|r-s|} + jf_{|r-s|} = (k' - j\eta'h')^{|r-s|} \qquad (4\text{-}199)$$

and

$$g_{|-m-t|} + jh_{|-m-t|} = (\bar{k} - j\eta\bar{h})^{|-m-t|} \qquad (4\text{-}200)$$

then, after performing the complex multiplications and equating the real and imaginary parts, the coefficients $A^{r,m}_{s,t}$ and $B^{r,m}_{s,t}$ are found to be

$$A^{r,m}_{s,t} = e_{|r-s|}\, g_{|-m-t|} - f_{|r-s|}\, h_{|-m-t|} \tag{4-201}$$

$$B^{r,m}_{s,t} = e_{|r-s|}\, h_{|-m-t|} + f_{|r-s|}\, g_{|-m-t|} \tag{4-202}$$

From eq. (4-201) and (4-202), one obtains the following relations

$$\frac{\partial A^{r,m}_{s,t}}{\partial \bar{h}} = e_{|r-s|} \frac{\partial g_{|-m-t|}}{\partial \bar{h}} - f_{|r-s|} \frac{\partial h_{|-m-t|}}{\partial \bar{h}} \tag{4-203}$$

$$\frac{\partial A^{r,m}_{s,t}}{\partial \bar{k}} = e_{|r-s|} \frac{\partial g_{|-m-t|}}{\partial \bar{k}} - f_{|r-s|} \frac{\partial h_{|-m-t|}}{\partial \bar{k}} \tag{4-204}$$

$$\frac{\partial A^{r,m}_{s,t}}{\partial h'} = \frac{\partial e_{|r-s|}}{\partial h'} g_{|-m-t|} - \frac{\partial f_{|r-s|}}{\partial h'} h_{|-m-t|} \tag{4-205}$$

$$\frac{\partial A^{r,m}_{s,t}}{\partial k'} = \frac{\partial e_{|r-s|}}{\partial k'} g_{|-m-t|} - \frac{\partial f_{|r-s|}}{\partial k'} h_{|-m-t|} \tag{4-206}$$

and

$$\frac{\partial B^{r,m}_{s,t}}{\partial \bar{h}} = e_{|r-s|} \frac{\partial h_{|-m-t|}}{\partial \bar{h}} + f_{|r-s|} \frac{\partial g_{|-m-t|}}{\partial \bar{h}} \tag{4-207}$$

$$\frac{\partial B^{r,m}_{s,t}}{\partial \bar{k}} = e_{|r-s|} \frac{\partial h_{|-m-t|}}{\partial \bar{k}} + f_{|r-s|} \frac{\partial g_{|-m-t|}}{\partial \bar{k}} \tag{4-208}$$

$$\frac{\partial B^{r,m}_{s,t}}{\partial h'} = \frac{\partial e_{|r-s|}}{\partial h'} h_{|-m-t|} + \frac{\partial f_{|r-s|}}{\partial h'} g_{|-m-t|} \tag{4-209}$$

$$\frac{\partial B^{r,m}_{s,t}}{\partial k'} = \frac{\partial e_{|r-s|}}{\partial k'} h_{|-m-t|} + \frac{\partial f_{|r-s|}}{\partial k'} g_{|-m-t|} \tag{4-210}$$

The coefficients of eqs. (4-199) and (4-200) and their partial derivatives can be computed by recurrence. Since there are no parity constraints between r and s or between m and t, the recurrences are designed to relate coefficients corresponding to exponents that differ by 1. The techniques of the prior section may be used to achieve the desired results:

$$e_{|r-s|+1} = k' e_{|r-s|} + \eta' h' f_{|r-s|} \tag{4-211}$$

$$f_{|r-s|+1} = -\eta' h' e_{|r-s|} + k' f_{|r-s|} \tag{4-212}$$

$$\left.\begin{aligned} e_0 &= 1 \\ f_0 &= 0 \end{aligned}\right\} \quad |r-s| = 0 \tag{4-213, 4-214}$$

$$g_{|-m-t|+1} = \bar{k} g_{|-m-t|} + \eta \bar{h} h_{|-m-t|} \tag{4-215}$$

$$h_{|-m-t|+1} = -\eta \bar{h} g_{|-m-t|} + \bar{k} h_{|-m-t|} \tag{4-216}$$

$$\left.\begin{aligned} g_0 &= 1 \\ h_0 &= 0 \end{aligned}\right\} \quad |-m-t| = 0 \tag{4-217, 4-218}$$

$$\frac{\partial e_{|r-s|+1}}{\partial k'} = (|r-s| + 1)\, e_{|r-s|} \tag{4-219}$$

$$\frac{\partial f_{|r-s|+1}}{\partial k'} = (|r-s| + 1)\, f_{|r-s|} \tag{4-220}$$

$$\left.\begin{aligned} \frac{\partial e_0}{\partial k'} &= 0 \\ \frac{\partial f_0}{\partial k'} &= 0 \end{aligned}\right\} \quad |r-s| = 0 \tag{4-221, 4-222}$$

$$\frac{\partial e_{|r-s|+1}}{\partial h'} = (|r-s| + 1)\, \eta'\, f_{|r-s|} \tag{4-223}$$

$$\frac{\partial f_{|r-s|+1}}{\partial h'} = -(|r-s| + 1)\, \eta'\, e_{|r-s|} \tag{4-224}$$

$$\left.\begin{aligned} \frac{\partial e_0}{\partial h'} &= 0 \\ \frac{\partial f_0}{\partial h'} &= 0 \end{aligned}\right\} \quad |r-s| = 0 \tag{4-225, 4-226}$$

$$\frac{\partial g_{|-m-t|+1}}{\partial \bar{k}} = (|-m-t| + 1)\, g_{|-m-t|} \tag{4-227}$$

$$\frac{\partial h_{|-m-t|+1}}{\partial \bar{k}} = (|-m-t| + 1)\, h_{|-m-t|} \tag{4-228}$$

$$\left.\begin{aligned} \frac{\partial g_0}{\partial \bar{k}} &= 0 \qquad (4\text{-}229) \\ \frac{\partial h_0}{\partial \bar{k}} &= 0 \qquad (4\text{-}230) \end{aligned}\right\} \quad |-m-t| = 0$$

$$\frac{\partial g_{|-m-t|+1}}{\partial \bar{h}} = (|-m-t| + 1)\, \eta\, h_{|-m-t|} \tag{4-231}$$

$$\frac{\partial h_{|-m-t|+1}}{\partial \bar{h}} = -(|-m-t| + 1)\, \eta\, g_{|-m-t|} \tag{4-232}$$

$$\left.\begin{aligned} \frac{\partial g_0}{\partial \bar{h}} &= 0 \qquad (4\text{-}233) \\ \frac{\partial h_0}{\partial \bar{h}} &= 0 \qquad (4\text{-}234) \end{aligned}\right\} \quad |-m-t| = 0$$

4.4.5 Recurrence Relations for the Third Body Hansen Coefficient Kernel $K_s^{-n-1,r}$ and its Derivative

The modified Hansen coefficients for the third body have the form

$$Y_s^{-n-1,r} = (k' - jn' h')^{|r-s|} K_s^{-n-1,r} \qquad (4\text{-}235)$$

Mathematical expressions for the calculation of the complex polynomial in eq. (4-235) and its partial derivatives have already been introduced. The recurrence relations for the computation of the kernel function $K_s^{-n-1,r}$ and its derivative are now examined. The two cases corresponding to $s \neq 0$ and $s = 0$ are considered separately.

Case I; $s \neq 0$

The recurrence relation governing the third body kernel functions when the subscript is non-zero may be taken from an 1855 Hansen manuscript [26]:

$$K_s^{c,r} = \frac{x'^2}{(c+4)[(c+2)^2-r^2]} \{(c+2)(c+4)(2c+5)\, K_s^{c+1,r} -$$

$$- (c+3)[(c+2)(c+4)+2sr\sqrt{1-e'^2}\,]\, K_s^{c+2,r} + s^2(c+2)\, K_s^{c+4,r} \} \qquad (4\text{-}236)$$

where

$$c = -n - 1 \qquad (4\text{-}237)$$

and

$$x' = (1 - e'^2)^{-1/2} \qquad (4\text{-}238)$$

The initialization of the recurrence is accomplished by evaluating the explicit power series representation of $K_s^{c,r}$ given in eq. (4-69) for $c = -n_\ell-1$, $-n_\ell-2$, $-n_\ell-3$, $-n_\ell-4$, where n_ℓ is the lower bound on the index n given by

$$n_\ell = \max(2, m, |r|) \tag{4-239}$$

Note that this initialization ensures that the apparent singularities in eq. (4-236) for $c = -|r| - 2$ and $c = -4$ are never encountered in practice.

The derivative of the kernel function with respect to e'^2 is seen to obey the recurrence relation,

$$\frac{dK_s^{c,r}}{de'^2} = x'^2 K_s^{c,r} + \frac{x'^2}{(c+4)[(c+2)^2 - r^2]} \{(c+2)(c+4)(2c+5) \cdot$$

$$\cdot \frac{dK_s^{c+1,r}}{de'^2} - (c+3)\left[(c+2)(c+4) + 2sr\sqrt{1-e'^2}\right] \frac{dK_s^{c+2,r}}{de'^2} +$$

$$+ s\, r\, (c+3)\, x'\, K_s^{c+2,r} + s^2 (c+2) \frac{dK_s^{c+4,r}}{de'^2} \}$$

(4-240)

The recurrence is explicitly initialized by evaluating the derivative of eq. (4-69), viz.,

$$\frac{dK_s^{c,r}}{de'^2} = \sum_{j=0}^{\infty} (j+1) \; x^{c,r}_{j+\frac{|q|+q}{2}+1,\, j+\frac{|q|-q}{2}+1} \; e'^{2j}$$

(4-241)

for $c = -n_\ell - 1,\ -n_\ell - 2,\ -n_\ell - 3,\ -n_\ell - 4$.

Case II; s = 0

If s is set equal to zero in eq. (4-236) then the following specialized recurrence relation results:

$$K_0^{c,r} = \frac{(c+2)x'^2}{[(c+2)^2 - r^2]} \{(2c+5)\, K_0^{c+1,r} - (c+3)\, K_0^{c+2,r}\}$$

(4-242)

The zero subscript kernel function can be represented by a series which terminates after a finite number of terms and hence may be computed in closed form. Accordingly, the initial values for eq. (4-242) are given by the simple expressions

$$K_0^{-|r|-1,r} = 0 \qquad (4\text{-}243)$$

$$K_0^{-|r|-2,r} = (1/2)^{|r|}\, x'^{2|r|+1} \qquad (4\text{-}244)$$

The derivative recurrence is readily obtained by setting s to zero in eq. (4-240)

$$\frac{dK_0^{c,r}}{de'^2} = x'^2\, K_0^{c,r} + \frac{(c+2)\, x'^2}{[(c+2)^2 - r^2]} \left\{(2c+5) \frac{dK_0^{c+1,r}}{de'^2} - (c+3) \frac{dK_0^{c+2,r}}{de'^2}\right\} \qquad (4\text{-}245)$$

The initial conditions are given by

$$\frac{dK_0^{-|r|-1,r}}{de'^2} = 0 \qquad (4\text{-}246)$$

$$\frac{dK_0^{-|r|-2,r}}{de'^2} = (1/2)^{|r|+1}\, (2|r| + 1)\, x'^{2|r|+3} \qquad (4\text{-}247)$$

4.4.6 Recurrence Relations for the Satellite Hansen Coefficient Kernel $K_t^{n,-m}$ and its Derivative

The modified Hansen coefficients for the satellite have the form

$$Y_t^{n,-m} = (\bar{k} - j\eta\bar{h})^{|-m-t|} K_t^{n,-m} \qquad (4\text{-}248)$$

The recurrence relations for the kernel function $K_t^{n,-m}$ and its derivative are now discussed for $t \neq 0$ and $t = 0$.

Case I; $t \neq 0$

The recurrence relation governing the satellite kernel functions when the subscript is non-zero is given by:

$$K_t^{n,-m} = \frac{1}{t^2(n-2)} \{(n-1)[n(n-2) - 2tm\sqrt{1-\bar{e}^2}\,]\, K_t^{n-2,-m} -$$

$$- n(n-2)(2n-3)\, K_t^{n-3,-m} + n[(n-2)^2 - m^2](1-\bar{e}^2)\, K_t^{n-4,-m} \} \qquad (4\text{-}249)$$

The initialization of the recurrence is accomplished by evaluating the explicit power series representation of $K_t^{n,-m}$ in eq. (4-73) for $n = n_\ell$, $n_\ell+1$, $n_\ell+2$, $n_\ell+3$, where n_ℓ is defined in eq. (4-239). This initialization ensures that the apparent singularity at n=2 is not encountered.

The derivative of the kernel function with respect to $\bar{e}^2$ is seen to obey the recurrence relation

$$\frac{dK_t^{n,-m}}{d\bar{e}^2} = \frac{1}{t^2(n-2)} \left\{ tm(n-1) \chi K_t^{n-2,-m} + \right.$$

$$+ (n-1)\left[n(n-2) - 2tm\sqrt{1-\bar{e}^2}\right] \frac{dK_t^{n-2,-m}}{d\bar{e}^2} - n(n-2)(2n-3) \cdot$$

$$\cdot \frac{dK_t^{n-3,-m}}{d\bar{e}^2} - n\left[(n-2)^2 - m^2\right]K_t^{n-4,-m} + n\left[(n-2)^2 - m^2\right] \cdot$$

$$\left. \cdot (1 - \bar{e}^2) \frac{dK_t^{n-4,-m}}{d\bar{e}^2} \right\}$$

(4-250)

where

$$\chi = (1 - \bar{e}^2)^{-1/2} \qquad (4\text{-}251)$$

The recurrence is explicitly initialized by evaluating the derivative of eq. (4-73), viz.,

$$\frac{dK_t^{n,-m}}{d\bar{e}^{\,2}} = \sum_{j=0}^{\infty} (j+1)\, X^{n,-m}_{j+\frac{|q|+q}{2}+1,\, j+\frac{|q|-q}{2}+1}\, \bar{e}^{\,2j} \qquad (4\text{-}252)$$

for $n = n_\ell,\ n_\ell+1,\ n_\ell+2,\ n_\ell+3$.

Case II; t = 0

If both sides of eq. (4-249) are multiplied by the factor $t^{2(n-2)}$ and the index t is then set to zero,

$$0 = (n-1)(n-2)\, K_0^{n-2,-m} - (n-2)(2n-3)\, K_0^{n-3,-m} + \\ + [(n-2)^2 - m^2](1 - \bar{e}^{\,2})\, K_0^{n-4,-m} \qquad (4\text{-}253)$$

Setting n = n+2 in eq. (4-253) leads to the specialized recurrence relation:

$$K_0^{n,-m} = \frac{1}{n(n+1)} \{n(2n+1)K_0^{n-1,-m} - (n^2 - m^2)(1-\bar{e}^{\,2})\, K_0^{n-2,-m}\} \qquad (4\text{-}254)$$

The zero subscript kernel may be computed in closed form. Hence, the initial values for eq. (4-254) are given by the simple expressions

$$K_0^{m,-m} = (-1)^m \frac{(2m+1)!!}{(m+1)!} \tag{4-255}$$

$$K_0^{m+1,-m} = (-1)^m \frac{(2m+1)!!}{(m+2)!} [2(m+1)+\bar{e}^{\,2}] \tag{4-256}$$

The derivative recurrence is obtained by differentiating eq. (4-254)

$$\frac{dK_0^{n,-m}}{d\bar{e}^{\,2}} = \frac{1}{n(n+1)} \{n(2n+1) \frac{dK_0^{n-1,-m}}{d\bar{e}^{\,2}} - (n^2 - m^2) [(1 - \bar{e}^{\,2}) \frac{dK_0^{n-2,-m}}{d\bar{e}^{\,2}} - K_0^{n-2,-m}]\} \tag{4-257}$$

The initial conditions are given by

$$\frac{dK_0^{m,-m}}{d\bar{e}^2} = 0 \qquad (4\text{-}258)$$

$$\frac{dK_0^{m+1,-m}}{d\bar{e}^2} = (-1)^m \frac{(2m+1)!!}{(m+2)!} \qquad (4\text{-}259)$$

4.5 Restriction of Indices in the Third Body Theory

In a numerical orbit prediction program, a procedure must be established for limiting the number of terms in the third body disturbing potential to the minimum required to accurately predict the motion of a satellite in a particular orbital regime. Once free truncation parameters have been set, this task entails the determination of constraining relations governing the indices of the multiple sum

$$\sum_{t=T_1}^{T_2} \sum_{s=S_1}^{S_2} \sum_{r=R_1}^{R_2} \sum_{m=0}^{M} \sum_{n=\max(2,m,|r|)}^{N} \qquad (4\text{-}260)$$

In the numerical implementation of the third body theory derived in this thesis, the truncation parameters are:

1) $N \equiv$ Maximum power of the parallax factor, $(\bar{a}/a')$

2) $M^* \equiv$ Upper bound on the satellite Hansen coefficient d'Alembert characteristic, $|-m-t|$.

3) $R^* \equiv$ Upper bound on the third body Hansen coefficient d'Alembert characteristic, $|r-s|$.

The bound on the satellite Hansen coefficient d'Alembert characteristic may be mathematically expressed by

$$|-m-t| \leq M^* \qquad (4\text{-}261)$$

which translates directly to an inequality on m:

$$-M^* - t \leq m \leq M^* - t \qquad (4\text{-}262)$$

The index m is not allowed to take on arbitrary values since the application of the Addition Theorem introduced the additional constraint:

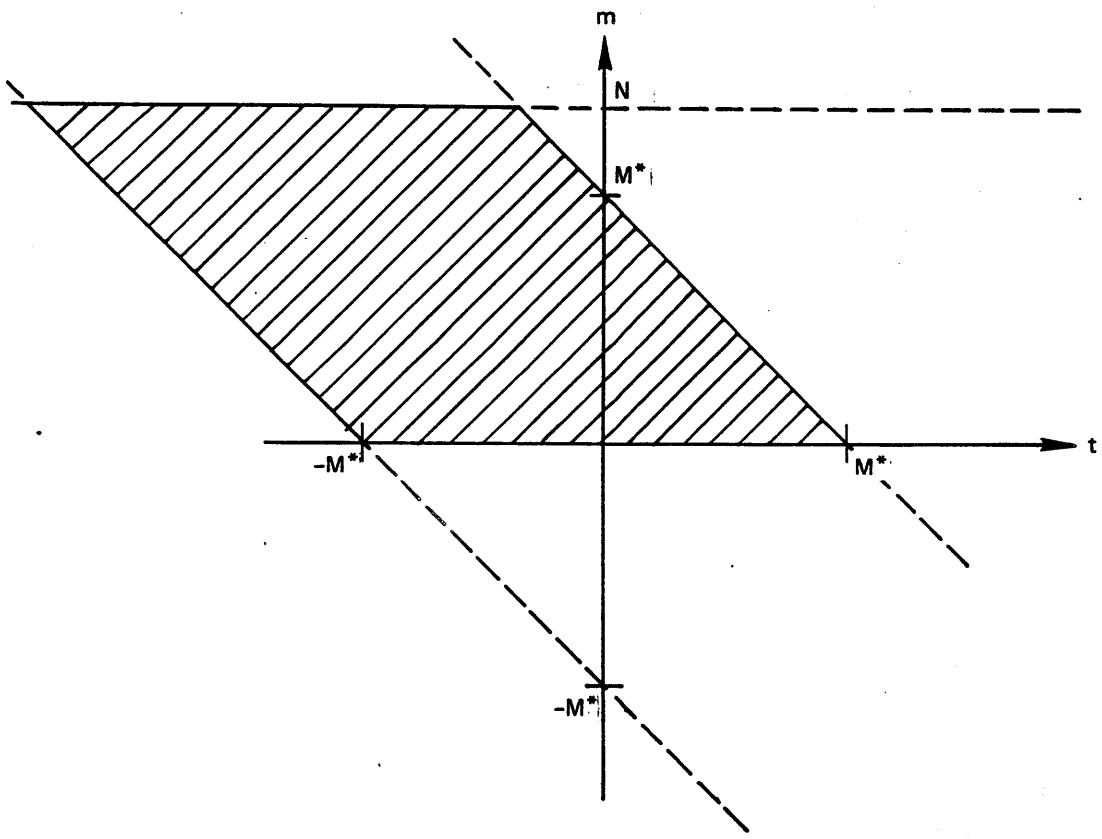
$$0 \leq m \leq N \tag{4-263}$$

The intersection of eq. (4-262) with eq. (4-263) leads to a parallelogram shaped region of admissible m versus t. The region is graphically displayed in Figure 4-1 for the special case of $M^* < N$. Solving eq. (4-262) for t and substituting eq. (4-263) yields the necessary bound:

$$-M^* - N \leq t \leq M^* \tag{4-264}$$

This same solution can be derived using Figure 4-1. Notice that eq. (4-264) shows that an increase in the number of multiples of the satellite mean longitude can be accomodated only by retaining more powers of the satellite eccentricity in the disturbing potential. With the t index restricted in accordance with eq. (4-264), it is now possible to write a well behaved constraint on m, viz.,

Figure 4-1. Admissible Values of the Index m vs. t



$$\max(\ 0,\ -M^*-t\ ) \leq m \leq \min(\ M^*-t,\ N\ ) \qquad (4\text{-}265)$$

The bound on the third body Hansen coefficient d'Alembert characteristic takes the mathematical form:

$$|r-s| \leq R^* \qquad (4\text{-}266)$$

which leads to

$$-R^* + s \leq r \leq R^* + s \qquad (4\text{-}267)$$

As in the satellite case, the index r cannot vary arbitrarily because the rotation theorem for spherical harmonics provides the auxiliary inequality:

$$-N \leq r \leq N \qquad (4\text{-}268)$$

The intersection of eq. (4-267) with eq. (4-268) leads to another parallelogram shaped region of admissible r versus s. The region is seen graphically in Figure 4-2 for the special case of $R^* < N$. Solving eq. (4-267) for s and substituting eq. (4-268) provides the required bound:

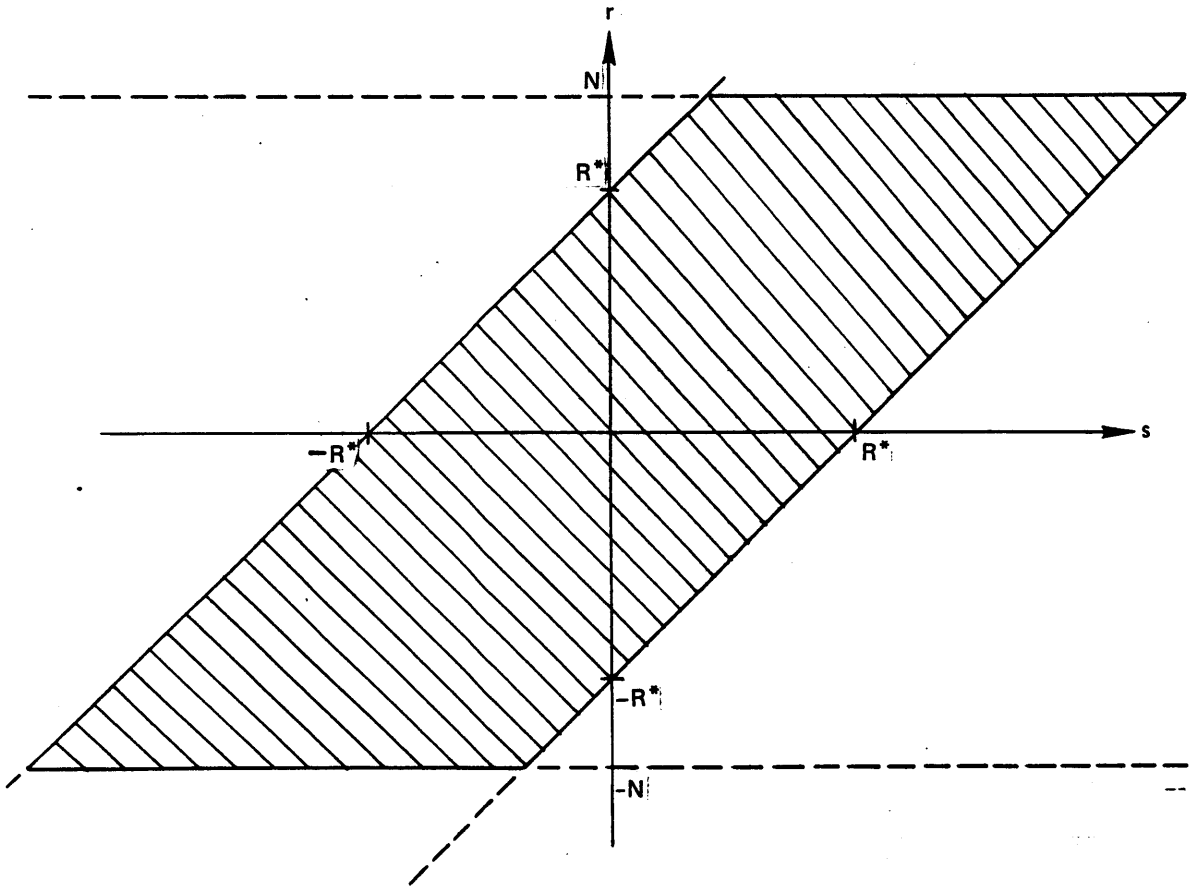
$$-R - N \leq s \leq R^* + N \qquad (4\text{-}269)$$

With the s index restricted in this way, a uniformly valid constraint on r can be written, viz.,

$$\max(-N, -R^*+s) \leq r \leq \min(R^*+s, N) \qquad (4\text{-}270)$$

Making use of the constraints of eqs. (4-264), (4-265), (4-269) and (4-270), the multiple sum of eq. (4-260) can be recast as

Figure 4-2. Admissible Values of the Index r vs. s



$$\sum_{t=-M^*-N}^{M^*} \sum_{s=-R^*-N}^{R^*+N} \sum_{r=\max(-N,-R^*+s)}^{\min(R^*+s,N)} \cdot \sum_{m=\max(0,-M^*-t)}^{\min(M^*-t,N)} \sum_{n=\max(2,m,|r|)}^{N}$$

(4-271)

Of course, for a given selection of N, M* and R* it is not necessary to use the full range of t, s, r, and m. Eq. (4-271) simply shows the maximum allowable ranges.

Chapter 5

Numerical Verification of the First Order Third Body Theory

The first order third body averaging theory developed in this thesis was designed to substantially reduce the computational expense of mission analysis and long term studies of orbital stability. This chapter presents the results of a numerical implementation of the third body theory that tests the design. The results show that the theory can be used to accurately predict the long term motion of a high altitude satellite with an efficiency that makes it decisively superior to conventional mission analysis techniques.

The theory is applied to the long term prediction of five test orbits which span a broad range of eccentricity and semi-major axis. For each test orbit, initial conditions for the averaged equations of motion are determined from the high precision orbital elements at epoch using a least squares differential correction algorithm. The averaged equations of motion are then integrated and compared for speed and accuracy against Cowell integration.

The equations for the first order third body averaging theory are programmed and interfaced with a version of the Goddard Trajectory Determination System (GTDS) modified at the Charles Stark Draper Laboratory in Cambridge, Massachusetts. This version of GTDS operates on CSDL's Amdahl 470 V/8 digital computer. GTDS furnishes test facilities that include numerical integrators, interpolation algorithms for the short periodic coefficients, and auxiliary perturbation models.

The software implementation of the third body theory consists of an Averaged Orbit Generator (AOG) and a Short Periodic Generator (SPG) which interface with the executive routines for the semianalytical satellite theory software in GTDS. The AOG is capable of constructing the right hand sides of the averaged equations of motion for third body perturbation that correspond to the double averaged and resonant satellite dynamics. The SPG computes the short periodic coefficients for the zonal, tesseral and m-daily analogs on the integration grid of the AOG. At all other times the coefficients are interpolated by GTDS. Since the averaged equations of motion and the short periodics have a similar analytical structure, the AOG and SPG share a great many subroutines. Nevertheless, the two

components of the averaging software are independent and different fields of indices can be specified for each. A discussion of the program flow and subroutine interactions can be found in Appendix B.

Section 5.1 describes the method employed for the determination of the AOG initial conditions from high precision data. Section 5.2 presents a method for computing disturbing body ephemerides over the time spans required for long term satellite orbit prediction. The numerical results of applying the averaging theory to selected test orbits are discussed in Section 5.3.

5.1 Initialization of the Averaged Equations of Motion

Given a set of high precision satellite orbital elements at epoch, a corresponding set of initial mean elements for a long term integration must be determined in a way which is consistent with the harmonic content of the averaged equations of motion. This requires the elimination of contributions to the high precision elements arising from frequencies that have been removed from the satellite equations of motion. If the conversion from osculating element space to mean element space is inaccurate, then a divergence is apparent between the averaged element

histories and the long term trends of the high precision trajectory [27].

For the test cases discussed in this chapter, the AOG was initialized using the Precise Conversion of Elements (PCE) capability of GTDS. The PCE procedure is a least squares differential correction algorithm that solves for epoch mean elements based on the fit of a semi-analytical trajectory to the output of a high precision Cowell integration. The PCE can be performed over any time span.

The exact initialization procedure is as follows:

1) Given a set of initial osculating elements and an appropriate perturbation model, a high precision trajectory is produced by Cowell integration. At fixed intervals within the integration span, the inertial rectangular components of the satellite position and velocity are output to a file to represent actual observations.

2) With a compatible perturbation field and an a priori estimate of the mean elements at epoch, $\underset{\sim}{\bar{a}}^*_0$, where

$$\underset{\sim}{\tilde{\bar{a}}}^{*T}_0 = [\tilde{\bar{a}}_0, \tilde{\bar{h}}_0, \tilde{\bar{k}}_0, \tilde{\bar{p}}_0, \tilde{\bar{q}}_0, \tilde{\bar{\lambda}}_0] \qquad (5\text{-}1)$$

a semi-analytical approximation to the osculating element histories is generated over the same span as the Cowell integration. The SPG is used to recover the first order short periodic corrections to the integrated mean elements. It must be stressed that an accurate short periodic recovery model is essential to ensure the convergence of the differential correction algorithm.

3) At each observation time, two body relations are employed to compute satellite position and velocity components from the orbital elements determined by semi-analytical methods. A vector of observation residuals, $\delta\underline{b}$, is obtained by subtracting the observations computed in this step from the actual observations. For a single

observation time, τ, where the six components of satellite position and velocity are computed through the equations

$$\begin{bmatrix} \underline{r}_c(\tau) \\ \dot{\underline{r}}_c(\tau) \end{bmatrix} = \begin{bmatrix} \underline{X}\ [\bar{a}(\tau)+\nu\eta_{1,1}, \bar{h}(\tau)+\nu\eta_{2,1}, \ldots, \bar{\lambda}(\tau)+\nu\eta_{6,1}] \\ \dot{\underline{X}}\ [\bar{a}(\tau)+\nu\eta_{1,1}, \bar{h}(\tau)+\nu\eta_{2,1}, \ldots, \bar{\lambda}(\tau)+\nu\eta_{6,1}] \end{bmatrix} \tag{5-2}$$

the correction to the mean elements at epoch is given by the expression

$$\delta\underline{\bar{a}}^*_0 = (A^T W A)^{-1} A^T W \delta\underline{b} \tag{5-3}$$

In eq. (5-3), W is a weighting matrix and A is the Jacobian of $\underline{X}$ and $\dot{\underline{X}}$ with respect to $\underline{\bar{a}}^*_0$ evaluated at the observation time, viz.,

$$A = \left[\frac{\partial \underline{X}(t)}{\partial \underline{\bar{a}}^*_0} \;\vdots\; \frac{\partial \dot{\underline{X}}(t)}{\partial \underline{\bar{a}}^*_0} \right] \Bigg|_{t=\tau} \tag{5-4}$$

Eq. (5-4) can be expanded by chain rule partial differentiation to yield:

$$A = \left\{ \left[\frac{\partial \underline{X}(t)}{\partial \underline{a}^*(t)} \;\middle|\; \frac{\partial \dot{\underline{X}}(t)}{\partial \underline{a}^*(t)} \right] \left[\begin{array}{c|c} \dfrac{\partial \underline{a}^*(t)}{\partial \bar{\underline{a}}^*(t)} & 0_{6x6} \\ \hline 0_{6x6} & \dfrac{\partial \underline{a}^*(t)}{\partial \bar{\underline{a}}^*(t)} \end{array} \right] \cdot \right.$$

$$\left. \cdot \left[\begin{array}{c|c} \dfrac{\partial \bar{\underline{a}}^*(t)}{\partial \bar{\underline{a}}^*_0} & 0_{6x6} \\ \hline 0_{6x6} & \dfrac{\partial \bar{\underline{a}}^*(t)}{\partial \bar{\underline{a}}^*_0} \end{array} \right] \right\} \Bigg|_{t=\tau} \tag{5-5}$$

where $\underline{a}^*(t)$ is the vector of osculating elements

$$\underline{a}^{*T}(t) = [a,h,k,p,q,\lambda] \tag{5-6}$$

At first order, the partial derivative matrix, $\partial \underline{a}^*(t)/\partial \bar{\underline{a}}^*(t)$, is given by

$$\frac{\partial \underline{a}^*(t)}{\partial \bar{\underline{a}}^*(t)} = I_{6x6} + \nu \frac{\partial \underline{\eta}}{\partial \bar{\underline{a}}^*(t)} \qquad (5\text{-}7)$$

where I_{6x6} is a 6x6 identity matrix. The least squares differential correction algorithm in GTDS is found to converge even for very crude estimates of eq. (5-7). For all runs in this thesis, eq. (5-7) was approximated by the identity matrix, so that eq. (5-5) reduces to

$$A = \left\{ \left[\frac{\partial \underline{X}(t)}{\partial \underline{a}^*(t)} \;\vdots\; \frac{\partial \dot{\underline{X}}(t)}{\partial \underline{a}^*(t)} \right] \left[\begin{array}{c:c} \dfrac{\partial \bar{\underline{a}}^*(t)}{\partial \bar{\underline{a}}^*_0} & 0_{6x6} \\ \hdashline 0_{6x6} & \dfrac{\partial \bar{\underline{a}}^*(t)}{\partial \bar{\underline{a}}^*_0} \end{array} \right] \right\} \Bigg|_{t=\tau} \qquad (5\text{-}8)$$

The partial derivatives, $\partial \bar{\underline{a}}^*(t)/\partial \bar{\underline{a}}^*_0$, are governed by the differential equation [22]

$$\frac{d}{dt}\left[\frac{\partial \bar{\underline{a}}^*(t)}{\partial \bar{\underline{a}}^*_0}\right] = \left[\frac{\partial [\dot{\bar{\underline{a}}}^*(t)]}{\partial \bar{\underline{a}}^*(t)}\right]\left[\frac{\partial \bar{\underline{a}}^*(t)}{\partial \bar{\underline{a}}^*_0}\right] \tag{5-9}$$

with the initial conditions

$$\frac{\partial \bar{\underline{a}}^*(t_0)}{\partial \bar{\underline{a}}^*_0} = I_{6x6} \tag{5-10}$$

The partial derivatives are obtained at the observation times by interpolating on the integrated output of eq. (5-9). The matrix, $\partial[\dot{\bar{\underline{a}}}^*(t)]/\partial \bar{\underline{a}}^*(t)$, is computed in GTDS using a double-sided finite differencing algorithm where the mean elements are varied by an amount [22],

$$\Delta\bar{\underline{a}}^*(t) = 10^{-5}\,\bar{\underline{a}}^*(t) \qquad (5\text{-}11)$$

4) After all the observations have been processed, the revised estimate to the mean elements at epoch is given by

$$\hat{\bar{\underline{a}}}^*_0 = \tilde{\bar{\underline{a}}}^*_0 + \delta\bar{\underline{a}}^*_0 \qquad (5\text{-}12)$$

This new estimate replaces the a priori estimate in Step 2.

5) Steps 2 through 4 are repeated until a convergence criterion is met.

5.2 The Computation of Third Body Ephemerides

In GTDS, the geocentric position and velocity components of the sun and moon are usually obtained by evaluating Chebyshev polynomials. The coefficients of these polynomials are computed from ephemerides supplied on magnetic tape by the Jet Propulsion Laboratory (JPL) and are stored on permanent files. At the present time, these files can accomodate requests for third body ephemerides that fall

within a period between 1 January 1971 and 14 January 1984. If very long numerical integrations are necessary or if the option to choose an arbitrary epoch of integration is desired, than an extended capability is required.

For the numerical integrations discussed in this chapter, the extended capability is provided by the use of analytical theories for the secular motion of the sun and moon. These theories are taken from the Explanatory Supplement to the Astronomical Ephemeris [28] and are based on the solar tables of Newcomb and the lunar tables of Brown. The mean equinoctial elements for the sun and moon, in mean ecliptic of date coordinates, are given by:

Mean Solar Elements

$$a' = 149598412.7 \text{ km}$$

$$h' = 0.01675104 \sin\Gamma$$

$$k' = 0.01675104 \cos\Gamma$$

$$p' = 0.0$$

$$q' = 0.0$$

$$\lambda' = 279^\circ.69668 + 0^\circ.9856473354\, d + 0^\circ.000303\, C^2$$

where Γ is the longitude of pericenter which is computed according to

$$\Gamma = 281^\circ.22083 + 0^\circ.0000470684\ d + 0^\circ.000453\ C^2$$

and

d = Julian days from 1900.0

C = Julian centuries from 1900.0

($C = d/36525$)

Mean Lunar Elements

$$a' = 384388.1743 \text{ km}$$

$$h' = 0.054900489 \sin\Gamma'$$

$$k' = 0.054900489 \cos\Gamma'$$

$$p' = 0.0449322554 \sin\Omega$$

$$q' = 0.0449322554 \cos\Omega$$

$$\lambda' = 270^\circ.434164 + 13^\circ.1763965268\ d - 0.001133\ C^2$$

where Γ' is the longitude of pericenter given by,

$$\Gamma' = 334^\circ.329556 + 0^\circ.1114040803\ d - 0^\circ.010325\ C^2$$

and Ω is the longitude of the lunar ascending node on the ecliptic,

$$\Omega = 259^\circ.183275 - 0^\circ.0529539222\ d + 0^\circ.002078\ C^2$$

At each evaluation of the third body equinoctial elements, two body relations are used to compute the rectangular components of the position and velocity vectors in mean ecliptic of date coordinates. The position and velocity vectors are then transformed to mean of date equatorial coordinates by rotating them through the mean obliquity of the ecliptic given by [28],

$$\begin{aligned}\bar{\varepsilon} &= 23^\circ.452294 - 0^\circ.0130125\ T - \\ &- 0^\circ.00000164\ T^2 + \\ &+ 10^\circ.000000503\ T^3\end{aligned}$$

where T is the number of Julian centuries since 1950.0. Further rotations depend on the reference system of the numerical integration.

5.3 Analysis of the Numerical Results

This section describes the performance of the first order third body averaging theory, in comparison with Cowell integration, for five test orbits. These test satellite orbits demonstrate the ability of the theory to predict long term motion accurately and efficiently over a wide range of orbital geometries.

For each test orbit, the third body ephemerides were computed by the same method for both the averaging theory and the Cowell integration. Hence, the source of the ephemerides does not enter into any of the comparisons. Except for the ISEE test case, which used the JPL ephemeris, all of the results of this section were obtained using the analytical ephemeris described in Section 5.2.

5.3.1 IUE Test Case

The International Ultraviolet Explorer (IUE) orbit provides an accuracy baseline for the third body AOG and SPG before moving on to more demanding test cases. The initial osculating elements of the orbit are defined in Table 5-1.

Table 5-1. Epoch Osculating Elements for the IUE Test Case

a = 42143.48243 km	Epoch = 7 March 1972
e = 0.2353378723	$0^h.0, 0^m.0, 0^s.0$
i = 28.30116521°	
Ω = 199.6137090°	Period = 0.996 day
ω = 264.6988766°	
M = 270.4208456°	

Radius of Perigee = 32225.5 km

Radius of Apogee = 52061.4 km

Lunar Parallax Factor $(a/a')_\ell \simeq 0.1$

Solar Parallax Factor $(a/a')_S \simeq 0.0003$

The IUE orbit was chosen to demonstrate the following points:

1) The validity of the PCE procedure for obtaining epoch mean elements from osculating elements.

2) The ability of the AOG to track the mean of a high precision trajectory over an arc which is long in comparison to the time span of the PCE initialization.

3) The accuracy of the third body short periodic model.

4) The remarkably long integration step size that is permitted by the third body averaging theory.

The initial mean elements for the averaged equations of motion were obtained by performing a PCE fit to 184 sets of high precision position and velocity components evenly spaced over sixty days. The a priori elements for the initialization were provided by the GTDS numerical osculating-to-mean conversion which used a 96 point Gaussian quadrature to average the osculating trajectory over one period of the satellite [29]. The perturbation models used

in the PCE are given in Table 5-2. The truncation parameters N, M* and R*, in the lunar and solar models, were chosen on the basis of experience and the relative sizes of parameters such as the third body and satellite orbital eccentricities. Given the truncation parameters, the maximum ranges on the frequency indices, t and s, are given by the inequality relations in eqs. (4-264) and (4-269) of Chapter 4. The symmetry of the ranges chosen for the PCE reflects the present capability of the third body software to handle only symmetrical frequency fields. It should be noted that the parameters specified for the lunar and solar models in Table 5-2 are actually conservative choices. Model truncation studies are required with a view towards improving numerical efficiency without sacrificing accuracy (see Chapter 6).

Table 5-2. PCE Perturbation Models for the IUE Test Case

1) AOG + SPG Perturbation Model:

SUN	MOON	EARTH
N = 6	N = 10	J_2
M* = 6	M* = 8	
R* = 4	R* = 4	
$-5 \leq t \leq 5$	$-5 \leq t \leq 5$	
$-5 \leq s \leq 5$	$-5 \leq s \leq 5$	

NOTE: AOG retains only double averaged terms for the third body

N ≡ maximum power of the parallax factor, $(\bar{a}/a')$

M* ≡ upper bound on the satellite Hansen coefficient d'Alembert characteristic

R* ≡ upper bound on the third body Hansen coefficient d'Alembert characteristic

2) Cowell Perturbing Acceleration:

point mass sun
point mass moon
J_2

Since the IUE orbit is non-resonant with respect to a third body, only the double averaged terms are retained in the third body AOG for the initialization process. The mean elements determined in the PCE are shown in Table 5.3. In order to judge the quality of the converged solution, these mean elements were used to initialize an integration of the averaged equations of motion over the sixty day fit span of the PCE. Short periodic recovery at the output times of the numerical integration produced a semi-analytical approximation to the osculating trajectory which was then compared to a Cowell prediction over the same span. Representative element histories are shown in Figures 5-1 through 5-4. The Cowell trajectory is represented by the symbol (+), while the semi-analytical trajectory is denoted by the symbol (*). Whenever the element histories agree to within the resolution of the plot scale, then the (+) overwrites the (*). The plots demonstrate the high accuracy of the averaging theory. In particular, the semi-monthly oscillation in the orbital eccentricity and inclination, induced by the motion of the moon, is seen to be reproduced by the third body short periodic model. A more graphic demonstration of the fit span accuracy is provided by the element difference plots in Figures 5-5 through 5-8. The element differences are very small fractions of the elements themselves. For example, the semi-analytical semi-major axis

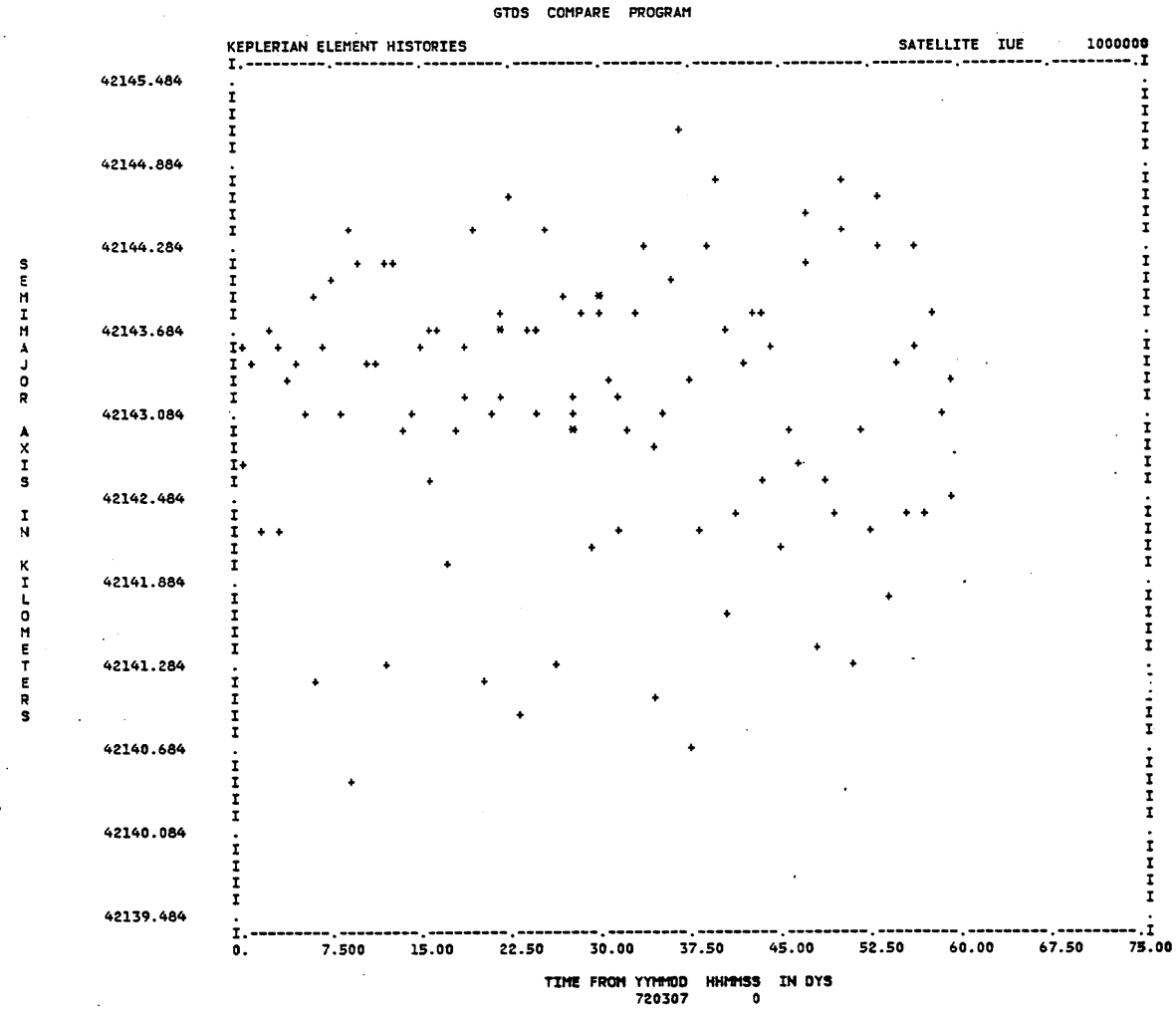
differs from its Cowell generated counterpart by no more than fifteen meters at any point within the sixty day fit span. Similarly, the averaging theory holds to within 10^{-4} degree of the Cowell computed mean longitude. Further evidence that the PCE fit was accurate is the absence of an appreciable bias in the element difference plots.

Table 5-3. Epoch Mean Elements for the IUE Test Case

Keplerian	Equinoctial
$\bar{a}$ = 42143.09386 km	$\bar{a}$ = 42143.09386 km
$\bar{e}$ = 0.2357026946	$\bar{h}$ = 0.2284825453
$\bar{i}$ = 28.27923713°	$\bar{k}$ = -0.0578920263
$\bar{\Omega}$ = 199.6755329°	$\bar{p}$ = -0.0848190305
$\bar{\omega}$ = 264.5426255°	$\bar{q}$ = -0.2372094942
$\bar{M}$ = 270.4886538°	$\bar{\lambda}$ = 14.7068122°

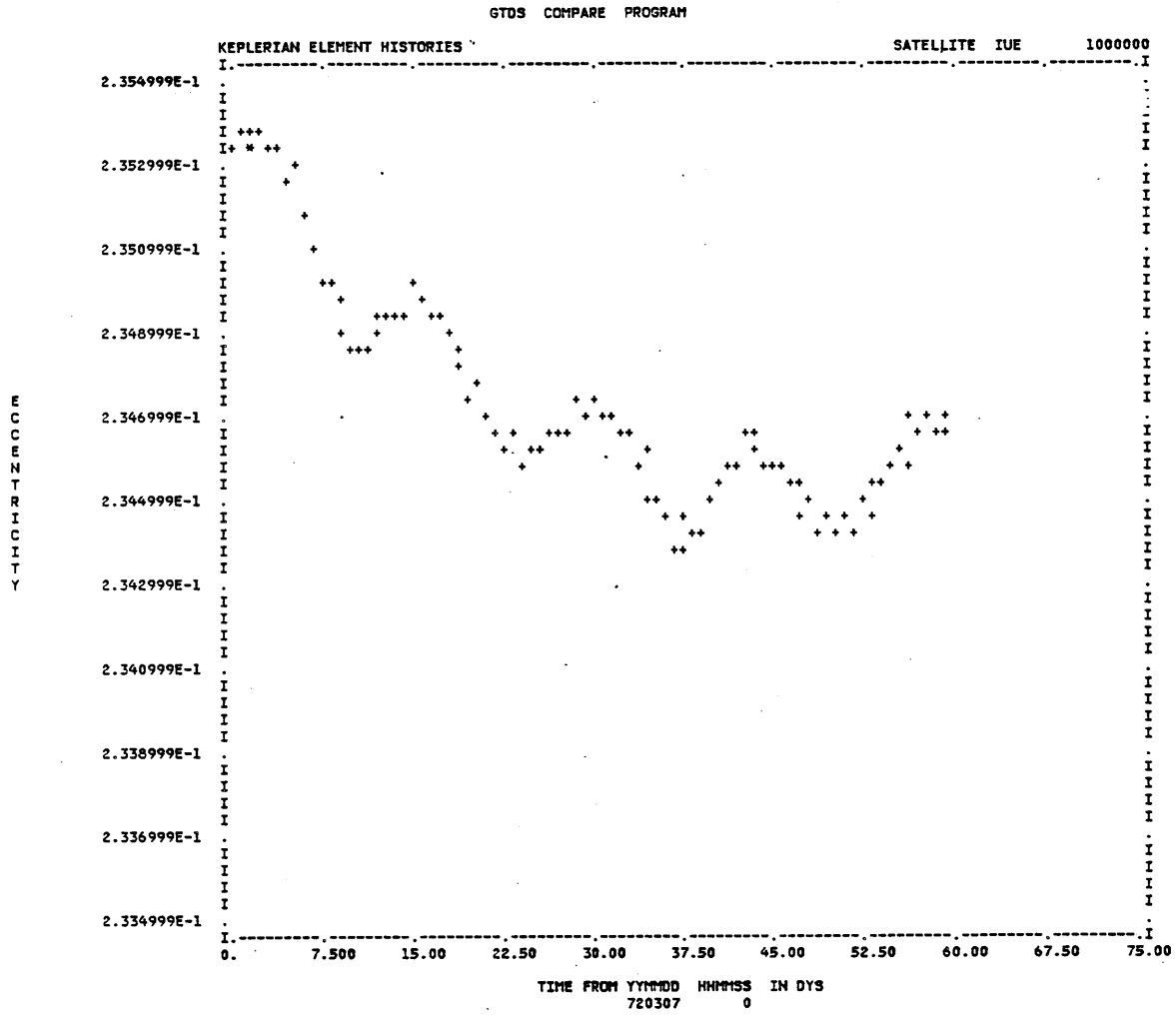
The PCE procedure adjusts the mean satellite elements at epoch to produce the "best" semi-analytical fit to Cowell generated data. As a result, the observed accuracy of an averaging theory over the fit span is not sufficient to

Figure 5-1. Osculating Semi-Major Axis Comparison within the 60 Day PCE Fit Span for the IUE Orbit/ Semi-Analytical versus Cowell



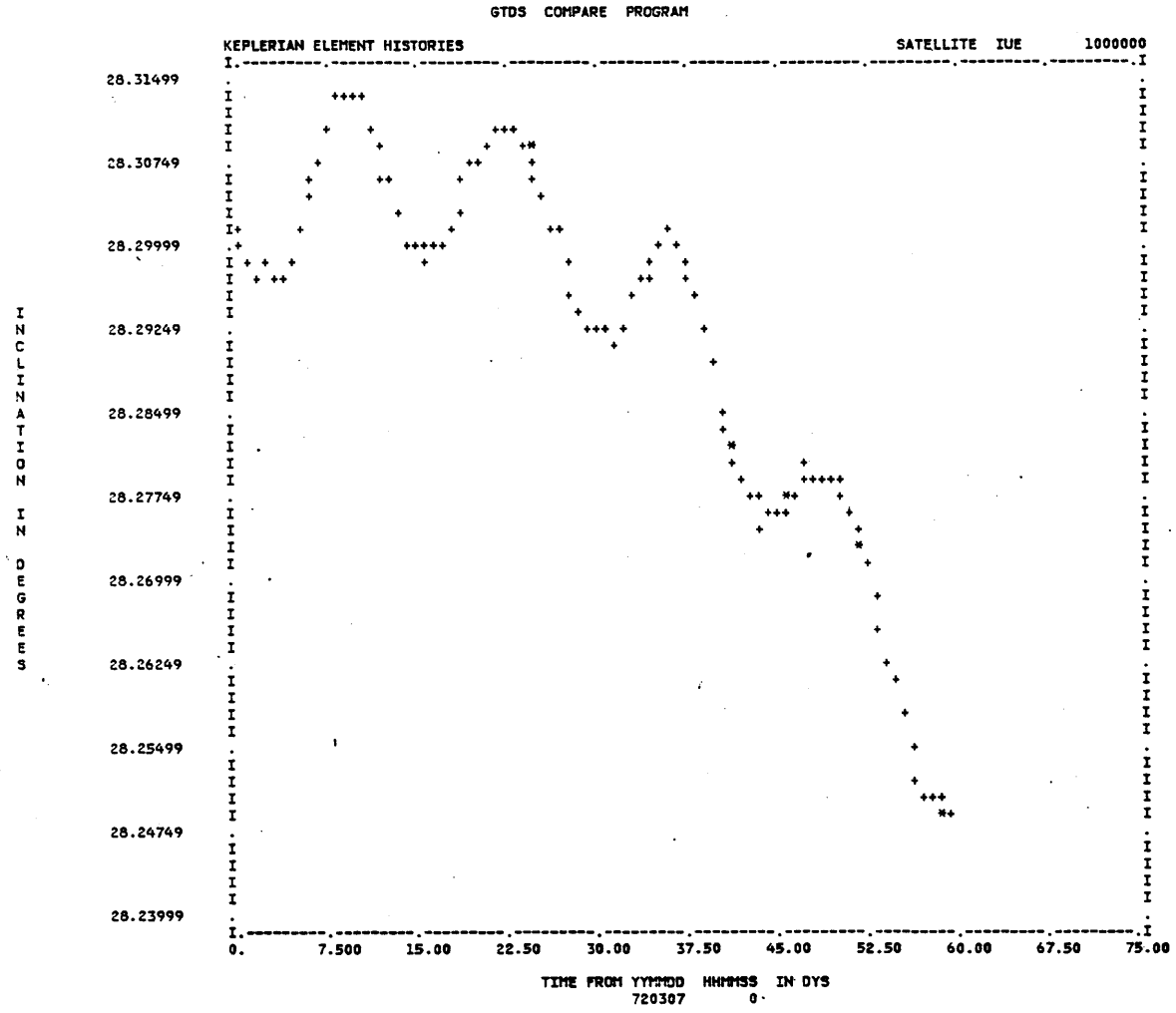
(+) = Cowell
(*) = AOG & SPG

Figure 5-2. Osculating Eccentricity Comparison within the 60 Day PCE Fit Span for the IUE Orbit/ Semi-Analytical versus Cowell



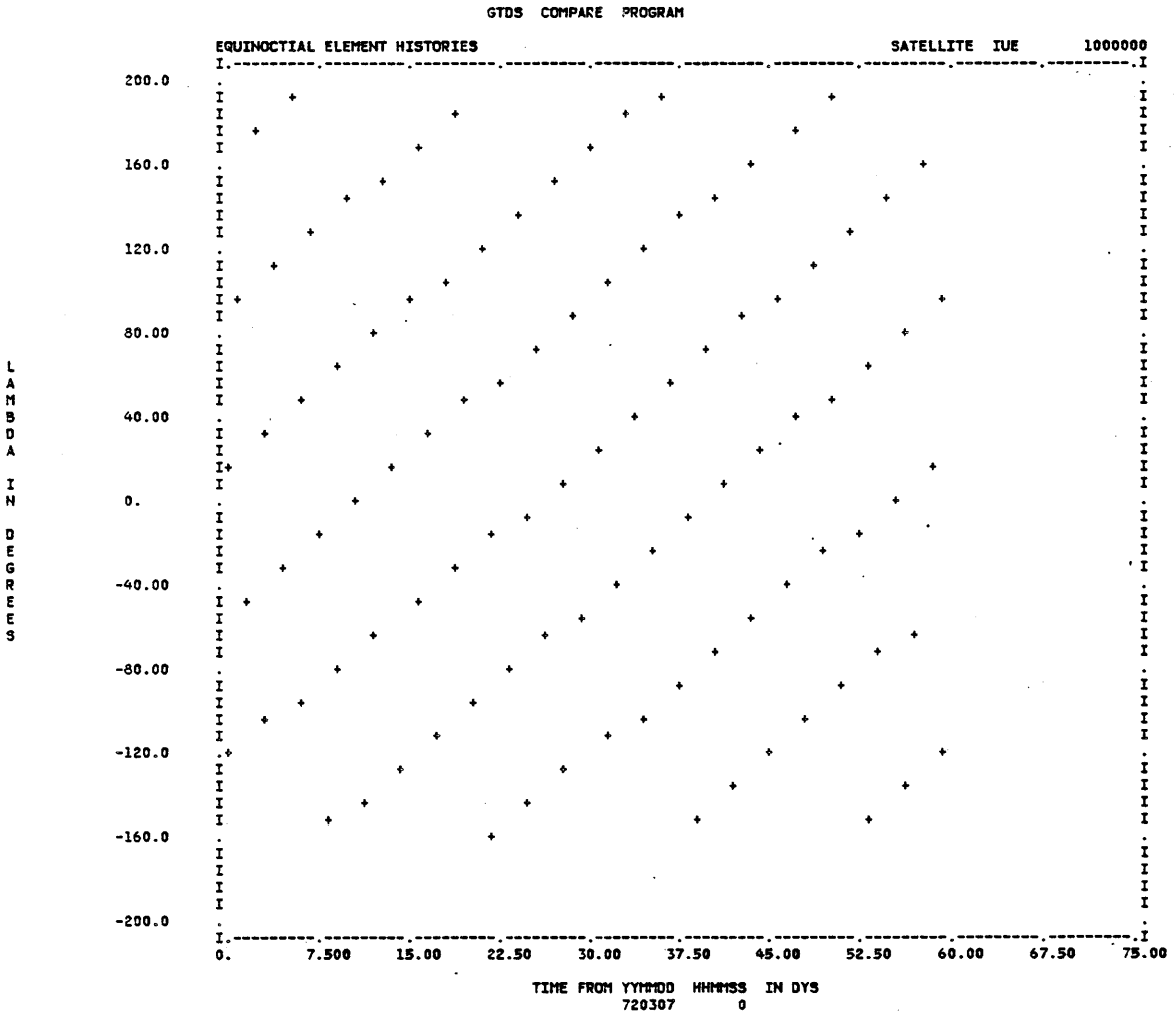
(+) = Cowell
(*) = AOG & SPG

Figure 5-3. Osculating Inclination Comparison within the 60 Day PCE Fit Span for the IUE Orbit/ Semi-Analytical versus Cowell



(+) = Cowell
(*) = AOG & SPG

Figure 5-4. Osculating Mean Longitude Comparison within the 60 Day PCE Fit Span for the IUE Orbit/ Semi-Analytical versus Cowell



(+) = Cowell
(*) = AOG & SPG

Figure 5-5. Osculating Semi-Major Axis Differences within the 60 Day PCE Fit Span for the IUE Orbit/ Semi-Analytical minus Cowell

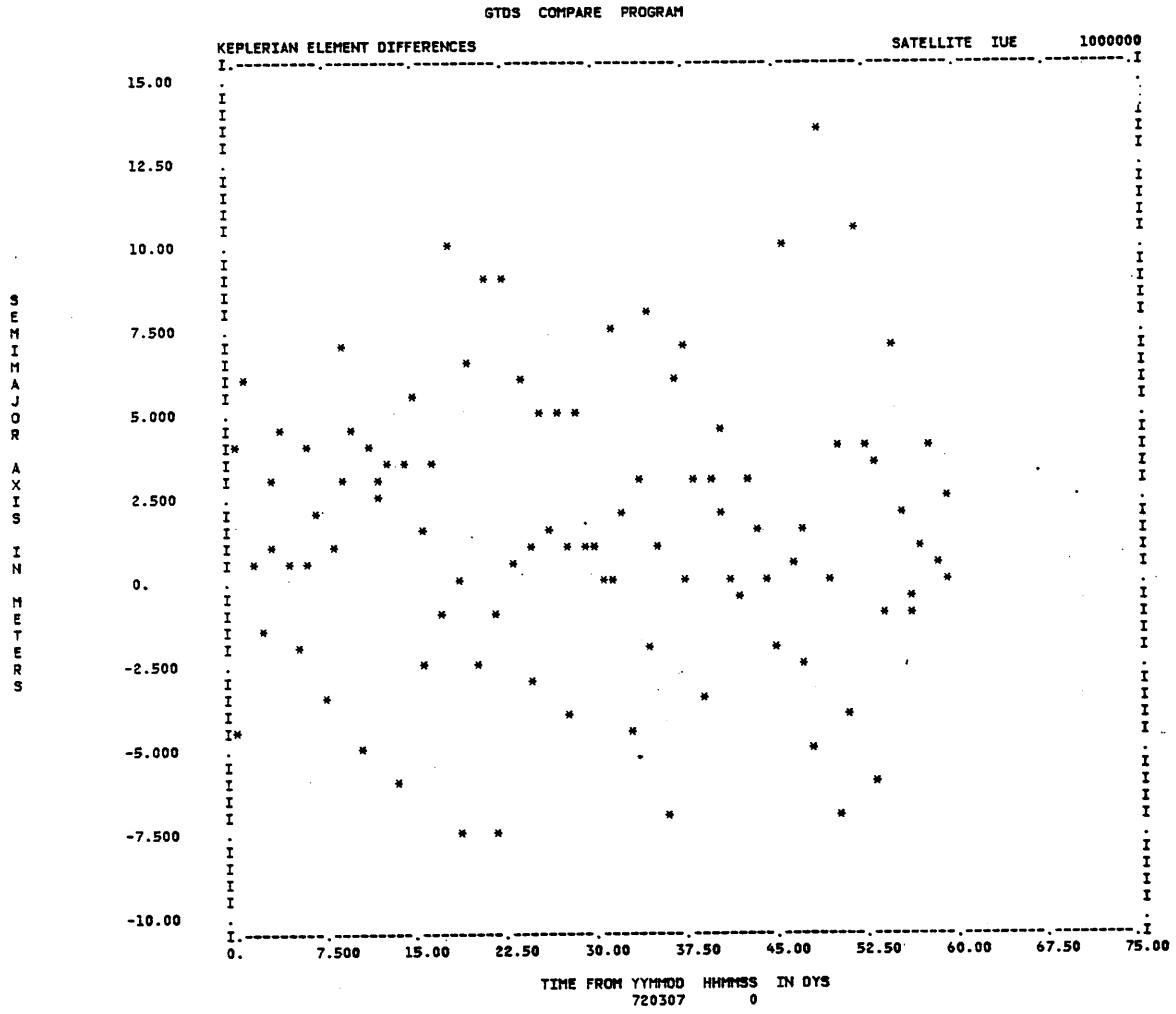


Figure 5-6. Osculating Eccentricity Differences within the 60 Day PCE Fit Span for the IUE Orbit/ Semi-Analytical minus Cowell

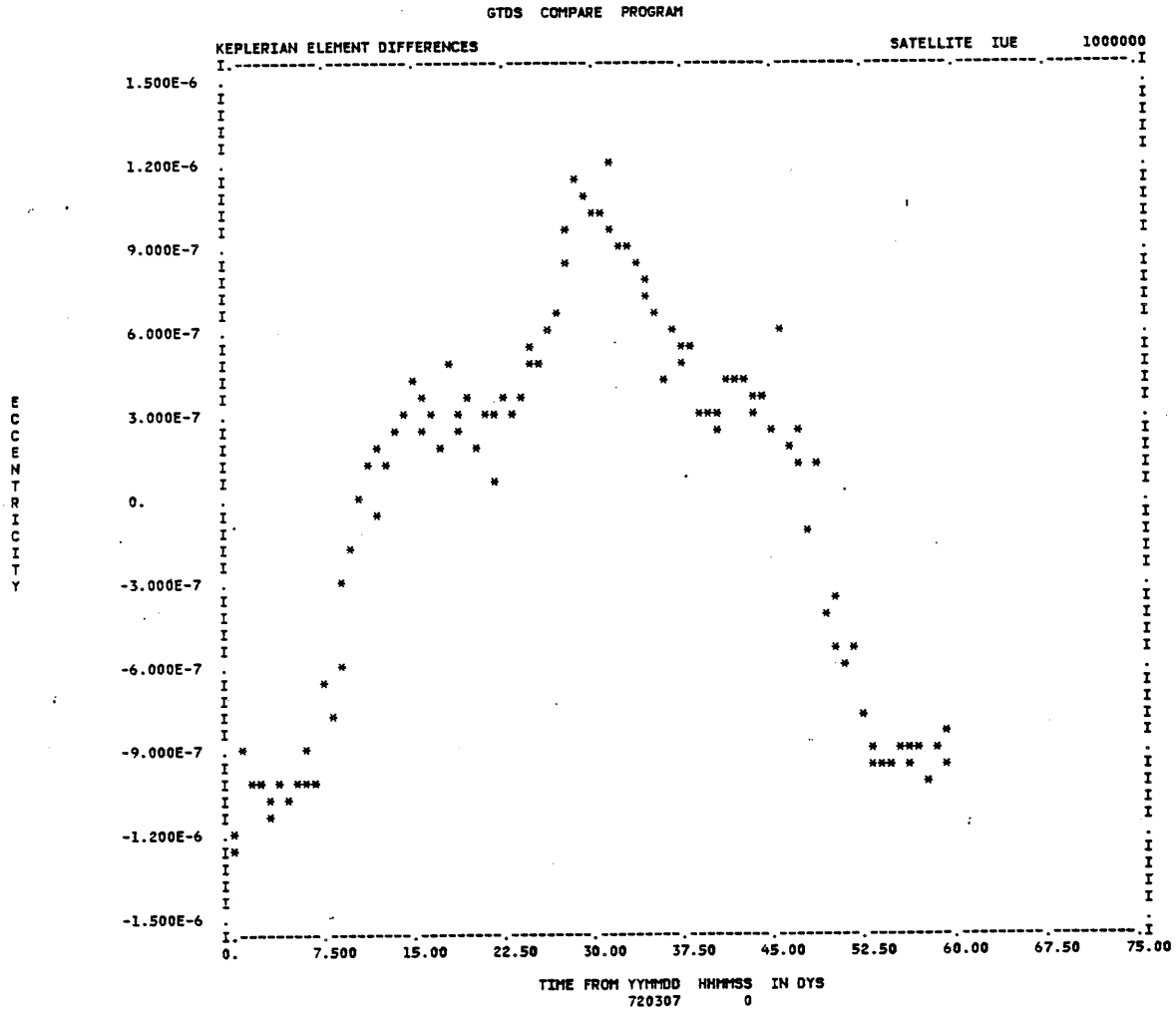


Figure 5-7. Osculating Inclination Differences within the 60 Day PCE Fit Span for the IUE Orbit/ Semi-Analytical minus Cowell

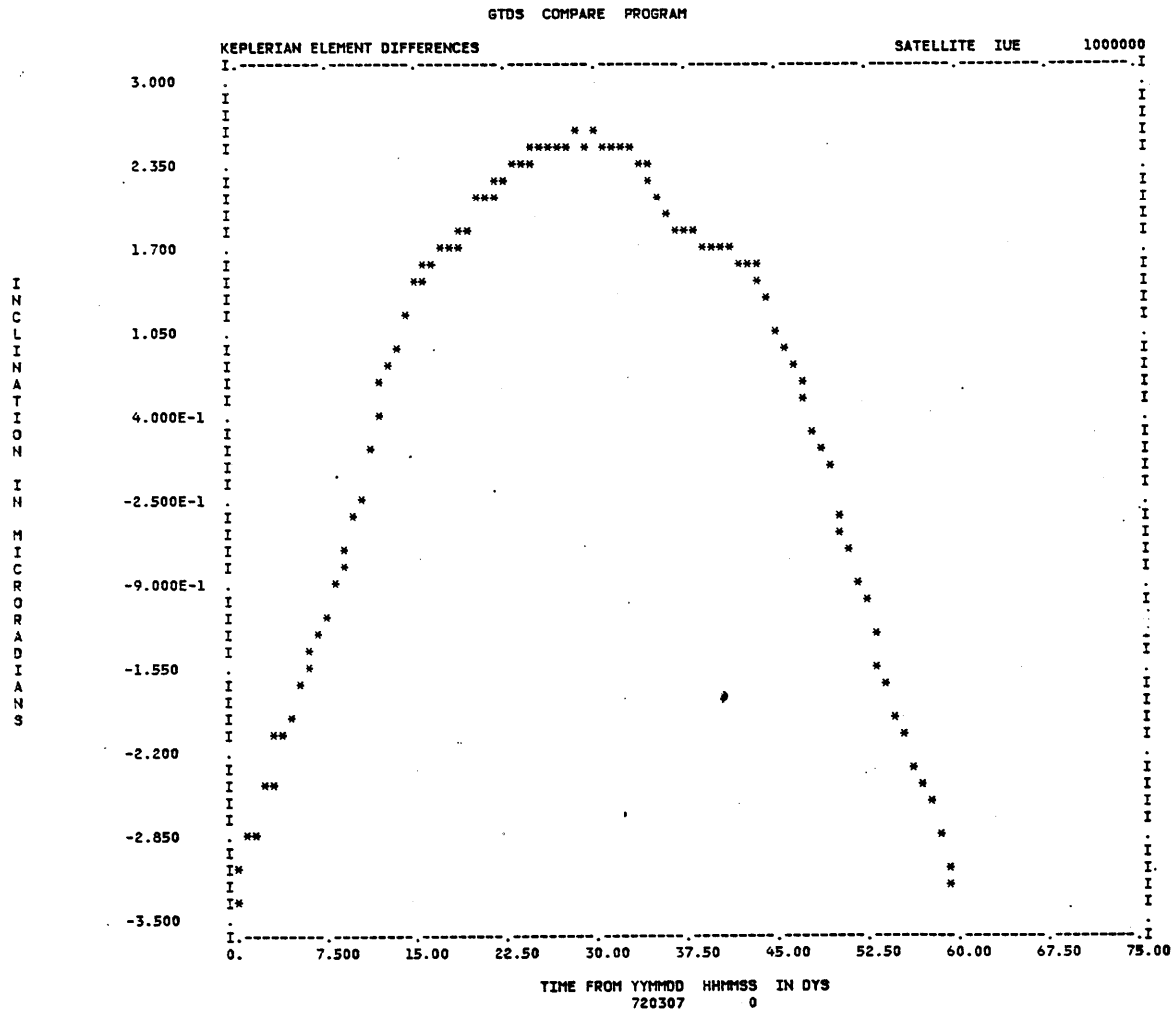
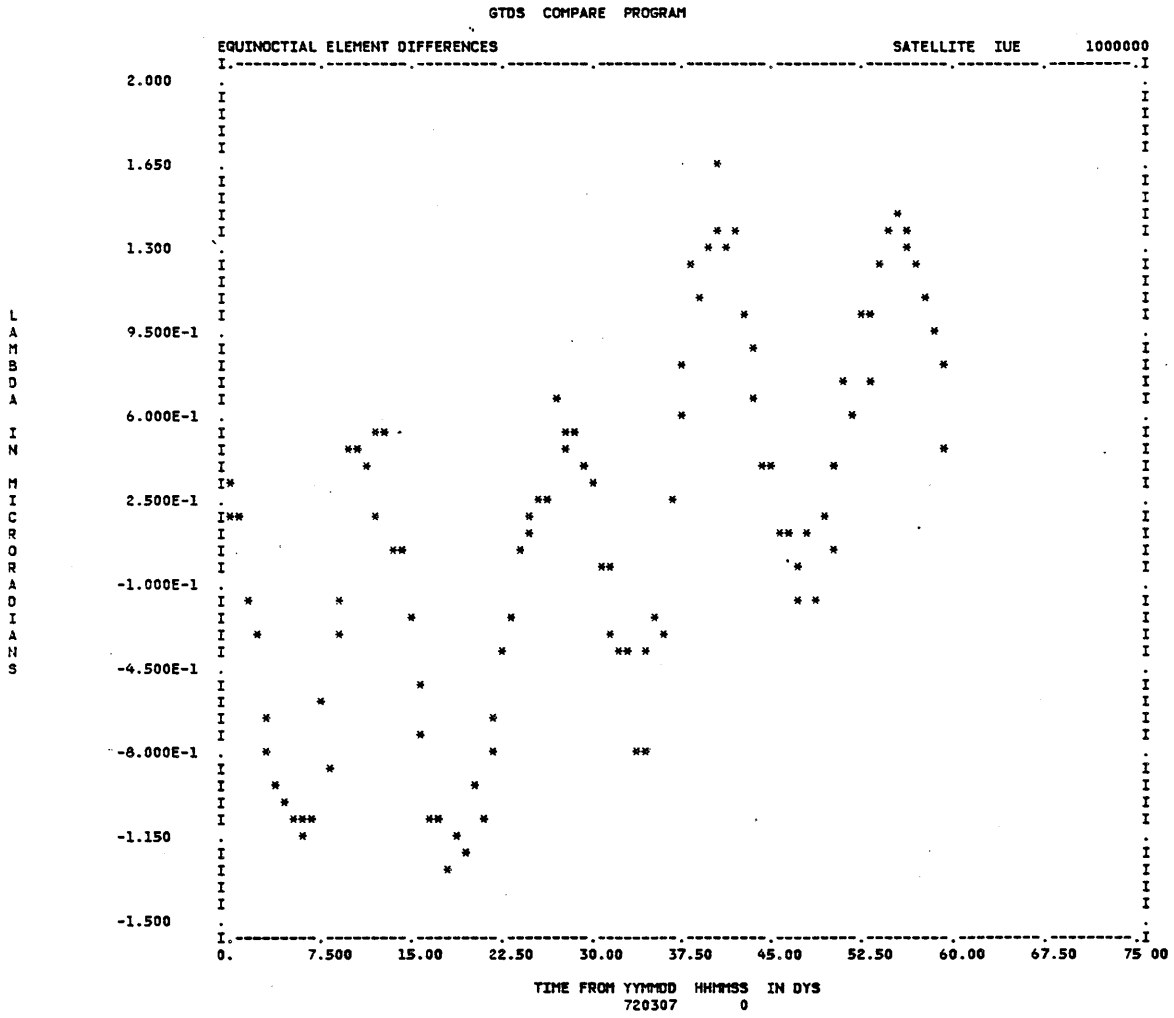
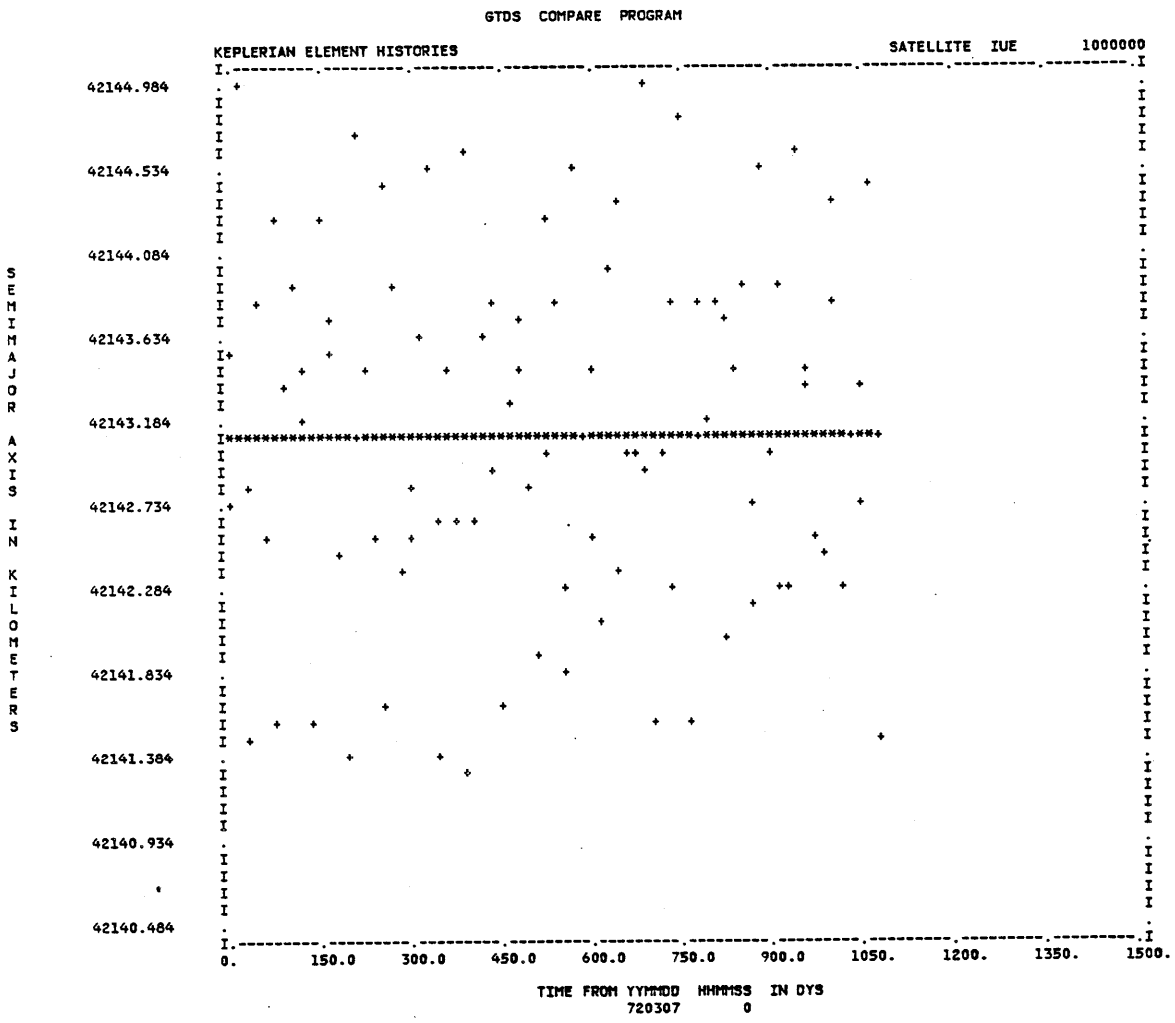


Figure 5-8. Osculating Mean Longitude Differences within the 60 Day PCE Fit Span for the IUE Orbit/ Semi-Analytical minus Cowell



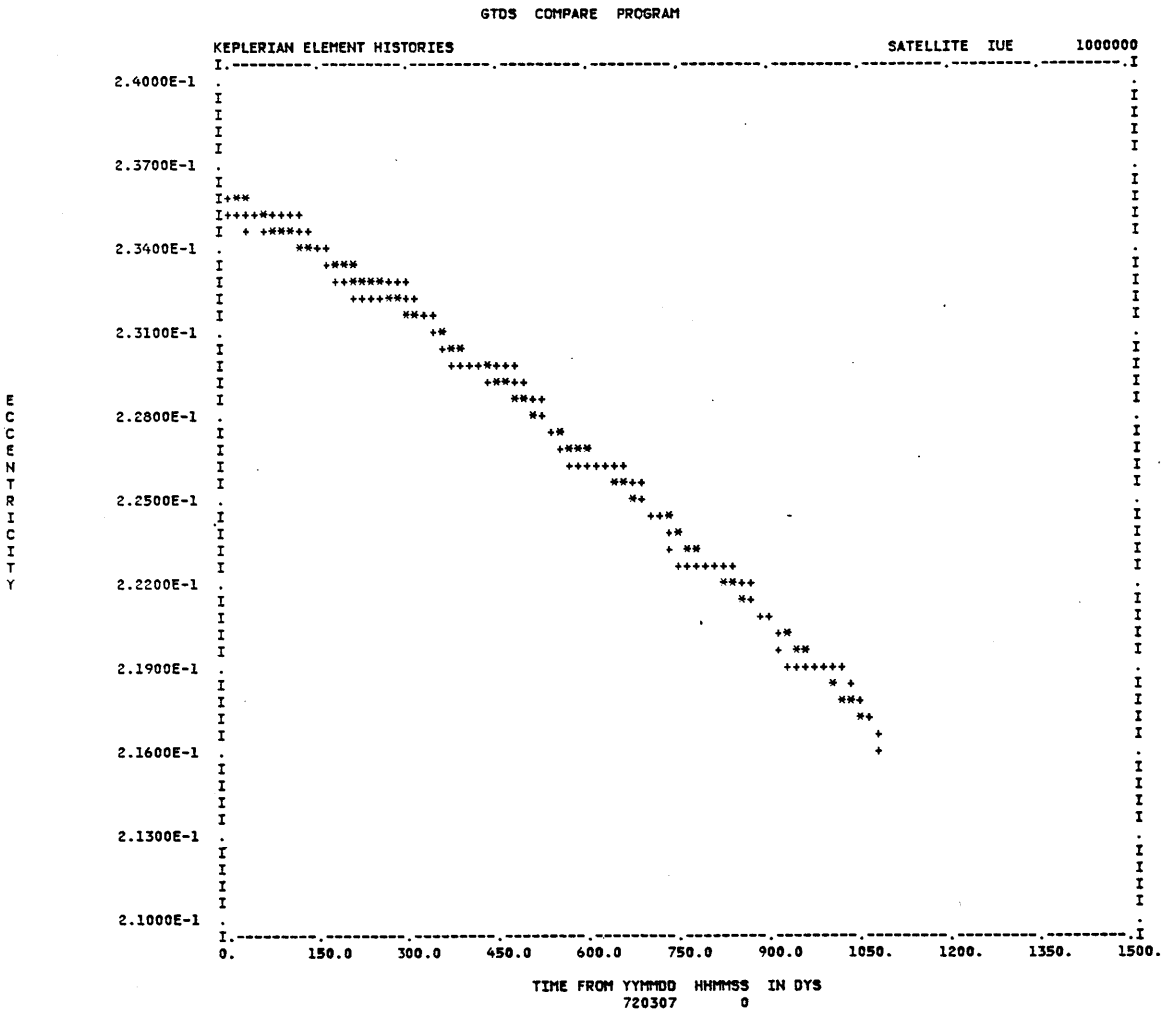
ensure acceptable behavior for a longer integration. The mean elements in Table 5-3 were used to initialize a three year AOG prediction to test the ability of the averaged equations of motion to predict the mean of the corresponding high precision trajectory over an arc that is much longer than the time span of the PCE initialization. The truncation parameters N, M* and R* for the lunar and solar models are the same as those given in Table 5-2. Element compare plots for the semi-major axis, eccentricity, and inclination are given in Figures 5-9 through 5-11 where the symbol (+) represents the Cowell trajectory and the symbol (*) represents the mean output of the AOG. The mean semi-major axis is constant since all dependence on the satellite mean longitude has been removed from the averaged perturbation models. The 180 day oscillations in the high precision element histories for the eccentricity and the inclination are the semi-annual variations introduced by the motion of the sun. Evidently, the AOG follows the mean of the high precision trajectory very closely over the three year integration interval. The element difference plots corresponding to Figures 5-9 through 5-11 are found in Figures 5-12 through 5-14. The symmetry of the element differences is further verification of the PCE initialization and the accuracy of the averaged perturbation

Figure 5-9. Comparison of the Mean and Osculating Semi-Major Axis Histories for the 3 Year Integration of the IUE Orbit/AOG versus Cowell



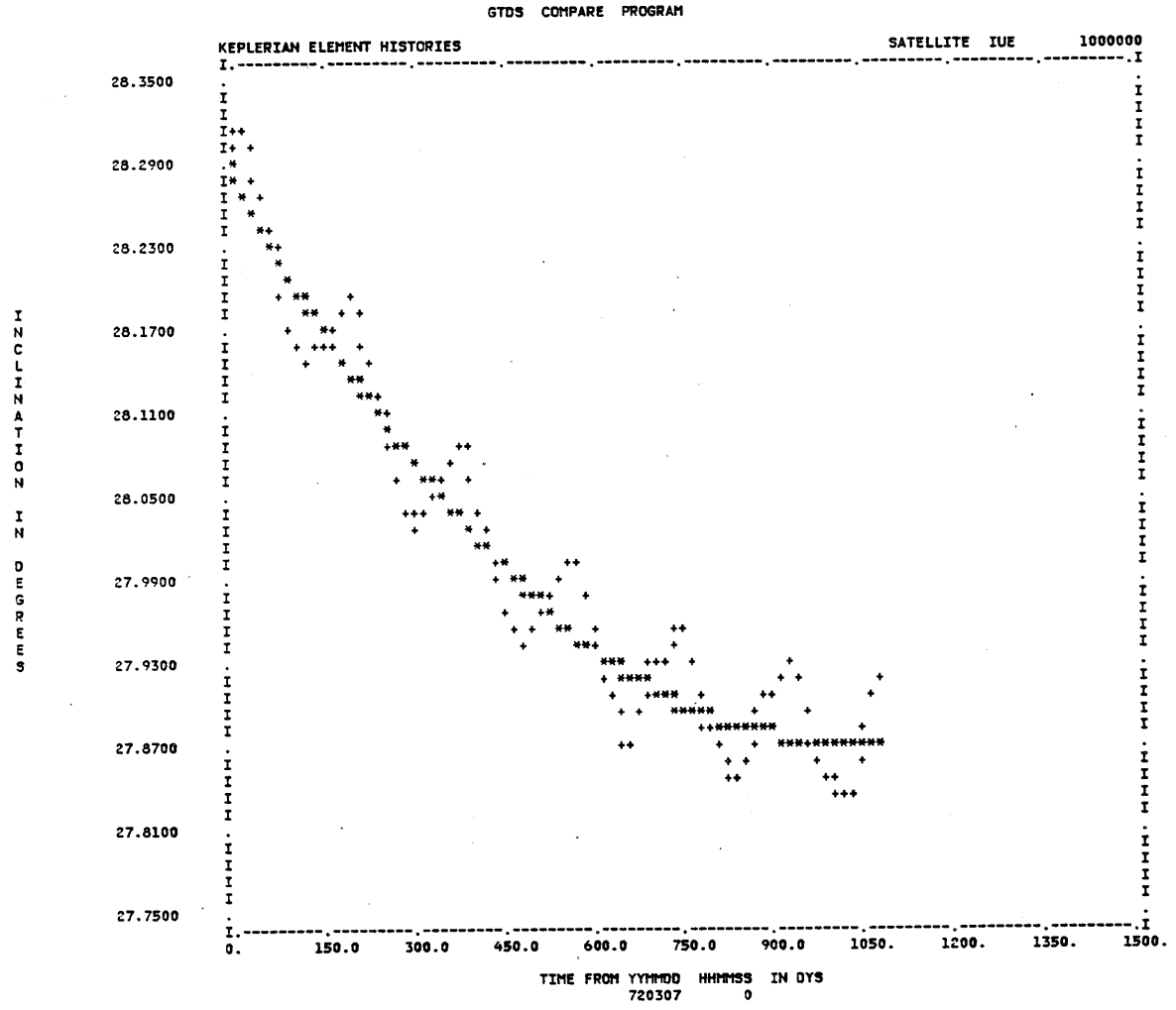
(+) = Cowell
(*) = AOG

Figure 5-10. Comparison of the Mean and Osculating Eccentricity Histories for the 3 Year Integration of the IUE Orbit/AOG versus Cowell



(+) = Cowell
(*) = AOG

Figure 5-11. Comparison of the Mean and Osculating Inclination Histories for the 3 Year Integration of the IUE Orbit/AOG versus Cowell



(+) = Cowell
(*) = AOG

Figure 5-12. Differences Between the Mean and Osculating Semi-Major Axis Histories for the 3 Year Integration of the IUE Orbit/AOG minus Cowell

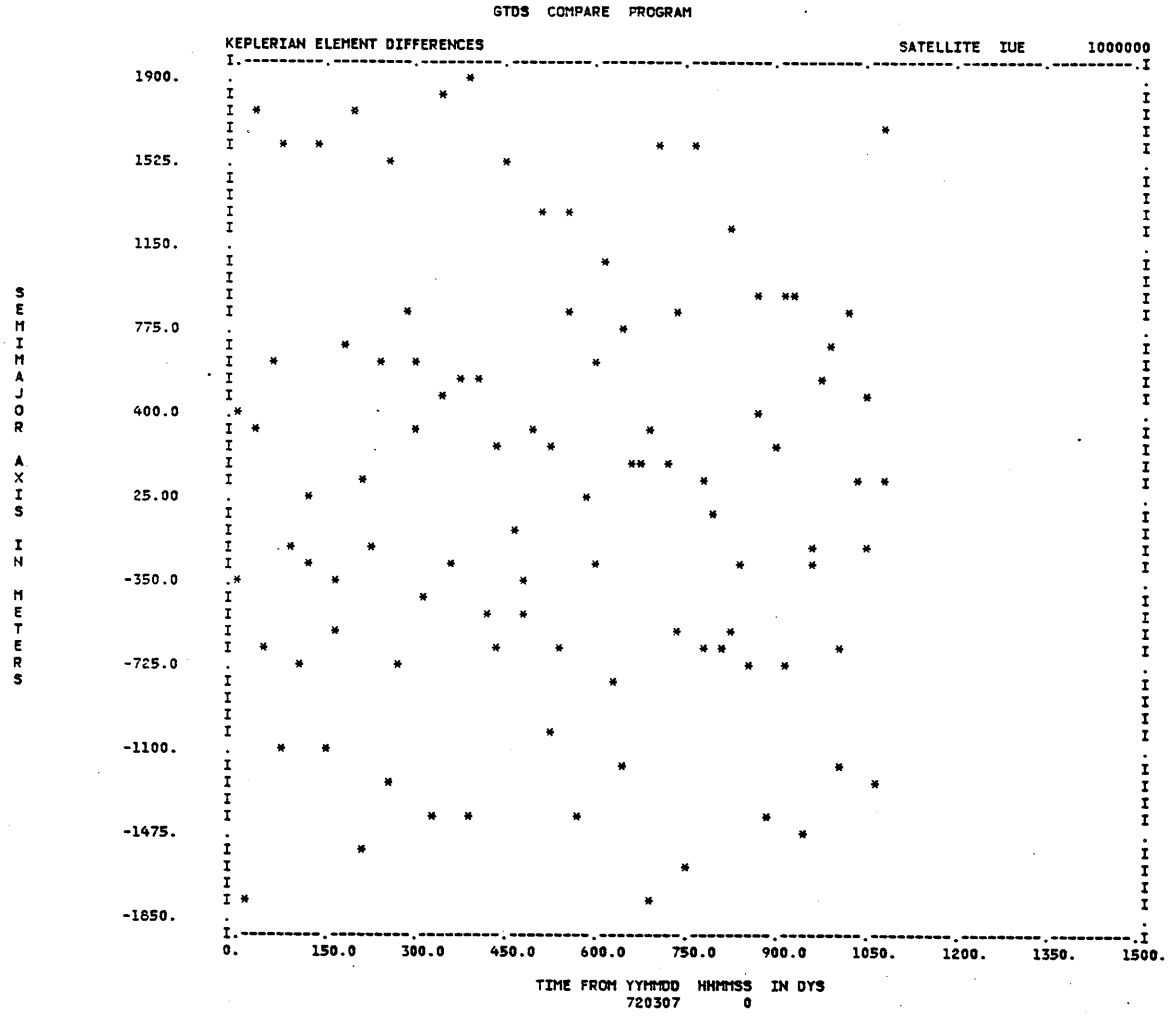


Figure 5-13. Differences Between the Mean and Osculating Eccentricity Histories for the 3 Year Integration of the IUE Orbit/AOG minus Cowell

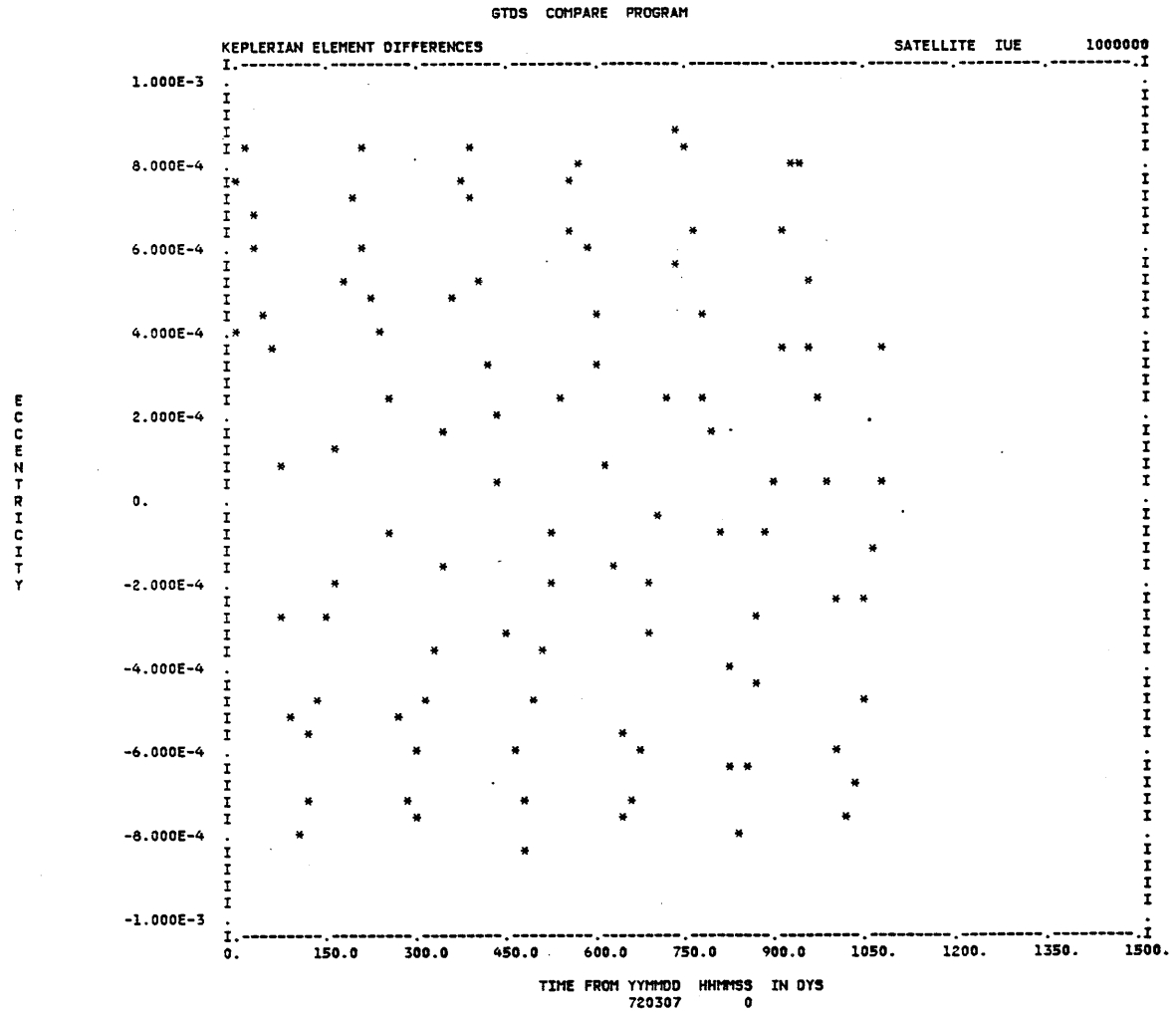
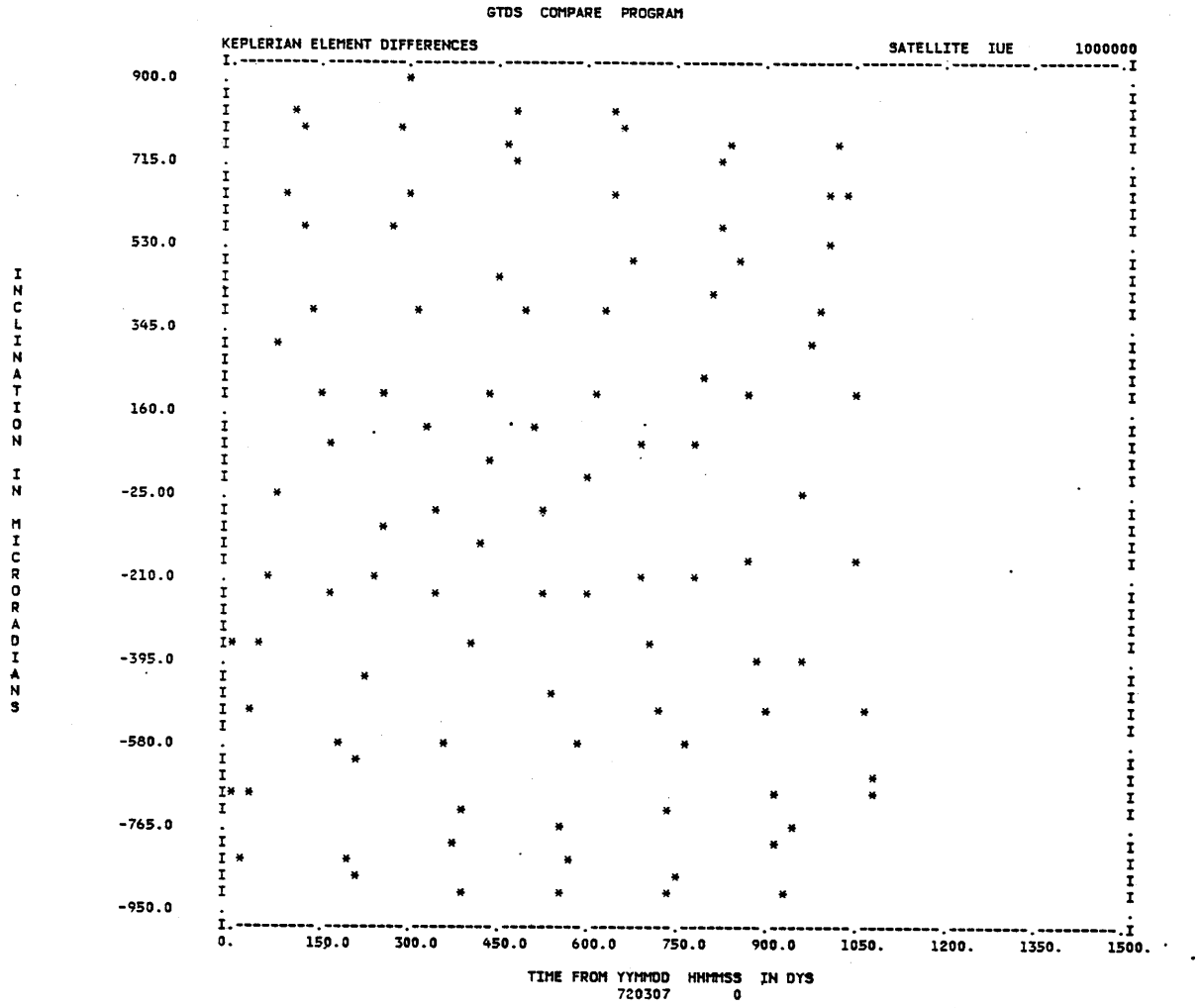
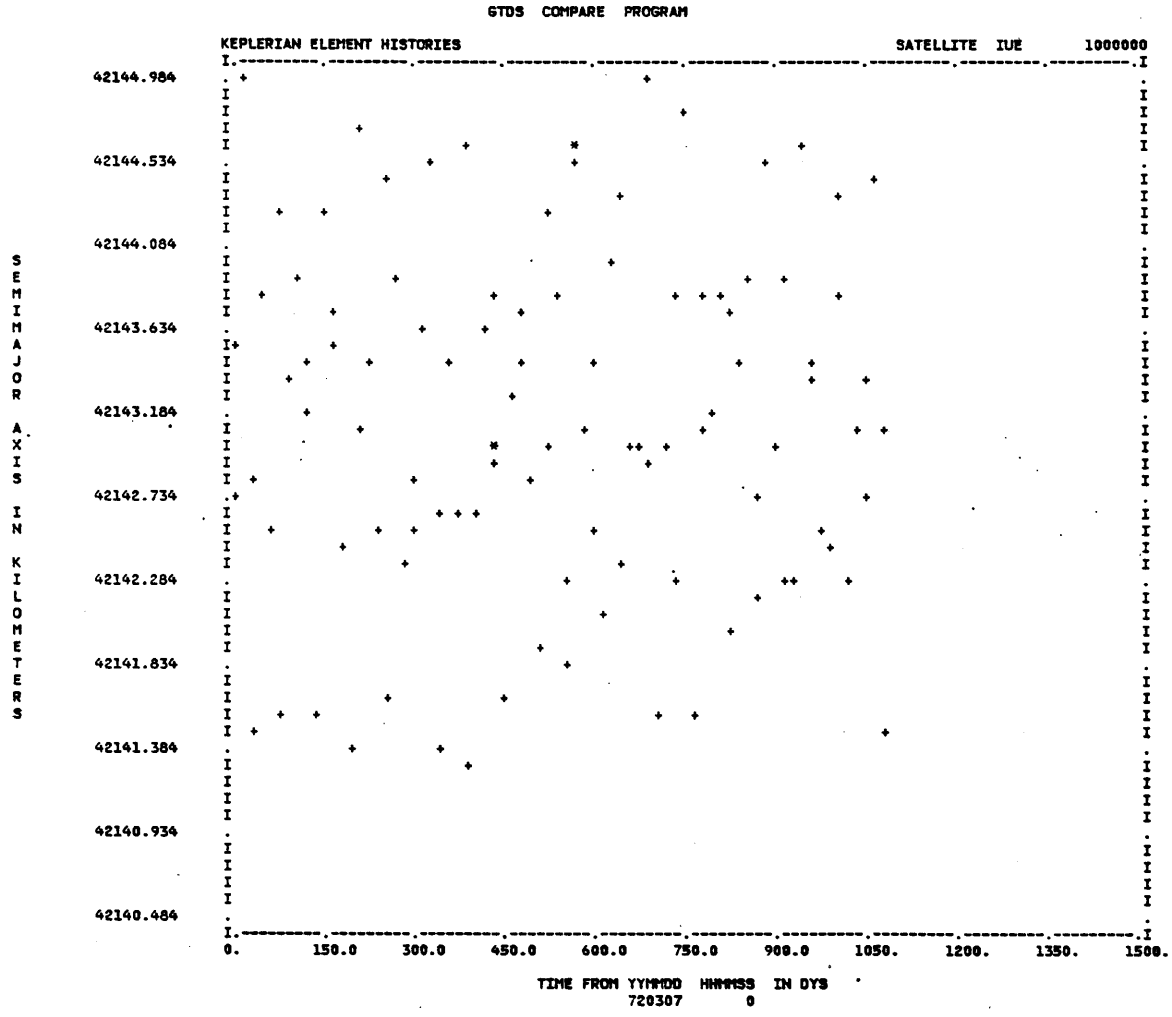


Figure 5-14. Differences Between the Mean and Osculating Inclination Histories for the 3 Year Integration of the IUE Orbit/AOG minus Cowell



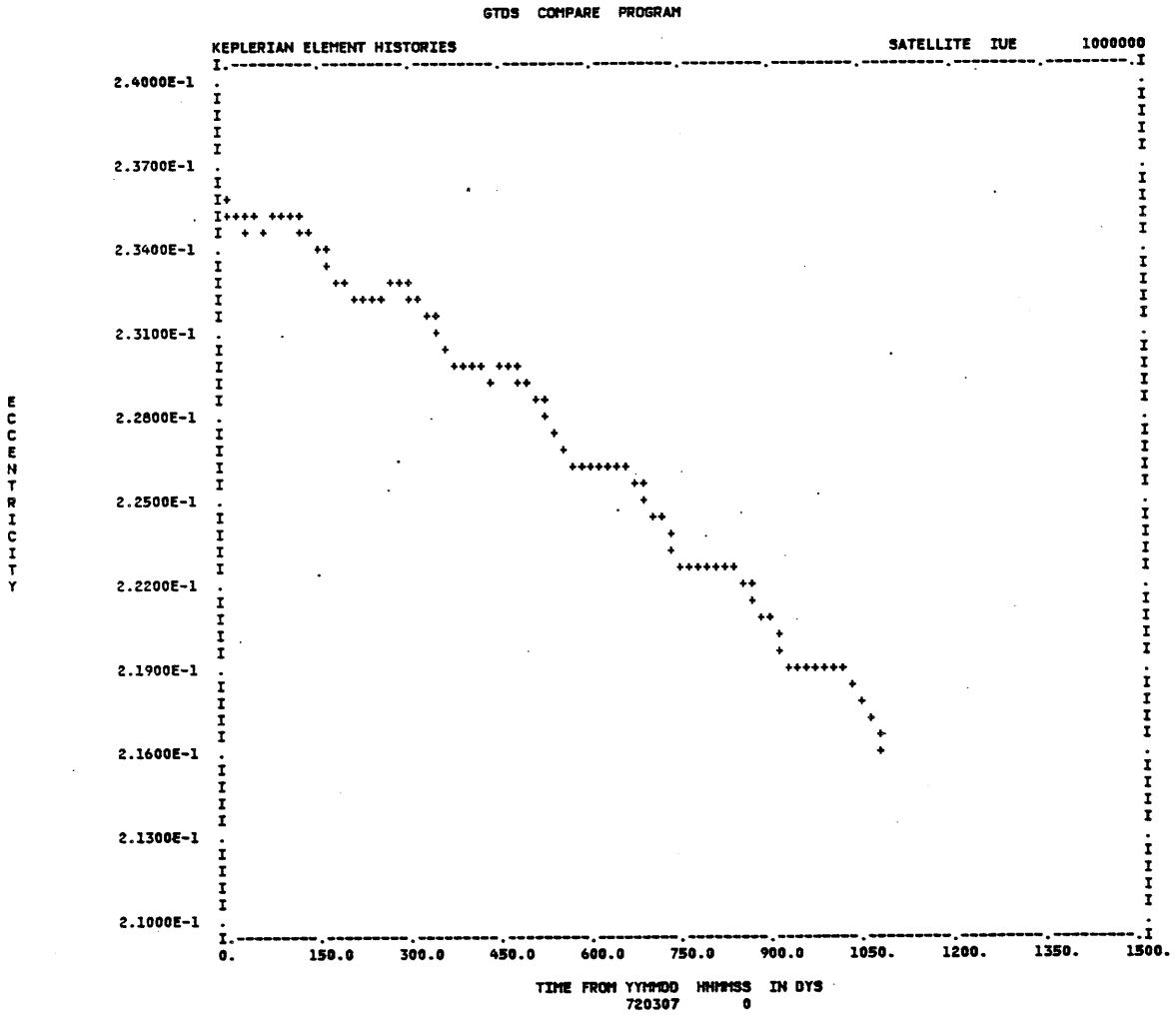
models. A semi-analytical recovery of the high precision orbital elements at the compare times of the AOG leads to the element history plots in Figures 5-15 through 5-17. At the altitude of IUE, the short periodic variations in the semi-major axis caused by third body perturbations amount to a large percentage of the total variation. The lunar short periodics by themselves cause the semi-major axis to vary about its mean value by as much as 1 kilometer. A comparison of Figure 5-9 with Figure 5-15 shows that short periodic corrections to the constant mean semi-major axis have reproduced the Cowell generated element, to within the resolution of the plot scale, at all but two points in the three year prediction span. This is powerful evidence that the third body short periodic model is working well. Similarly, short periodic corrections to the mean eccentricity in Figure 5-10, notably the semi-annual variation induced by the sun, produce an approximation to the Cowell generated eccentricity in Figure 5-16 that is exact to within the resolution of the plot scale. A comparison of the inclination plots in Figures 5-11 and 5-17 provides yet another example of the accuracy with which the semi-annual variations have been modelled in the third body SPG. Hence, the three year integration provides the first indications that extremely accurate long term orbital predictions that include the third body models developed in

Figure 5-15. Osculating Semi-Major Axis Comparison for the 3 Year IUE Integration/Semi-Analytical versus Cowell



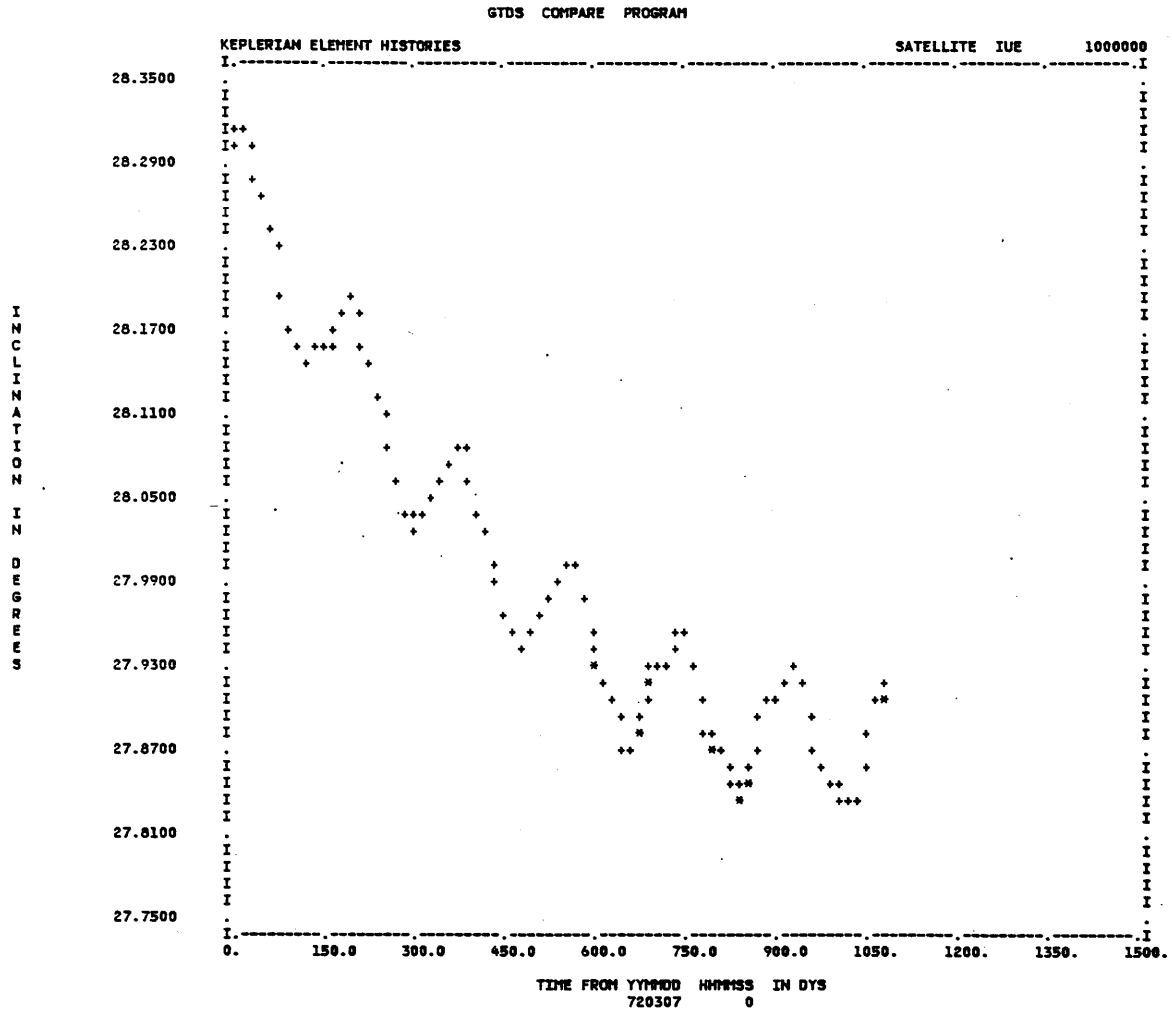
(+) = Cowell
(*) = AOG & SPG

Figure 5-16. Osculating Eccentricity Comparison for the 3 Year IUE Integration/Semi-Analytical versus Cowell



(+) = Cowell
(*) = AOG & SPG

Figure 5-17. Osculating Inclination Comparison for the 3 Year IUE Integration/Semi-Analytical versus Cowell



(+) = Cowell
(*) = AOG & SPG

this thesis can be initialized from relatively short spans of high precision data.

The Cowell file for the three year comparison was generated from an integration that used 150 time regularized steps per revolution of tne satellite. This is a conservative step size, although it is not unreasonable for a satellite orbit of moderate eccentricity. In contrast, the AOG used a step size of one year. This was made possible by removing fast variable dependent frequencies from the third body equations of motion. Since the circulation periods for satellite angles, such as the argument of perigee and the longitude of the ascending node, are generally quite long at the altitude of IUE, the shortest period oscillation of considerable amplitude retained in the AOG was the 8.9 year advance of lunar perigee. Hence, an AOG step size of one year was permitted without loss of accuracy. This remarkably large integration step size has enormous consequences for the efficient analysis of high altitude orbital stability over decades or centuries. A one hundred year AOG prediction of the IUE orbit was made with a one year integration step size, using the epoch mean elements of Table 5-3. The AOG executed in 33 seconds of CPU time. The element histories for the eccentricity and inclination are plotted in Figures 5-18 and 5-19. At present, there are no precision benchmarks against

Figure 5-18. Evolution of the Mean Eccentricity for the 100 Year AOG Prediction of the IUE Orbit

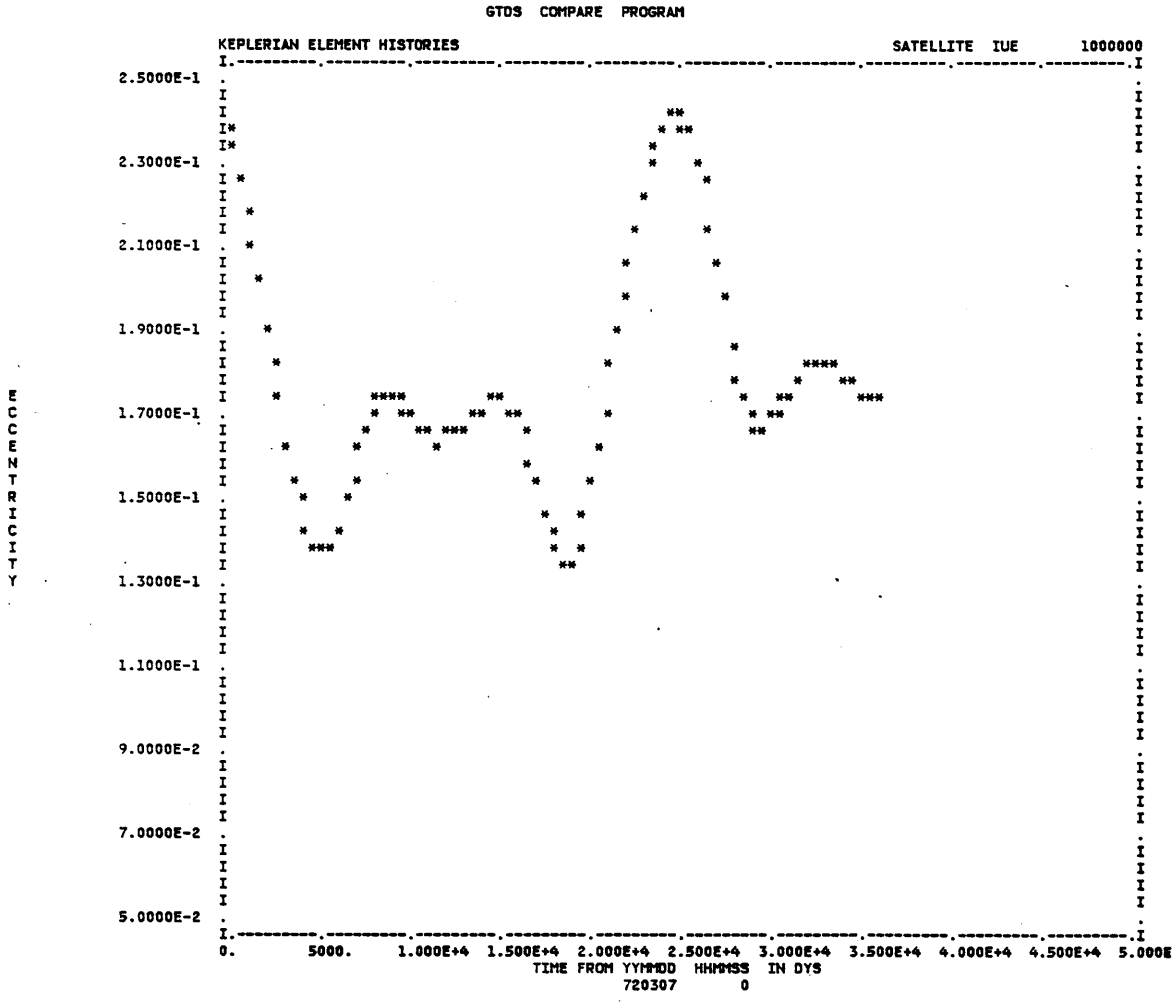
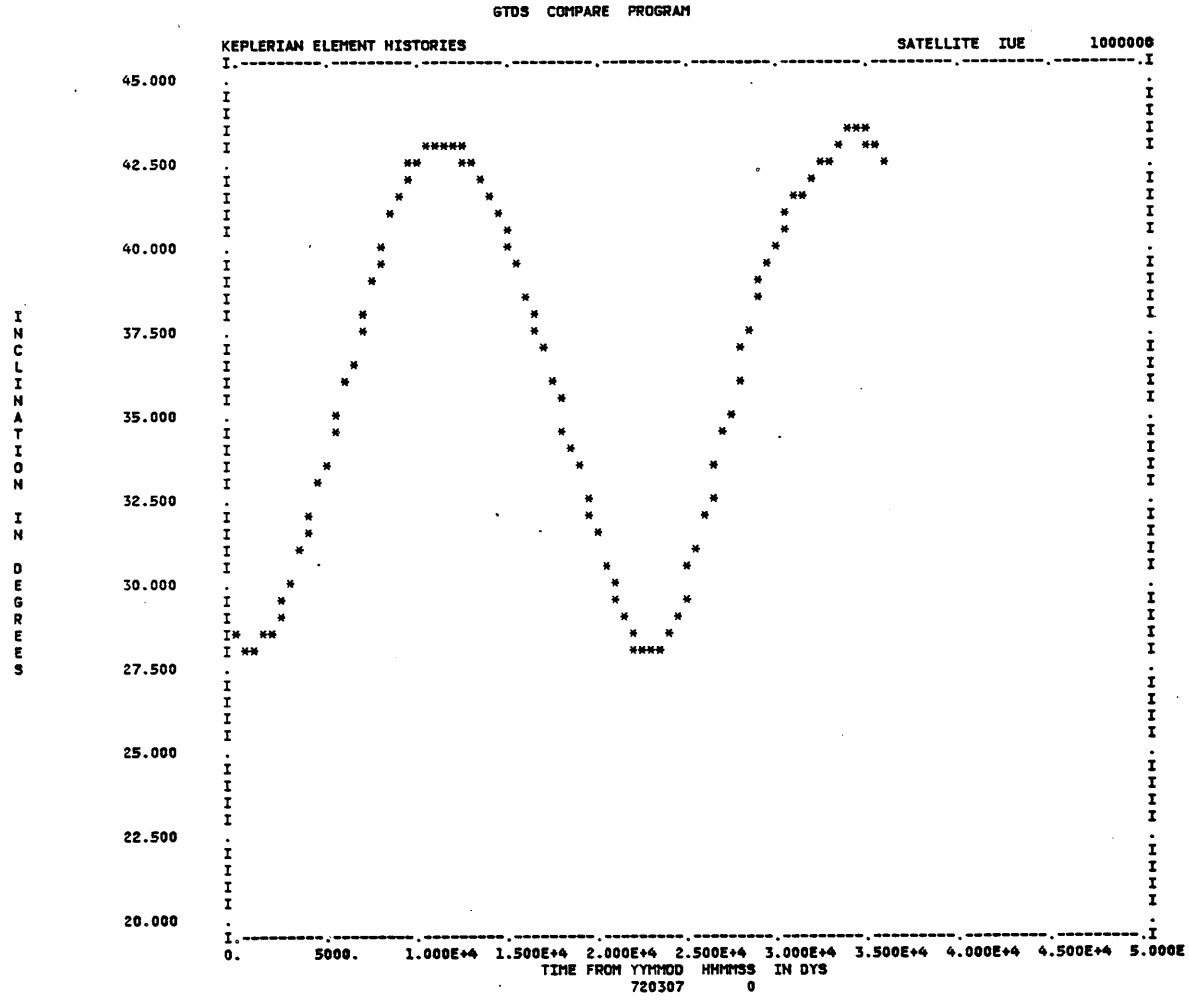


Figure 5-19. Evolution of the Mean Inclination for the 100 Year AOG Prediction of the IUE Orbit



which the correctness of this prediction can be measured. However, the basic regularity of the element histories is a good indication that their deviation from the physical world is at least a slow process. Furthermore, the 54 year period of oscillation in the inclination, predicted by Kozai [30] for the geosynchronous orbit, is clearly seen in Figure 5-19. The corresponding Cowell trajectory cannot be integrated. It would be prohibitively time consuming. In addition, the build-up of numerical error over time, associated with intensive computations on a fixed word length computer, would make the output points increasingly suspect.

5.3.2 ISEE Test Case

The International Sun-Earth Explorer (ISEE) orbit demonstrates the accuracy of the first order third body theory when the satellite orbital eccentricity is large. The initial orbital elements are shown in Table 5-4.

Table 5-4. Epoch Osculating Elements for the ISEE Test Case

$a = 70850.0$ km	Epoch = 7 March 1972
$e = 0.89$	$0^h.0, 0^m.0, 0^s.0$
$i = 29.0°$	
$\Omega = 49.5°$	Period = 2.2 days
$\omega = 0.21°$	
$M = 0.0°$	

Radius of Perigee = 7793.5 km
Radius of Apogee = 133906.5 km
Lunar Parallax Factor, $(a/a')_\ell \simeq 0.18$
Solar Parallax Factor, $(a/a')_S \simeq 0.00047$

The epoch mean elements for the AOG were obtained by a PCE procedure over sixty days. The *a priori* elements for the initialization were provided by averaging the osculating trajectory over one period of the satellite using the GTDS numerical osculating-to-mean conversion. The perturbation models used in the PCE are shown in Table 5-5. The ISEE

orbit is non-resonant with respect to a third body so that only the double averaged terms for the third body are retained in the AOG. The mean elements determined from the PCE are given in Table 5-6. These elements were used to initialize an eight year integration of the averaged equations of motion. A one year integration step size was used. A high precision Cowell integration over the same time was performed using 200 time regularized steps per revolution of the satellite. The five slow Keplerian element histories are shown in Figures 5-20 through 5-24 for both the AOG and Cowell predictions. The Cowell elements are represented by the symbol (+), while the mean elements are designated by a (*). As in the previous test case, the (+) overwrites the (*) when the two histories agree to within the resolution of the plot scale. The mean elements are seen to closely follow the mean of the osculating element histories. One will note that the scale of the semi-major axis plot in Figure 5-20 was set by the single Cowell point at epoch corresponding to 70850 kilometers. This point occurs at perigee where the short periodic variation in the semi-major axis caused by J_2 is on the order of 400 kilometers. Since the time over which this variation acts is extremely short in comparison to the orbital period, the PCE procedure tended to smooth its effects. This accounts for the apparent discrepancy between the single Cowell point and the predicted mean. The absence

of any further points at perigee in Figure 5-20 is a point selection phenomenon. The pronounced oscillatory behavior evidenced in the eccentricity and inclination plots of Figures 5-21 and 5-22 is caused by the second multiple of the lunar argument of perigee which was not removed by the averaging operation.

Table 5-5. PCE Perturbation Models for the ISEE Test Case

1) AOG + SPG Perturbation Model:

SUN	MOON	EARTH
N = 5	N = 12	J_2, J_3, J_4
M* = 5	M* = 12	
R* = 4	R* = 6	
$-5 \leq t \leq 5$	$-6 \leq t \leq 6$	
$-5 \leq s \leq 5$	$-6 \leq s \leq 6$	

NOTE: AOG retains only the double averaged terms for the third body

N ≡ maximum power of the parallax factor, $(\bar{a}/a')$

M* ≡ upper bound on the satellite Hansen coefficient d'Alembert characteristic

R* ≡ upper bound on the third body Hansen coefficient d'Alembert characteristic

2) Cowell Perturbing Acceleration:

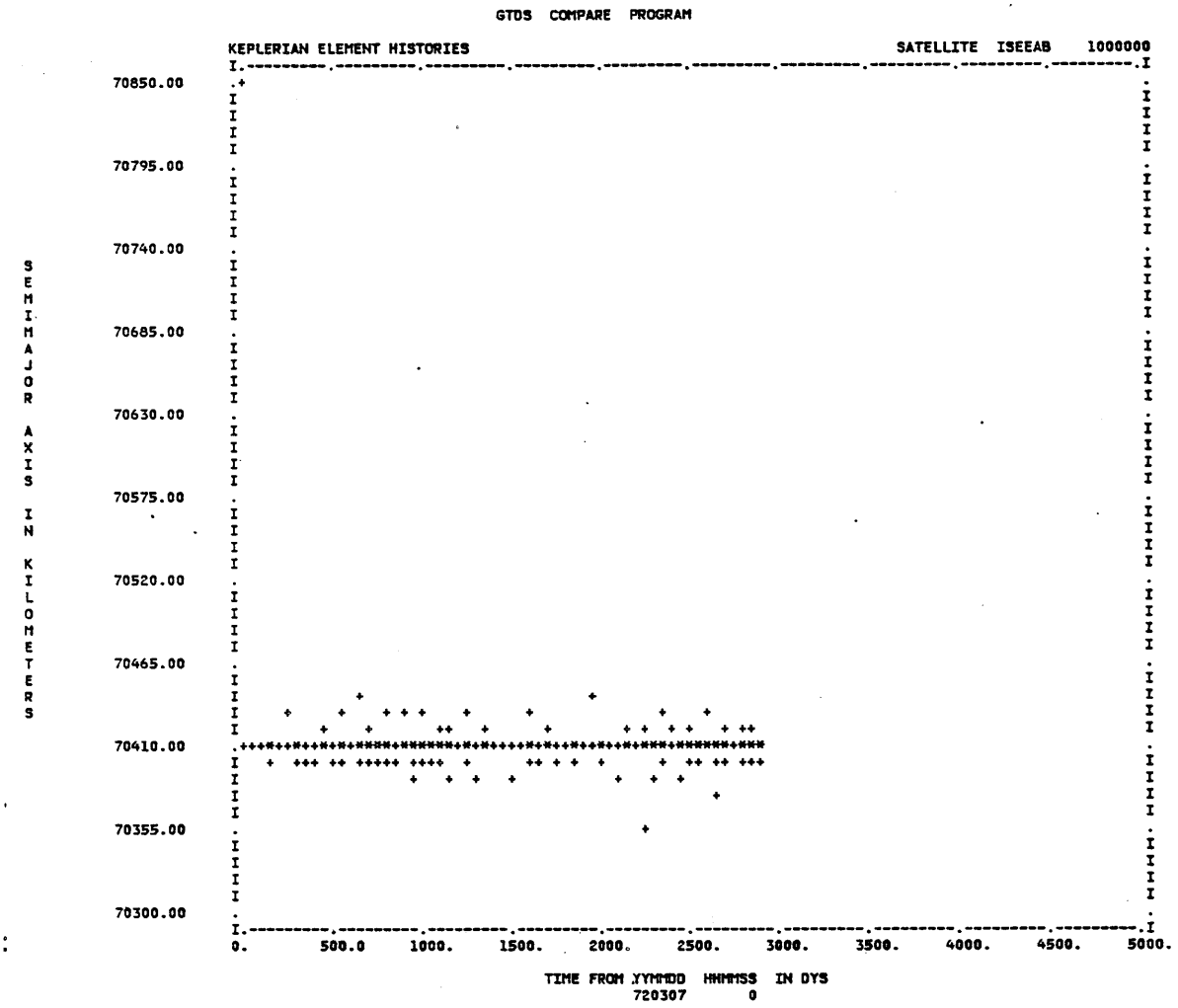
point mass sun
point mass moon
J_2, J_3, J_4

Table 5-6. Epoch Mean Elements for the ISEE Test Case

Keplerian	Equinoctial
$\bar{a}$ = 70405.55206 km	$\bar{a}$ = 70405.55206 km
$\bar{e}$ = 0.8908091435	$\bar{h}$ = 0.6816570336
$\bar{i}$ = 29.24922760°	$\bar{k}$ = 0.5734846282
$\bar{\Omega}$ = 49.50104656°	$\bar{p}$ = 0.1984228809
$\bar{\omega}$ = 0.4247283997°	$\bar{q}$ = 0.169462882
$\bar{M}$ = 359.2566209°	$\bar{\lambda}$ = 49.18239586°

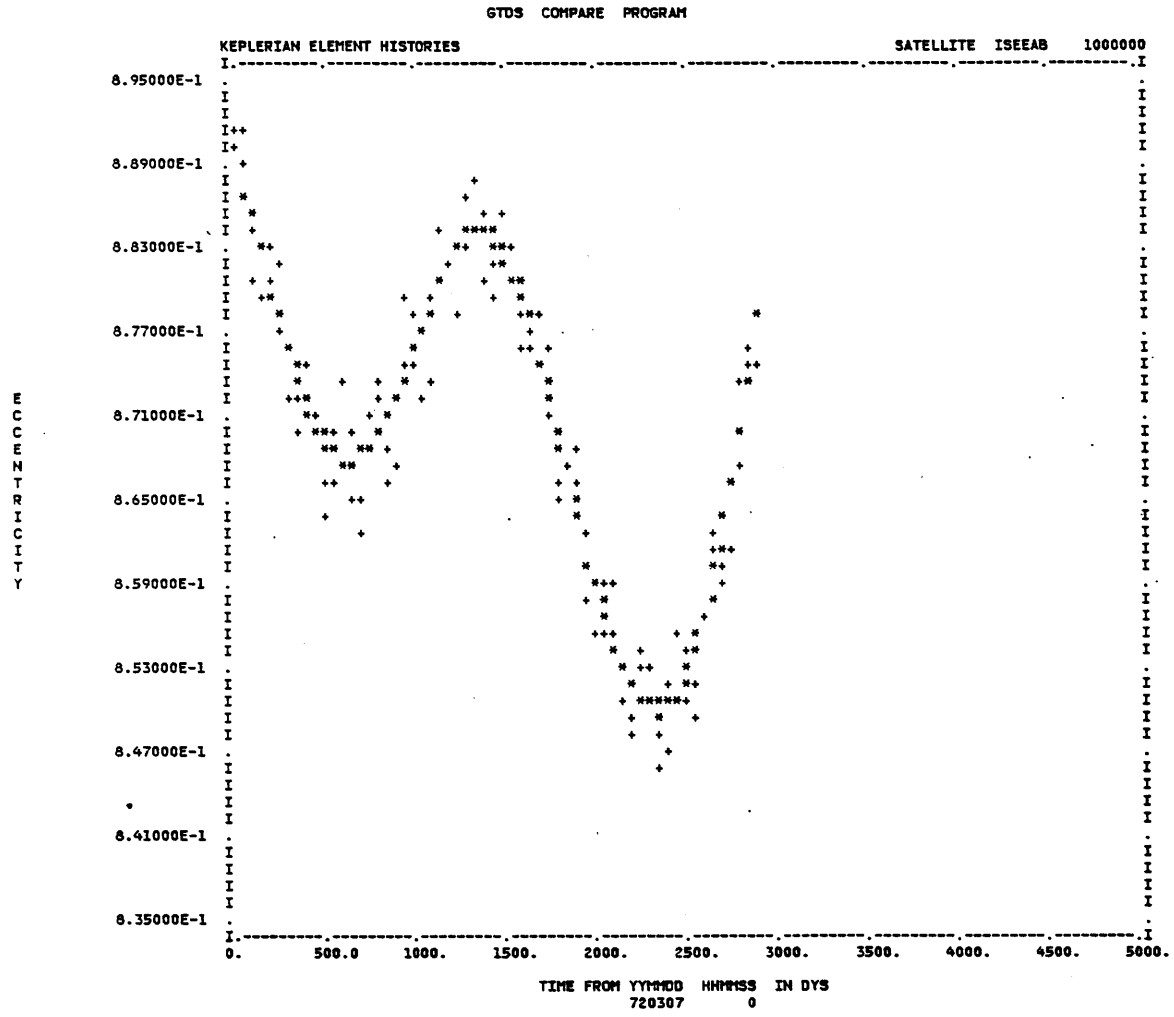
A look at the element plots for the satellite argument of perigee and longitude of the ascending node reveals that their circulation periods are approximately 16 years and 21 years respectively. This indicates that a one year integration step size for the AOG is appropriate even for an orbit with strong zonal perturbations arising from the low perigee height. Hence, it would appear that the benefit of retaining only the double averaged third body terms in the AOG is not diminished by the inclusion of other

Figure 5-20. Comparison of the Mean and Osculating Semi-Major Axis Histories for the 8 Year Integration of the ISEE Orbit/AOG versus Cowell



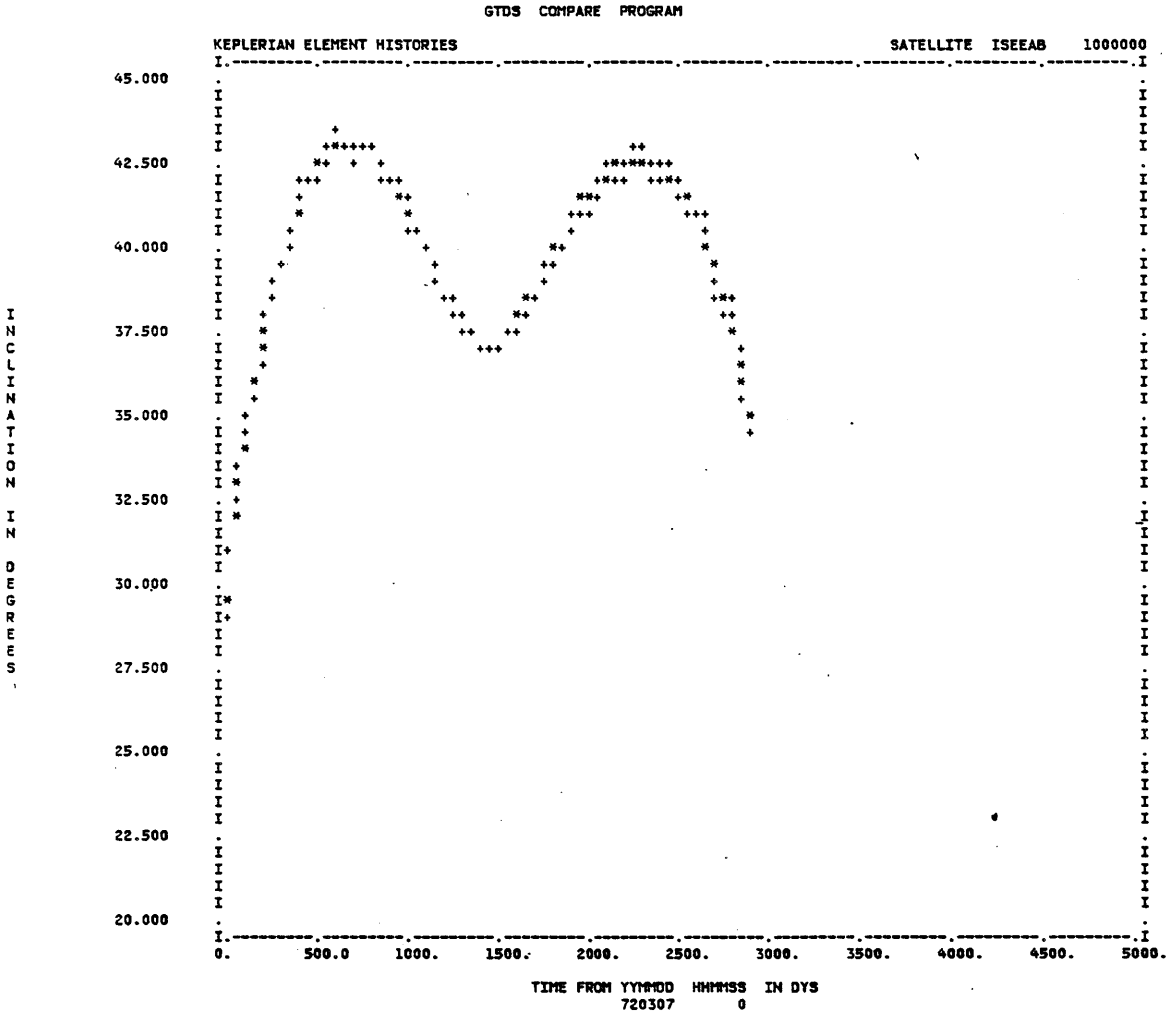
(+) = Cowell
(*) = AOG

Figure 5-21. Comparison of the Mean and Osculating Eccentricity Histories for the 8 Year Integration of the ISEE Orbit/AOG versus Cowell



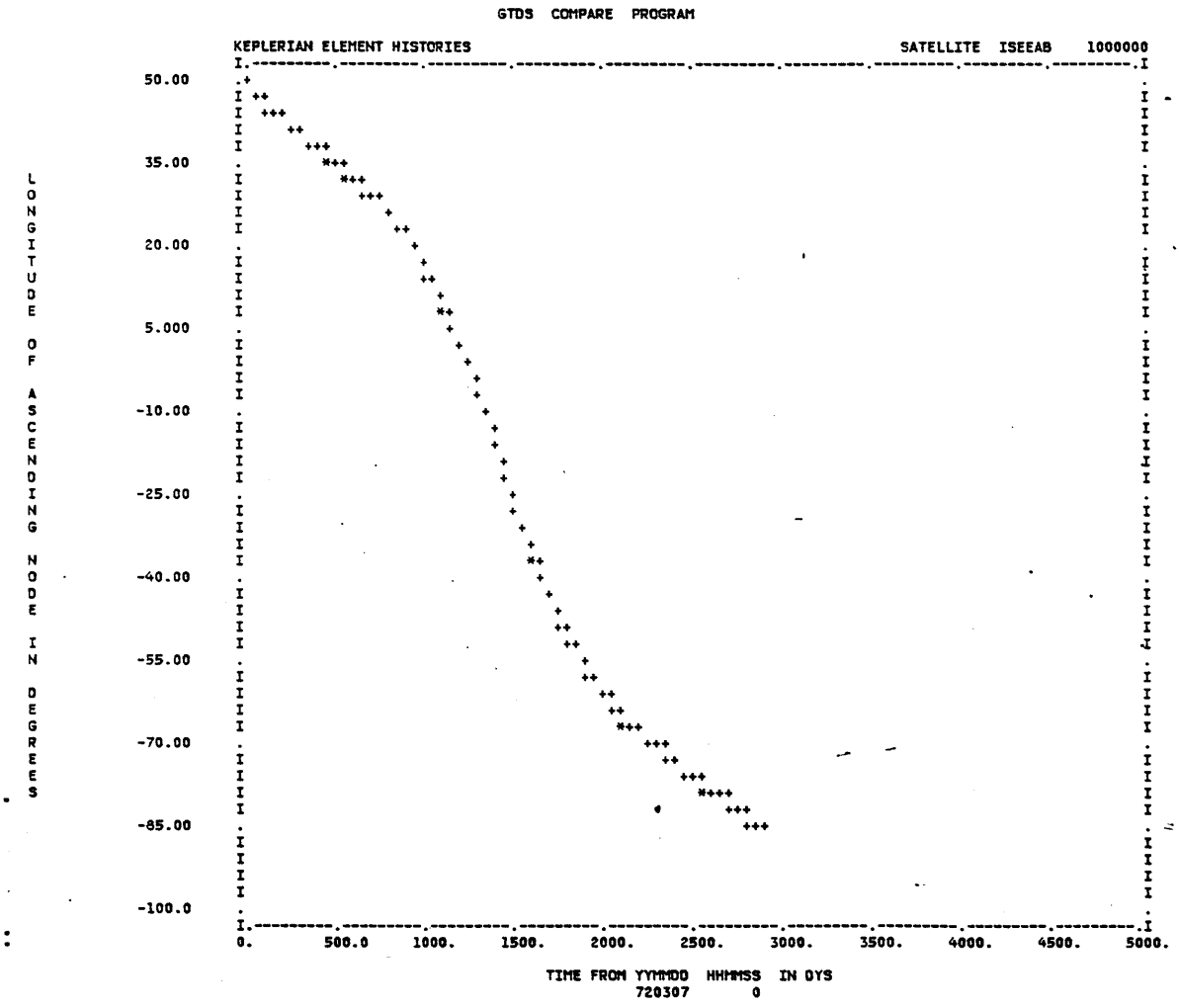
(+) = Cowell
(*) = AOG

Figure 5-22. Comparison of the Mean and Osculating Inclination Histories for the 8 Year Integration of the ISEE Orbit/AOG versus Cowell



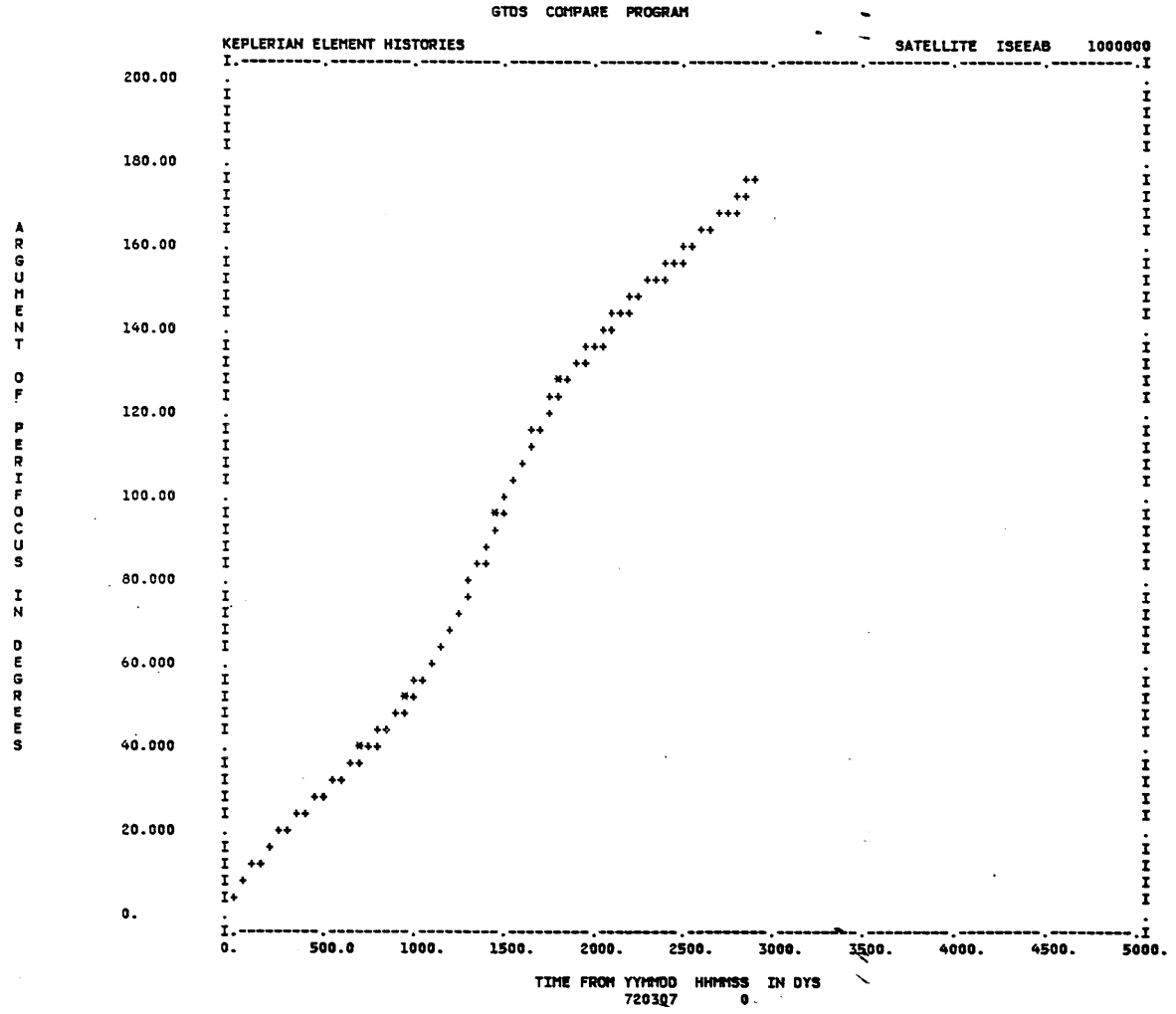
(+) = Cowell
(*) = AOG

Figure 5-23. Comparison of the Mean and Osculating Longitude of Ascending Node Histories for the 8 Year Integration of the ISEE Orbit/ AOG versus Cowell



(+) = Cowell
(*) = AOG

Figure 5-24. Comparison of the Mean and Osculating Argument of Perifocus Histories for the 8 Year Integration of the ISEE Orbit/AOG versus Cowell



(+) = Cowell
(*) = AOG

averaged perturbation models. This allows very efficient long term predictions to be made with a realistic force field.

A comparison of integration times between Cowell and the AOG is given in Table 5-7. The AOG is observed to execute in approximately 1/30 the time of the Cowell integration over the eight year span. It should be noted that the comparison is even more favorable, since the AOG execution time also includes the creation of the ephemeris comparison plots described above.

Table 5-7. Comparison of Cowell and AOG Execution Times for the Eight Year ISEE Integration

Orbit Generator	Step Size	Execution Time
Cowell	200 steps/rev., time regularized	300 seconds
AOG	31536000 seconds (1 year)	9.95 seconds

Notes

1) The Cowell integrator is based on the 12th order Adams-Bashforth Predictor / Adams-Moulton Corrector Algorithm
2) The AOG uses a 4th order Runge-Kutta integration algorithm
3) The execution time for the Cowell integration contains overhead associated with file creation.
4) The execution time for the AOG contains overhead assciated with file creation and includes the ephemeris comparison step.

5.3.3 VELA Test Case

The evolution and stability of the high altitude VELA orbit are almost exclusively determined by the action of the sun and the moon. At this altitude lunar and solar perturbations can induce short periodic variations in the semi-major axis that are on the order of 100 kilometers. The initial orbital elements are shown in Table 5-8.

Table 5-8. Epoch Osculating Elements for the VELA Test Case

$a = 118230.0$ km	Epoch = 8 April 1970
$e = 0.003$	$0^h.0, 0^m.0, 0^s.0$
$i = 32.52°$	
$\Omega = 0.0°$	Period = 4.68 days
$\omega = 47.0°$	
$M = 0.0°$	

Radius of Perigee = 117875.31 km
Radius of Apogee = 118584.69 km
Lunar Parallax Factor, $(a/a')_\ell \simeq 0.3075$
Solar Parallax Factor, $(a/a')_S \simeq 0.0008$

The initial mean elements for the AOG prediction were obtained from a PCE procedure over sixty days. The osculating satellite elements were used as the a priori input to the least squares differential correction algorithm. The perturbation models used in the PCE are given in Table 5-9. The frequencies included in the SPG reflect the shallow 6:1 resonance of the VELA orbit with the moon. The critical argument of the resonance has a period of approximately 167 days, while the second multiple of the critical argument circulates with a period of around 83 days. Both periods are far too short to be included in the AOG which still retains only the double averaged terms for the third body. However, the resonance should be modelled in the SPG since it produces terms with periods that are long in comparison to the fit span of the PCE. Failure to model the effect can cause a noticeable bias in the computed mean elements at epoch. The mean elements determined from the PCE are found in Table 5-10.

Table 5-9. PCE Perturbation Models for the VELA Test Case

1) AOG + SPG Perturbation Model:

SUN	MOON
N = 4	N = 8
M* = 4	M* = 4
R* = 4	R* = 8
$-4 \leq t \leq 4$	$-4 \leq t \leq 4$
$-4 \leq s \leq 4$	$-12 \leq t \leq 12$

NOTE: AOG retains only the double averaged third body terms

N ≡ maximum power of the parallax factor, $(\bar{a}/a')$

M* ≡ upper bound on the satellite Hansen coefficient d'Alembert characteristic

R* ≡ upper bound on the third body Hansen coefficient d'Alembert characteristic

2) Cowell Perturbing Acceleration:

point mass sun
point mass moon

Table 5-10. Epoch Mean Elements for the VELA Test Case

Keplerian	Equinoctial
$\bar{a}$ = 118095.5461 km	$\bar{a}$ = 118095.5461 km
$\bar{e}$ = 0.0020558154	$\bar{h}$ = 0.0017593771
$\bar{i}$ = 32.48414636°	$\bar{k}$ = 0.0010634702
$\bar{\Omega}$ = 359.9590416°	$\bar{p}$ = -0.000208255
$\bar{\omega}$ = 58.88974402°	$\bar{q}$ = 0.2913232484
$\bar{M}$ = 348.2477284°	$\bar{\lambda}$ = 47.09651402°

The mean elements in Table 5-10 were used to initialize a ten year AOG prediction of the VELA orbit. The numerical integration used a step size of one year. The truncation parameters N, M*, R* for the AOG prediction are slightly different than those used in the PCE and are compiled in Table 5-11. The upper bound on the d'Alembert characteristic for the satellite Hansen coefficient has been increased to accomodate some growth in the satellite orbital eccentricty over the ten year prediction span. The new third body model is not inconsistent with the model used in the PCE since at the very small epoch eccentricity of the VELA orbit the same fit would be achieved by both. The Cowell compare file was created using the same models as those used in the PCE. The integration step size was 2700 seconds. Ephemeris comparison plots over the ten year integration are provided in Figures 5-25 through 5-30 for the five slow elements of the equinoctial set and the inclination. The Cowell trajectory is represented by the symbol (+), while the mean output of the AOG is denoted by (*). Figure 5-25 shows that the PCE has effectively determined the mean semi-major axis. The other averaged element histories show a similar ability to track the mean of the Cowell generated elements. The slight divergence in the k element at the end of ten years may be an initial conditions error.

Table 5-11. AOG Perturbation Model for the Ten Year VELA Integration

SUN	MOON
N = 4	N = 8
M* = 4	M* = 6
R* = 4	R* = 8

NOTE: AOG retains only the double averaged third body terms.

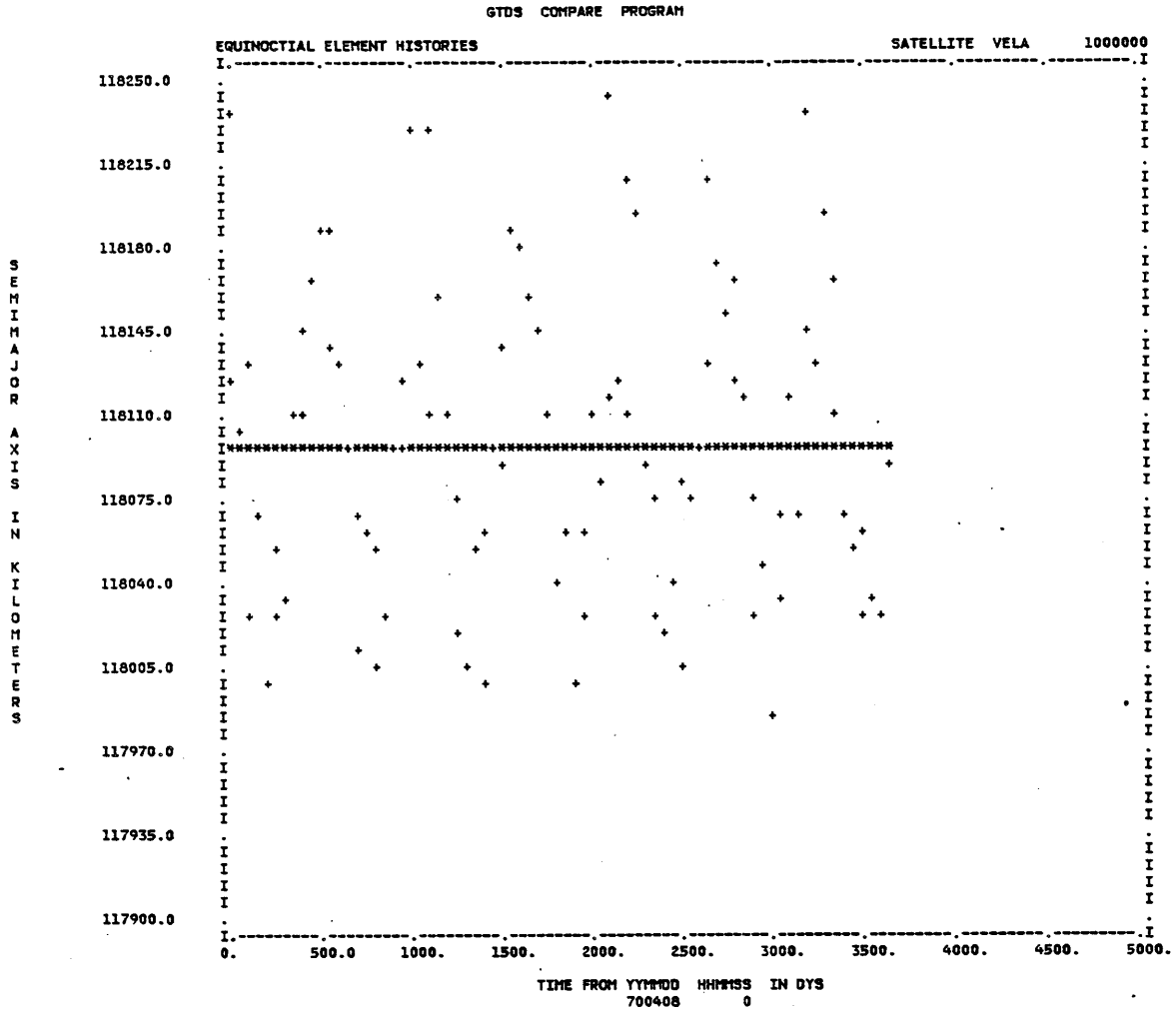
N ≡ maximum power of the parallax factor, $(\bar{a}/a')$

M* ≡ upper bound on the satellite Hansen coefficient d'Alembert characteristic

R* ≡ upper bound on the third body Hansen coefficient d'Alembert characteristic

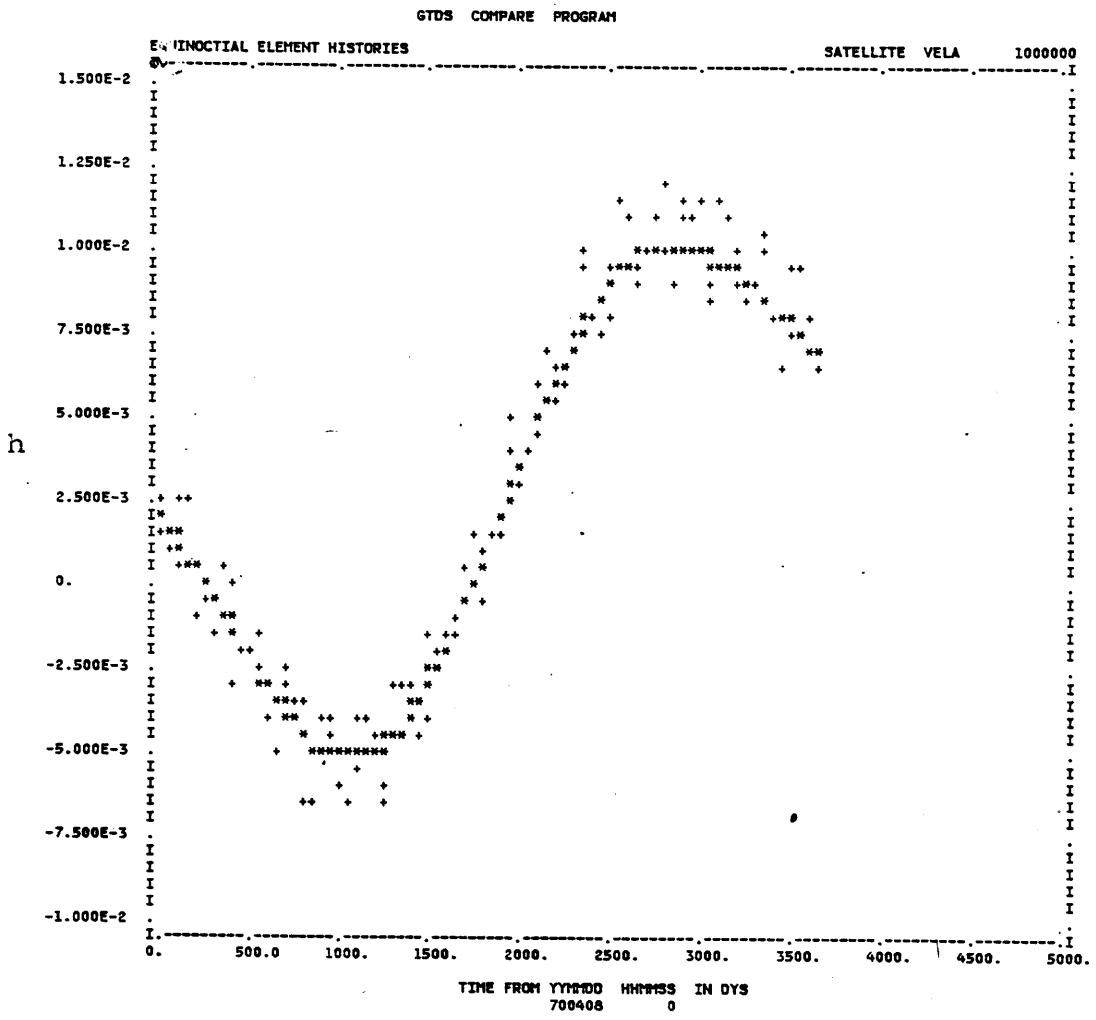
Table 5-12 compares the execution times of the Cowell and AOG predictions. The use of the first order third body theory with a one year step has reduced the execution time for a ten year run by at least a factor of 50. Again, it should be noted that the AOG run time includes the ephemeris comparison step so that the efficiency of the third body theory is even better than indicated.

Figure 5-25. Comparison of the Mean and Osculating Semi-Major Axis Histories for the 10 Year Integration of the VELA Orbit/AOG versus Cowell



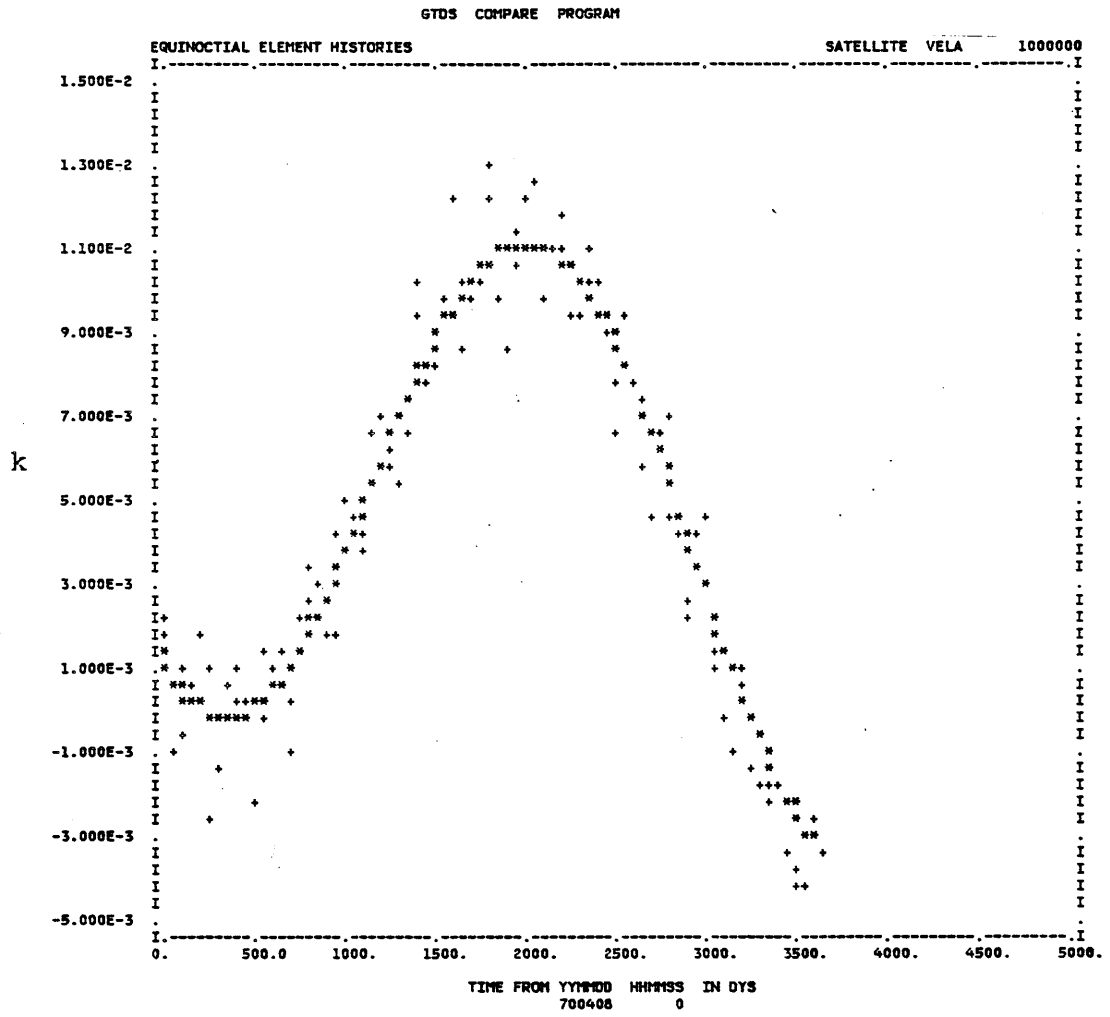
(+) = Cowell
(*) = AOG

Figure 5-26. Comparison of the Mean and Osculating h Element Histories for the 10 Year Integration of the VELA Orbit/AOG versus Cowell



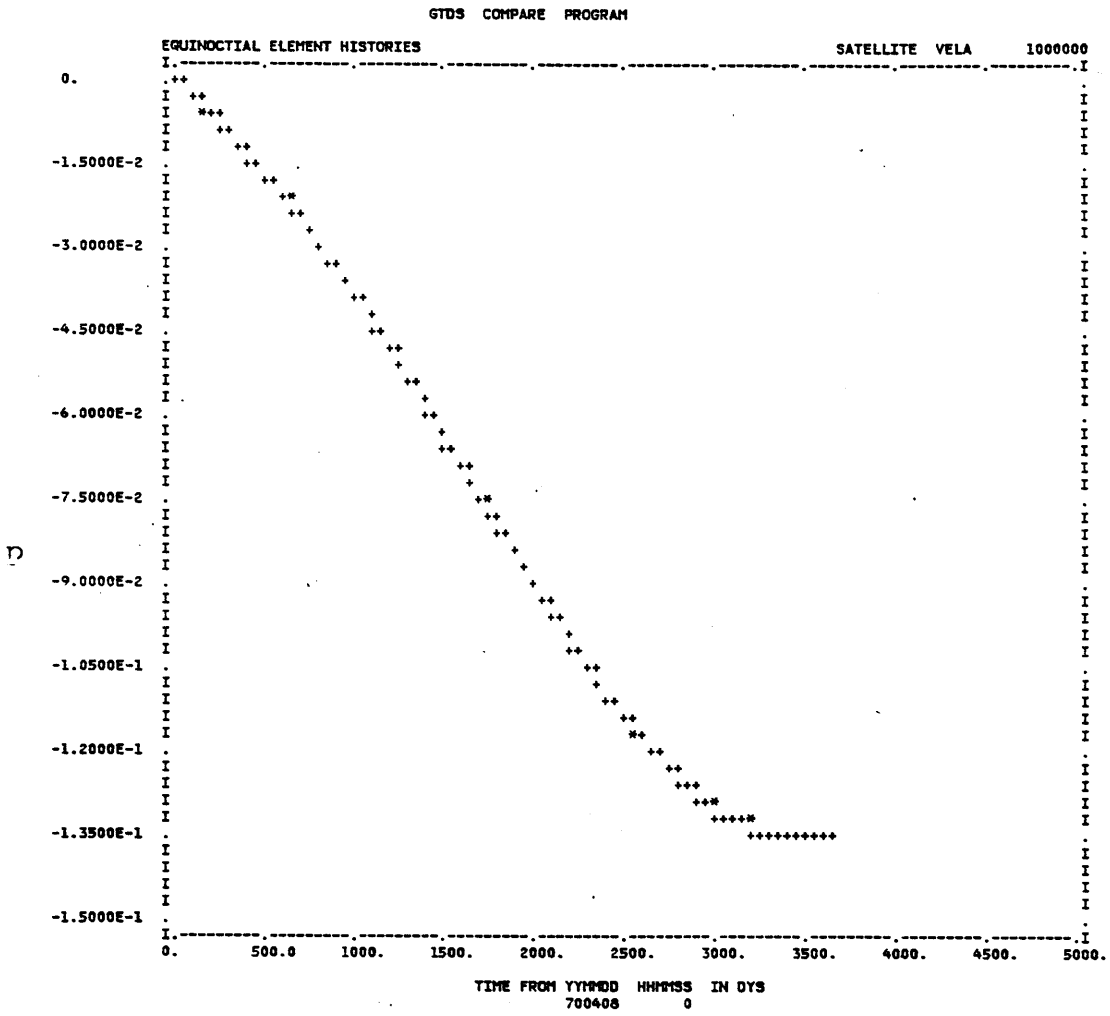
(+) = Cowell
(*) = AOG

Figure 5-27. Comparison of the Mean and Osculating k Element Histories for the 10 Year Integration of the VELA Orbit/AOG versus Cowell



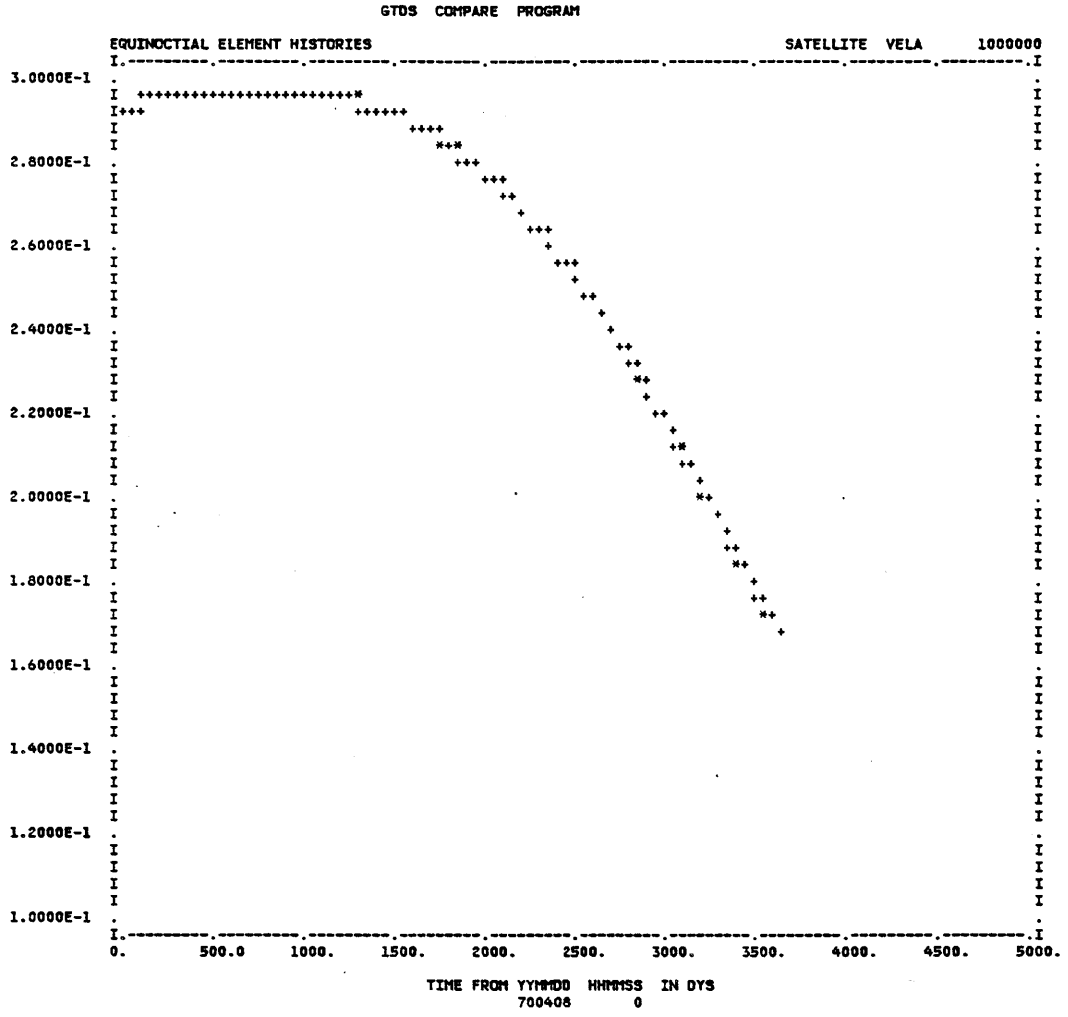
(+) = Cowell
(*) = AOG

Figure 5-28. Comparison of the Mean and Osculating p Element History for the 10 Year Integration of the VELA Orbit/AOG versus Cowell



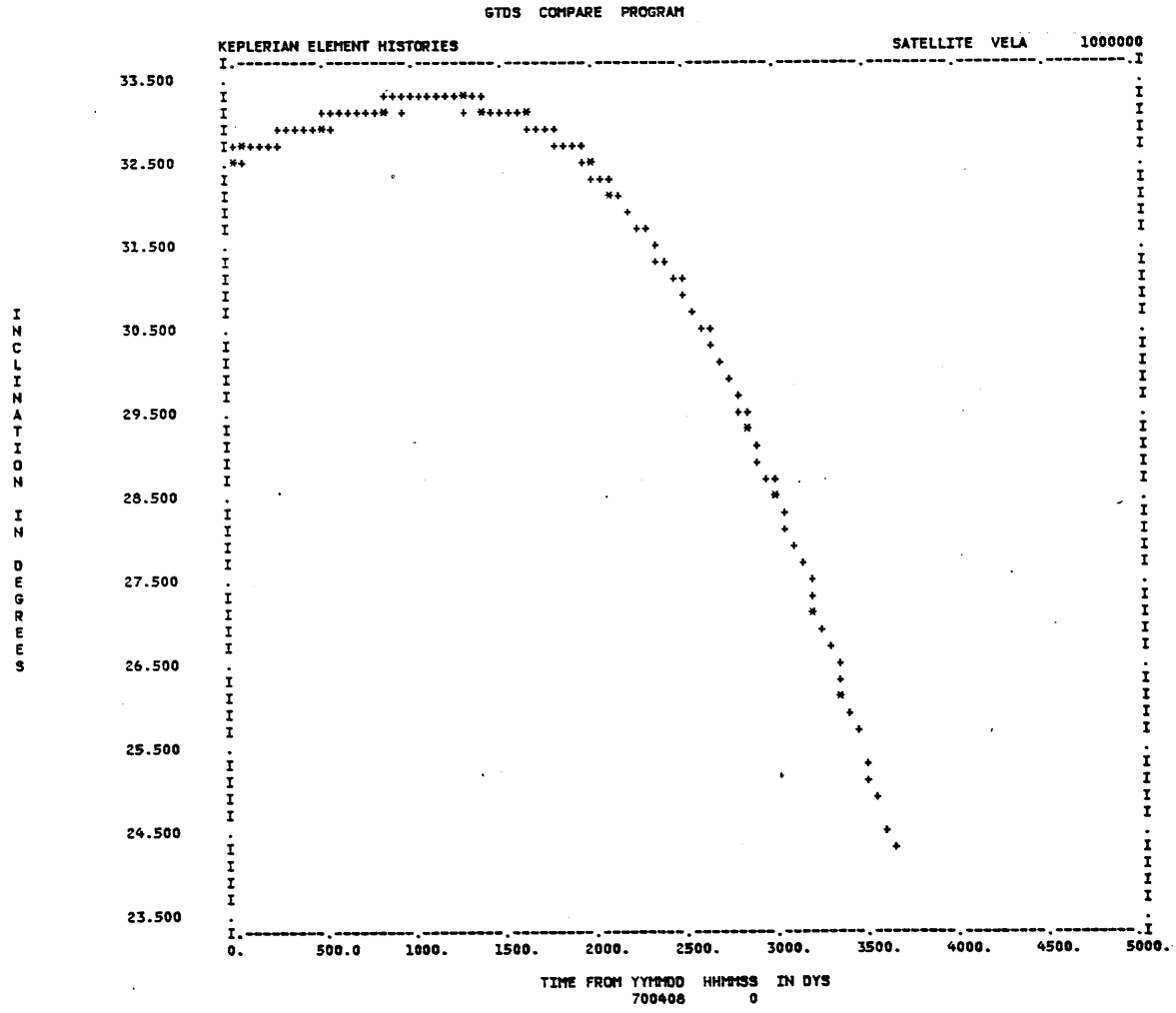
(+) = Cowell
(*) = AOG

Figure 5-29. Comparison of the Mean and Osculating q Element Histories for the 10 Year Integration of the VELA Orbit/AOG versus Cowell



(+) = Cowell
(*) = AOG

Figure 5-30. Comparison of the Mean and Osculating Inclination Histories for the 10 Year Integration of the VELA Orbit/AOG versus Cowell



(+) = Cowell
(*) = AOG

Table 5-12. Comparison of Cowell and AOG Execution Times for the Ten Year VELA Integration

Orbit Generator	Step Size	Execution Time
Cowell	2700 seconds, fixed step	482 seconds
AOG	31536000 sec. (1 year)	9.63 seconds

Notes

1) The Cowell integrator is based on the 12th order Adams-Bashforth Predictor / Adams-Moulton Corrector algorithm.
2) The AOG uses a 4th order Runge-Kutta integration algorithm.
3) The execution time for the Cowell integration contains overhead associated with file creation
4) The execution time for the AOG contains overhead associated with file creation and includes the ephemeris comparison step.

5.3.4 STRATSAT Test Case

The STRATSAT orbit is the most demanding test case discussed in this thesis. The initial orbital elements are presented in Table 5-13. Extremely strong lunar perturbations cause the orbit to decay within ten years of epoch. During this period, the eccentricity grows rapidly to very large values. The capability of the third body AOG to predict an orbit which evolves radically with respect to its epoch conditions is demonstrated by the STRATSAT test case. The ability of the third body theory to converge for high values of the parallax factor is also demonstrated.

Table 5-13. Epoch Osculating Elements for the STRATSAT Test Case

$a = 211868.8$ km	Epoch = 21 March 1985
$e = 0.001$	$0^h.0, 0^m.0, 0^s.0$
$i = 90.0°$	
$\Omega = 180.0°$	Period = 11.23 days
$\omega = 0.0°$	
$M = 0.0°$	

Radius of Perigee = 211656.93 km
Radius of Apogee = 212080.67 km
Lunar Parallax Factor, $(a/a')_\ell \simeq 0.55$

The initial mean elements for the AOG prediction were obtained from a PCE procedure over sixty days. The osculating satellite elements were used as the a priori quantities. The perturbation models used in the PCE are given in Table 5-14. The frequencies included in the SPG reflect the shallow 5:2 resonance of the STRATSAT orbit with the moon. The critical argument of the resonance has a period of approximately 233 days, while the second multiple of the critical argument circulates with a period of about 116 days. These periods are too short to be included in the AOG which retains only the double averaged lunar terms. However, the resonance should be modelled in the SPG to prevent a bias in the mean elements at epoch. The mean elements determined from the PCE are given in Table 5-15.

Table 5-14. PCE Perturbation Models for the STRATSAT Test Case

1) AOG + SPG Perturbation Model:

MOON

N = 12
M* = 6
R* = 8
$-4 \leq t \leq 4$
$-10 \leq s \leq 10$

NOTE: AOG retains only the double averaged third body terms

N ≡ maximum power of the parallax factor, $(\bar{a}/a')$

M* ≡ upper bound on the satellite Hansen coefficient d'Alembert characteristic

R* ≡ upper bound on the third body Hansen coefficient d'Alembert characteristic

2) Cowell Perturbing Acceleration:

point mass moon

Table 5-15. Epoch Mean Elements for the STRATSAT Test Case

Keplerian	Equinoctial
$\bar{a}$ = 211134.9014 km	$\bar{a}$ = 211134.9014 km
$\bar{e}$ = 0.0044788188	$\bar{h}$ = -0.0022599939
$\bar{i}$ = 90.11755585°	$\bar{k}$ = 0.0038668133
$\bar{\Omega}$ = 180.0375365°	$\bar{p}$ = -0.000656481
$\bar{\omega}$ = 149.6579277°	$\bar{q}$ = -1.002053629
$\bar{M}$ = 208.9757986°	$\bar{\lambda}$ = 178.6712628°

The mean elements in Table 5-15 were used to initialize an eight year AOG prediction of the STRATSAT orbit. The numerical integration used a step size of one year. The truncation parameters N, M*, R* for the AOG prediction are found in Table 5-16. The maximum power of the parallax factor has been conservatively chosen to ensure the accuracy of the eight year prediction. The upper bound on the satellite Hansen coefficient d'Alembert characteristic has been allowed to assume its maximum value to accomodate the anticipated growth of the satellite orbital eccentricity.

Table 5-16. AOG Perturbation Model for the Eight Year STRATSAT Integration

MOON

N = 15
M* = 15
R* = 8

NOTE: AOG retains only the double averaged third body terms.

N ≡ maximum power of the parallax factor, $(\bar{a}/a')$

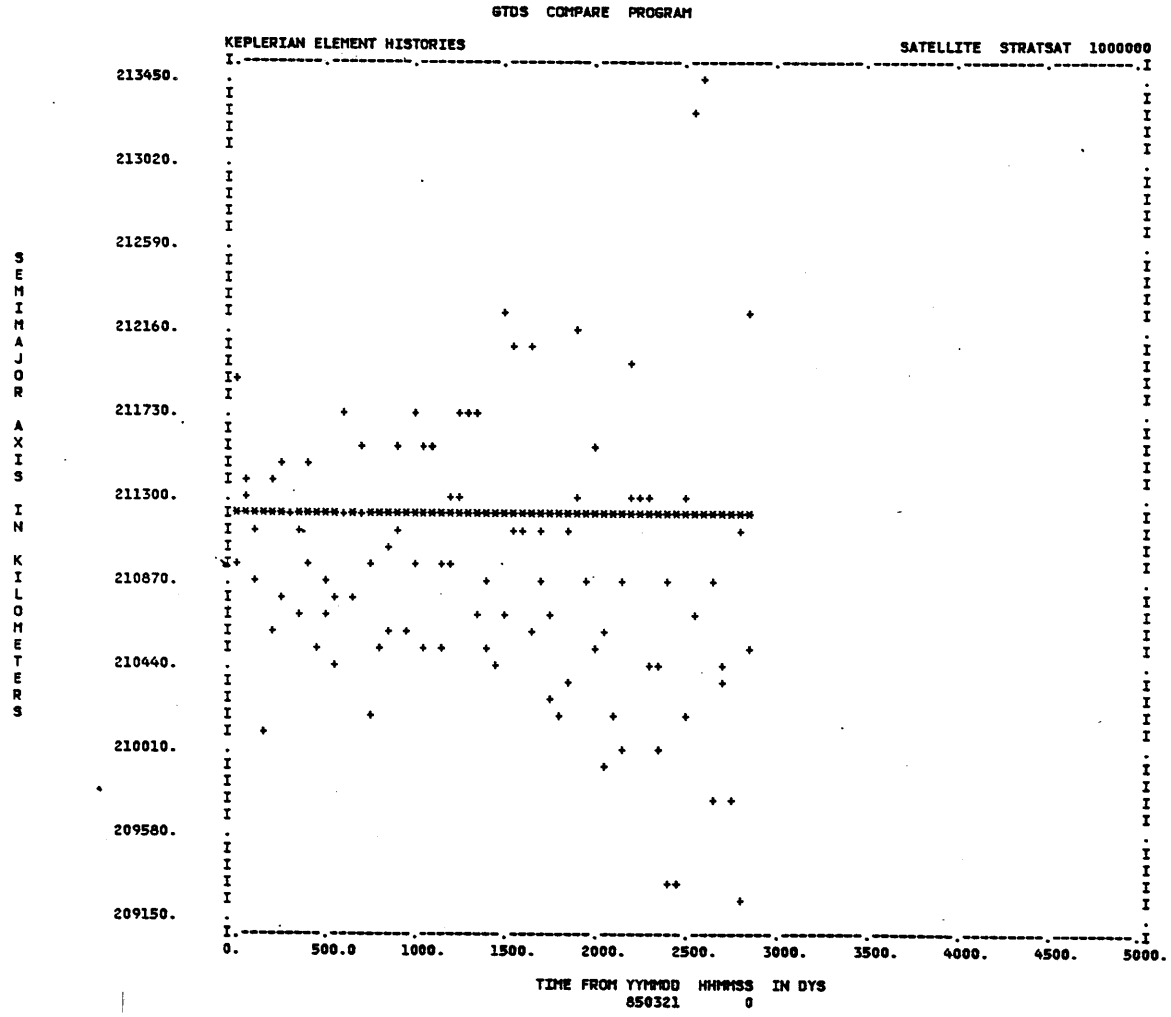
M* ≡ upper bound on the satellite Hansen coefficient d'Alembert characteristic

R* ≡ upper bound on the third body Hansen coefficient d'Alembert characteristic

The Cowell compare file was created from an integration that used 150 time regularized steps per revolution of the satellite. Ephemeris comparison plots for the semi-major axis, eccentricity, and inclination are shown in Figures 5-31 through 5-33. The radius of perigee is plotted in Figure 5-34. Special attention should be focused on the eccentricity plot in Figure 5-32. The AOG (*) is observed to accurately follow the Cowell integration (+) up to an eccentricity of 0.8 over the eight year prediction span. The plots indicate that the third body theory developed in this thesis can be reliably used to monitor the evolution and stability of rapidly evolving orbits.

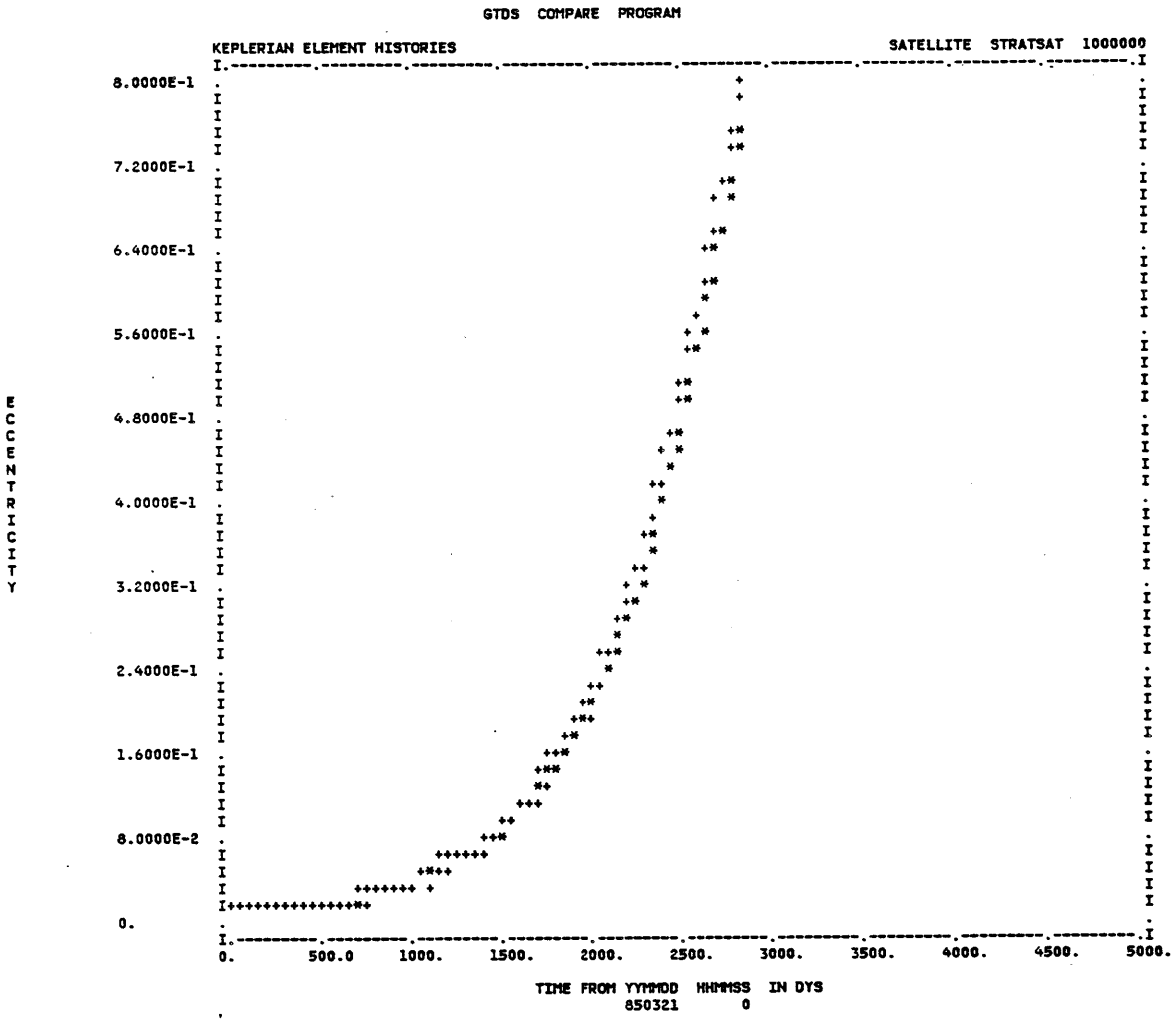
Table 5-17 compares the execution times of the AOG and Cowell predictions. The execution time of the AOG for an eight year run is seen to be at least a factor of 14 less than that of the corresponding Cowell integration.

Figure 5-31. Comparison of the Mean and Osculating Semi-Major Axis Histories for the 8 Year Integration of the STRATSAT Orbit/AOG versus Cowell



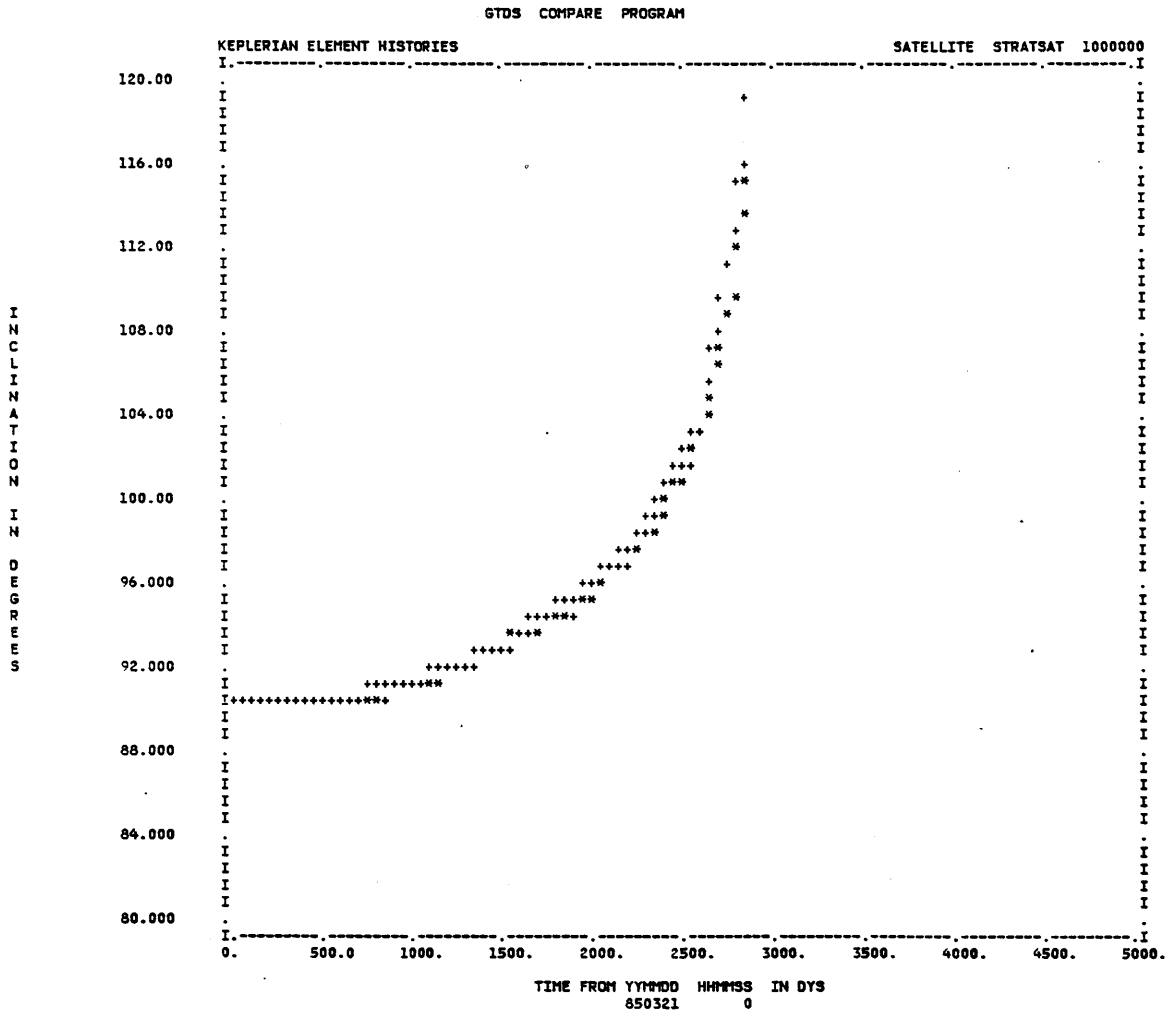
(+) = Cowell
(*) = AOG

Figure 5-32. Comparison of the Mean and Osculating Eccentricity Histories for the 8 Year Integration of the STRATSAT Orbit/AOG versus Cowell



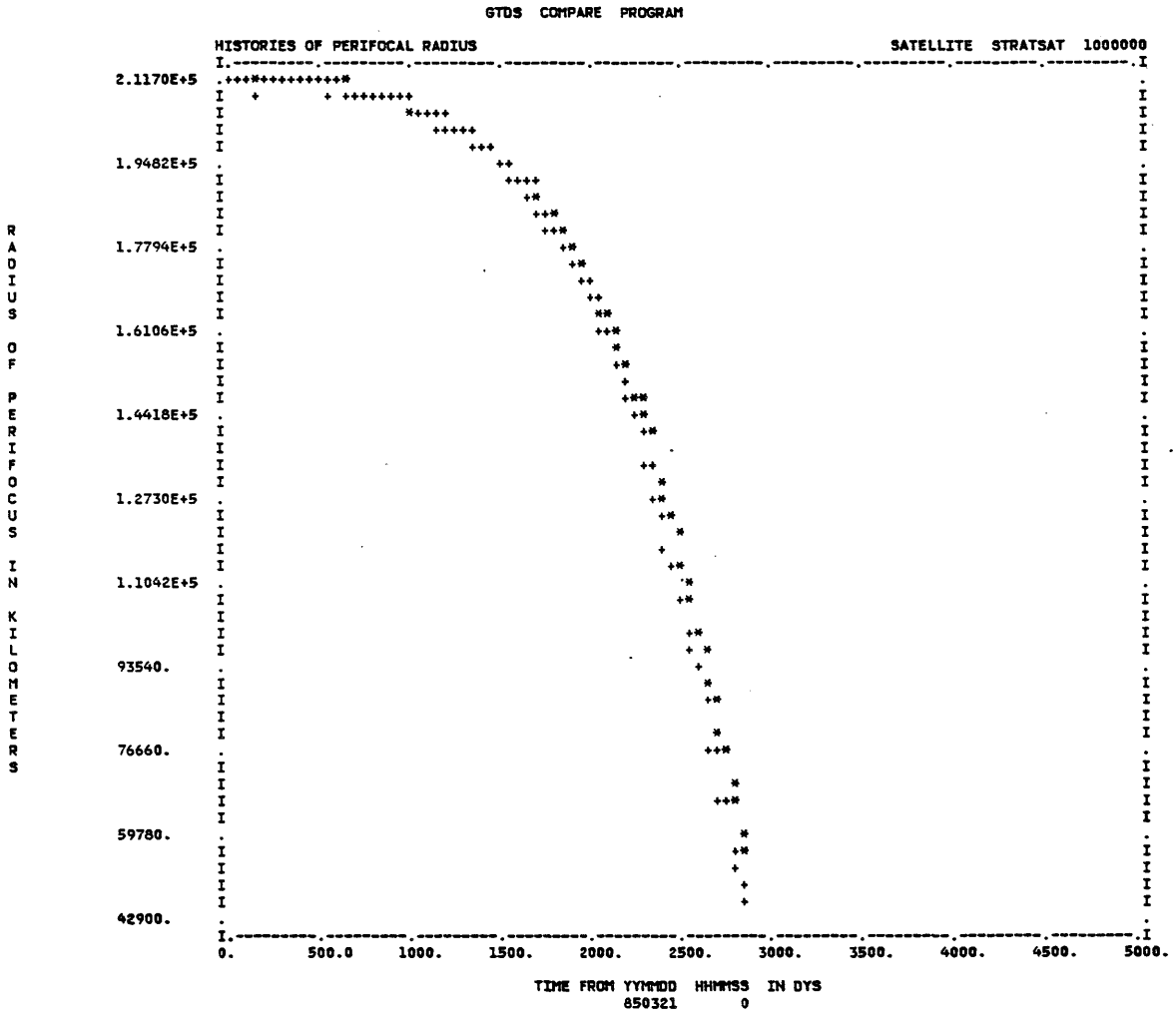
(+) = Cowell
(*) = AOG

Figure 5-33. Comparison of the Mean and Osculating Inclination Histories for the 8 Year Integration of the STRATSAT Orbit/AOG versus Cowell



(+) = Cowell
(*) = AOG

Figure 5-34. Comparison of the Mean and Osculating Radius of Perifocus Histories for the 8 Year Integration of the STRATSAT Orbit/AOG versus Cowell



(+) = Cowell
(*) = AOG

Table 5-17. Comparison of Cowell and AOG Execution Times for the Eight Year STRATSAT Integration

Orbit Generator	Step Size	Execution Time
Cowell	150 steps/rev., time regularized	170 seconds
AOG	31536000 seconds (1 year)	12.44 seconds

Notes

1) The Cowell integrator is based on the 12th order Adams-Bashforth Predictor / Adams-Moulton Corrector algorithm.
2) The AOG uses a 4th order Runge-Kutta integration algorithm.
3) The execution time for the Cowell integration contains overhead associated with file creation.
4) The execution time for the AOG contains overhead associated with file creation and includes the ephemeris comparison step.

5.3.5 Lunar Resonance Test Case

This test case examines the capability of the third body AOG to accomodate resonance terms. The initial orbital elements are given in Table 5-18. The orbit is in a near 5:2 resonance with the moon. The critical argument of the resonance has a period of approximately 1340 days, while the second multiple of the critical argument circulates with a period of 670 days.

Table 5-18. Epoch Osculating Elements for the Lunar Resonance Test Case

$a = 209831.6$ km	Epoch = 21 March 1985
$e = 0.001$	$0^h.0, 0^m.0, 0^s.0$
$i = 90.0°$	
$\Omega = 90.0°$	Period = 11.07 days
$\omega = 0.0°$	
$M = 0.0°$	

Radius of Perigee = 209621.76 km
Radius of Apogee = 210041.43 km
Lunar Parallax Factor, $(a/a')_\ell \simeq 0.546$

The initial mean elements for the AOG prediction were obtained from a PCE over sixty days. The osculating satellite elements were used as the a priori input to the PCE. The perturbation model used in the PCE is given in Table 5-19. Resonant terms with periods of 670 days or over were included in the AOG. Care was taken to ensure that these terms were not also modelled in the SPG. The mean elements determined from the PCE are given in Table 5-20.

Table 5-19. PCE Perturbation Models for the Lunar Resonance Test Case

1) AOG + SPG Perturbation Model:

MOON

N = 12
M* = 6
R* = 8
$-4 \leq t \leq 4$
$-10 \leq s \leq 10$

NOTE: AOG retains the double averaged terms and the resonant terms corresponding to the index pairs (t=2,s=-5), (t=-2,s=5), (t=4,s=-10), and (t=-4,s=10). These index pairs are deleted from the SPG.

N ≡ maximum power of the parallax factor, $(\bar{a}/a')$

M* ≡ upper bound on the satellite Hansen coefficient d'Alembert characteristic

R* ≡ upper bound on the third body Hansen coefficient d'Alembert characteristic

2) Cowell Perturbing Acceleration:

point mass moon

Table 5-20. Epoch Mean Elements for the Lunar Resonance Test Case

Keplerian	Equinoctial
$\bar{a}$ = 209702.4301 km	$\bar{a}$ = 209702.4301 km
$\bar{e}$ = 0.0049611077	$\bar{h}$ = 0.0023951282
$\bar{i}$ = 90.09639511°	$\bar{k}$ = -0.0043446461
$\bar{\Omega}$ = 90.04588787°	$\bar{p}$ = 1.001683508
$\bar{\omega}$ = 61.08692413°	$\bar{q}$ = -0.0008022429
$\bar{M}$ = 298.1680329°	$\bar{\lambda}$ = 89.3008449°

The mean elements in Table 5-20 were used to initialize a five year AOG prediction of the lunar resonance test orbit. The numerical integration of the averaged equations of motion used a step size of 115 days. The AOG model is shown in Table 5-21. The upper bound on the satellite Hansen coefficient d'Alembert characteristic has been increased to allow for eccentricity growth over the five year prediction span. The Cowell compare file was generated from an integration that used 150 time regularized steps per revolution of the satellite. Ephemeris comparison

plots for the semi-major axis, eccentricity and inclination are provided in Figures 5-35 through 5-37. The AOG histories (*) are in general agreement with the long term motion observed in the Cowell generated histories (+).

Table 5-22 compares the execution times of the Cowell and AOG predictions. The execution time of the AOG for the five year run is seen to be at least a factor of 3.5 less than that of the corresponding Cowell integration.

Table 5-21. AOG Perturbation Model for the Five Year Lunar Resonance Integration

MOON

N = 12
M* = 12
R* = 8

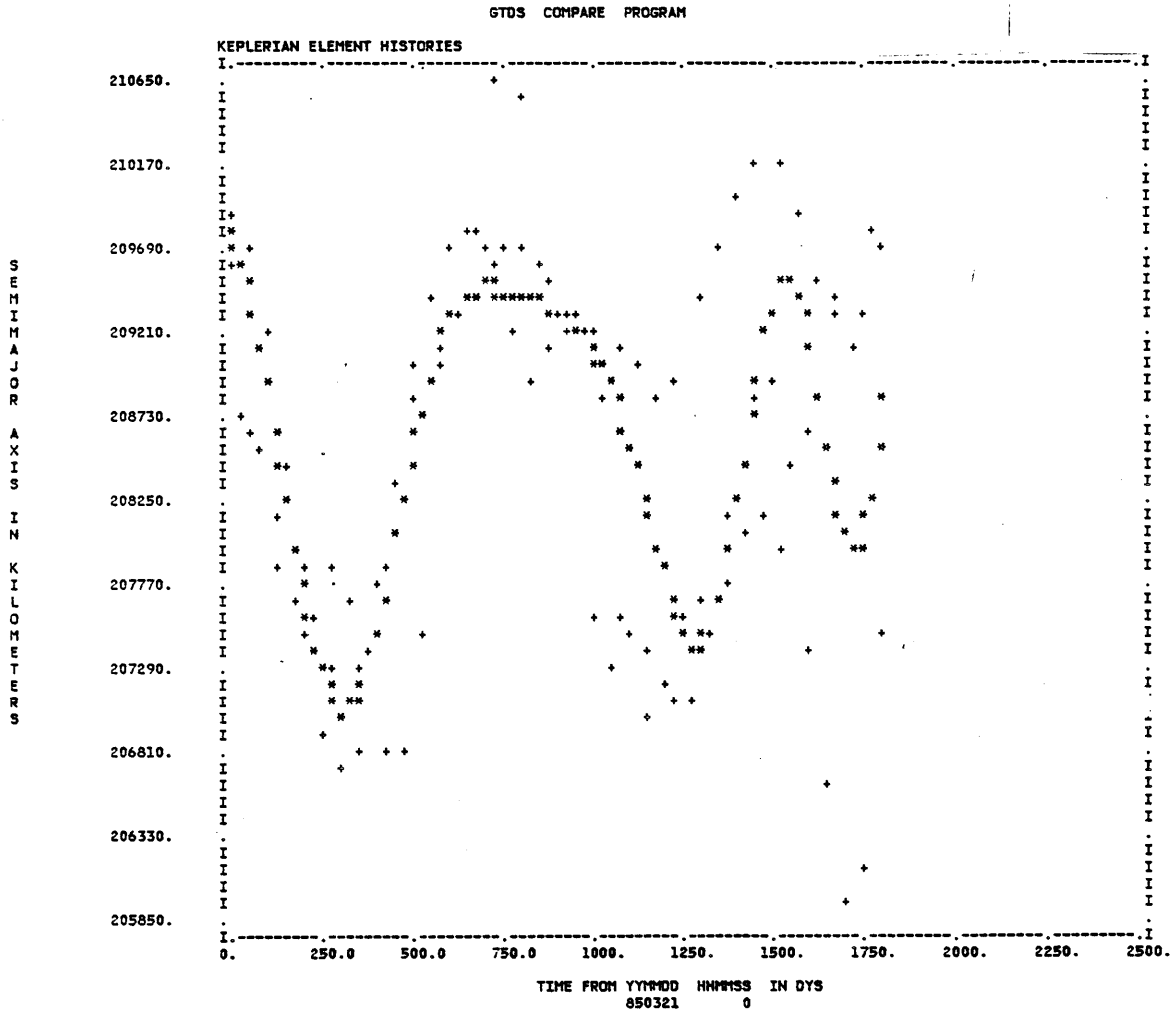
NOTE: AOG retains the double averaged terms and the resonant terms corresponding to the index pairs (t=2,s=-5), (t=-2,s=5), (t=4,s=-10), and (t=-4,s=10).

N ≡ maximum power of the parallax factor, $(\bar{a}/a')$

M* ≡ upper bound on the satellite Hansen coefficient d'Alembert characteristic

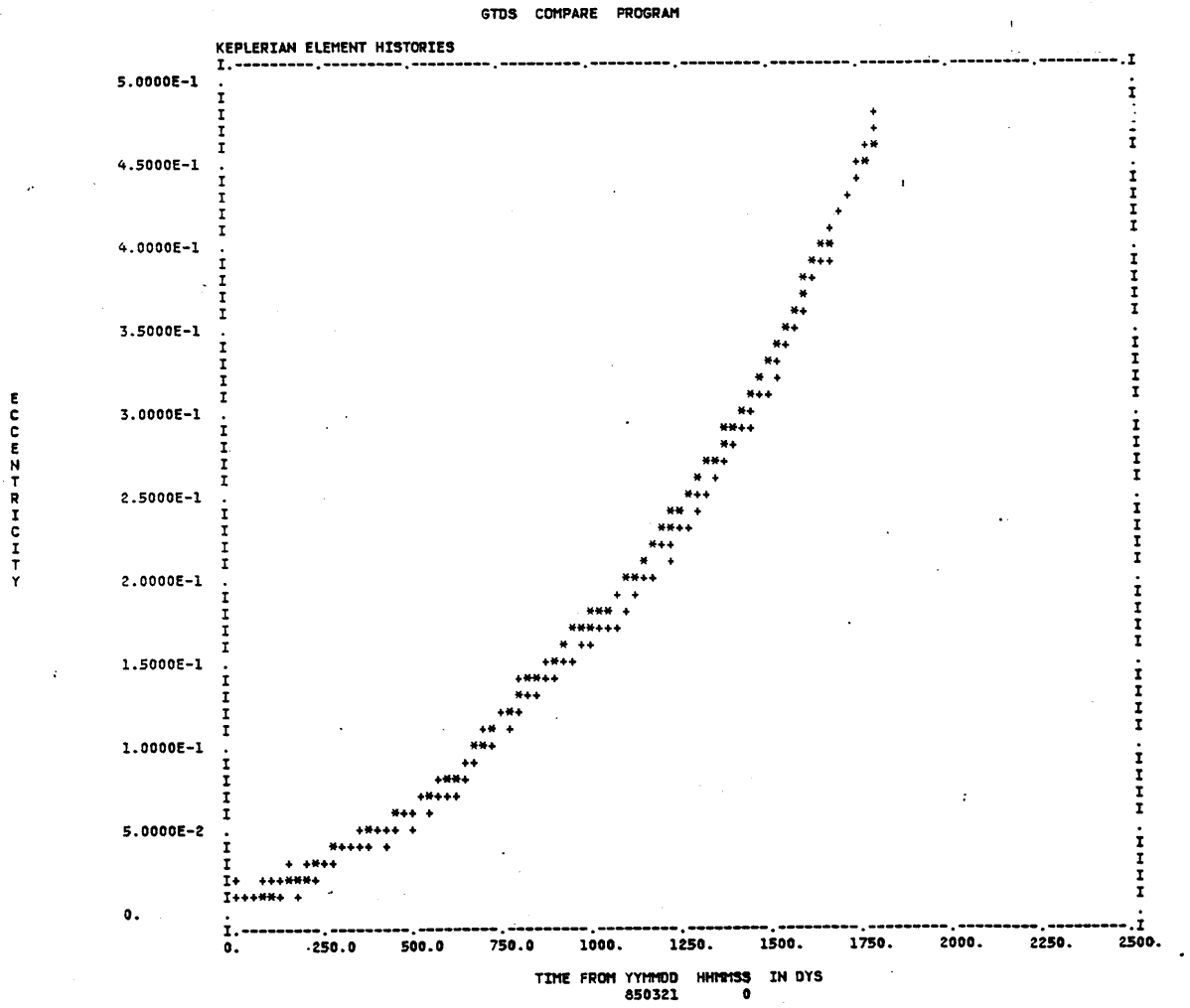
R* ≡ upper bound on the third body Hansen coefficient d'Alembert characteristic

Figure 5-35. Comparison of the Mean and Osculating Semi-Major Axis Histories for the 5 Year Integration of the Lunar Resonance Test Orbit/AOG versus Cowell



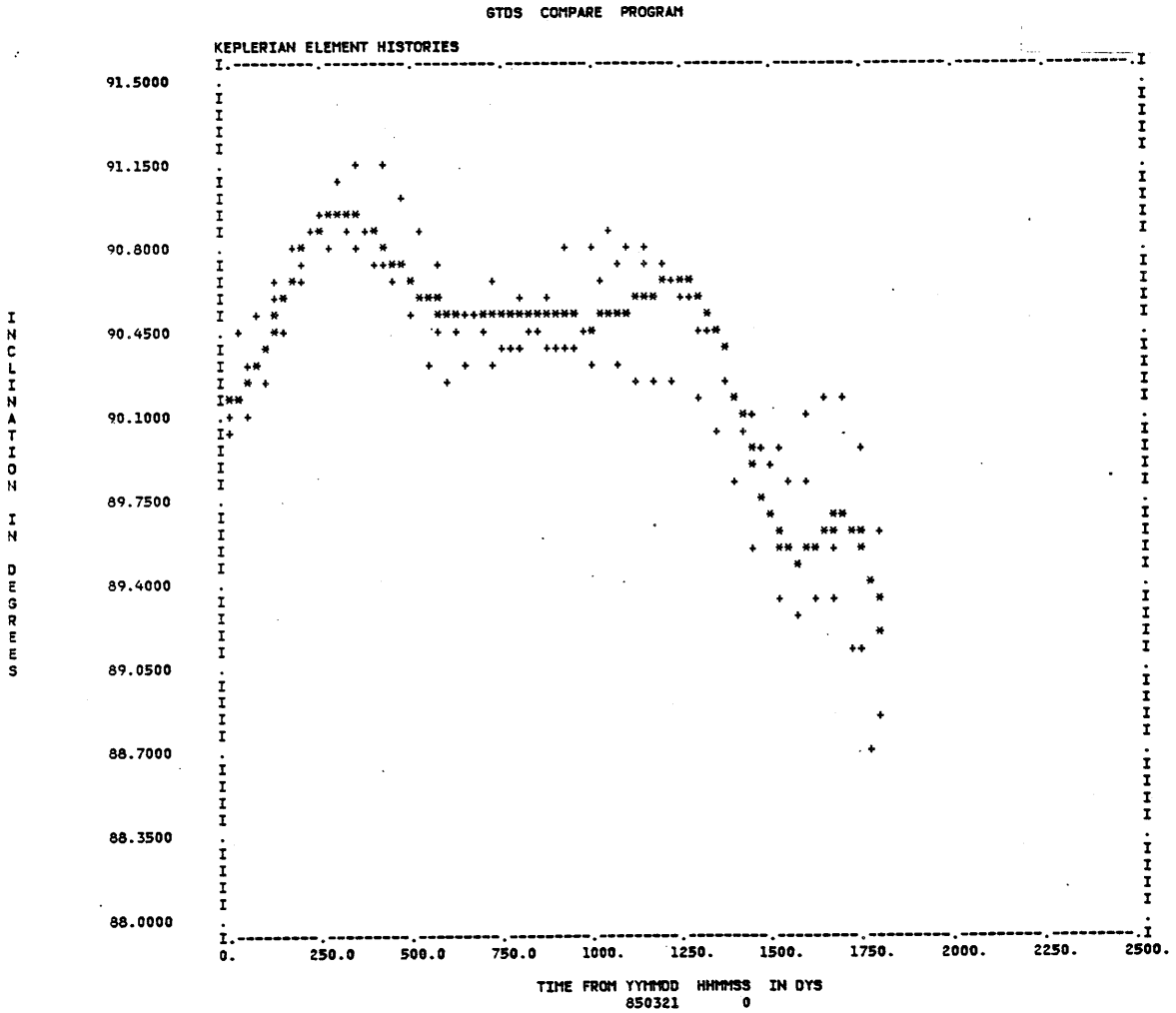
(+) = Cowell
(*) = AOG

Figure 5-36. Comparison of the Mean and Osculating Eccentricity Histories for the 5 Year Integration of the Lunar Resonance Test Orbit/AOG versus Cowell



(+) = Cowell
(*) = AOG

Figure 5-37. Comparison of the Mean and Osculating Inclination Histories for the 5 Year Integration of the Lunar Resonance Test Orbit/AOG versus Cowell



(+) = Cowell
(*) = AOG

Table 5-22. Comparison of Cowell and AOG Execution Times for the Five Year Lunar Resonance Integration

Orbit Generator	Step Size	Execution Time
Cowell	150 steps/rev. time regularized	111 seconds
AOG	9936000 seconds (115 days)	32 seconds

Notes

1) The Cowell integrator is based on the 12th order Adams-Bashforth Predictor / Adams-Moulton Corrector algorithm.
2) The AOG uses a 4th order Runge-Kutta integration algorithm.
3) The execution time for the Cowell integration contains overhead associated with file creation.
4) The execution time for the AOG contains overhead associated with file creation and includes the ephemeris comparison step.

This test case has demonstrated the capability of the third body AOG to incorporate resonance terms. However, Table 5-22 shows that the efficiency of the AOG with respect to Cowell integration is substantially degraded in comparison to the previous test cases. This is because the resonant terms that were included in the averaged equations of motion have periods that are still too short in relation to the double averaged terms. The result is an unnecessary restriction of the integration step size.

An attempt was made to perform a PCE initialization with only the double averaged terms retained in the AOG and with the resonance modelled in the SPG. Inspection of the semi-major axis plot in Figure 5-35 would indicate that the PCE should have converged to a constant semi-major axis of around 208395 kilometers, which seems well removed from the exact resonance value of 207830 kilometers. Nevertheless, the PCE procedure did not converge. This was probably caused by "overshoot" in the least squares differential correction algorithm. For an iteration of the PCE, it is possible that a correction to the mean semi-major axis was computed that placed the orbit in a region of nearly exact resonance with the moon. Since the tesseral analog short periodics are numerically ill-conditioned in the vicinity of exact resonance because of the presence of small divisors,

the semi-analytical trajectory generated over the fit span for the subsequent iteration was erroneous. Hence, the residuals between the semi-analytical approximation to the osculating orbit and the Cowell data were so large as to prevent convergence of the PCE.

It is desirable to model all but the sharpest commensurabilities as short periodics, while retaining only the double averaged terms in the AOG, so that the full benefit of averaging can be exploited. Accordingly, the study of initialization procedures that are more highly constrained with respect to the solution point is required to avoid the problems encountered in this test case.

Chapter 6

Conclusions and Future Work

The goal of this thesis has been to construct a semi-analytical third body theory that can be used to predict the long term evolution of high altitude satellite orbits both accurately and with an efficiency that exceeds the capability of conventional mission analysis techniques.

The mathematical development of the third body averaged equations of motion and short periodic recovery functions was based on the application of the Generalized Method of Averaging to the Lagrangian form of the high precision satellite equations. A representation of the third body disturbing potential in satellite orbital elements was essential to the development. The analysis for the potential was performed in Chapter 2, with the final result being given in eq. (2-110). The potential retains the parallax factor to an arbitrary power and no assumptions are made on the geometry of the third body orbit. Non-singular equinoctial orbital elements were used as part of a unified approach to the elimination of artificial singularities in the satellite dynamical equations for near-circular and near-equatorial orbits. The potential was developed with

respect to the reference frame of the satellite to minimize the analytical complexity of the first order theory. Special functions were employed wherever possible to modularize the analytical structure with a view towards efficient computation in a numerical program. The potential was also expanded into the mean longitudes of the satellite and the disturbing body so that resonance could be studied.

Substitution of the potential into the Lagrange Planetary equations leads to a system of satellite equations of motion that depend on the two fast angles of the satellite and the third body. Chapter 3 developed an averaging theory, based on the Generalized Method of Averaging, for the removal of undesired components of the equations of motion depending on rapidly varying linear combinations of the satellite and disturbing body mean longitudes. At first order, the right hand sides of the averaged equations of motion, shown in eq. (3-25), are obtained by a multiple average of the high precision equations of motion with respect to each of the rapidly varying angles, where all osculating elements have been replaced by the corresponding mean quantities. The short periodic recovery functions, formulated in terms of the mean elements output by the

averaged equations of motion, are obtained from the evaluation of the indefinite integrals in eqs. (3-32) and (3-33).

Chapter 4 synthesized the results of Chapters 2 and 3 to produce mathematical expressions for the numerical implementation of the third body theory. The form of the averaged equations of motion is shown in Table 4-2. The Fourier series coefficients for the short periodic variations were developed in Section 4.2 for the tesseral, zonal and m-daily analogs of the third body potential. The forms of partial derivatives of the potential with respect to satellite related quantities were investigated in detail in Section 4.3. Of particular interest are the partial derivatives of h', k' and λ' with respect to the mean satellite elements $\bar{p}$ and $\bar{q}$. These expressions relate the third body elements to the dynamical system of reference through the evolution of the satellite orbital plane and are the result of having chosen a non-inertial frame to develop the potential. Section 4.4 contained a complete discussion of recurrence relations for the computation of special functions and auxiliary quantities. Truncation parameters for the third body theory were introduced in Section 4.5. Constraining relations on the indices of the third body potential were derived on the basis of these parameters.

The choice of the non-inertial satellite reference frame over the inertial frame for the development of the third body disturbing potential led to the elimination of the satellite inclination function and the associated summation. In exchange for the more compact analytical structure of the disturbing body potential the orbital elements of the third body assumed a dependence on the orbital elements of the satellite which had to be accounted for when partial derivatives were taken in the averaged equations of motion and in the short periodic recovery functions. However, the net computational advantage was in favor of the potential formulated in the non-inertial frame since the analytical forms of the third body elements and their partial derivatives are known and have to be computed only once for each evaluation of the averaged element rates and the short periodics. A central result relating to the use of a relative coordinate frame for the first order theory was the proof that the partial derivatives of $\overline{\phi}_{t,s}$ with respect to the mean satellite elements $\overline{p}$ and $\overline{q}$ are not periodic. Hence, averaging integrals of the form in eq. (4-19) vanish. This means that no residual secular contributions are retained in the first order averaged equations of motion for terms that do not satisfy the constraint of eq. (4-31).

Chapter 5 described the results of a numerical implementation of the first order third body averaging theory. The third body software consisted of two components: the Averaged Orbit Generator (AOG) and the Short Periodic Generator (SPG). The capability to construct a semi-analytical approximation to high precision satellite ephemerides is provided by a combination of the AOG and SPG algorithms. This capability was used in the Precise Conversion of Elements (PCE) initialization procedure to produce accurate epoch mean elements from osculating elements for long term integrations of the averaged equations of motion. Long term predictions of five test orbits were performed using the AOG and compared against Cowell integration for speed and accuracy.

6.1 Conclusions

The principal conclusion of this thesis is that the first order semi-analytical third body theory can be used to accurately predict the long term motion of a high altitude satellite with an efficiency that makes it decisively superior to conventional mission analysis techniques. A further conclusion is that the large integration step sizes (on the order of one year) permitted by the third body

theory are compatible with other averaged perturbation models that might be included in a general mission analysis program.

The numerical test results verify that the AOG is capable of predicting the mean of a high precision trajectory over a time span that is very long in comparison to the span of the initialization process. The SPG was also found to provide a highly accurate representation of the third body short periodic variations.

The excellent agreement of long term AOG predictions, based on the PCE-generated epoch mean elements, with the Cowell precision ephemeris validates both the AOG and SPG algorithms.

The semi-analytical third body theory was shown to be successful in predicting the long term motion of high altitude satellites over a broad range in orbital geometry. The theory produced very fine results for high values of the satellite orbital eccentricity and for large values of the parallax factor. The capability to model third body resonance in the AOG was also demonstrated.

Several conclusions can be drawn regarding the numerical behavior of the third body software. First, the recursive processes used to speed computation in the third body theory are stable for the test cases examined. In particular, the recurrence relations for the non-zero subscripted Hansen coefficients of the satellite and the third body appear well behaved. This conclusion is supported by "stand-alone" investigations of the recurrence relations, found in Sections 4.4.5 and 4.4.6, using the symbolic manipulation package MACSYMA [31]. The resolution of the stability issue was required since some of Hansen's recurrences have received little attention since their derivation in 1855. Furthermore, the theory converges rapidly along powers of the parallax factor even when the parallax factor is quite large. Finally, interpolator concepts are applicable to the computation of the third body short periodic coefficients, since the coefficients meet the requirement of being slowly varying.

6.2 Future Work

Several areas of future investigation have been suggested by the present research. Some are concerned with the analysis, refinement, and application of algorithms developed in this thesis. Others are concerned with the exploration of new algorithmic approaches.

Further numerical testing is required to determine the accuracy limits of the first order third body theory. At present, the importance of including second order coupling terms in the averaged equations of motion remains an unresolved question. Coupling terms can arise from the interactions of lunar and solar perturbations with each other and with non-spherical central body perturbations. The effect of neglecting these terms on a long term integration is often difficult to distinguish from the propagation of small errors in the initial conditions. Insight into this problem could be provided by initializing the Averaged Orbit Generator over a data span that is substantially longer than the 60 day fit span used for the test cases in Chapter 5. This would allow greater advantage to be taken of the PCE error smoothing properties. Any residual discrepancies between the resulting semi-analytical trajectory and Cowell integration could then be more realistically attributed to second order terms. The effect of such second order terms would become more important as the prediction span is lengthened.

Continuing with the question of model accuracy, orbit determination tests using the semi-analytical theory and long arcs of actual tracking data for high altitude satellites would provide another stringent end-to-end test.

Improvements to the third body software are possible through algorithmic optimization. A careful examination of the flow of indices in the third body theory could lead to a more completely recursive software architecture which places less reliance on the storage of special functions. Recurrence relations would be helpful for computing the coefficient $Z^m_{n,r}$ discussed in Section 4.4.1. These recurrences are easy to derive, but are not implemented in the current software. Furthermore, while the work to date has demonstrated both accuracy and efficiency, these results have usually been achieved with conservative values of the various indices. Automatic algorithms to rationally select these indices for an arbitrary semi-major axis and eccentricity would be quite valuable.

The capability to parametrically map stability regions for high altitude satellite orbits can be of immense value for the study of orbits in the STRATSAT class, where strong lunar and solar perturbations can cause rapid decay if initial conditions are not judiciously chosen. The first order third body theory can provide this capability with an efficiency that was not previously possible. A great many test orbits can be generated in averaged element space in the time that it would take to integrate one high precision trajectory. Having found a mean orbit that satisfies the mission constraints, a corresponding set of osculating

elements could then be computed using analytical short periodic recovery. These osculating elements might be sufficiently accurate to determine real world injection conditions. If not, they could be used as a priori input to a PCE which would refine the estimate of the real world orbit.

The Legendre polynomial expansion for the inverse of the distance between the satellite and the disturbing body, given in eq. (2-17), was performed under the assumption that the satellite orbit was interior to the orbit of the third body. By assuming that the satellite orbit is exterior to the orbit of the disturbing body, a new Legendre polynomial expression can be developed which will extend the applicability of the third body theory to satellites moving in the translunar region.

The development of the third body disturbing potential in the satellite reference frame introduces partial derivatives of third body orbital elements with respect to satellite orbital elements into the equations of motion. The cross coupling of these partial derivatives in a second order averaging theory can lead to significant analytical complexity. This is clearly illustrated in eqs. (3-19) and (3-20). Hence, the representation of the third body potential in inertial coordinates, seen in eq. (2-111), may offer substantial advantages if an attempt is made to develop second order terms.

Appendix A

Computation and Storage of the Newcomb Operators in the Third Body Theory

In the software implementation of the third body theory, the non-zero subscripted Hansen coefficient kernel functions for the satellite and the disturbing body are computed using the recurrence relations in eqs. (4-249) and (4-236). Similarly, the derivatives of the kernel functions are computed using the recurrence relations in eqs. (4-250) and (4-240). The recurrences require the explicit calculation of initial values from the power series expressions:

Satellite

$$K_t^{n,-m} = \sum_{i=0}^{\infty} X^{n,-m}_{i+\frac{|q|-q}{2},\, i+\frac{|q|-q}{2}} e^{-2i} \qquad \text{(A-1)}$$

and

$$\frac{dK_t^{n,-m}}{d\bar{e}^2} = \sum_{j=0}^{\infty} (j+1)\, X^{n,-m}_{j+\frac{|q|+q}{2}+1,\; j+\frac{|q|-q}{2}+1}\, \bar{e}^{2j} \qquad \text{(A-2)}$$

where

$$q = (t + m) \qquad \text{(A-3)}$$

Disturbing Body

$$K_s^{-n-1,r} = \sum_{i=0}^{\infty} X^{-n-1,r}_{i+\frac{|q|+q}{2},\; i+\frac{|q|-q}{2}}\, e'^{2i} \qquad \text{(A-4)}$$

and

$$\frac{dK_s^{-n-1,r}}{de'^2} = \sum_{j=0}^{\infty} (j+1)\, X^{-n-1,r}_{j+\frac{|q|+q}{2}+1,\; j+\frac{|q|-q}{2}+1}\, e'^{2j} \qquad \text{(A-5)}$$

where

$$q = s - r \tag{A-6}$$

The series coefficients, $X^{u,v}_{\rho,\sigma}$, are the Newcomb operators and are governed by the recurrence relations [17]:

$\underline{\sigma = 0}$

$$4\rho\, X^{u,v}_{\rho,0} = 2(2v - u)\, X^{u,v+1}_{\rho-1,0} + (v - u)\, X^{u,v+2}_{\rho-2,0} \tag{A-7}$$

$\underline{\rho = 0}$

$$4\sigma\, X^{u,v}_{0,\sigma} = -2(2v + u)\, X^{u,v-1}_{0,\sigma-1} - (v + u)\, X^{u,v-2}_{0,\sigma-2} \tag{A-8}$$

$\rho > 1,\ \sigma = 1$

$$4(\rho + 1)\, X^{u,v}_{\rho,1} = 2(2v - u)\, X^{u,v+1}_{\rho-1,1} - 2(2v + u)\, X^{u,v-1}_{\rho,0} +$$

$$+ (v - u)\, X^{u,v+2}_{\rho-2,1} + 2(2\rho - 2 - u)\, X^{u,v}_{\rho-1,0}$$

(A-9)

$\rho = 1,\ \sigma > 1$

$$4(1 + \sigma)\, X^{u,v}_{1,\sigma} = 2(2v - u)\, X^{u,v+1}_{0,\sigma} - 2(2v + u)\, X^{u,v-1}_{1,\sigma-1} -$$

$$- (v + u)\, X^{u,v-2}_{1,\sigma-2} + 2(2\sigma - 2 - u)\, X^{u,v}_{0,\sigma-1}$$

(A-10)

$\rho > 1,\ \sigma > 1$

$$4(\rho + \sigma)\, X^{u,v}_{\rho,\sigma} = 2(2v - u)\, X^{u,v+1}_{\rho-1,\sigma} - 2(2v + u)\, X^{u,v-1}_{\rho,\sigma-1} +$$

$$+ (v - u)\, X^{u,v+2}_{\rho-2,\sigma} - (v + u)\, X^{u,v-2}_{\rho,\sigma-2} +$$

$$+ 2(2\rho + 2\sigma - 4 - u)\, X^{u,v}_{\rho-1,\sigma-1} \qquad \text{(A-11)}$$

The initial conditions for these recurrence relations are given by,

$$X^{u,v}_{0,0} = 1 \qquad \text{(A-12)}$$

$$X^{u,v}_{1,0} = v - \frac{u}{2} \qquad \text{(A-13)}$$

$$X^{u,v}_{0,1} = -v - \frac{u}{2} \qquad \text{(A-14)}$$

The Newcomb operators with negative subscripts are identically zero.

The Newcomb operators are computed "offline" by the recurrence relations and are stored in FORTRAN block data subprograms (see Appendix B). The compiled versions of these subprograms are linked to GTDS at run time, along with the rest of the third body software, to initialize three dimensional Newcomb operator arrays.

At the present time, there are Newcomb operator arrays that can be accessed to explicitly develop the satellite and disturbing body kernel functions for each value of the index n, up to and including n = 20.

For a given value of n, the satellite Newcomb operator arrays are valid for Hansen coefficients with d'Alembert characteristics up to 20 and can be used to construct kernel functions with subscripts that fall within the range,

$$-41 \leq t \leq 41 \qquad \text{(A-15)}$$

Likewise, for a particular value of n, the disturbing body Newcomb operator arrays are valid for Hansen coefficients with d'Alembert characteristics up to 10 and can be used to construct kernel functions with subscripts that fall within the range,

$$-31 \leq s \leq 31 \qquad \text{(A-16)}$$

Appendix B

Software Implementation of the Third Body Theory

The theory for the averaged equations of motion and for the short periodic corrections to the mean elements has been implemented into GTDS for both double averaged non-resonant and resonant third body perturbations. The GTDS executive subroutine for the third body Averaged Orbit Generator (AOG) is ANAVR which constructs the averaged orbital element rates for time independent perturbations. The Short Periodic Generator (SPG) is driven by the GTDS subroutine SPANAL which governs the computation of short periodic coefficients for analytically averaged perturbations.

B.1 Subroutine Descriptions

This section describes the subroutines which implement the third body theory. With the exception of EVAL, all of the subroutines were expressly written to test the analysis of this thesis and were included in GTDS as temporary updates. The GTDS subroutine EVAL was extensively modified to incorporate the analytical ephemeris discussed in Chapter 5 and is thus included in the list of third body

subroutines. Wherever appropriate, references to the thesis text that link the software to the analysis are included in the subroutine descriptions.

The twenty-four subroutines that follow form the core of the third body averaging software. They are used to generate the right hand sides of the averaged equations of motion for double averaged third body perturbations.

1) AAPRIM: Computes and stores $(\bar{a}/a')^n$ up to and including n = N, where N is the maximum degree of the third body Legendre polynomial expansion.

2) AVEXEC: Computes the real and imaginary parts of $\bar{\Psi}_{t,s}$ and its partial derivatives for the third body averaged orbit generator [eqs. (4-81) to (4-83), eqs. (4-86) to (4-91)]. Computes sines and cosines of $t\bar{\lambda}+s\lambda'$ for the third body resonance implementation.

3) BROLUN: Computes the mean equinoctial elements of the Moon in mean ecliptic of date coordinates using Brown's theory [Section 5.2].

4) BROSOL: Computes the mean equinoctial elements of the Sun in mean ecliptic of date coordinates using Newcomb's theory [Section 5.2].

5) CMRDMR: Computes and stores the real and imaginary parts of the complex polynomials $C_m^r(\alpha,\beta) + j\ D_m^r(\alpha,\beta)$ [eqs. (4-168) to (4-171), eqs. (4-184) to (4-187)] and its partial derivatives with respect to α and β [eqs. (4-175) to (4-182), eqs. (4-188) to (4-195)].

6) DUBFAC: Computes and stores double factorials required for the averaged orbit generator and the short periodic generator.

7) EPRIM: Computes the h' and k' elements of the disturbing body orbit in satellite frame coordinates [Table 2-3]. Computes the partial derivatives of h' and k' with respect to the satellite elements $\bar{p}$ and $\bar{q}$ [eq. (4-92), eqs. (4-94) to (4-96)].

8) EVAL: Computes position and velocity components for the Sun and Moon in the reference system of the numerical integration using the analytical ephemeris. Computes rotation matrices for converting inertial coordinates to body fixed coordinates and mean of 1950.0 coordinates to true of date coordinates.

9) FACT: Computes and stores factorials required for the averaged orbit generator and the short periodic generator.

10) HANST0: Computes in closed form and stores the satellite Hansen coefficient kernel functions of subscript zero, $K_0^{n,-m}$ [eqs. (4-254) to (4-256)]. Computes the partial derivatives of the satellite kernel functions with respect to $\bar{h}$ and $\bar{k}$ [eqs. (4-257) to (4-259)].

11) HANTD0: Computes in closed form and stores the disturbing body Hansen coefficient kernel functions of subscript zero, $K_0^{-n-1,r}$ [eqs. (4-242) to (4-244)]. Computes the partial derivatives of the disturbing body kernel functions with respect to h' and k' [eqs. (4-245) to (4-247)].

12) HKSAT: Computes and stores the real and imaginary parts of the complex polynomials $(\bar{k} - j\eta\bar{h})^{|-m-t|}$ [eqs. (4-215) to (4-218)] and its partial derivatives with respect to $\bar{h}$ and $\bar{k}$ [eqs. (4-277) to (4-234)].

13) HPKP: Computes and stores the real and imaginary parts of the complex polynomials $(k' - j\eta'h')^{|r-s|}$ [eqs. (4-211) to (4-214)] and its partial derivatives with respect to h' and k' [eqs. (4-219) to (4-226)].

14) JACPOL: Computes and stores the function $\Lambda(\gamma)$ and its derivative with respect to γ [eqs. (4-65) to (4-67), Section 4.4.2].

15) MEXEC: Executive routine for the summation over m in $\bar{\psi}_{t,s}$.

16) NEXCF: Executive routine for the summation over n in $\bar{\psi}_{t,s}$ that is used when the satellite Hansen coefficient kernel functions are of subscript zero.

17) NOD: Computes the nutation matrix for a rotation from mean of date coordinates to true of date coordinates.

18) OBLIQ: Computes the rotation matrix that transforms ecliptic coordinates to equatorial coordinates.

19) PRECES: Computes the precession matrix to transform mean of 1950.0 coordinates to mean of date coordinates. Computes the inverse of the precession matrix.

20) REXCF: Executive routine for the summation over r in $\bar{\psi}_{t,s}$ that is used when the disturbing body Hansen coefficient kernel functions are of subscript zero.

21) THIRD: Computes the disturbing body semi-major axis, the disturbing body eccentricity vector in inertial coordinates and the direction cosines of the disturbing body unit orbit normal with respect to the unit vectors of the satellite frame [Section 2.2.4].

22) XYZPOS: Computes the components of the disturbing body position vector in mean ecliptic of date coordinates.

23) XYZVEL: Computes the components of the disturbing body velocity vector in mean ecliptic of date coordinates.

24) ZCOEFF: Computes the coefficient $Z^{m}_{n,r}$ [eqs. (4-142) and (4-144)].

In order to model third body resonance in the averaged orbit generator or to model the short periodic corrections to the mean elements, the following subroutines are required:

25) ASSGN: Transfers the contents of the common blocks containing the third body Newcomb operators into a single common block.

26) NEXNEW: Executive routine for the summation over n in $\bar{\psi}_{t,s}$ that is used when the satellite Hansen coefficient kernel functions have non-zero subscripts.

27) REXNEW: Executive routine for the summation over r in $\bar{\psi}_{t,s}$ that is used when the disturbing body Hansen coefficient kernel functions have non-zero subscripts.

28) SATNEW: Computes by recurrence and stores the satellite Hansen coefficient kernel functions of non-zero subscript starting from initial values that have been constructed from the Newcomb operator expansions [eq. (4-249)]. Computes the partial derivatives of the satellite kernel functions with respect to $\bar{h}$ and $\bar{k}$ [eqs. (4-250) to (4-252)].

29) SATONE: Computes by recurrence and stores the satellite Hansen coefficient kernel functions of subscript one starting from initial values that have been constructed from the Newcomb operator expansions. Computes the partial derivatives of the satellite kernel functions with respect to $\bar{h}$ and $\bar{k}$. The recurrence relations are explicitly re-initialized beginning with n = 11 to avoid instability for high values of n when the kernel function subscript is one.

30) THDNEW: Computes by recurrence and stores the disturbing body Hansen coefficient kernel functions of non-zero subscript starting from initial values that have been constructed from the Newcomb operator expansions [eq. (4-236)]. Computes the partial derivatives of the disturbing body kernel functions with respect to h' and k' [eqs. (4-240) and (4-241)].

The Newcomb operator block data subprograms, which are used to initialize the satellite kernel function recurrence relations in SATNEW and SATONE, are loaded under names having the form NEWSn, where n is the degree of the third body potential Legendre polynomial expansion. The present third body software incorporates 19 of these subprograms, that is, NEWS2 through NEWS20. Likewise, the Newcomb operator block data subprograms, used to initialize the recurrence relations for the disturbing body kernel functions in THDNEW, are loaded under names having the form NEWn. There are presently 19 of these subprograms corresponding to NEW2 through NEW20.

The subroutine which is specifically required for the third body resonance implementation in the averaged orbit generator is:

31) THDLAM: Computes the mean longitude of the third body for use in the resonant averaged orbit generator [Section 2.2.3.2]. Computes the partial derivatives of the third body mean longitude with respect to the $\bar{p}$ and $\bar{q}$ satellite elements [eqs. (4-116) and (4-117), eqs. (4-118) to (4-133)].

The subroutines which are specifically required for the third body short periodic implementation are:

32) SPTHDB: Computes the analytical short periodic coefficients for third body perturbations [eqs. (4-37) and (4-38), eqs. (4-48) to (4-62)].

33) DBLANG: Computes the third body mean longitude and its partial derivatives with respect to p and q.

A schematic representation of the overall subroutine structure for the third body AOG and SPG is given in Figure B-1.

At present the third body software resides in partitioned data sets on the CSDL Amdahl 470 V/8 which are cataloged under the following names:

Non-Resonant Software

(1) SKC1756.GTDS.UPDATE. { FORT / LOAD }

(2) SKC1756.GTDS.SP. { FORT / LOAD }

Resonance Software

(3) SKC1756.GTDS.RESON. {FORT / LOAD}

(4) SKC1756.GTDS.SP.RESON. {FORT / LOAD}

Satellite Hansen Coefficient Newcomb Operators

(5) SKC1756.GTDS.NEWSAT1. {FORT / LOAD}

(6) SKC1756.GTDS.NEWSAT2. {FORT / LOAD}

Third Body Hansen Coefficient Newcomb Operators

(7) SKC1756.GTDS.NEWTHD1. {FORT / LOAD}

(8) SKC1756.GTDS.NEWTHD2. {FORT / LOAD}

Table B-1 indicates which data sets are needed for a given third body option and the minimum region size that is required for the resulting updated GTDS load module.

Third Body Option	Data Sets Required by Identifying no. (see text)	Required Region Size
AOG without resonance	(1)	1052K
AOG+SPG without resonance	(1),(2),(5),(6), (7),(8)	4976K
AOG with resonance	(3),(4),(5),(6), (7),(8)	4980K
AOG+SPG with resonance	(3),(4),(5),(6), (7),(8)	4980K

Table B-1. Datasets and Region Sizes Required for the Various Third Body Options

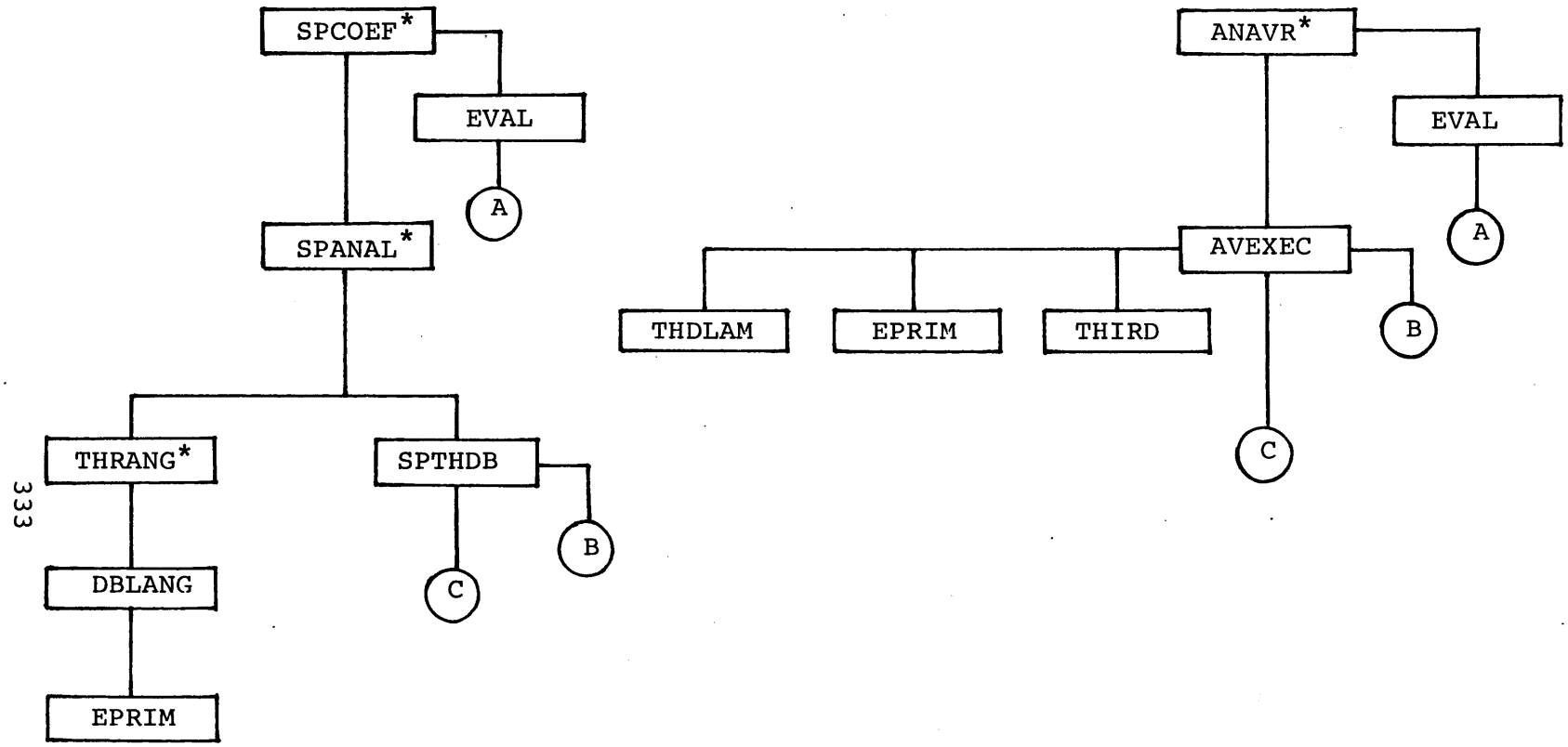


Figure B-1. Subroutine Interaction Diagram for the Third Body Software (page 1 of 4)

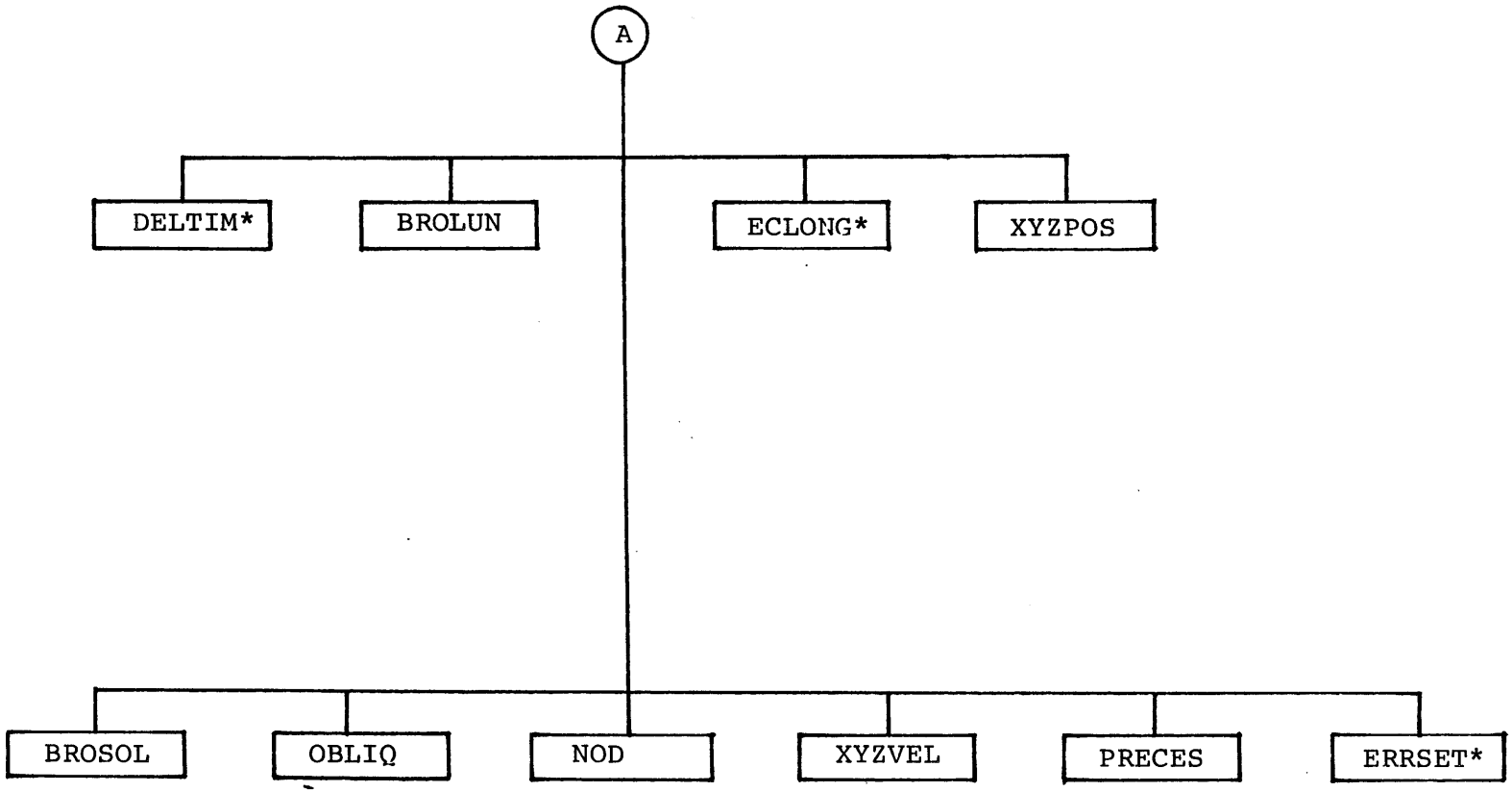


Figure B-1. Subroutine Interaction Diagram for the Third Body Software (page 2 of 4)

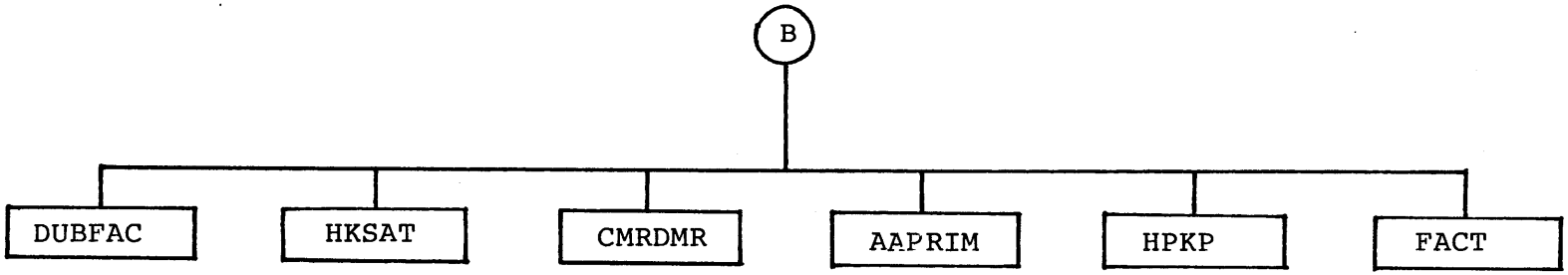


Figure B-1. Subroutine Interaction Diagram for the Third Body Software (page 3 of 4)

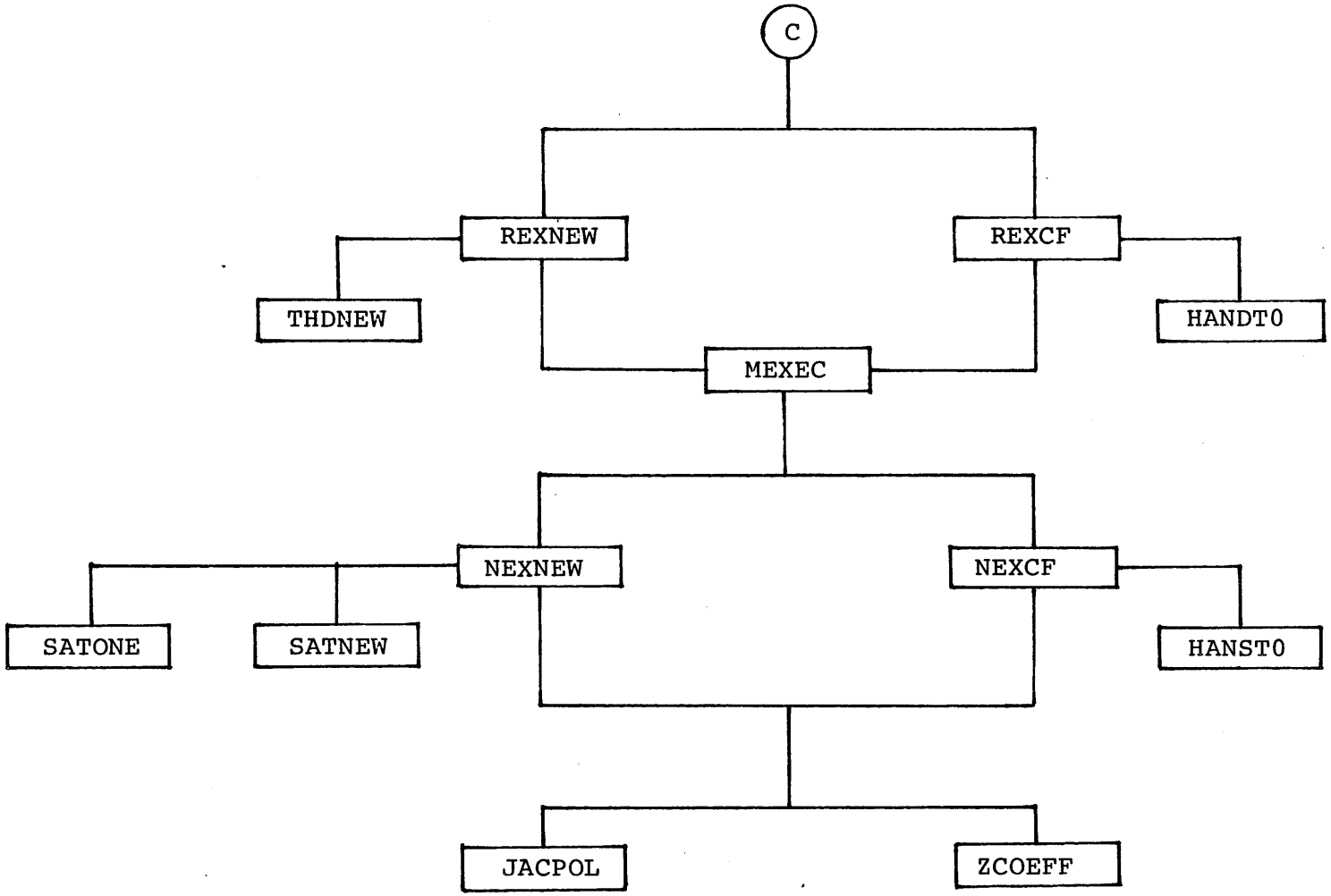


Figure B-1. Subroutine Interaction Diagram for the Third Body Software (page 4 of 4)

References

1. Kozai, Y., "Analytical Orbital Theories for Satellites," The Use of Artificial Satellites for Geodesy and Geodynamics (Proceedings of the International Symposium on the Use of Geodesy and Geodynamics, Athens, May 1973), ed. G. Veis, Athens, 1974, pp. 237-242.

2. Graf, Otis F., "The Elimination of Short and Intermediate Period Terms from the Problem of a High Altitude Earth Satellite," Celestial Mechanics, Vol. 14, No. 3, November 1976, pp. 321-329.

3. Krylov, N., and N. N. Bogoliubov, Introduction to Nonlinear Mechanics, Princeton University Press, Princeton, N.J., 1947.

4. Mitropolsky, Y. A., Problems of the Asymptotic Theory of Non-Stationary Vibrations, Daniel Davey, New York, 1965.

5. Hagihara, Y., Celestial Mechanics, Vol. II, Part I, MIT Press, Cambridge, Massachusetts, 1972.

6. Musen, P., "A Discussion of Halphen's Method of Secular Perturbations and Its Application to the Determination of Long-Range Effects in the Motion of Celestial Bodies," Reviews of Geophysics, Vol. 1, No. 1, February 1963, pp. 85-122.

7. Musen, P., "On Determining the Secular and Critical Effects in the Motion of Satellites by Means of a Nonsingular Set of Vectorial Elements," Journal of Geophysical Research, Vol. 68, No. 23, December 1, 1963, pp. 6255-6260.

8. Smith, A. J., "A Discussion of Halphen's Method for Secular Perturbations and Its Application to the Determination of Long Range Effects in the Motions of Celestial Bodies, Part 2," NASA TR R-194, Goddard Space Flight Center, Greenbelt, Maryland, June 1964.

9. Baxter, B. E., "On the Determination of Mean Elements for High Altitude Orbits," Aerospace Technical Memorandum 79(4404-30)-20, The Aerospace Corporation, El Segundo, California, 9 July 1979.

10. Ash, M. E., "Doubly Averaged Effect of the Moon and Sun on a High Altitude Earth Satellite Orbit," Celestial Mechanics, Vol. 14, No. 2, September 1976, pp. 209-238.

11. Sridharan, R., and W. P. Seniw, "An Intermediate Averaged Theory for High Altitude Orbits," Lincoln Laboratory Technical Note 1979-25, Lincoln Laboratory, Lexington, Massachusetts, 27 June 1979.

12. Lidov, M. L. "The Evolution of Orbits of Artificial Satellites of Planets Under the Action of Gravitational Perturbations of External Bodies," Planetary Space Sciences, Vol. 9, 1962, pp. 719-759.

13. Cook, G. E., "Basic Theory for PROD, A Program for Computing the Development of Satellite Orbits," Celestial Mechanics, Vol. 7, No. 3, April 1973, pp. 301-314.

14. Kaula, W. M., "A Development of the Lunar and Solar Disturbing Functions for a Close Satellite," NASA Technical Note D-1126, Goddard Space Flight Center, Greenbelt, Maryland, January 1962.

15. Computer Sciences Corporation, CSC/TR-77/6010, A Recursively Formulated First-Order Semianalytic Artificial Satellite Theory Based on the Generalized Method of Averaging, Vol. I: The Generalized Method of Averaging Applied to the Artificial Satellite Problem, Wayne D. McClain, November 1977.

16. Handbook of Mathematical Functions, eds. M. Abramowitz and I. A. Stegun, Dover Publications, Inc., New York, 1972.

17. Computer Sciences Corporation, CSC/TR-78/6001, A Recursively Formulated First-Order Semianalytic Artificial Satellite Theory Based on the Generalized Method of Averaging, Vol. II: The Explicit Development of the First-Order Averaged Equations of Motion for the Nonspherical Gravitational and Nonresonant Third-Body Perturbations, Wayne D. McClain, May 1978.

18. Cefola, P., "A Recursive Formulation for the Tesseral Disturbing Function in Equinoctial Variables," presented to the AIAA/AAS Astrodynamics Conference, San Diego, California, August 18-20, 1976, paper no. 76-839.

19) Morse, P. M., and H. Feshbach, Methods of Theoretical Physics, Part II, McGraw-Hill Book Company, Inc., New York, 1953.

20) Courant, R., and D. Hilbert, Methods of Mathematical Physics, Volume I, Interscience Publishers, Inc., New York, 1953.

21) McClain, W., and M. Slutsky, "A Theory for the Short Period Motion of an Artificial Satellite," presented to the AIAA/AAS Astrodynamics Conference, Danvers, Massachusetts, August 11-13, 1980, paper no. 80-1658.

22) Green, A. J., "Orbit Determination and Prediction Processes for Low Altitude Satellites," Ph.D. dissertation, Massachusetts Institute of Technology, Cambridge, MA, December 1979.

23) McClain, W. D., A. C. Long, and L. W. Early, "Development and Evaluation of a Hybrid Averaged Orbit Generator," presented to the AIAA/AAS Astrodynamics Conference, Palo Alto, California, August 7-9, 1978, paper no. 78-1382.

24) Early, L. W., GTDS software documentation in progress, Charles Stark Draper Laboratory, Inc., Cambridge, MA.

25) Shaver, J. S., "Formulation and Evaluation of Parallel Algorithms for the Orbit Determination Problem," Ph.D. dissertation, Massachusetts Institute of Technology, Cambridge, MA, March 1980.

26) Hansen, P. A., "Expansion of the Product of a Power of the Radius Vector with the Sine or Cosine of a Multiple of the True Anomaly in Terms of Series Containing the Sines and Cosines of the Multiples of the True, Eccentric or Mean Anomaly," Abhandlungen der Koniglichen Sachsischen Gesellschaft fur Wissenschraft, Vol. 2, No. 3, pp. 183-281, 1855; translated from the German by J. C. Van der Ha.

27) Collins, S. K., and P. J. Cefola, "Double Averaged Third Body Model for Prediction of Super-Synchronous Orbits Over Long Time Spans," presented to the AAS/AIAA Astrodynamics Specialist Conference, Provincetown, Massachusetts, June 25-27, 1979, paper no. 79-135.

28) Explanatory Supplement to the Astronomical Ephemeris and the American Ephemeris and Nautical Almanac, printed and published by Her Majesty's Stationery Office, London, 1974.

29) Computer Sciences Corporation, CSC/SD-78/6020, System Description and User's Guide for the GTDS R&D Averaged Orbit Generator, A. C. Long and L. W. Early, November 1978.

30) Kozai, Y., "A New Method to Compute Lunisolar Perturbations in Satellite Motions," Smithsonian Astrophysical Observatory Special Report 349, February 1, 1973.

31) MACSYMA Reference Manual, The Mathlab Group, Laboratory for Computer Science, Massachusetts Institute of Technology, Cambridge, MA, December 1977.

BIOGRAPHY

Sean Kevin Collins was born 21 February 1952 on the Fort Belvoir military reservation in Virginia to John M. and Gloria O. Collins. He attended Fort Hunt High School in Alexandria, Virginia from 1966 to 1970. In June of 1974 he received the Bachelor of Science Degree with High Distinction in Aerospace Engineering at the University of Virginia in Charlottesville, Virginia. Having entered the graduate school of the Massachusetts Institute of Technology in September of 1974, he was granted a Master of Science degree in Aeronautics and Astronautics in February 1977. He married Susan Jane Howling in July 1980. At present Mr. Collins is a Draper Fellow at the Charles Stark Draper Laboratory in Cambridge, Massachusetts.